Synthesis and Physical Properties of Porphyrins Having Five-Membered Fused Rings at the Periphery

Yuta Saegusa

February 2017

Synthesis and Physical Properties of Porphyrins Having Five-Membered Fused Rings at the Periphery

Yuta Saegusa
Doctoral Program in Chemistry

Submitted to the Graduate Schoool of
Pure and Applied Sciences
in Partial Fulfillment of the Requirements
for the Degree of Doctor of Philosophy in
Science

at
University of Tsukuba

Contents Page

Chapter 1

General introduction

1-1. Functionality of polycyclic aromatic hydrocarbons

A lot of π-conjugated molecules having one-, two- and three-dimensional structures have been well investigated, because of the fascinating physical and chemical properties (Figure 1-1).[1-4] Among them, polycyclic aromatic hydrocarbons (PAH) has widely attracted attention, because of interests in the intense absorption in the visible region,[5]

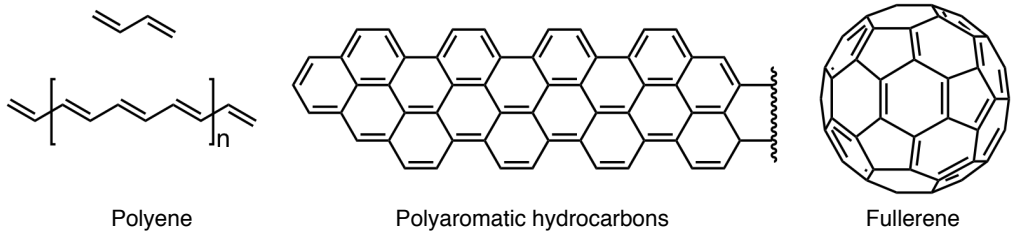

Figure 1-1. Representative examples of π-conjugated compounds.

and highly electron-conducting properties,[6] by virtue of expansion of the π-conjugated circuits. PAHs also can easily form one- and two-dimensional supramolecular assemblies using strong π-π interactions based on the planar structures.[7,8] Introduction of substituents showing electrostatic or hydrogen-bonding interaction to PAHs prompts PAHs to more easily form multi-dimensional assemblies accompanying more complicated structures and more useful functionalities.[9] For example, an amphiphilic PAH molecule, having a hexabenzocoronene (HBC) moiety at the core

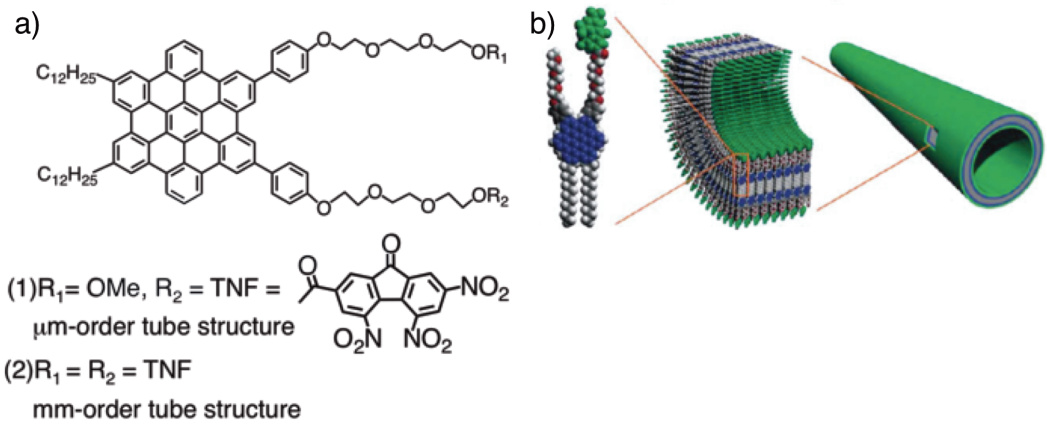

Figure 1-2. The molecular structure of the TNF-appended HBC amphiphile (a) and schematic description of one-dimensional supramolecular assembly to form the nanotube structure (b).[9a]

and a trinitro-fluorenone (TNF) moiety at the periphery, selectively formed nanotubes or microfibers, depending on the assembling conditions, and the nanotubes and microfibers exhibited different photochemical properties (Figure 1-2).[9a] The coaxial nanotubular structure of the amphiphilic HBC derivative performed photochemical generation of spatially separated charge carries and a quick photoconductive response, whereas the microfibers consisting of the amphiphilic HBC derivative exhibit almost no photocurrent generation.[9a]

Various PAHs, having not only six-membered rings but also five-membered rings, have been also synthesized. PAHs consisting of only six-membered rings generally exhibit planar structures, whereas those involving five-membered rings displayed curved surfaces.[1c] Based on π-π interaction of the curved surfaces, π-conjugated molecules including five-membered ring have been employed as host molecule for fullerenes;[10] for instance, a corannulene derivative, **a**, (Figure 1-3), which consists of five benzene rings fused with a central five-membered ring, formed 1:1 complexes with C_{60} in toluene with the association constant, K_{assoc}, of 450 M^{-1}.[11] The association constant of a π-expanded corannulene derivative, **b**, with C_{60} was improved to *ca.* 1400 M^{-1},[11] and thus, the expansion of the size of π-systems is important for efficient binding of fullerenes in solution.

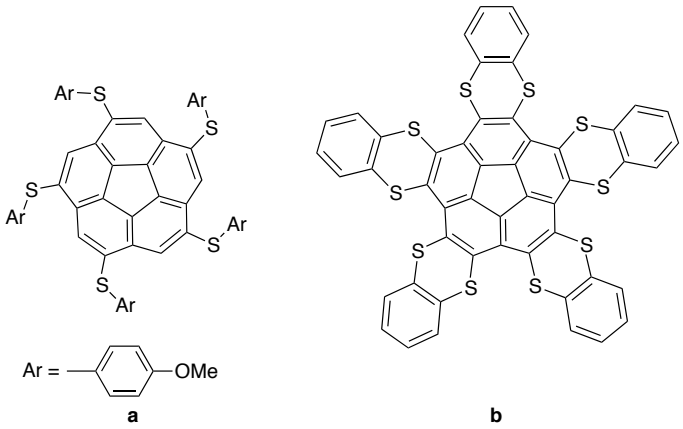

Figure 1-3. The molecular structures of the corannulene based host molecules.[11]

The number of atoms to form fused rings of PAHs also strongly affects its aromaticity. In PAHs consisting of only six-membered rings, each six-membered ring maintains the independent aromatic circuit, and additionally, an aromatic circuit across the whole structure of the PAH also can be drawn to exhibit the aromaticity.[12] In contrast, PAHs having five-membered rings as components can exhibit an anti-aromatic circuit across the whole structure (Fig 1-4).[12] As an example of such kinds of PAHs, pyracylene has been well known; pyracylene has a naphthalene moiety at the center and two fused five-membered rings, and the pyracylene structure can be found in fullerenes such as C_{60} and C_{70} as a partial structure.[12] Pyracylene is considered to be an aromatic compound, since it can be regarded as a molecule consisting of 10π-electron naphthalene core and two etheno moieties at the periphery (Figure 1-4A).[13] However, pyracylene also has an antiaromatic character, since it can be viewed as a 12π-electron cyclododecahexaene having an internal cross-linked etheno unit (Figure 1-4B). The ^{1}H NMR spectrum of pyracylene indicates that the most

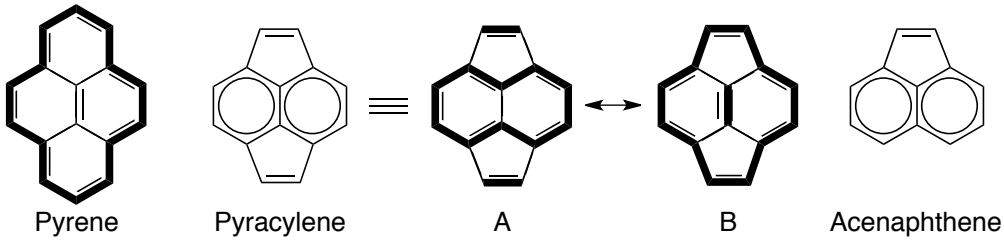

Figure 1-4. Structures of pyrene, pyracylene, and acenaphthene. In pyracylene, two resonance structures can bedrawn; a 10π-electron naphthalene unit connected to two 2π-electron etheno systems (A) and a 12 π-electron cyclododecahexaene periphery having an internal cross-linked etheno unit.

appropriate structure of pyracylene, reflecting its real electronic structure, is model B. In fact, the ^{1}H NMR signals of pyracylene appeared at relatively higher field (δ 6.01 and 6.52 ppm in CCl_4) in comparison to those of naphthalene (δ = 7.67 and 7.32 ppm in CCl_4).[13] The upfield shifts indicate the influence of a paramagnetic ring current of 12π-electron antiaromatic circuit. This paratropic shifts of the ^{1}H NMR signals of pyracylene are smaller than those of pure antiaromatic systems,[14] and thus, this shift can be viewed as a result of partial contribution of the antiaromatic circuits. Other compounds having fused five-membered rings at the periphery have been also reported to show characteristic properties derived from the partial contribution of the antiaromaticity to the electronic structures.[15]

In addition, as a characteristics of PAHs having five-membered fused rings, pyracylene has been reported to show a lower energy level of LUMO than that of isomeric anthracene, having a similar molecular size, and than that of acenaphthene, lacking a five-membered fused ring from pyracylene; the first reduction potential, E_{red1}, were reported to be = –1.06 V vs SCE for pyracylene, –2.10 V vs SCE for anthracene, –1.80 V vs SCE for acenaphthene.[16] It can be explained by the fact that the $2e^-$-reduced form of PAHs having fused five-membered rings is stabilized by the formation of an aromatic cyclopentadienide structure, showing the (4n+2)π Hückel aromaticity.[17] Therefore, PAHs having five-membered rings have been proposed as a candidate for components of n-type organic semiconductors.[16]

1-2. Structural features and optoelectronic properties of porphyrin and its derivatives

Porphyrin is a macrocyclic system consisting of four pyrroles and four methine carbons, along which an 18π electron π-conjugated circuit can be drawn. Porphyrin shows a strong diatropic current and strong optical absorption bands in the visible region with large absorption coefficients.[18] Therefore, porphyrins have been extensively investigated in diverse fields to construct artificial photosynthetic systems,[19] to develop efficient oxidation catalysts,[20] to form supramolecular assemblies,[21] to obtain host molecules for molecular recognitions,[22] and to apply porphyrin chromophores to nonlinear optical materials.[23] As another attractive point of porphyrins, structures of porphyrins can be easily modified; through the modification, their optical and electrochemical properties and self-assembling structures can be finely controlled.[18, 24-26]

A lot of porphyrin derivatives have been synthesized to utilize their characteristic optical properties and reversible multi-redox processes for various applications,[18,19,24-26] and for the purposes, many synthetic methods have

been reported so far.[18] Syntheses of *meso*-aryl porphyrins, which have been the most widely used, can be achieved by condensation of pyrroles and arylaldehydes in the presence of an acid catalyst, and subsequent oxidation.[27,28] Furthermore, porphyrin derivatives can be obtained with a stepwise manner using various dipyromethane derivatives as starting materials to obtain porphyrins unsymmetrically substituted with different aryl moieties.[29]

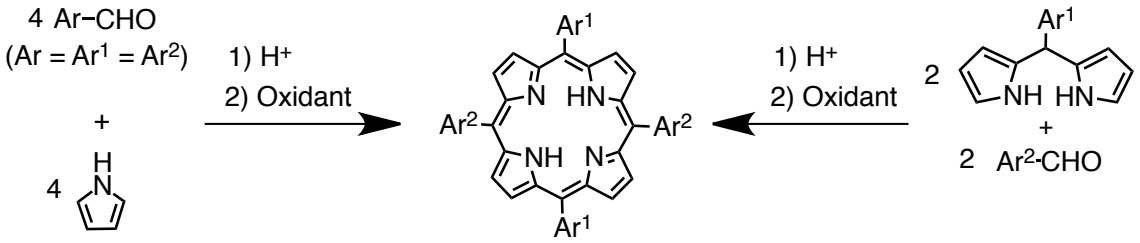

Scheme 1-1. Synthetic routes of *meso*-aryl porphyrins.

Porphyrin and its derivatives exhibit characteristic absorption bands in the visible region; the intense absorption band around 400 nm is mentioned as the Soret band and the relatively weak-split absorption bands observed in the range of 500 – 600 nm are called as Q bands. The origins of these absorption bands can be explained by the Gouterman's four-orbital model;[30] in this model, Soret and Q bands are derived from transitions between four frontier orbitals, HOMO, HOMO–1, LUMO, and LUMO+1 (Figure 1-5). Because of the small HOMO-LUMO gap and expanded π-conjugation, porphyrin derivatives also have been used to produce nonlinear optical materials.[23] The structural requirement to obtain high molecular first hyperpolalizability, β, is well understood from both of theoretical

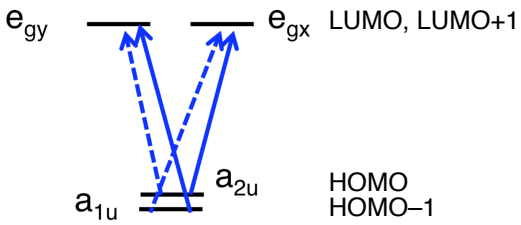

Figure 1-5. The Gouterman's model of four frontier orbitals of metalloporphyrins.[30]

and experimental aspects (see Chapter 7 in this thesis).[31]Organic chromophores, having electron-donating and -withdrawing groups that are connected by a large π-conjugated molecular bridge, are known to show high β values and the molecular design is known as a "push-pull" strategy. A "push-pull" porphyrin derivative, having two *p*-nitrophenyl groups at 5 and 10 positions and *p*-aminophenyl groups at 15 and 20 positions, shows a moderate β value, (30 ± 10) × 10^{-30} esu (Figure 1-6).[32] The reason for the small β value obtained by even introduction of the "push-pull" design to the porphyrin framework is that the intramolecular electronic conjugation between the electron-donating and -withdrawing groups are relatively weak in the tetraarylporphyrins, due to tilting of the *meso*- aryl-groups relative to the porphyrin plane.

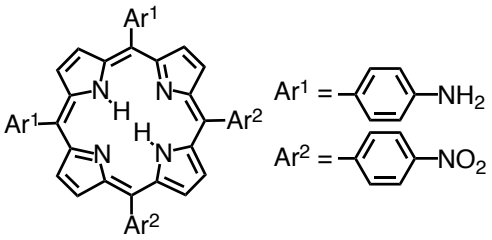

Figure 1-6. Molecular structure of the "push-pull" porphyrin.[32]

Porphyrin and its derivatives show reversible redox processes; for instance, tetraphenylporphyrin (H_2TPP) exhibited stepwise two oxidation and two reduction processes in CH_2Cl_2 containing 0.1 M (n-butyl)$_4NClO_4$ as an electrolyte (Figure 1-5).[25b] ESR studies have revealed that the redox processes proceed on the π-conjugated circuit of the porphyrin,[33] and thus, introduction of substituents to the π-conjugation pathway of porphyrins intensively affects the redox properties. Therefore, it is possible to obtain porphyrin derivatives showing desired redox potentials for various purposes by changing the substituents.[18,24-26]

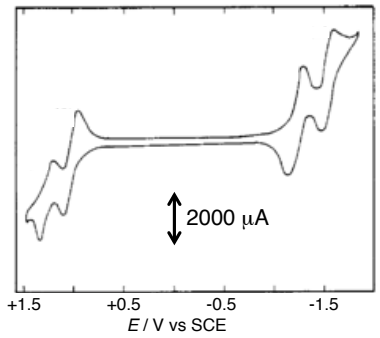

Figure 1-7. Cyclic voltamogram of H_2TPP. [H_2TPP] = 2.6×10^{-3} M. Electrolyte: (n-butyl)$_4NClO_4$ (0.1 M). Solvent: CH_2Cl_2. Scan Rate: 0.05 V/s.[26b]

Freebase porphyrins have two imino-nitrogen atoms, which play a role as a weak base ($pK_a \sim 4$).[34] The basicity of the imino-nitrogen atoms has attracted much attention, since protonation of the imino-nitrogen atoms causes bathochromic shifts of absorption bands of the porphyrins and also induces positive shifts of the redox potentials. Therefore, protonated porphyrins can be utilized as electron acceptors in photoinduced electron transfer.[35] In addition, freebase porphyrins exhibit NH tautomerism induced by proton transfer between the intramolecular hydrogen-bonded pair of the pyrrolic N-Hs and imino-nitrogen atoms of the non-protonated pyrroles. The NH tautomerism has been regarded as an important issue in the porphyrin chemistry toward development of single-molecule switchs, which are an essential component of single-molecule-based devices.[36]

Porphyrin forms stable metal complexes with most of the metals in the periodic table using four coordinating inner-nitrogen atoms, suitable for forming square-planar coordination structures.[18,37] Metal complexes of porphyrins

exhibit various reactivity and catalysis, depending on the characteristics of the metal centers.[20,38] They can also form coordination polymers using axial ligation at the central metals.[21b] In addition, introduction of substituents at the periphery of the porphyrin ligand has been known to be effective to control the chemical properties of the metal centers;[26] for example, an iron(III) complex of a porphyrin derivative having cyano groups at the *meso*-aryl groups shows positive shifts of the reduction potentials not only for the porphyrin core but also for the iron(III) center.[26c]

Using the expanded π-conjugation and strong electron-donating ability, porphyrin derivatives have been employed to form associated complexes with fullerenes as π-conjugated electron-accepting molecules.[39] However, supramolecular interaction between porphyrin derivatives showing planar structures and fullerenes having curved surfaces[40] generally are not so strong to maintain the associated structures in solution, since the structures are not complementary each other.[41] Therefore, for efficient recognition of fullerenes with porphyrins in solution, porphyrin hosts need to be dimers or higher oligomers (Figure 1-8) to enhance intermolecular π-π interaction with fullerenes.[39,42,43] Using the associated complexes, photoinduced electron transfer from the porphyrin to the fullerene included has been also investigated.[44]

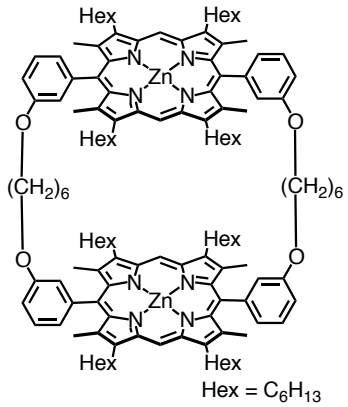

Figure 1-8. Host molecule based on porphyrin dimer.[42a]

1-3. Syntheses and physical properties of ring-fused porphyrins

Recent studies have revealed that porphyrin derivatives bearing fused aromatic moieties at the periphery show unique optical and magnetic properties on the basis of coplanarity between the porphyrin core and the fused aromatic moieties and the resultant expansion of π-conjugated circuits.[45] Introduction of ring-fused structures to porphyrins allows us to access bathochromic shifts of the absorption bands reaching to near-IR region,[46] two-photon absorption as a nonlinear optical response[47] and strong intermolecular π-π interaction for supramolecular assemblies.[48] The supramolecular assemblies of ring-fused porphyrins are highly promising as building blocks to develop efficient transporters of electrons, holes and excitation energies.[48] In this section, recent development of ring-fused porphyrin derivatives are briefly reviewed with focus on the synthesis, structure, aromatic and optical properties. Herein, the structures of ring-fused porphyrins are categorized into *β*-*β* fusion and *meso*-*β* fusion types (Figure 1-9).

A lot of ring-fused porphyrins having the fused aromatic moieties at the *β*-*β* positions have been

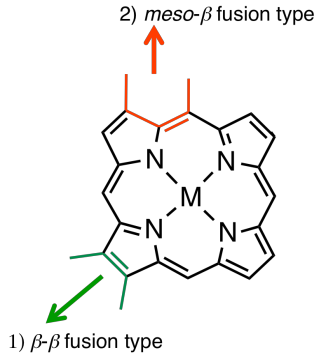

Figure 1-9. Classification of ring-fused porphyrins.

prepared by various procedures. One of the representative synthetic procedures of *β*-*β* fusion type ring-fused porphyrins is macrocyclization of *β*-*β*-ring fused pyrroles (Scheme 1-2).[49] To date, the procedure using the ring-fused pyrroles have been successfully utilized to synthesize various *β*-*β* ring-fused porphyrins;[49,50] however, one of the problems of this procedure is the low solubility of pyrrole derivatives having large planar aromatic moieties at the *β*-*β* positions and that of the porphyrin products obtained from the pyrroles, which causes low reaction yields.[50] To solve this problem, a retro-Diels-Alder strategy for the synthesis of the *β*-*β* aryl fused porphyrins has been developed;[51] the Diels-Alder

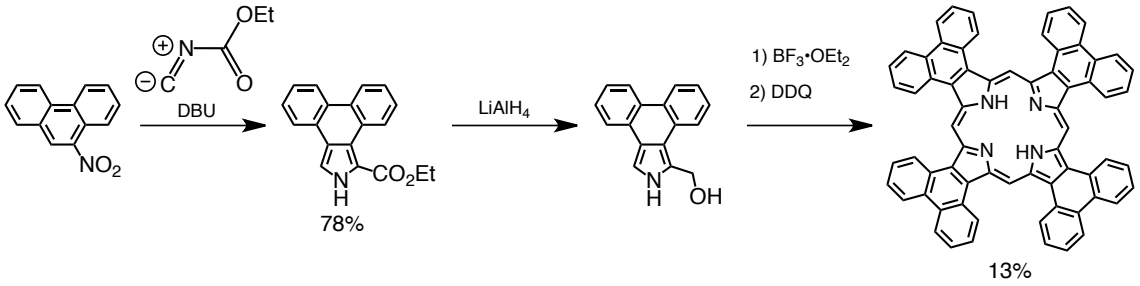

Scheme 1-2. Synthesis of phenanthrene-fused pyrrole and its porphyrin derivative.[50]

precursor of tetrabenzoporphyrin is quite soluble in many organic solvents, whereas tetrabenzoporphyrin is an expanded planar molecule and poorly soluble in any solvents (Scheme 1-3). Therefore, this procedure has been employed to produce a homogeneous spin-coat film, which is applied to organic thin-film transistors[51b] and photovoltaic cells.[52] Other porphyrin having fused aromatic moieties at the periphery have been also prepared by the retro-Diels-Alder

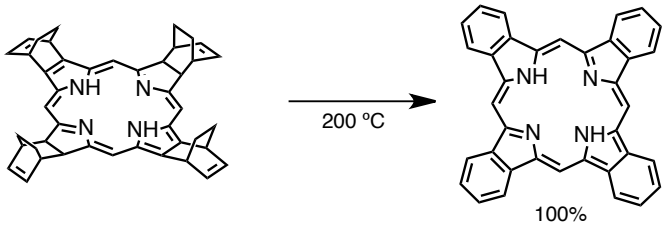

Scheme 1-3. Synthesis of tetrabenzoporphyrin using a retro-Diels-Alder reaction.[51]

strategy.[53] All of the *β*-*β*-type ring-fused porphyrins described above show moderate bathochromic shifts of the Soret and Q bands in the UV-Vis spectra relative to *meso*-*β*-type ring-fused porphyrins.[54,55] In comparison to the *β*-*β*-type ring-fused porphyrins, a fewer examples of *meso*-*β*-type ring-fused porphyrins have been prepared so far.[45] The *meso*-*β* ring-fusion on porphyrins, however, induces larger bathochromic shifts in the absorption spectra, in comparison to the *β*-*β* fused porphyrins, and thus, the *meso*-*β* ring-fusion more influences the electronic structures of porphyrins than the *β*-*β*-type ring-fusion.[45] In addition, both of the *meso*-*β* and *β*-*β* fusion types of ring-fused porphyrins have exhibited strong tendency to form supramolecular assemblies based on the intermolecular

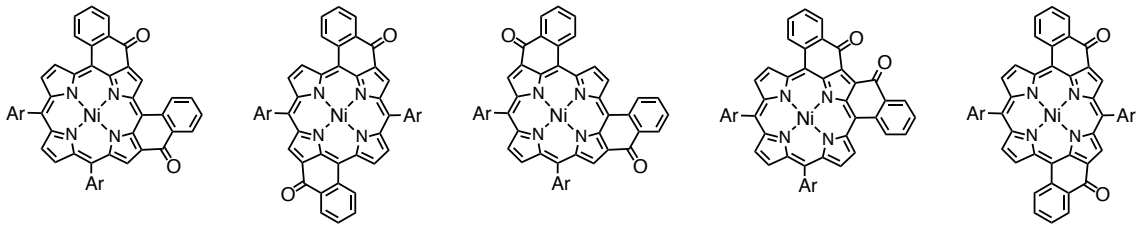

Figure 1-10. Structure of the fused porphyrins synthesized with an intramolecular Friedel-Crafts reaction.[56] Ar = 3,5-di-*tert*-butylphenyl.

π-π interaction. A series of *meso*-*β*-type ring-fused porphyrins have been synthesized using an intramolecular Friedel-Crafts reaction,[56] and the porphyrin derivatives showing different symmetries have been isolated (Figure 1-10). These ring-fused porphyrins have been reported to form π-π-stacked dimeric structures in the solid state owing to co-planarization of the carboxyphenyl moieties by ring-fusion, despite the fact that they had sterically bulky substituents such as 3,5-di-*tert*-butylphenyl groups.[56]

The synthetic route of another example of *meso*-*β*-ring-fused porphyrins, which has a thiophen- fused moiety, is shown in Scheme 1-4.[57] The thiophene-fused porphyrins show reduced aromaticity due to contribution of their antiaromatic resonance forms; a 20π-conjugated antiaromatic circuit can be drawn for the thiophene-fused porphyrin, **c**, with involving a fused five-membered ring at the periphery. In contrast, porphyrin **d** shows the weak antiaromatic contribution to the electronic structure, because of the disruption of the possible 24π antiaromatic circuit by the sulfur atom. The NICS values[58] for **c** and **d** are both positive (+30.5 and +13.1 ppm, respectively), and the larger positive NICS value for **c** indicates a larger contribution of the antiaromatic 20π circuit to the electronic structure of **c**. In the ^{1}H NMR spectra, the signals of the *meso* and *β* protons of **c** were shifted to further upfield relative to those of **d**, reflecting the increasing contributions of antiaromatic resonance forms to the electronic structures. On the other hand, in the UV-Vis absorption spectra of **c** and **d**, the Soret and Q bands were weakly and broadly observed in comparison with those of the precursor compounds, which is also due to contribution of the antiaromatic resonance forms.[59]

Meso-*β* fused porphyrins can be prepared with oxidative fusing reactions between the porphyrin core and aromatic moieties at the *meso*-positions, using a chemical oxidant such as $FeCl_3$ and DDQ.[46, 60-65] Based on this method,

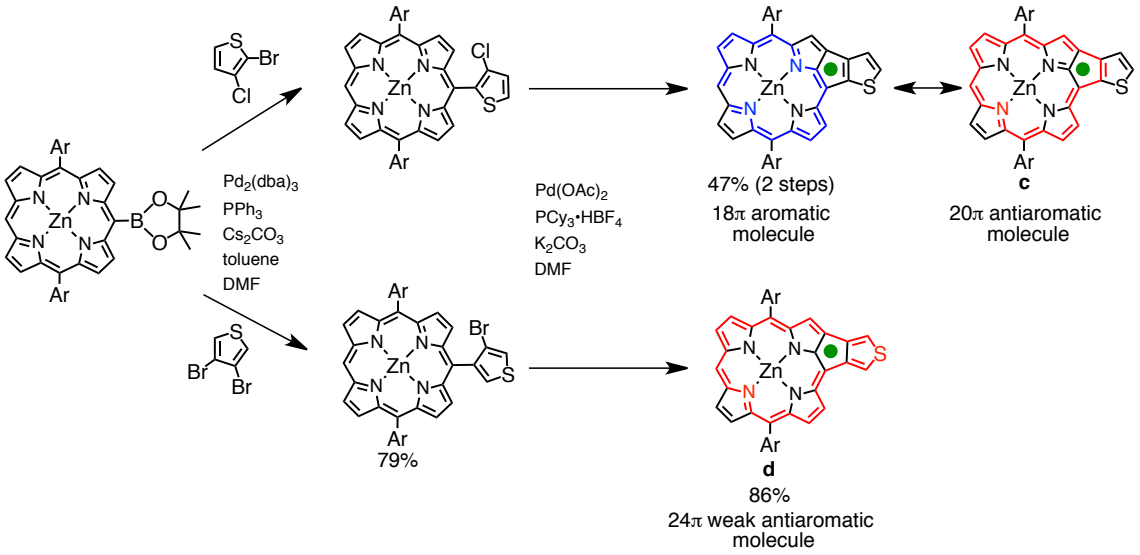

Scheme 1-4. Synthesis of thiophene-fused porphyrins.[57]

various aromatic compounds have been introduced as ring-fused moieties at the periphery of porphyrins. For example, *meso*-*β*-fused porphyrins having fused anthracene moieties have been synthesized by oxidative ring-fusion of the porphyrin core with electron-rich anthracene groups at the *meso*-positions using $FeCl_3$ as an oxidant. (Figure 1-11).[46] The anthracene-fused porphyrins exhibit intense Q-bands at 855 nm for **e**, 973 nm for **f**, and 1417 nm for **g**, indicating that increase on the number of fused anthracene units causes further bathochromic shifts of the absorption

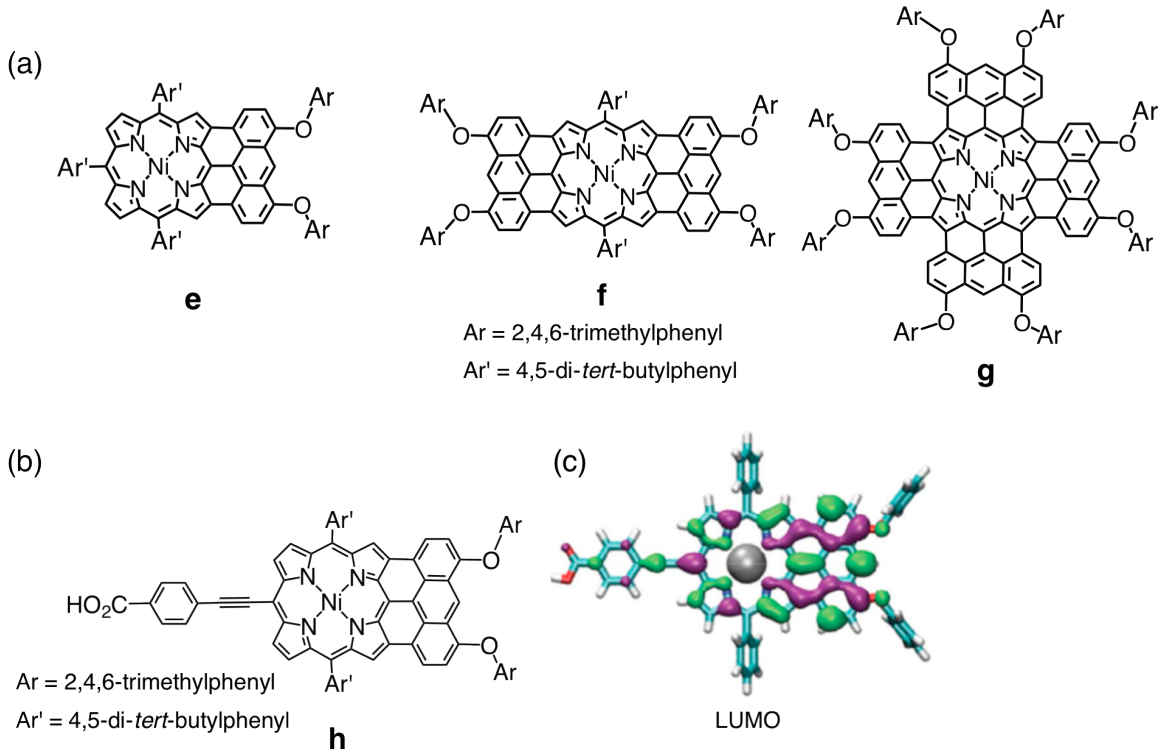

Figure 1-11. (a), (b) Molecular structures of anthracene-fused porphyrins.[46] (c) The distribution of the LUMO of an anthracene-fused porphyrin derivative.[66]

bands. In the crystal packing, porphyrin **g** formed a π-π stacked dimer. An anthracene-fused porphyrin derivative (**h**) has expanded π-conjugation to the aryl-ethynyl group and shows red-shifted absorption, and thus, it is expected to perform efficient charge-transfer from **h** to metal-oxide upon forming organic thin-layer photovoltaic cells by introduction of **h** on a metal-oxide substrate.[66] However, the incident photon-to-current conversion efficiency (IPCE) was determined to be only 0.1%. The low efficiency can be accounted for by the fact that the fused porphyrin **h** has the LUMO away from the anchor moiety, the carboxyl group at the arylethynyl group, to the metal oxide surface (Figure 1-11c), which disturbs efficient electron injection from the photoexcited **h** to the conduction band of the metal-oxide substrate.

Recently, thermal fusion methods of a porphyrin core having unactivated PAH groups such as naphthalene, pyrene, coronene, and perylene, introduced at the *meso*-positions, have been developed (Scheme 1-5).[67] However, the fusing positions under the thermal conditions are difficult to be controlled, and thus, the product selectivity is inherently low and the isolation of the products is highly difficult.

On the other hand, intramolecular ring-fusion reactions of porphyrins with aryl moieties at the periphery using Pd catalysts have been also reported;[68] for instance, singly- and doubly-fused porphyrins were prepared from halogen-appended precursors at the *meso*-aryl moieties using a Pd catalyst (Scheme 1-6).[68] Unfortunately, the corresponding quadruply-fused compounds was not detected at all in the

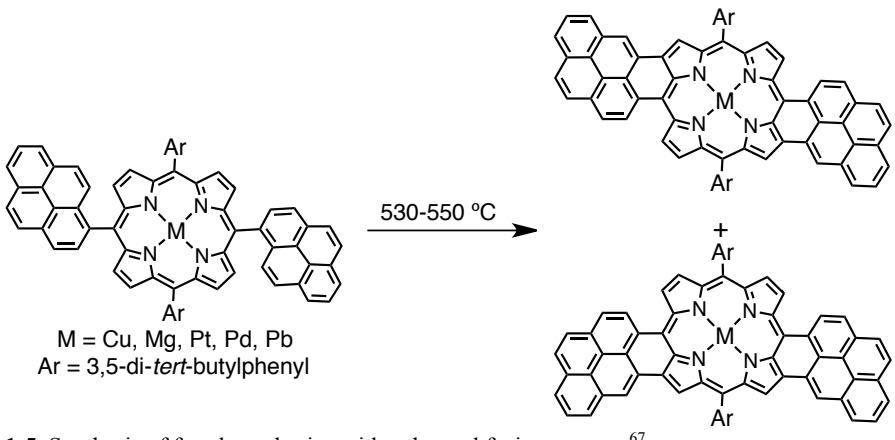

Scheme 1-5. Synthesis of fused porphyrins with a thermal fusion process.[67]

MALDI-TOF-MS spectrum of the reaction mixture, even when the tetrabromo-precursor was used (Scheme 1-6b).[68b] Additionally, the mixture including doubly fused porphyrins and the isomers could not be separated, although the compounds were obtained in moderate yields as estimated by the ^{1}H NMR spectroscopy. On the other hand, the singly fused porphyrin, obtained and isolated by a different procedure (Scheme 1-6c),[69] was utilized as a building block of dye-sensitized solar cells (Figure 1-11); as a result, the light harvesting properties of the solar cell made of the singly fused porphyrin in the visible and NIR regions were remarkably improved relative to that of tetraphenylporphyrin as a reference.[69]

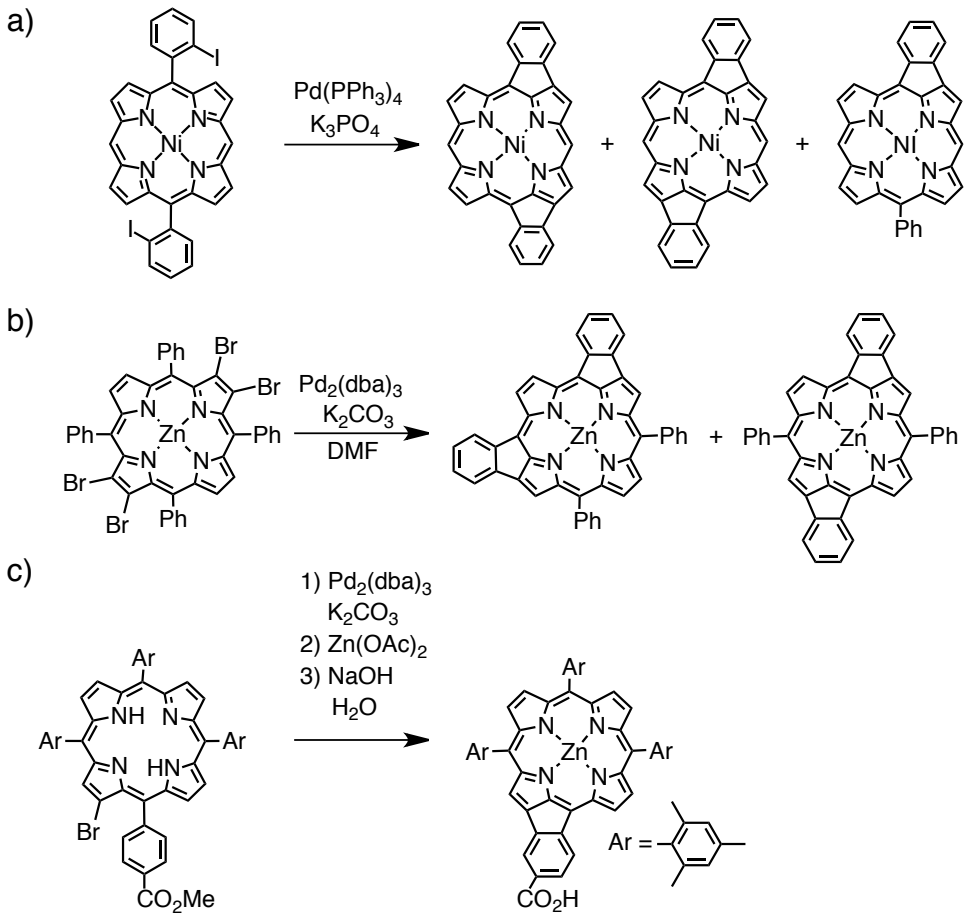

Scheme 1-6. Synthesis of five-membered-ring-fused porphyrins by C-H activation reactions using a Pd catalyst. dba = dibenzylideneacetone.

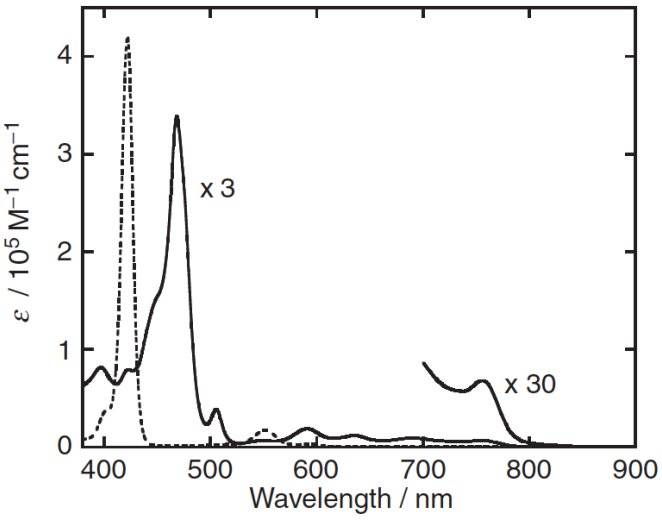

Figure 1-11. UV-vis absorption spectra of the singly fused porphyrin (solid line) and the corresponding tetraphenylporphyrin derivative (dashed line) in CH_2Cl_2.[69]

Problems of syntheses of ring-fused porphyrins revealed to date are summarized as follows: The oxidative ring-fusion reactions requires introduction of electron-donating groups to the aryl groups to be fused,[70] and thus, the possible substituents to be introduced are highly limited. Moreover, the synthesis of precursors for the oxidative

ring-fusion is time-consuming.[46] Synthetic problems of thermal fusion reactions are the low product selectivity and severe ring-fusion conditions. The product selectivity is also a problem for the intramolecular ring-fusion reactions using Pd catalysts.

1-4. Purpose of this research

In this research, the author has developed a facile synthetic method of novel quadruply fused porphyrins (QFPs), having four five-membered fused rings at the periphery, and has investigated their structural, aromatic and optical properties. QFP derivatives exhibit the expansion of the aromatic circuits to the fused *meso*-aryl groups, judging from the crystal structures and the ESR studies of the $1e^-$-reduced and $1e^-$-oxidized species. Furthermore, the impact of peripheral substitution of QFP on the structures and optical properties has been revealed. The author also has examined the effects of formation of ring-fused structure at the periphery on the properties of the metal center of the QFP-metal complexes and on the basicity of inner-imino nitrogen atoms of the freebase form. Furthermore, the nonlinear optical properties of QFP derivatives, having "push-pull" substituents, have been studied by the hyper-Rayleigh light-scattering method. Using the expanded π-conjugation circuit and the curved surface formed by the axial ligation of the metal center, QFP has been used as a host molecule for recognition of fullerenes in solution.

One of the advantages of QFP over other ring-fused porphyrin derivatives is the facile and efficient procedure for the preparation of QFP itself and its precursors. The ring-fusion reactions can be applied to a lot of porphyrins synthesized so far and having various functional groups, and the plentiful knowledge of porphyrin syntheses can be used to synthesize the ring-fusion precursors. Therefore, through the facile procedure, QFP derivatives exhibiting unique optical and electrochemical properties, which derive from the ring-fused structures, are easily prepared and they can be applied to optoelectronic devices. In addition, another interesting feature of QFP is the rhombic distortion around the metal center. As a result of the distortion, the mean length of the coordination bonds is elongated relative to those of the corresponding tetraphenylporphyrin complexes, which results in the increase of the Lewis acidity of the metal centers. Owing to the enhanced Lewis acidity, the metal center of the QFP metal complex can strongly hold axial ligands, and the axial ligation can induce a dome-like distortion of the QFP core plane, which is originally planar. Therefore, the two characteristic structures can be facilely switched by axial ligation, and resultantly, the functions and properties of QFP as supramolecular hosts can be controlled. Through this research, the author has provided a novel molecular design of functional molecules to develop the molecular devices utilizing a wide range of solar energy and exhibiting high efficiencies as optoelectronic materials.

Reference and notes

1 (a) F. Diederich, M. Kivala, *Adv. Mater.* **2010**, *22*, 803. (b) J. Cornil, D. Beljonne, J.-P. Calbert, J.-L. BrØdas, *Adv. Mater.* **2001**, *13*, 1053. (c) M. Stępień, E. Gońka, M. Żyła, N. Sprutta, *Chem. Rev.* **2017**, ASAP (DOI: 10.1021/acs.chemrev. 6b00076).

2 (a) F. Sondheimer, D. A. Ben-Efraim, R. Wolovsky, *J. Am. Chem. Soc.* **1960**, *83*, 1675. (b) J. Roncali, *Chem. Soc. Rev.* **2005**, *34*, 483.

3 (a) J. Wu, W. Pisula, K. Müllen, *Chem. Rev.* **2007**, *107*, 718. (b) T. Aida, E. W. Meijer, S. I. Stupp, *Science*, **2012**, *335*, 813. (c) D. Görl, X. Zhang, F. Würthner, *Angew. Chem. Int. Ed.* **2012**, *51*, 6328.

4 (a) *Acc. Chem. Res.* **1992**, *25*, 97-176 (special issues on buckminsterfullerenes). (b) M. Terrones, *Int. Mater. Rev.* **2004**, *49*, 325.

5 (a) J. L. Delgado, P.-A. Bouit, S. Filippone, M. Á. Herranza, N. Martín, *Chem. Commun.* **2010**, *46*, 4853. (b) A. Kaeser, A. P. H. J. Schenning, *Adv. Mater.* **2010**, *22*, 2985. (c) O. S. Wenger, *Chem. Soc. Rev.* **2011**, *40*, 3538.

6 (a) J.-L. Brédas, D. Beljonne, V. Coropceanu, J. Cornil, *Chem. Rev.* **2004**, *104*, 4971. (b) M. Wan, *Adv. Mater.* **2008**, *20*, 2926. (c) W. Wu, Y.Liu, D. Zhu, *Chem. Soc. Rev.* **2010**, *39*, 1489. (c) W. Jiang, Y. Li, Z. Wang, *Chem. Soc. Rev.* **2013**, *42*, 6113.

7 (a) A. P. H. J. Schenning, E. W. Meijer, *Chem. Commun.* **2005**, 3245. (b) Z. Chen, A. Lohr, C. R. Saha-Möller, F. Würthner, *Chem. Soc. Rev.* **2009**, *38*, 564.

8 S. Santhosh Babu, V. K. Praveen, A. Ajayaghosh, *Chem. Rev.* **2014**, *114*, 1973.

9 (a) Y. Yamamoto, T. Fukushima, Y. Suna, N. Ishii, A. Saeki, S. Seki, S. Tagawa, M. Taniguchi, T. Kawai, T. Aida, *Science* **2006**, *314*, 1761. (b) E. Krieg, E. Shirman, H. Weissman, E. Shimoni, S. G. Wolf, I. Pinkas, B. Rybtchinski, *J. Am. Chem. Soc.* **2009**, *131*, 14365. (c) A. F. M. Kilbinger, R. H. Grubbs, *Angew. Chem. Int. Ed.* **2002**, *41*, 1563. (d) H.-L. Yip, J. Zou, H. Ma, Y. Tian, N. M. Tucker, A. K.-Y. Jen, *J. Am. Chem. Soc.* **2006**, *128*, 13042.

10 (a) T. Kawase, H. Kurata, *Chem. Rev.* **2006**, *106*, 5250. (b) E. M. Pérez, N Martín, *Chem. Soc. Rev.* **2008**, *37*, 1512.

11 S. Mizyed, P. E. Georghiou, M. Bancu, B. Cuadra, A. K. Rai, P. Cheng, L. T. Scott, *J. Am. Chem. Soc.* **2001**, *123*, 12770.

12 M. Randic, *Chem. Rev.* **2003**, *103*, 3449.

13 (a) B. M. Trost, G. M. Brigth, *J. Am. Chem. Soc.* **1967**, *89*, 4244. (b) Trost, B. M.; Brigth, G. M.; Frihart, C.; Britteli, D. R. *J. Am. Chem. Soc.* **1971**, *93*, 737.

14 R. H. Mitchell, *Chem. Rev.* **2001**, *101*, 1301.

15 H. A. Wegner, H. Reisch, K. Rauch, A. Demeter, K. A. Zachariasse, A. de Meijere, L. T. Scott, *J. Org. Chem.* **2006**, *71*, 9080.

16 C. Koper, M. Sarobe, L. W. Jenneskens, *Phys. Chem. Chem. Phys*. **2004**, *6*, 319.

17 *Science of Fullerenes and Carbon Nanotubes* (Eds.: M. S. Dresselhaus, G. Dresselhaus, P. C. Eklund), Academic Press, London, **1995**, Ch. 10.

18 (a) *The Porphyrin Handbook, Vol. 1–10* (Eds.: K. M. Kadish, K. M. Smith, R. Guilard), Academic Press, New York, **2000**. (b) *The Porphyrin Handbook*, *Vol. 11-20* (Eds.: K. M. Kadish, K. M. Smith, R. Guilard), Academic Press, San Diego, **2003**. (c) *The Porphyrins* (Eds.: D. Dolphin), Academic Press, New York, 1979.

19 D. Gust, T. A. Moore, A. L. Moore, *Acc. Chem. Res.* **2001**, *34*, 40.

20 M. Momenteau, C. A. Reed, *Chem. Rev.* **1994**, *94*, 659.

21 (a) M. R. Wasielewski, *Chem. Rev.* **1992**, *92*, 435. (b) I. Beletskaya, V. S. Tyurin, A. Y. Tsivadze, R. Guilard, C. Stern, *Chem. Rev.* **2009**, *109*, 1659.

22 H. Ogoshi, T. Mizutani, *Acc. Chem. Res.* **1998**, *31*, 81.

23 M. O. Senge, M. Fazekas, E. G. A. Notaras, W. J. Blau, M. Zawadzka, O. B. Locos, E. M. N. Mhuircheartaigh, *Adv. Mater.* **2007**, *19*, 2737.

24 (a) X. Huang, K. Nakanishi, N. Berova, *Chirality* **2000**, *12*, 237. (b) K. M. Kadish, M. M. Morison, *J. Am. Chem. Soc.* **1976**, *98*, 3326.

25 (a) A. Giraudeau, H. J. Callot, M. Gross, *Inorg. Chem.* **1979**, *18*, 201. (b) K. M. Kadish, M. M. Morrison, *J. Am. Chem. Soc.* **1976**, *98*, 3326. (c) A. Giraudeau, H. J. Callot J. Jordan, I. Ezhar, M. Gross, *J. Am. Chem. Soc.* **1979**, *101*, 3857.

26 (a) K. M. Kadish, M. M. Morrison, *Bioinorg. Chem.* **1977**, *7*, 107. (b) F. A. Walker, D. Beroiz, K. M. Kadish, *J. Am. Chem. Soc.* **1976**, *98*, 3484. (c) K. M. Kadish, M. M. Morrison, L. A. Constant, L. Dickens, D. G. Davis, *J. Am. Chem. Soc.* **1976**, *98*, 8387.

27 A. D. Adler, F. R. Longo, J. D. Finarelli, J. Goldmacher, J. Assour, L. Korsakoff, *J. Org. Chem.* **1967**, *32*, 476.

28 J. S. Lindsey, I. C. Schreiman, H. C. Hsu, P. C. Kearney, A. M. Marguerettaz, *J. Org. Chem.* **1987**, *52*, 827.

29 B. J. Littler, Y. Ciringh, J. S. Lindsey, *J. Org. Chem.* **1999**, *64*, 2864.

30 M. Gouterman, *J. Chem. Phys.* **1959**, *30*, 1139.

31 (a) S. J. Lalama, A. F. Garito, *Phys. Rev. A* **1979**, *20*, 1179. (b) J. L. Oudar, D. S. Chemia, *J. Chem. Phys.* **1977**, *66*, 2664. (c) X. Hu, D. Xiao, S. Keiman, I. Asselberghs, M. J. Therien, K. Clays, W. Yang, D. N. Beratan, *J. Phys. Chem. C* **2010**, *114*, 2349.

32 K. S. Suslick, C.-T. Chen, G. R. Meredith, L.-T. Cheng, *J. Am . Chem. Soc.* **1992**, *114*, 6928.

33 (a) K. Ichimori, H. Ohya-Nishiguchi, N. Hirota, *Bull. Chem. Soc. Jpn.* **1988**, *61*, 2753. (b) R. H. Felton, H. Linschitz, *J. Am. Chem. Soc.* **1966**, *88*, 1113. (c) G. L. Closs, L. E. Closs, *J. Am. Chem. Soc.* **1963**, *85*, 818. (d) J. Seth, D. F. Bocian, *J. Am. Chem. Soc.* **1994**, *116*, 143. (e) J. Pawlik, G. Lileta, S. Karabunarliev, M. Baugmgarten, *Chem. Phys.* **1997**, *221*, 121.

34 (a) P. Hambright, *Coord. Chem. Rev.* **1971**, *6*, 247. (b) S. Aronoff, *J. Phys. Chem.* **1958**, *62*, 428. (c) A. Stone, E. B. Fleischer, *J. Am. Chem. Soc.* **1968**, *90*, 2735. (d) R. Karaman, T. C. Bruice, *Inorg. Chem.* **1992**, *31*, 2455. (e) T. P. C. Sutter, P. Hambright, *Inorg. Chem.* **1992**, *31*, 5089.

35 (a) R. Harada, T. Kojima, *Chem. Commun.* **2005**, 716. (b) T. Kojima, T. Nakanishi, R. Harada, K. Ohkubo, S. Yamauchi, S. Fukuzumi, *Chem. Eur. J.* **2007**, *13*, 8714.

36 (a) T. Kumagai, F. Hanke, S. Gawinkowski, J. Sharp, K. Kotsis, J. Waluk, M. Persson, L. Grill, *Phys. Rev. Lett.* **2013**, *111*, 246101. (b) T. Kumagai, F. Hanke, S. Gawinkowski, J. Sharp, K. Kotsis, J. Waluk, M. Persson, L. Grill, *Nat. Chem.* **2014**, *6*, 41. (c) J. N. Ladenthin, T. Frederiksen, M. Persson, J. C. Sharp, S. Gawinkowski, J. Waluk, T.

Kumagai, *Nat. Chem.* **2016**, *8*, 935.

37 R. J. P. Williams, *Chem. Rev.* **1956**, *56*, 299.

38 (a) B. Meunier, *Chem. Rev.* **1992**, *92*, 1411. (b) J. P. Collman, X. Zhang, V. J. Lee, E. S. Uffelman, J. I. Brauman, *Science* **1993**, *261*, 1404. (c) P. Besse, H. Veschambre, *Tetrahedron* **1994**, *50*, 8885. (d) L. A. Campbell, T. Kodadek, *J. Mol. Catal. A: Chem.* **1996**, *113*, 293. (e) D. Mansuy, *Coord. Chem. Rev.* **1993**, *125*, 129; (f) M. C. Feiters, A. E. Rowan, R. J. M. Nolte, *Chem. Soc. Rev.* **2000**, *29*, 375. (g) E. Rose, B. Andrioletti, S. Zrig, M. Quelquejeu-Ethève, *Chem. Soc. Rev.* **2005**, *34*, 573. (h) G. Simonneaux, P. L. Maux, *Coord. Chem. Rev.* **2002**, *228*, 43.

39 (a) C. M. Drain, A. Varotto, I. Radivojevic, *Chem. Rev.* **2009**, *109*, 1630. (b) D. Canevet, E. M. Pérez, N. Martín, *Angew. Chem. Int. Ed.* **2011**, *50*, 9248. (c) P. D. W. Boyd, C. A. Reed, *Acc. Chem. Res.* **2005**, *38*, 235. (d) K. Tashiro, T. Aida, *Chem. Soc. Rev.* **2007**, *36*, 189.

40 (a) R. D. Jonson, D. S. Bethune, C. S. Yannoni, *Acc. Chem. Res.* **1992**, *25*, 169. (b) A. V. Nicolaev, T. J. S. Dennis, K. Prassides, A. K. Soper, *Chem. Phys. Lett.* **1994**, *223*, 143.

41 X. Fang, Y.-Z. Zhu, J.-Y. Zheng, *J. Org. Chem.* **2014**, *79*, 1184.

42 (a) K. Tashiro, T. Aida, J.-Y. Zheng, K. Kinbara, K. Saigo, S. Sakamoto, K. Yamaguchi, *J. Am. Chem. Soc.* **1999**, *121*, 9477. (b) J.-Y. Zheng, K. Tashiro, Y. Hirabayashi, K. Kinbara, K. Saigo, T. Aida, S. Sakamoto, K. Yamaguchi, *Angew. Chem. Int. Ed*. **2001**, *40*, 1857. (c) Y. Shoji, K. Tashiro, T. Aida, *J. Am. Chem. Soc.* **2004**, *126*, 6570. (d) M. Yanagisawa, K. Tashiro, M. Yamasaki, T. Aida, *J. Am. Chem. Soc.* **2007**, *129*, 11912. (e) F. Hajjaj, K. Tashiro, H. Nikawa, N. Mizorogi, T. Akasaka, S. Nagase, K. Furukawa, T. Kato, T. Aida, *J. Am. Chem. Soc.* **2011**, *133*, 9290.

43 (a) P. D. W. Boyd, M. C. Hodgson, C. E. F. Rickard, A. G. Oliver, L. Chaker, P. J. Brothers, R. D. Bolskar, F. S. Tham, C. A. Reed, *J. Am. Chem. Soc.* **1999**, *121*, 10487. (b) D. Sun, F. S. Tham, C. A. Reed, L. Chaker, P. D. W. Boyd, *J. Am. Chem. Soc.* **2002**, *124*, 6604. (c) A. Hosseini, S. Taylor, G. Accorsi, N. Armaroli, C. A. Reed, P. D. W. Boyd, *J. Am. Chem. Soc.* **2006**, *128*, 15903.

44 (a) H. Nobukuni, Y. Shimazaki, H. Uno, Y. Naruta, K. Ohkubo, T. Kojima, S. Fukuzumi, S. Seki, H. Sakai, T. Hasobe, F. Tani, *Chem. Eur. J.* **2010**, *16*, 11611. (b) B. Grimm, J. Schornbaum, C. M. Cardona, J. D. van Paauwe, P. D. W. Boyd, D. M. Guldi, *Chem. Sci.* **2011**, *2*, 1530. (c) T. Kamimura, K. Ohkubo, Y. Kawashima, H. Nobukuni, Y. Naruta, F. Tani, S. Fukuzumi, *Chem. Sci.* **2013**, *4*, 1451.

45 (a) S. Fox, R. W. Boyle, *Tetrahedron* **2006**, *62*, 10039. (b) J. P. Lewtak, D. T. Gryko, *Chem. Commun.* **2012**, *48*, 10069. (c) H. Mori, T. Tanaka, A. Osuka, *J. Mater. Chem. C* **2013**, *1*, 2500. (d) M. Stępień, E. Gońka, M. Żyła, N. Sprutta, *Chem. Rev.* **2017**, ASAP (DOI: 10.1021/acs.chemrev. 6b00076).

46 (a) N. K. S. Davis, M. Pawlicki, H. L. Anderson, *Org. Lett.*, **2008**, *10*, 3945. (b) N. K. S. Davis, A. L. Thompson, H. L. Anderson, *Org. Lett.* **2010**, *12*, 2124. (c) N. K. S. Davis, A. L. Thompson, H. L. Anderson, *J. Am. Chem. Soc.* **2011**, *133*, 30.

47 K. Kurotobi, K. S. Kim, S. B. Noh, D. Kim, A. Osuka, *Angew. Chem. Int. Ed.* **2006**, *45*, 3944.

48 D. Myśliwiec, B. Donnio, P. J. Chmielewski, B. Heinrich, M. Stępień**,** *J. Am. Chem. Soc.* **2012**, *134*, 4822.

49 (a) L. Edwards, M. Gouterman, C. B. Rose, *J. Am. Chem. Soc.* **1976**, *98*, 7638. (b) R. B. Koehorst, J. F. Kleibeuker, T. J. Schaafsma, D. A. de Bie, B. Geurtsen, R. N. Henrie, H. C. van der Plas, *J. Chem. Soc., Perkin Trans. 2* **1981**, 1005.

50 T. D. Lash, B. H. Novak, *Angew. Chem. Int. Ed. Engl.* **1995**, *34*, 683.

51 (a) S. Ito, T. Murashima, N. Ono, H. Uno, *Chem. Commun.* **1998**, 1661. (b) H. Yamada, T. Okujima, N. Uno, *Chem. Commun.* **2008**, 2957.

52 Y. Matsuo, Y. Sato, T. Niinomi, I. Soga, H. Tanaka, E. Nakamura, *J. Am. Chem. Soc.* **2009**, *131*, 16048.

53 (a) H. Yamada, T. Okujima, N. Ono, *Org. Lett.* **2008**, *10*, 2947. (b) S. Ito, N. Ochiai, H. Uno, T. Murashima, N. Ono. *Chem. Commun*. **2000**, 893. (c) R. Deshpande, L. Jiang, G. Schmidt, J. Rakovan, X. Wang, K. Wheelre, H. Wang, *Org. Lett.* **2009**, *11*, 4251. (d) L. Jiang, J. T. Engle, L. Sirk, C. S. Hartley, C. J. Ziegler, H. Wang, *Org. Lett.* **2011**, *13*, 3020.

54 (a) H. Aihara, L. Jaquinod, D. J. Nurco, K. M. Smith, *Angew. Chem. Int. Ed.* **2001**, *40*, 3439. (b) J. D. Spence, E. D. Cline, D. M. LLagostera, P. S. O'Toole, *Chem. Commun.* **2004**, 180.

55 S. Banala, T. Rühl, K. Wurst, B. Kraütler, *Angew. Chem. Int. Ed.* **2009**, *48*, 599.

56 S. Richiter, C. Jeandon, N. Kyrisakas, R. Ruppert, H. J. Callot, *J. Org. Chem.* **2003**, *68*, 9200.

57 Y. Mitsushige, S. Yamaguchi, B. S. Lee, Y. M. Sung, S. Kuhri, C. A. Schierl, D. M. Guldi, D. Kim, Y. Matsuo, *J. Am. Chem. Soc.* **2012**, *134*, 16540.

58 P. van Ragué Schleyer, C. Maerker, A. Dransfeld, H. Jiao, N. J. R. van Eikema Hommes, *J. Am. Chem. Soc.* **1996**, *118*, 6317.

59 (a) H. Song, J. A. Cissell, T. P. Vaid, D. Holten, *J. Phys. Chem. B* **2007**, *111*, 2138. (b) S. Cho, Z. S. Yoon, K. S. Kim, M.-C.Yoon, D.-G. Cho, J. L. Sessler, D. Kim, *J. Phys. Chem. Lett.* **2010**, *1*, 895. (c) J. M. Lim, Z. S. Yoon, J.-Y. Shin, K. S. Kim, M.-C. Yoon, D. Kim, *Chem. Commun.* **2009**, 261.

60 (a) M. Akita, S. Hiroto, H. Shinokubo, *Angew. Chem. Int. Ed.* **2012**, *51*, 2894. (b) N. Aratani, A. Osuka, *Macromol. Rapid Commun.* **2001**, *22*, 725. (c) N. Aratani, A. Osuka, *Bull. Chem. Soc. Jpn.* **2001**, *74*, 1361. (d) N. Aratani, A. Tsuda, A. Osuka, *Synlett* **2001**, 1663. (e) D. Kim, A. Osuka, *Acc. Chem. Res.* **2004**, *37*, 735.

61 (a) A. Tsuda, A. Nakano, H. Furuta, H. Yamochi, A. Osuka, *Angew. Chem. Int. Ed.*, **2000**, *39*, 558. (b) A. Tsuda, H. Furuta, A. Osuka, *Angew. Chem. Int. Ed.*, **2000**, *39*, 2549. (c) A. Tsuda, H. Furuta, A. Osuka, *J. Am. Chem. Soc.* **2001**, *123*, 10304. (d) A. Tsuda, A. Osuka, *Science* **2001**, *293*, 79.

62 (a) T. Tanaka, Y. Nakamura, A. Osuka, *Chem. Eur. J.* **2008**, *14*, 204. (b) B. J. Brennan, M. J. Kenny, P. A. Liddell, B. R. Cherry, J. Li, A. L. Moore, T. A. Moore, D. Gust, *Chem. Commun.* **2011**, *47*, 10034.

63 (a) Y. Nakamura, S. Y. Jang, T. Tanaka, N. Aratani, J. M. Lim, K. S. Kim, D. Kim, A. Osuka, *Chem. Eur. J.* **2008**, *14*, 8279. (b) Y. Nakamura, N. Aratani, H. Shinokubo, A. Takagi, T. Kawai, T. Matsumoto, Z. S. Yoon, D. Y. Kim, T. K. Ahn, D. Kim, A. Muranaka, N. Kobayashi, A. Osuka, *J. Am. Chem. Soc.* **2006**, *128*, 4119. (c) G.

Sedghi, L. J. Esdaile, H. L. Anderson, S. Martin, D. Bethell, S. J. Higgins, R. J. Nichols, *Adv. Mater.* **2012**, *24*, 653.

64 (a) T. Ikeda, N. Aratani, A. Osuka, *Chem. Asian J.* **2009**, *4*, 1248. (b) T. Ikeda, J. M. Lintuluoto, N. Aratani, Z. S. Yoon, D. Kim, A. Osuka, *Eur. J. Org. Chem.* **2006**, 3193. (c) T. Ikeda, A. Tsuda, N. Aratani, A. Osuka, *Chem. Lett.* **2006**, *35*, 946.

65 (a) A. K. Sahoo, Y. Nakamura, N. Aratani, K. S. Kim, S. B. Noh, H. Shinokubo, D. Kim, A. Osuka, *Org. Lett.* **2006**, *8*, 4141. (b) V. V. Diev, K. Hanson, J. D. Zimmerman, S. R. Forrest, M. E. Thompson, *Angew. Chem. Int. Ed.* **2010**, *49*, 5523. (c) M.-C. Yoon, S. B. Noh, A. Tsuda, Y. Nakamura, A. Osuka, D. Kim, *J. Am. Chem. Soc.* **2007**, *129*, 10080. (d) A. Tsuda, Y. Nakamura, A. Osuka, *Chem. Commun.* **2003**, 1096. (e) K. Sugiura, T. Matsumoto, S. Ohkouchi, Y. Naitoh, T. Kawai, Y. Takai, K. Ushiroda, Y. Sakata, *Chem. Commun.* **1999**, 1957.

66 J. M. Ball, N. K. S. Davis, J. D. Wilkinson, J. Kirkpatrick, J. Teuscher, R. Gunning, H. L. Anderson, H. J. Snaith, *RSC Adv.* **2012**, *2*, 6846.

67 V. V. Diev, C. W. Schlenker, K. Hanson, Q. Zhong, J. D. Zimmerman, S. R. Forrest, M. E. Thompson, *J. Org. Chem.* **2012**, *77*, 143.

68 (a) S. Fox, R. W. Boyle, *Chem. Commun.* **2004**, 1322. (b) D.-M. Shen, C. Liu, Q.-Y. Chen, *J. Org. Chem.* **2006**, *71*, 6508.

69 S. Hayashi, Y. Matsubara, S. Eu, H. Hayashi, T. Umeyama, Y. Matano, H, Imahori, *Chem. Lett.* **2008**, *37*, 846.

70 (a) N. Fukui, W.-Y. Cha, S. Lee, S. Tokuji, D. Kim, H. Yorimitsu, A. Osuka, *Angew. Chem. Int. Ed.* **2013**, *52*, 9728. (b) C.-M. Feng, Y.-Z. Zhu, S.-C. Zhang, J.-Y. Zheng, *Org. Biomol. Chem.* **2015**, *13*, 2566.

Chapter 2

Synthesis and characterization of multiply-fused porphyrins

2-1. Introduction

π-Conjugated organic molecules exhibiting long-wavelength absorption and a high tendency to form intermolecular π-π stacking structures have attracted considerable attention due to their potential for application in organic semiconductors and organic photovoltaic cells.[1-3] Tetraphenylporphyrin (TPP),[4] a representative of synthetic porphyrins,[5] and its derivatives are promising candidates as functional dyes for the purpose mentioned above, because of the highly-extended π-conjugation, facileness of the synthesis and introduction of functional groups, and the robustness among the organic dyes.[4] TPP, however, cannot form strong intermolecular π-π stacking with the porphyrin core due to the steric repulsion of the *meso*-phenyl groups,[6] and thus, it cannot be directly used to construct π-π stacked one-dimensional molecular wires, which are very important to construct molecule-based optoelectronic materials.[7] On the other hand, modification of porphyrins by introduction of fused rings at the periphery of the porphyrin aromatic circuit has been intensively studied recently,[8-14] because of the merits of the unique physical properties derived from the narrowed HOMO-LUMO gaps. The ring-fusion strategy has been successfully applied to obtain a chromophore showing an absorption band over 1400 nm based on one porphyrin unit,[12] and by increasing the number of porphyrin units included in the fused π-systems, the longest absorption band can reach the infrared region below 3000 cm^{-1}.[13] In particular, *meso*-*β*-arene- fused derivatives[10-14] exhibit larger red-shifts of the optical absorption bands and smaller HOMO-LUMO gaps, compared to *β*-*β*-arene fused derivatives.[9] However, the ring-fusing reactions reported so far are highly limited and the synthetic procedures for the precursors are time-consuming. Herein, the author reports a facile and efficient procedure for the preparation of a quadruply ring-fused porphyrin (QFP, **4a**, in Figure 2-1), in which the four *meso*-phenyl groups are covalently bonded to the *β*-carbons of the pyrrole rings at the *ortho*-positions. In addition, the ring-fused porphyrins are highly planar with expanded π-conjugation and are expected to show strong π-π stacking tendency and physical properties based on the narrowed HOMO-LUMO gaps.

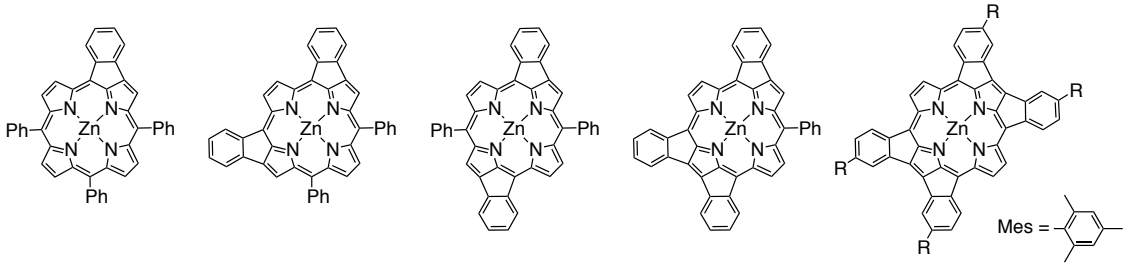

1 **2**-*cis* **2**-*trans* **3** **4a** (R = H) **4b** (R = Mes)

Figure 2-1. Molecular structures of fused porphyrins, **1** – **4**.

2-2. Synthesis of porphyrins having five-membered fused rings

The ring-fusion reactions of zinc(II) 2,3,12,13,-tetrabromo-5,10,15,20-tetraphenylporpyrinate (**5a**)[15] were conducted by direct C-H activation in the presence of a Pd catalyst.[16] The key factor of the reaction is the selection of the Pd catalyst. The usual molecular Pd catalysts, such as $Pd(PPh_3)_4$, did not afford the fully fused product **4a**, but the partially fused products, **1** and **2** (Table 2-1).[14c] In sharp contrast, when Pd-nanoclusters derived from $[Pd(\eta^3\text{-}C_3H_5)Cl]_2$ were employed as the catalyst (Scheme 1),[17] the quadruply fused **4a** was obtained in 79% yield, accompanying the triply fused **3** as a minor product in 11% yield. The isolation of **4a** was very easily performed on the basis of its low solubility in organic solvents; the reaction mixture was filtered to remove the Pd catalyst and other insoluble materials, and then the solvent of the filtrate was evaporated under vacuum. The residual solid was dissolved in THF and the remaining violet solid was filtered to give a red-brown filtrate. The solid obtained mainly

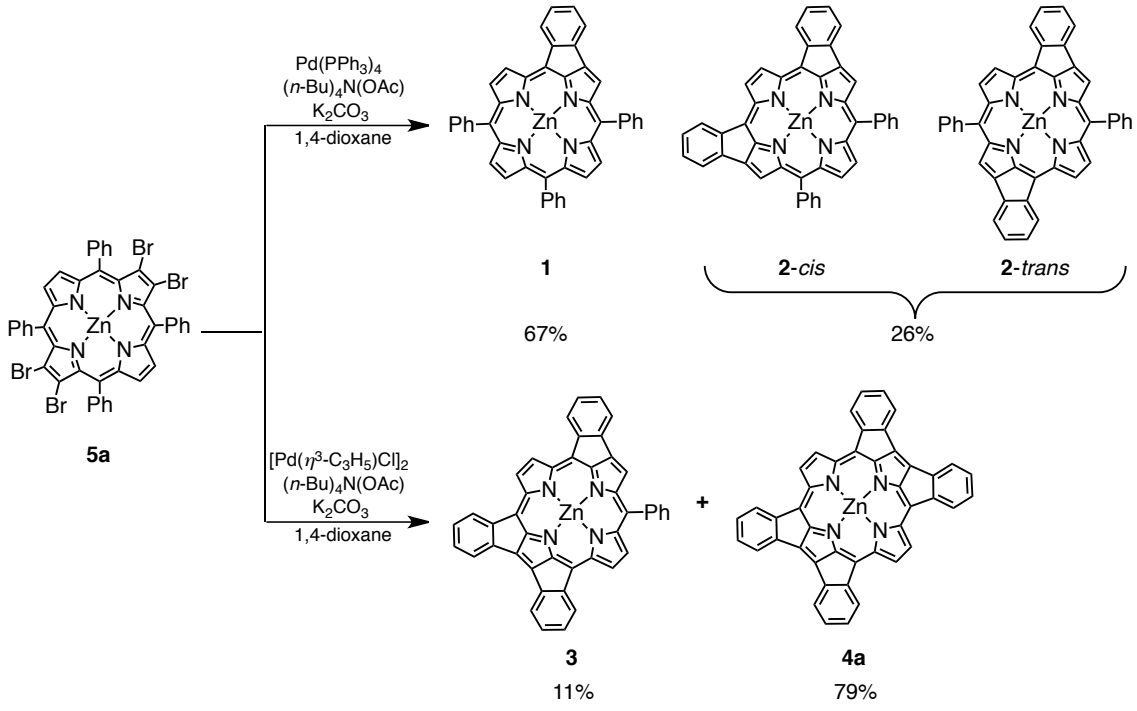

Scheme 2-1. Synthesis of a series of ring-fused porphyrin derivatives.

included **4a** and the recrystallization from THF-EtOH in the presence of one drop of pyridine to increase the solubility gave **4a** with a pyridine molecule as an axial ligand (**4a**-py) in the pure form. In addition, the major component of the red-brown filtrate in THF was the triply fused **3** and further purification using preparative-scale thin-layer chromatography on silica gel, followed by recrystallization from THF-hexane, gave violet crystals of **3**. The singly-fused **1** and doubly-fused **2** were also obtained from the reactions under different conditions using Pd-nanoclusters derived from $Pd(OAc)_2$ as catalysts (entry 2 in Table 2-1). The doubly-fused porphyrin contains three

isomers, 7,22;18,40-fused, **2**-*cis*, 7,22;17,34-fused, **2**-*trans*, as well as 7,22;8,28-fused, **2'** (Figure 2-2). **2**-*cis* and **2**-*trans* were the major products and could be easily isolated by column chromatography.

Table 2-1. Product yields of the ring-fused reactions dependent on the conditions.

	Yield of products (%)				
Catalyst	ZnTPP	**1**	**2**	**3**	**4a**
Pd-clusters from $[Pd^{II}(\eta^3\text{-}C_3H_5)Cl]_2$	0	0	trace	11	79
Pd-clusters from $Pd^{II}(OAc)_2$	10	25	40	15	trace
$Pd^0(PPh_3)_4$	12	67	26	trace	0

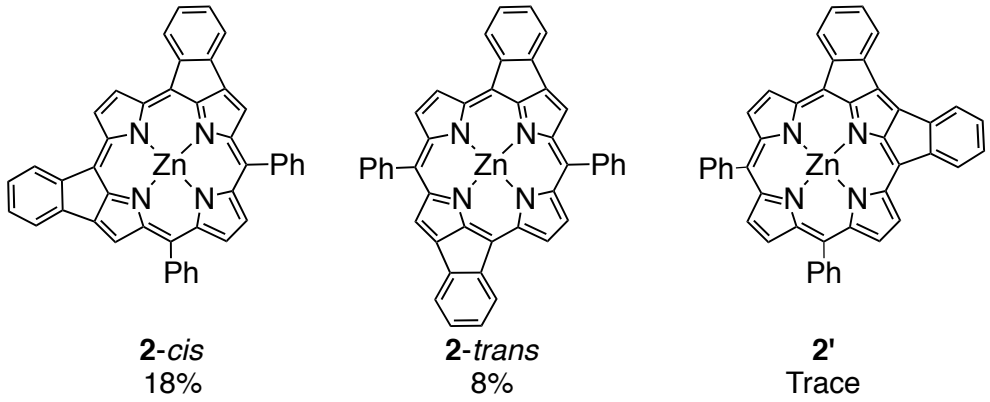

Figure 2-2. Structures of three isomers of the doubly-fused porphyrin.

2-3. Structural characterization of ring-fused porphyrins

Characterization of the ring-fused porphyrins was performed using ^{1}H NMR spectroscopy, MALDI-TOF-MS spectrometry, elemental analysis and X-ray crystallography (See below). The ^{1}H NMR spectrum of **4a** in DMSO-d_6 displayed a simple signal pattern reflecting the four-fold symmetric structure, and eight ^{1}H NMR signals including three signals assigned to a free pyridine molecule[18] were observed (Figure 2-3). Each signal of **4a** was assigned on the basis of the ^{1}H-^{1}H COSY spectrum (Figure 2-4). The ^{1}H NMR spectrum of **3** showed a relatively complicated pattern due to the low-symmetric structure (Figure 2-3b).

Recrystallization of **1** – **4a** gave single crystals appropriate for X-ray diffraction analysis.[19] The ORTEP drawings of **1**-THF, **2**-*cis*, **3**, and **4a**-py are shown in Figure 2-5. Compounds **1** and **4a** had a THF and a pyridine (py) molecules, respectively, derived from the recrystallization solvents as axial ligands on the central Zn^{II} ions, whereas **2**-*cis* and **3** did not have any axial ligand. As one of the characteristics of the ring-fused porphyrins in the crystal structures, the bond lengths between the central Zn^{II} ion and the nitrogen atoms of the pyrrole rings involved in the ring-fused structures were much shortened than those for the Zn^{II} and the nitrogen atoms of non-fused pyrrole rings

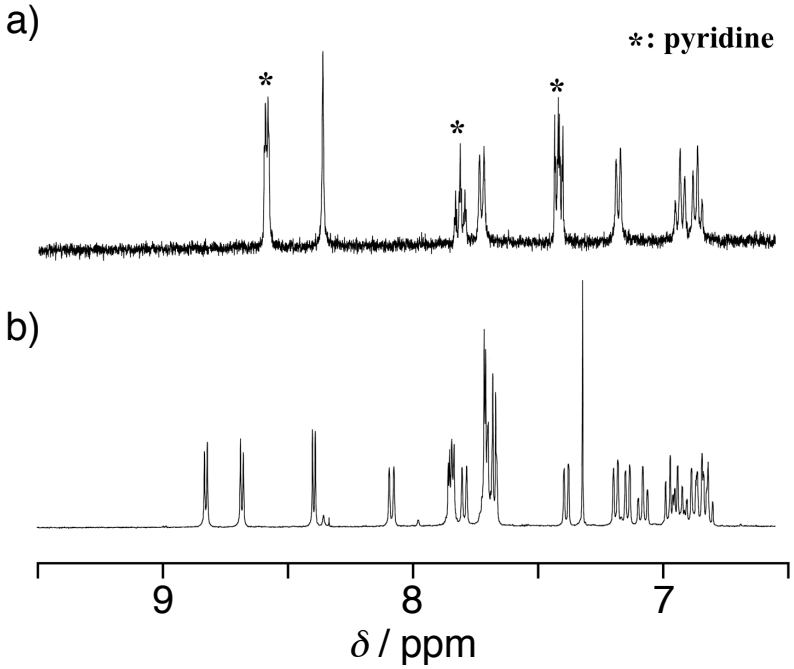

Figure 2-3. ^{1}H NMR spectra of **4a** (a) and **3** (b) in DMSO-d_6.

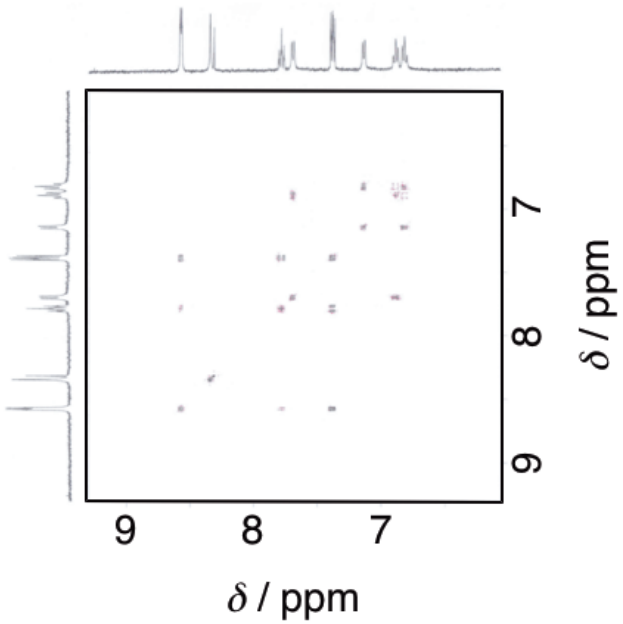

Figure 2-4. ^{1}H-^{1}H COSY spectrum of **4a** in DMSO-d_6. The sample solution of **4a** included 1 equiv of pyridine for improving the solubility.

(Table 2-2); for instance, in **4a**-py, the bond distances of Zn-N2 and Zn-N4 were found to be 1.894(2) Å and 1.900(2) Å, respectively, involving the fused-ring nitrogen atoms, whereas those of Zn-N1 and Zn-N3 were 2.196(5) Å and 2.126(5) Å, respectively, involving the non-fused pyrrole nitrogen atoms. On the other hand, the Zn-N bond lengths in ZnTPP were almost identical.[6] The difference in the Zn-N bond lengths observed for the fused and

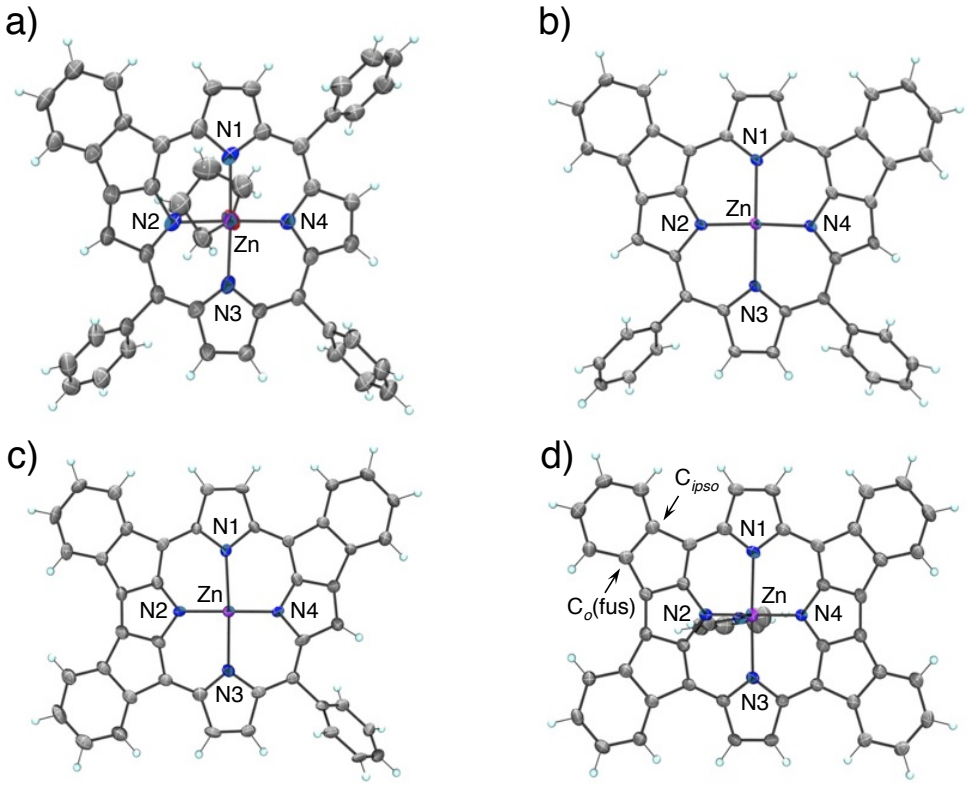

Figure 2-5. ORTEP drawings of crystal structures of **1**-THF (a), **2**-*cis* (b), **3** (c), and **4a**-py (d). The thermal ellipsoids are drawn with 50% probability.

non-fused pyrroles is probably caused by the rigidity of the fused ring structure, which results in shrinkage of the N2···N4 distance and elongation of the N1···N3 distance. The rhombic deformation of the porphyrin core by the ring fusion is confirmed by the density-functional-theory (DFT)-optimized structure of the free-base porphyrin of **4a** (Figure 2-6), where the N1···N3 distance is 4.59 Å and the N2···N4 distance is 3.43 Å. Another feature found in the crystal structures of the fused porphyrins was the long bond lengths between the *ipso*-carbon (C_{ipso}) of the fused phenyl groups and the *ortho*-carbon ($C_{o(fus)}$) of the same phenyl group in the ring-fused moieties (see Figure 2-5). The C-C bond lengths of non-fused phenyl groups and the C-C bond lengths except the C_{ipso}-$C_{o(fus)}$ bond in the fused phenyl rings were almost equal to *ca.* 1.39 Å, whereas the C_{ipso}-$C_{o(fus)}$ bond lengths were *ca.* 1.44 Å in common to all the crystal structures of the fused porphyrins. The elongation of the C_{ipso}-$C_{o(fus)}$ bond by *ca.* 0.05 Å indicates that a single bond is localized between C_{ipso} and $C_{o(fus)}$, and thus the π-conjugation circuit always avoids the C_{ipso}-$C_{o(fus)}$ bond and the isolated aromaticity of the *meso*-phenyl groups is almost lost. Therefore, larger aromatic circuits soaking into the fused phenyl rings in the fused porphyrins are recognized in the crystal structures. The fused porphyrins obviously showed intermolecular π-π stacking in the crystal packing and the π-π stacking distances gradually shortened as the number of the fused rings increased. The THF-ligated **1** formed π-π stacked dimers, in which the interplanar distance of the two

Table 2-2. Selected bond lengths (Å) and angles (°) in the crystal structures of the fused porphyrins and ZnTPP

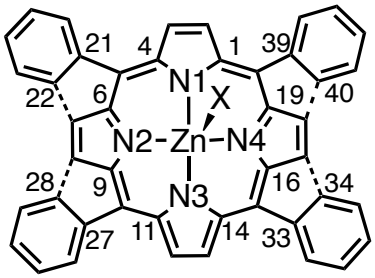

	1-THF	**2**-*cis*-THF[a]	**2**-*cis*	**3**	**4a**-py	ZnTPP[b]
Zn-N1	2.113(5)	2.1543(13)	2.1372(16)	2.196(5)	2.277(2)	2.037(5)
Zn-N2	2.003(5)	1.9652(14)	1.9619(16)	1.881(5)	1.894(2)	2.027(4)
Zn-N3	2.078(5)	2.1044(13)	2.0768(15)	2.126(5)	2.268(2)	—
Zn-N4	1.993(4)	1.9567(13)	1.9503(16)	1.880(5)	1.900(2)	—
Zn-X	2.208(4) (O)	2.1930(13) (O)	—	—	2.079(3) (N)	—
C21-C22	1.433(9)	1.430(2)	1.427(3)	1.441(8)	1.437(4)	1.392(7)
C27-C28	1.386(8)	1.391(2)	1.401(3)	1.438(8)	1.430(4)	1.375(7)
C33-C34	1.366(8)	1.395(2)	1.388(3)	1.384(8)	1.443(4)	—
C39-C40	1.402(8)	1.431(2)	1.429(3)	1.430(8)	1.434(4)	—
∠C1-N1-C4	105.6(5)	106.54(13)	106.66(15)	107.0(5)	107.2(2)	106.6(4)
∠C6-N2-C9	106.0(5)	105.77(13)	105.25(15)	104.1(5)	104.5(2)	106.0(4)
∠C11-N3-C14	106.3(4)	107.11(13)	106.90(15)	108.1(5)	106.9(4)	—
∠C16-N4-C19	107.2(4)	105.85(13)	105.72(16)	105.5(5)	104.4(2)	—

[a] ref 14c. [b] ref 6.

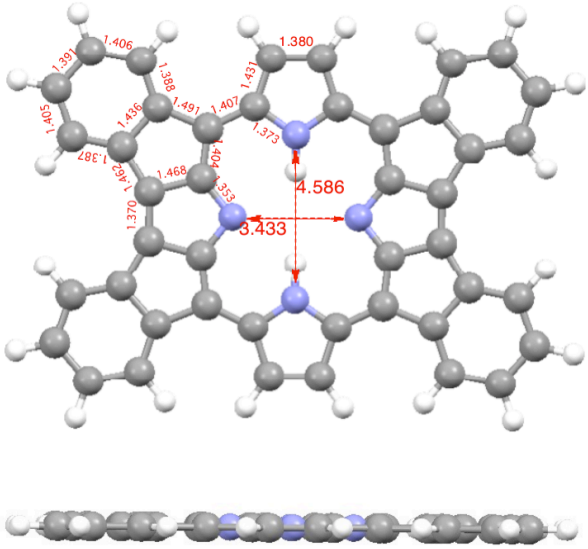

Figure 2-6. DFT-optimized structure of the freebase form of **4a**. The bond lengths and atom distances are in Å.

porphyrins was 3.46 Å (Figure 2-7). On the other hand, compounds **2**-*cis* and **3** having no axial ligands formedπ-stacked one-dimensional (1D) supramolecular arrays in the crystals (Figure 2-8 and 2-9). Both of the 1D arrays with **2**-*cis* and with **3** exhibit two interplanar distances of 3.43 and 3.58 Å for **2**-*cis*, and 3.28 and 3.36 Å for **3**, respectively. With respect to the π-π stacking distances of the three crystal structures, the order is **1**-THF (3.46 Å) > **2**-*cis* (3.43 Å) > **3** (3.28 Å). This order indicates that increasing the number of the fused rings enhances the planarity of the molecule and simultaneously increases the number of the π-electrons involved in the π-conjugation. Due to the axial pyridine ligand, **4a**-py showed a dome-type distortion of the fully fused porphyrin ligand in the crystal structure and the porphyrin core did not exhibit any intermolecular π-π stacking (Figure 2-10).

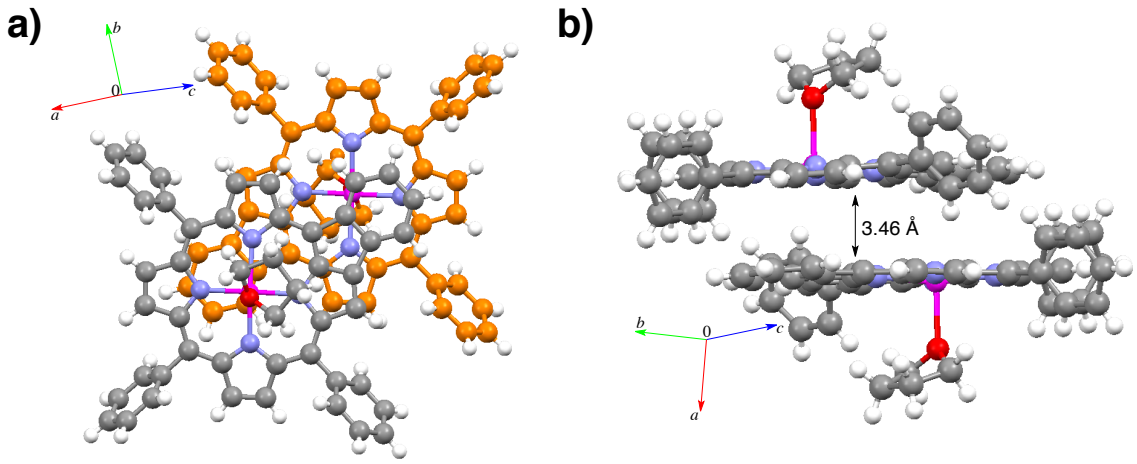

Figure 2-7. Description of the π-π stacking structure of **1**-THF. Top (a) and side (b) views. In the top view, the carbon atoms of the behind molecule are orange-colored.

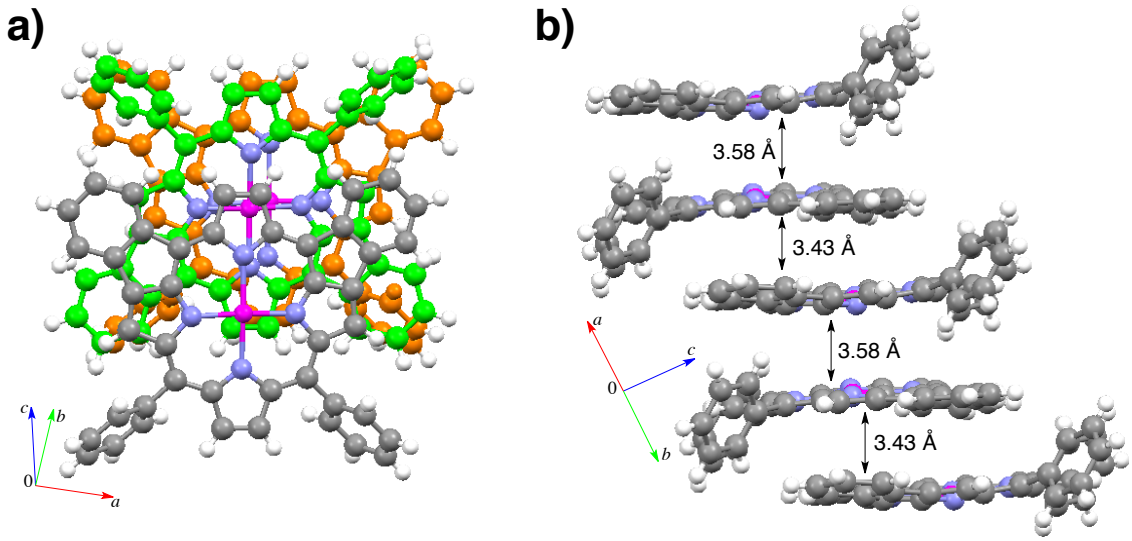

Figure 2-8. Description of the π-π stacking structure of **2**-*cis*. (a) Top and (b) side views. In the top view, the carbon atoms of the molecule in the second layer are green-colored and those of the molecule in the third layer are orange-colored.

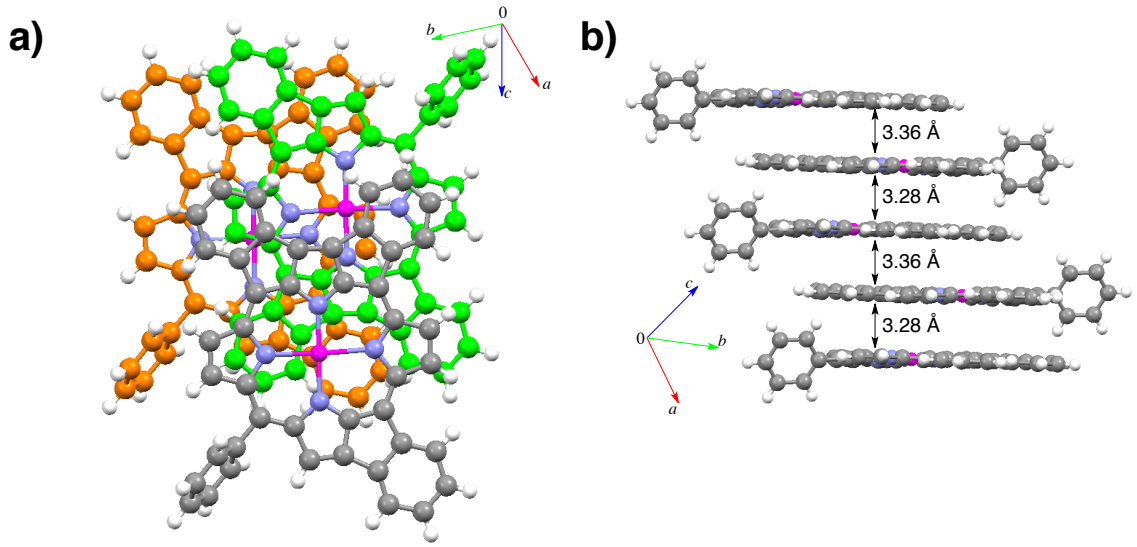

Figure 2-9. Description of the π-π stacking structure of **3**. Top (a) and side (b) views. In the top view, the carbon atoms of the molecule in the second layer are green-colored and those of the molecule in the third layer are orange-colored.

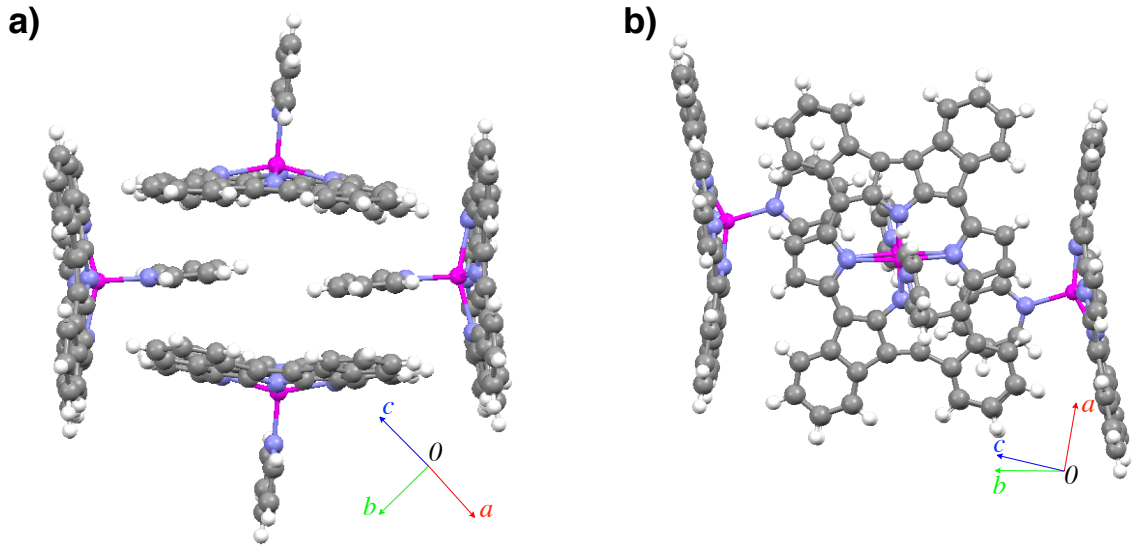

Figure 2-10. The packing diagram of **4a**-py from two directions.

2-4. The contribution of partially antiaromatic resonance forms to magnetic properties

In the ^{1}H NMR spectra of **1** – **4a** and ZnTPP in DMSO-d_6, increasing the number of fused rings causes the upfield shifts of the corresponding signals; for instance, the ^{1}H NMR signals of protons at the β-positions of non-fused pyrroles, adjacent to fused phenyl rings (blue circles in Figure 2-11), were observed at δ 9.31 ppm for **1**, 9.16 ppm for **2**-*cis*, 8.99 ppm for **2**-*trans*, 8.62 ppm for **3** (the mean value of those for the three corresponding signals), and 8.34 ppm for **4a**. This tendency seems contrary to the fact that the ring fusion makes the porphyrin molecules more planar and causes π-expansion to the fused phenyl groups to generate larger aromatic circuits. This can be explained by the

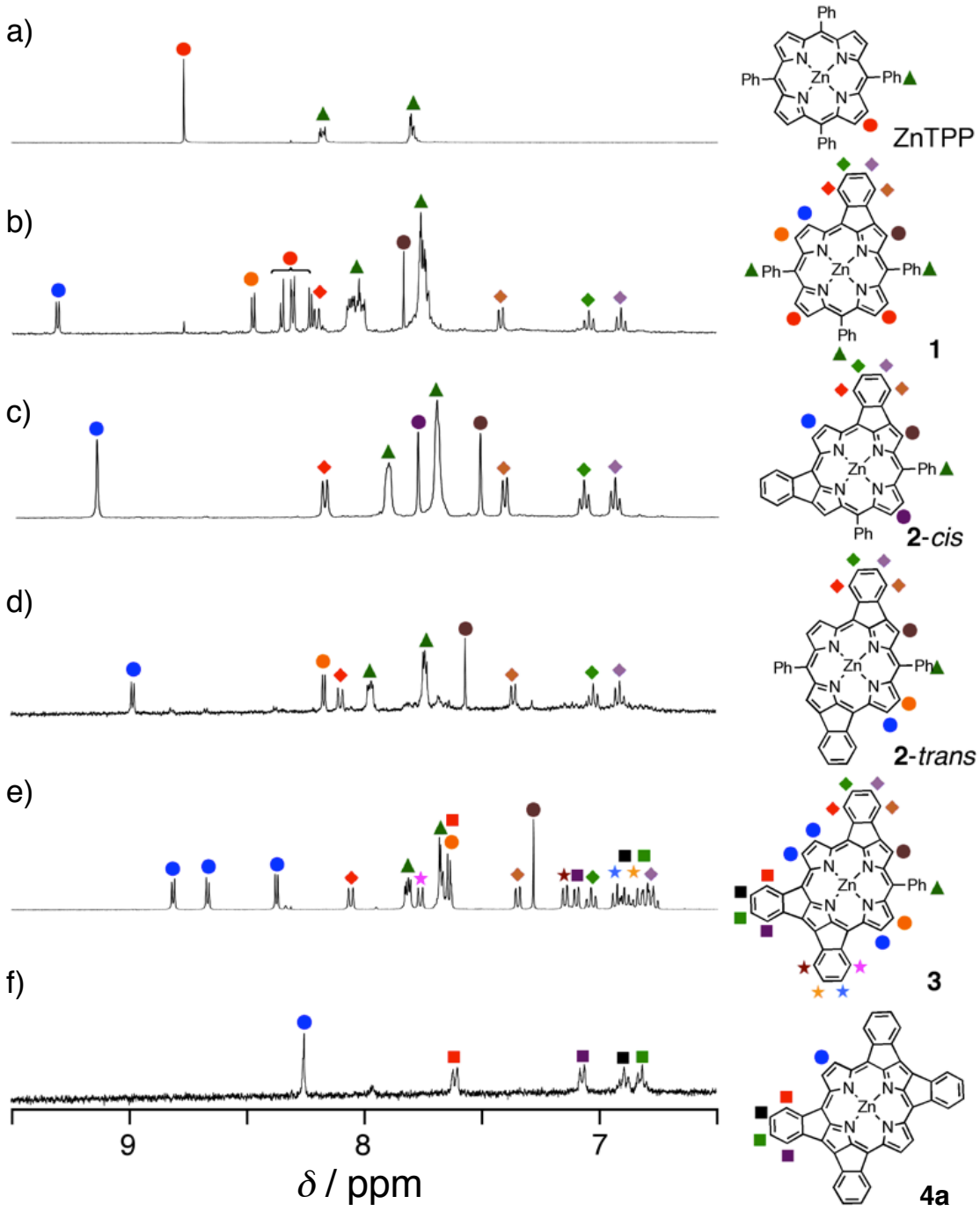

Figure 2-11. ^{1}H NMR spectra of the fused porphyrins in DMSO-d_6 at 298 K; (a) ZnTPP, (b) **1**, (c) **2**-*cis*, (d) **2**-*trans*, (e) **3**, and (f) **4a**.

contribution of resonance structures involving anti-aromatic circuits.[20-22] For instance, for quadruply fused **4a**, 30π (4), 26π (8), 22π (4) and 18π (2) aromatic circuits can be drawn (the numbers in parentheses indicate those of the circuit patterns having the number of π-electrons), whereas 24π (4) and 20π (4) anti-aromatic circuits can be expected simultaneously (Figure 2-12). In contrast to the aromatic and antiaromatic circuits expanding to the whole porphyrin molecule, more partial aromatic and anti-aromatic circuits such as 6π benzene rings (4), 8π azapentalene rings (4) and 12π benzoazapentalene rings (4) can also be drawn. The numbers of possible resonance structures for the other

ring-fused porphyrins are summarized in Table 2-3 (see also Figure 2-13 to 2-15). These various resonance structures contribute to the magnetic properties of the ring-fused porphyrins depending on the stabilization energy of each resonance structure. In particular, the number of anti-aromatic resonance structures increases with the increasing number of the fused rings. This contributes to the up-field shifts of the ^{1}H NMR signals upon increasing the number of the fusedrings. To elucidate the magnetic properties of the ring-fused porphyrins, DFT calculations have been performed on them to estimate nuclear-independent chemical shifts (NICS(1)[23]). The NICS(1) values were estimated at

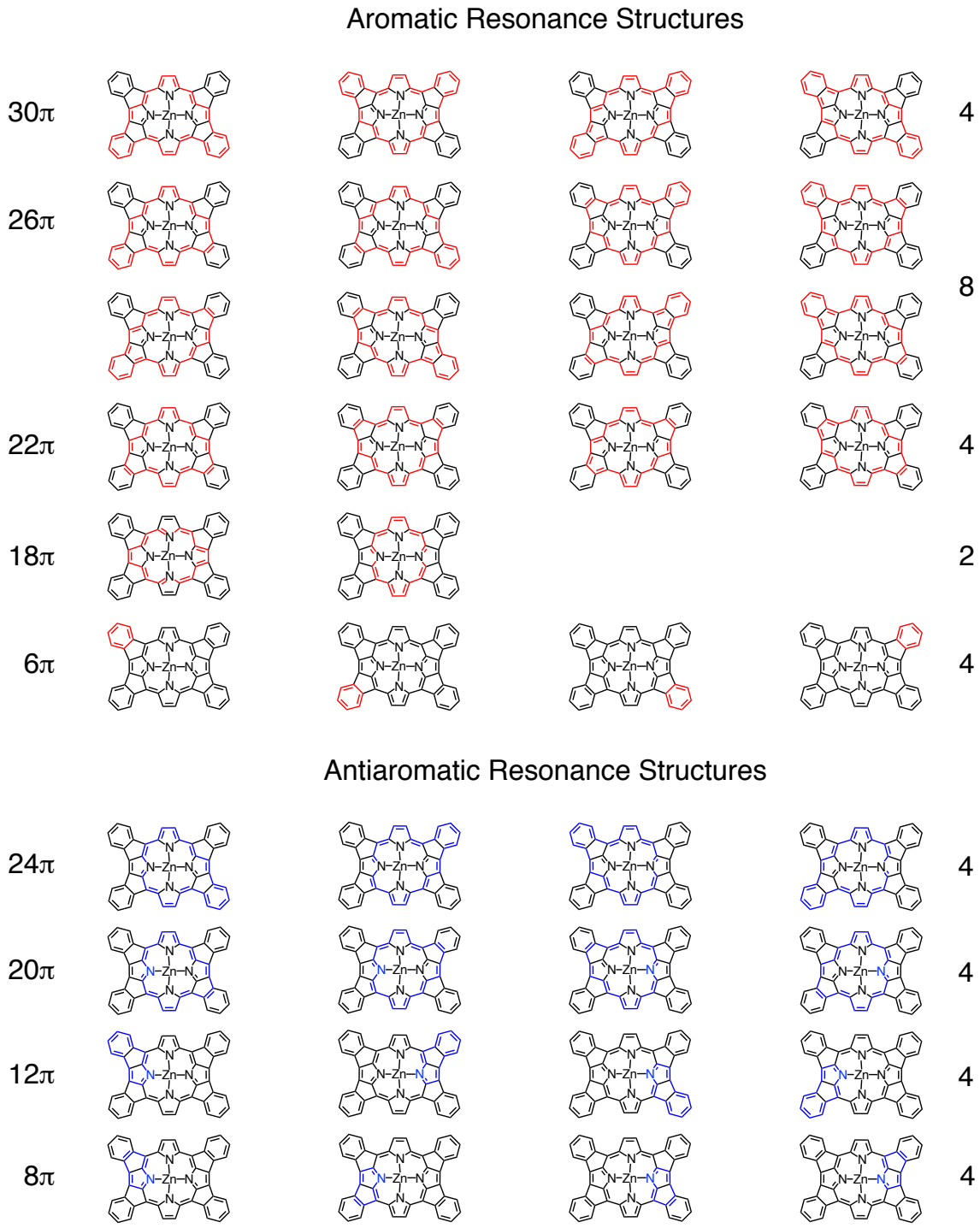

Figure 2-12. Possible resonance structures of **4a** having different aromatic circuits.

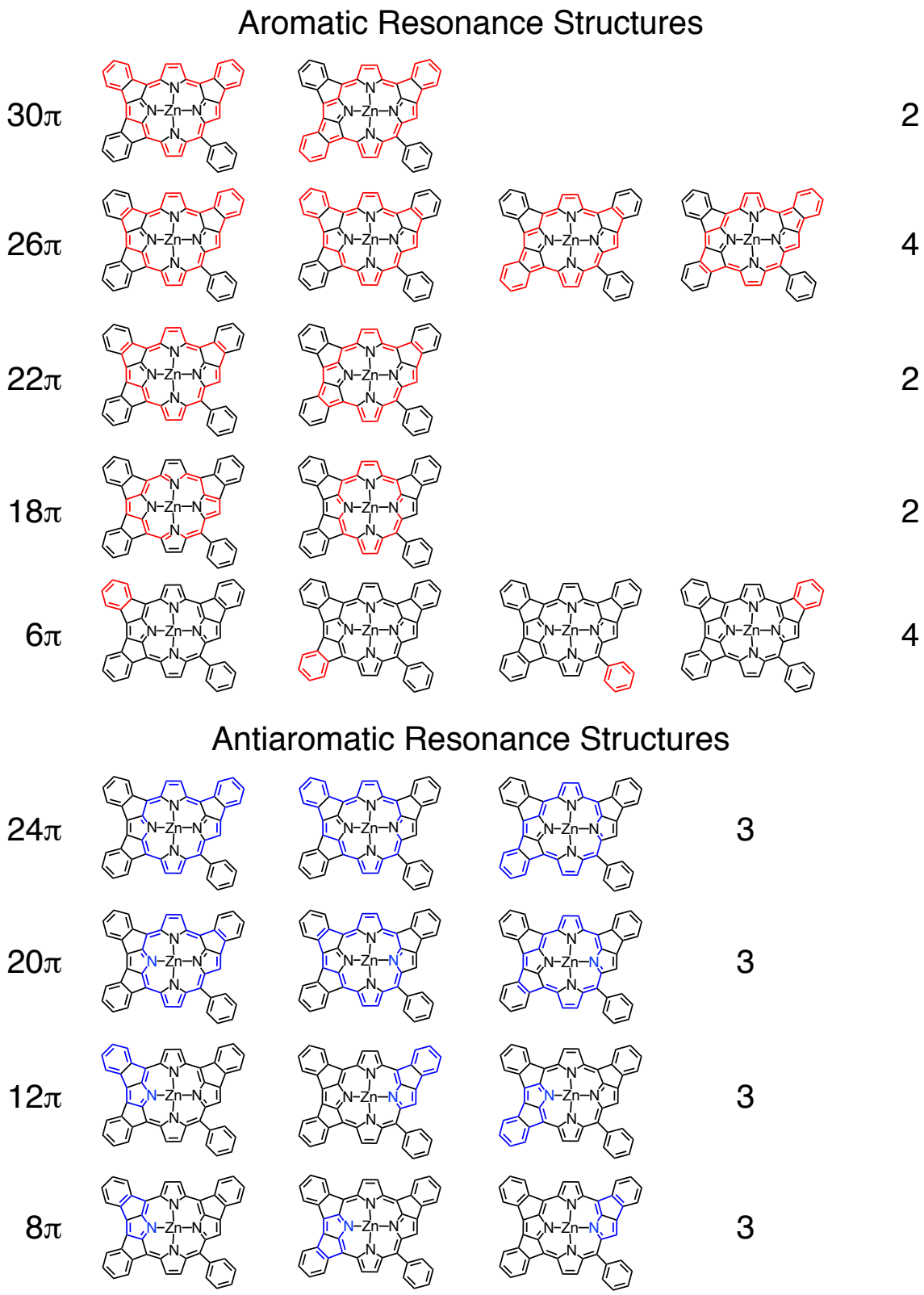

Figure 2-13. Possible resonance structures of **3** having different aromatic circuits.

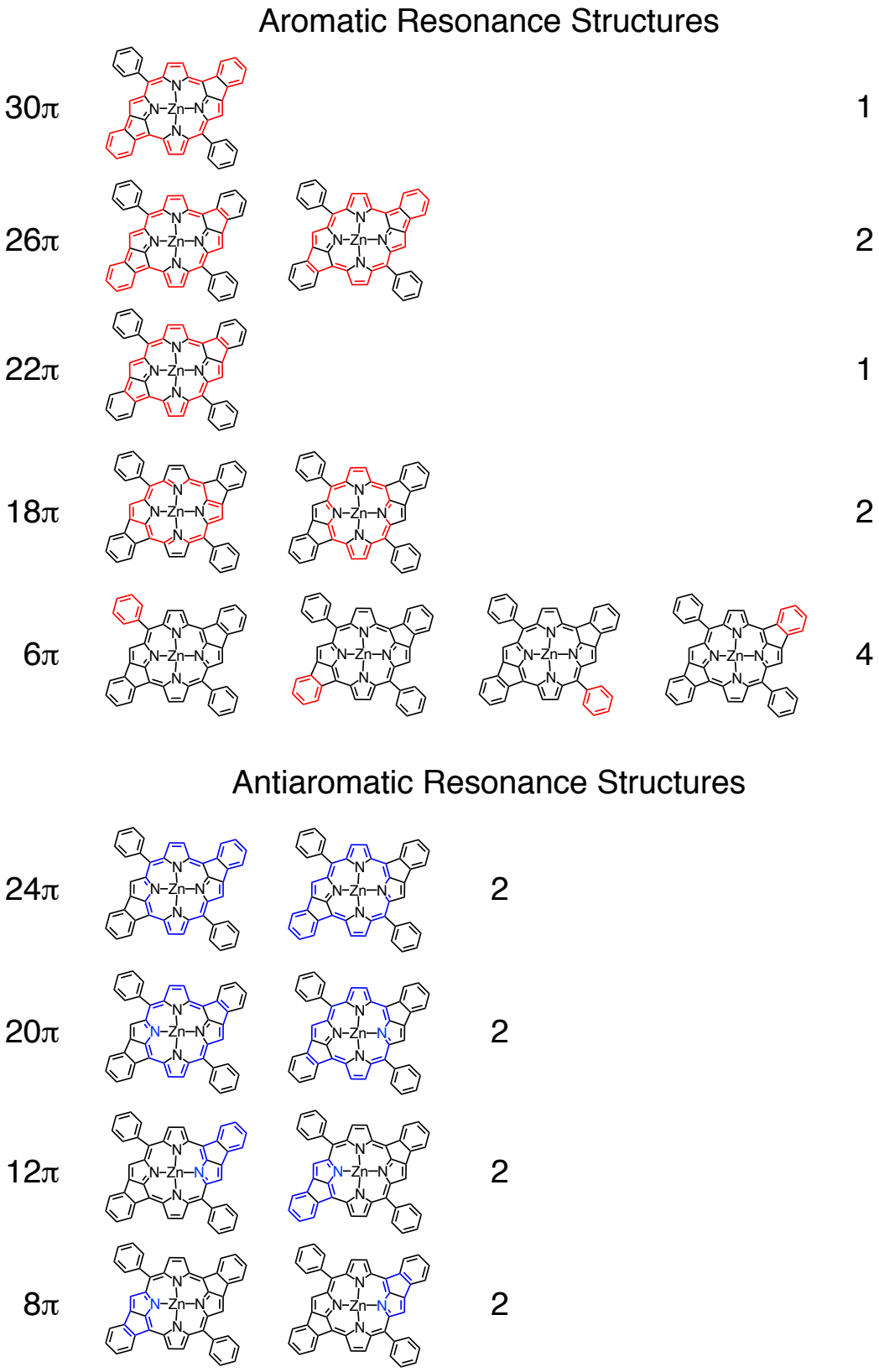

Figure 2-14. Possible resonance structures of **2**-*trans* having different aromatic circuits.

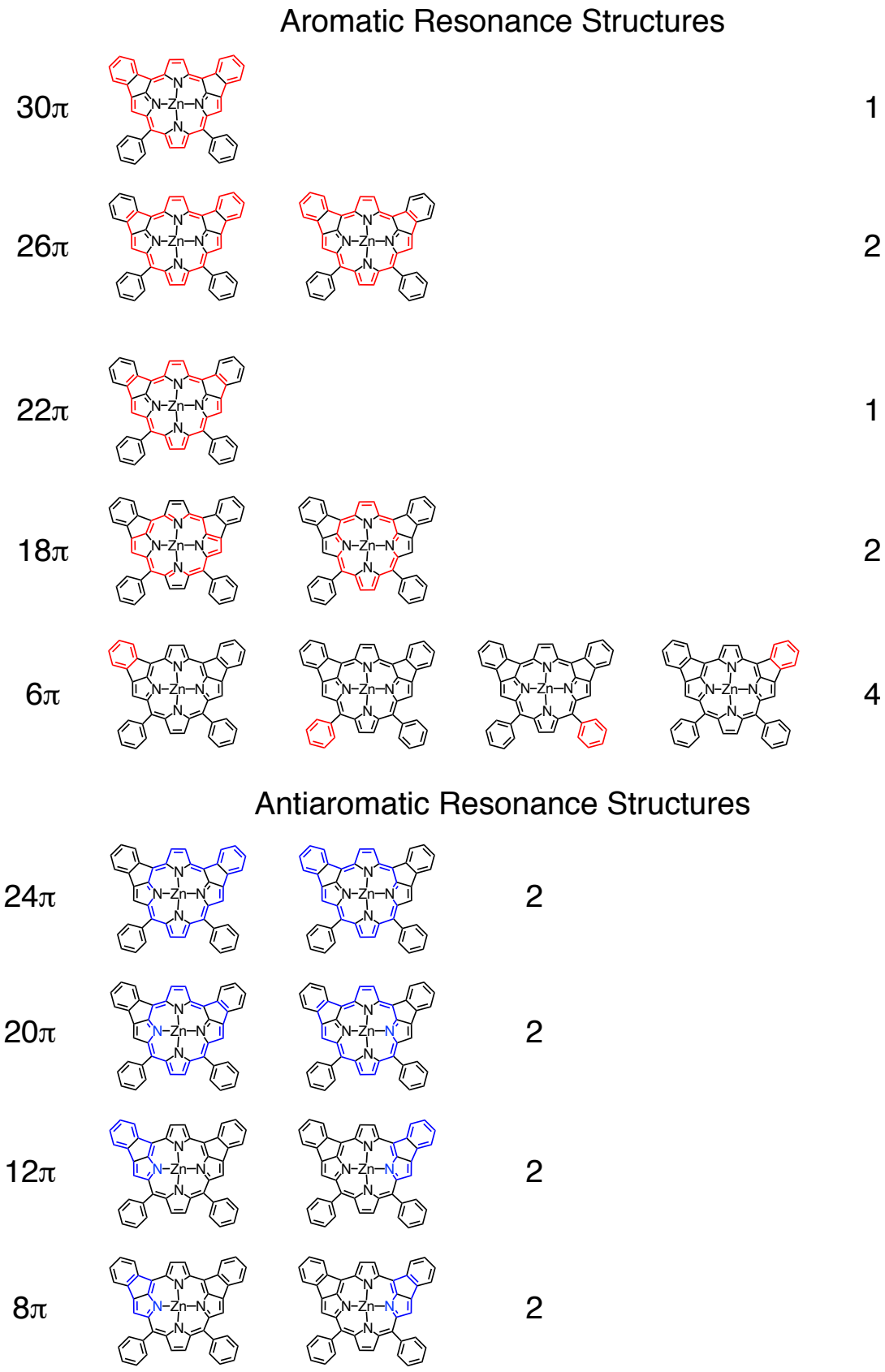

Figure 2-15. Possible resonance structures of **2**-*cis* having different aromatic circuits.

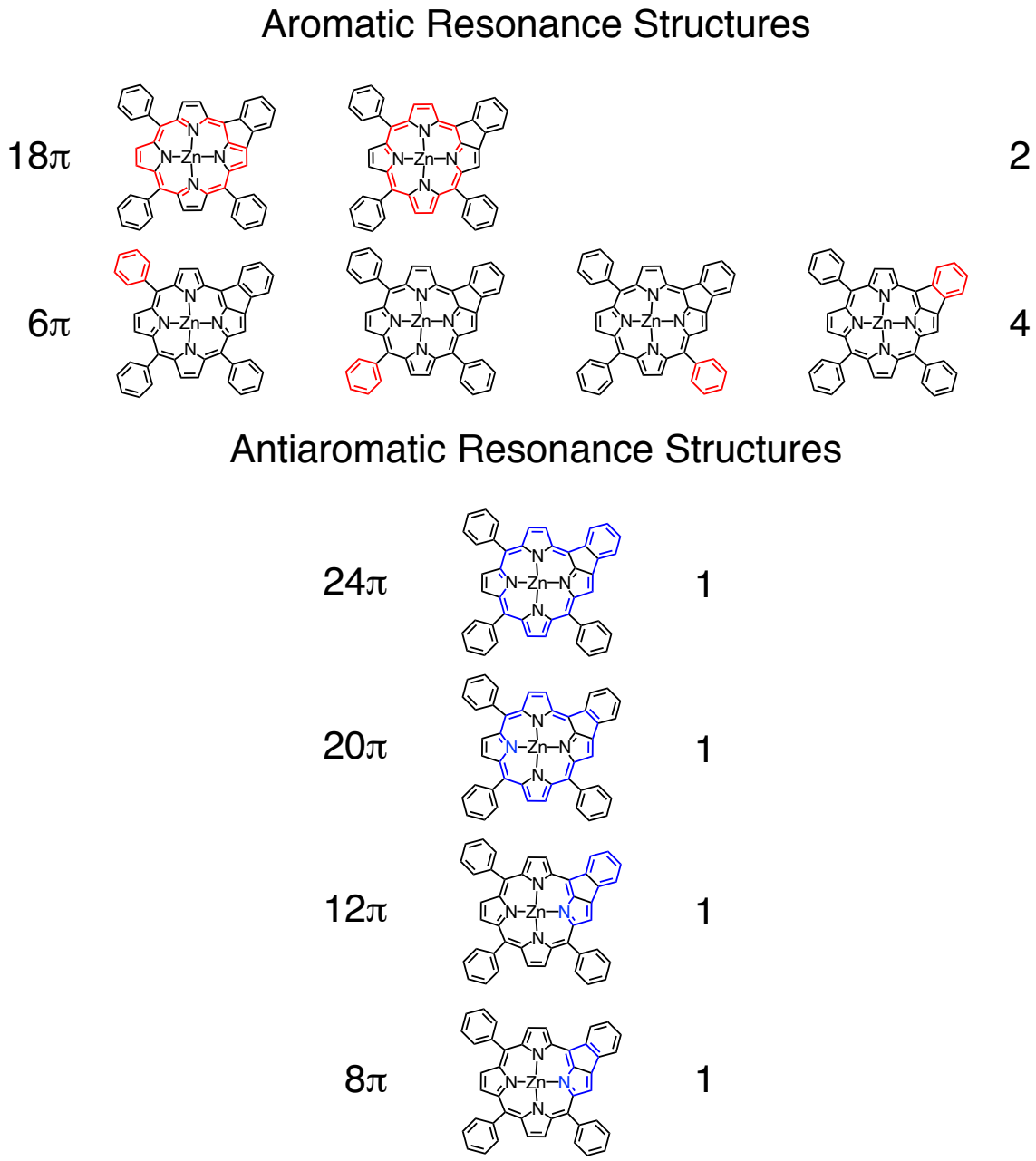

Figure 2-16. Possible resonance structures of **1** having different aromatic circuits.

various positions of the ring-fused porphyrins as summarized in Table 2-4. Negative NICS(1) values indicate diatropic (aromatic) current effects working at the positions and the positive values indicate paratropic (antiaromatic) current effects. The NICS(1) values for the centers of the six-membered chelate rings of the porphyrin core (position D) and for the centers of the non-fused pyrrole rings (position E) are largely negative, which is common for all the fused porphyrins, indicating the existence of strong aromatic currents in the porphyrin cores. Moreover, the NICS(1) values increased with increasing the number of fused rings. On the other hand, the five-membered rings formed by the ring-fusion exhibit largely positive values at the centers (position A). The positive values at position A can be accounted for by two factors; (1) the five-membered rings are positioned at the outside of the strong aromatic currents of the porphyrin cores, and (2) simultaneously, are involved in the antiaromatic circuits formed by the ring fusion. In

Table 2-3. Summary for the numbers of possible resonance structures having different aromatic and antiaromatic circuits for the fused porphyrin derivatives

Number of π-electrons	**1**	**2**-*cis*	**2**-*trans*	**3**	**4a**
		Aromatic and antiaromatic circuits with the whole porphyrin structure			
18π	2	2	2	2	2
20π	1	2	2	3	4
22π	—	1	1	2	4
24π	1	2	2	3	4
26π	—	2	2	4	8
30π	—	1	1	2	4
		Aromatic and antiaromatic circuits with the partial structure			
6π	4	4	4	4	4
8π	1	2	2	3	4
12π	1	2	2	3	4

Table 2-4. NICS(1) values of ZnTPP and the zinc(II) complexes of the fused porphyrins

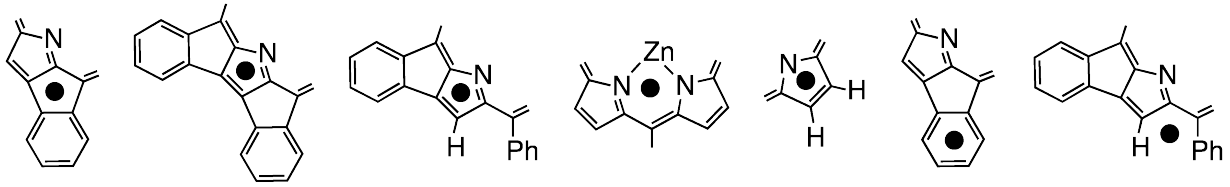

A B C D E F G

	A	B	C	D	E	F	G
ZnTPP	–	–	–	−15.00	−8.56	–	+1.81
1	+12.72	–	–1.24	–12.09 [a]	−9.55 [a]	−2.81	+1.03
2-*cis*	+9.66	–	−1.81	−9.60 [a]	−8.55 [a]	−4.01	+0.17
2-*trans*	+11.66	–	−1.16	−10.75 [a]	−9.01	−3.19	+0.05
3	+12.37 [a]	+6.29	−1.60	−8.59 [a]	−7.44 [a]	−2.47 [a]	−0.53
4a	+10.85	+6.21	–	−7.19	−7.33	−3.31	—

[a] Mean values of those for corresponding positions.

comparison with the NICS(1) values at the outside of the porphyrin aromatic circuits (position G), those at position A are quite larger and thus the positive values are mainly derived from the anti-aromatic contributions. Additionally, the NICS(1) values at the centers of the fused pyrroles (position B and C) gradually increase with increase in the number of the fused rings, from a negative value for **1** to a positive value for **4a**. The tendencies are well matched with the ^{1}H NMR observations (see above) and well explained with the contribution of the anti-aromatic resonance structures.

2-5. Optical spectroscopic characterization of a series of fused porphyrins

The fused porphyrins show more bathochromically shifted absorption bands by increasing the number of fused rings, indicating the expansion of π-conjugation circuits of the porphyrins. The narrowing of the HOMO-LUMO gaps with increasing the number of fused rings was also reflected on the redox potentials of the fused porphyrins and the values obtained by DFT calculations (Table 2-5); the HOMO-LUMO gaps obtained from the three methods linearly correlated with each other. In addition, the molar coefficients of the absorption bands and the total oscillator strengths decreased with increasing the number of fused rings. This tendency can be also explained by the contribution of the aforementioned anti-aromatic circuits; *i.e.* the anti-aromatic molecules exhibit smaller molar extinction coefficients,

Table 2-5. Summary of HOMO-LUMO gaps obtained the UV-Vis spectroscopy, electrochemical studies and DFT calculations for the ring-fused porphyrins

	Oscillator Strength			Δ(HOMO-LUMO), eV		
	Soret	Q	total	CV[a]	UV-Vis-NIR[b]	DFT
ZnTPP	1.497 (389 – 444 nm)[c]	0.123 (497 – 647 nm)[c]	1.620	2.19	2.07	2.86
1	1.110 (430 – 538 nm)[c]	0.103 (540 – 821 nm)[c]	1.213	1.81	1.60	2.41
2-*cis*	0.884 (374 – 475 nm)[c]	0.077 (621 – 851 nm)[c]	0.961	1.73	1.56	2.37
2-*trans*	1.149 (445 – 614 nm)[c]	0.128 (615 – 967 nm)[c]	1.277	1.45	1.39	2.07
3	0.568 (495 – 676 nm)[c]	0.059 (690 – 1130 nm)[c]	0.627	1.42	1.30	2.04
4a	0.499 (513 – 693 nm)[c]	0.039 (720 – 1155 nm)[c]	0.538	1.32	1.21	1.94

[a] Obtained from the difference between the first oxidation and first reduction potentials. [b] Obtained from the wavelength of the lowest absorption band. [c] The oscillator strength was calculated with the wavelength range indicated in the parenthesis.

because the paratropic character makes the electronic transition spin-forbidden.[24] To rationalize the observed spectral properties, the electronic absorption spectra were calculated using the TD-DFT method at the B3LYP/6-31G(d) level using the corresponding DFT-optimized structures of the fused porphyrins. The calculated electronic transition wavelengths and intensities are summarized in Table 2-6 and are schematically depicted in Figure 2-18. The calculated stick spectra in Figure 2-18 reproduce the excitation wavelengths and intensities of the experimental spectra. The lowest absorption bands of the fused porphyrins commonly derive from the HOMO-to-LUMO π-π* transitions (Figure 2-19 and 2-20).[25]

To gain in-depth insight into the electronic structures of the ring-fused porphyrins based on spectroscopic techniques, their magnetic circular dichroism (MCD) spectra were measured in DMF (Figure 2-17).[26-28] Due to the molecular symmetries being lower than C_3, the MCD signals consist of Faraday B terms. Despite the less intense and more complicated MCD signal patterns compared to those of regular porphyrins, which can also be accounted for in

Table 2-6. TD-DFT results for low-energy π-π* states of the ring-fused porphyrin derivatives [a]

compound	wavelength, nm	oscillator strength	contribution (weight %)[b]
1	652.91	0.0347	H→L (85), H–1→L+1 (10)
	476.70	0.0982	H–1→L+1 (43), H–2→L (39), H→L+1 (6)
	425.07	0.8041	H–1→L (33), H→L+1 (28), H–2→L+1 (18)
2-*cis*	674.00	0.0032	H–1→L (55), H→L+1 (44)
	671.24	0.0169	H→L (82), H–1→L+1 (16)
	567.23	0.0760	H–1→L+1 (73), H–2→L (10), H→L (10)
	484.07	0.6550	H→L+1 (43), H–1→L (33), H–3→L (18)
2-*trans*	766.49	0.0471	H→L (90), H–1→L+1 (6)
	480.73	0.2510	H–1→L+1 (41), H–3→L (29), H–1→L (16)
	443.79	0.5036	H–4→L (39), H–4→L+1 (18), H→L+1 (14)
	429.24	0. 7010	H–4→L (51), H–1→L (15)
3	812.01	0.0162	H→L (92), H–1→L+1 (5)
	590.67	0.0310	H–1→L+1 (66), H–2→L (10), H–3→L (9)
	518.38	0.6563	H→L+1 (33), H–2→L+2 (26), H–1→L (21)
	407.17	0.4693	H–5→L+1 (33), H–4→L (32), H–1→L+2 (13)
4a	884.12	0.0061	H→L (94)
	818.53	0.0056	H–1→L (70), H→L+1 (29)
	534.38	0.9019	H→L+1 (64), H–1→L (26)
	461.65	0.3157	H–4→L (79), H–1→L+1 (8), H–2→L+2 (8)
	402.97	0.5580	H–6→L (67), H–3→L+2 (22)

[a] At the B3LYP/6-31G(d) level of theory. [b] H = HOMO, L = LUMO.

terms of contributions from other resonance structures to the electronic structures of these compounds, changes in the MCD sign sequence can be observed upon increasing the number of fused rings. In the Q-band region, **1** and **2**-*cis* show a negative to positive sign sequence (–, +) in ascending energy, which becomes less intense and unclear for **2**-*trans*,and finally the reverse sign sequence (+, –) was observed for **3** and **4a**. According to the Michl's perimeter model for predicting MCD signs,[26,29] which was successfully applied by Djerassi *et al.* to explain the sign sequence of reduced porphyrins such as chlorin and bacteriochlorin, (–, +) and (+, –) sequences in ascending energy related to the cases of ΔHOMO > ΔLUMO and ΔHOMO < ΔLUMO, respectively (ΔHOMO and ΔLUMO stand for the energy gap between HOMO and HOMO–1 and that between LUMO and LUMO+1, respectively).[29,30] It was also demonstrated that in the case of ΔHOMO ≈ ΔLUMO, the MCD signal in the Q band region becomes (–, –) and basically very weak.[30] By applying this structure-spectrum correlation to the fused porphyrin systems presented here, it can be proposed that the degeneracy of the LUMO and LUMO+1 of the D_{4h}-type porphyrin macrocycle is loosened with the increasing number of fused rings, *i.e.* ΔHOMO > ΔLUMO for **1** and **2**-*cis*, ΔHOMO ≈ ΔLUMO for **2**-*trans*, and ΔHOMO < ΔLUMO for **3** and **4a** (Figure 2-20). In addition, DFT calculations on the fused porphyrins supported well the relative energy changes

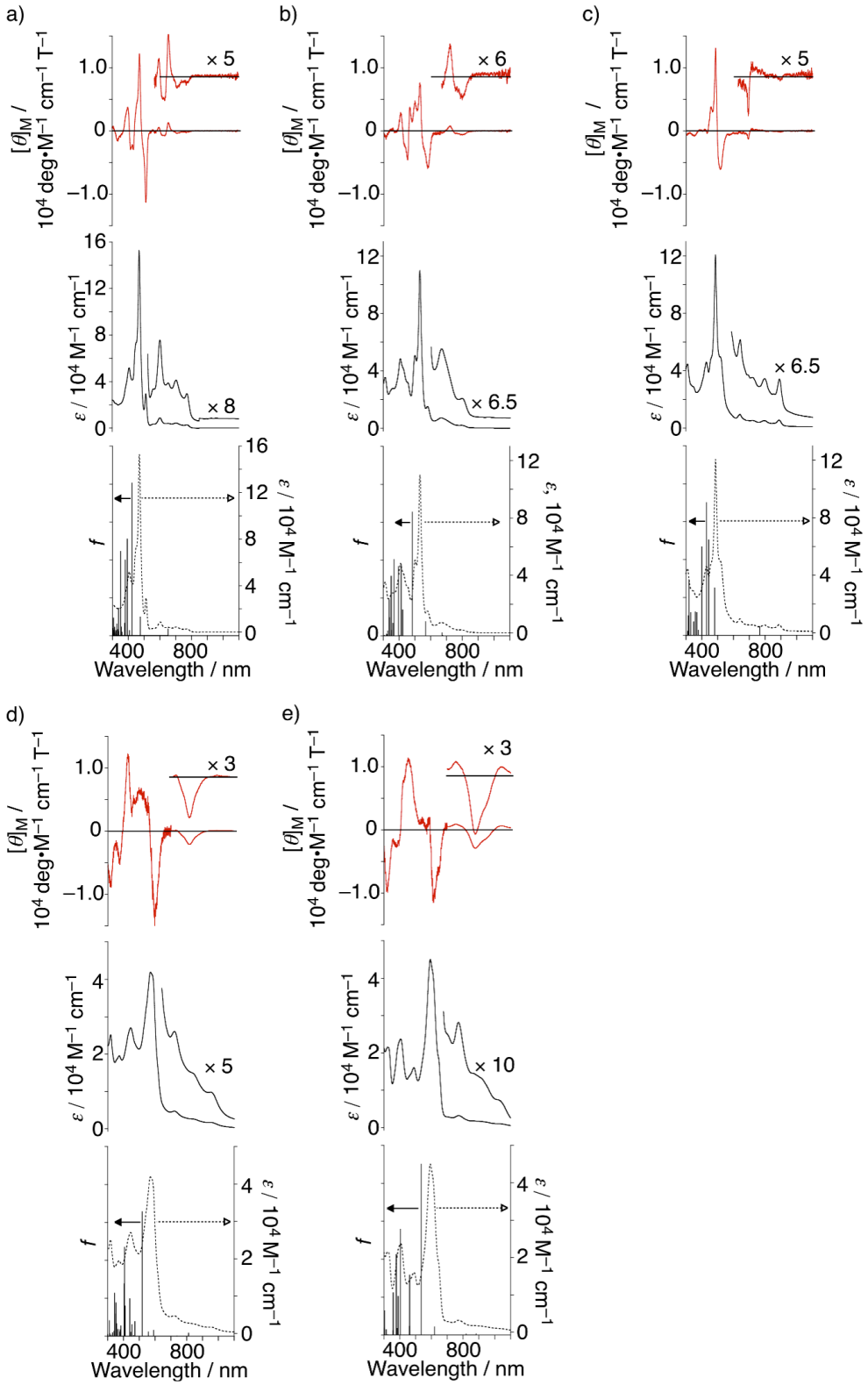

Figure 2-17. MCD (top) and experimental absorption (middle) spectra, recorded in DMF at room temperature, and calculated transition energies and oscillator strengths (*f*) obtained with TD-DFT calculations at the B3LYP/6-31G(d) level of theory (bottom) of **1** (a), **2**-*cis* (b), **2**-*trans* (c), **3** (d) and **4a** (e). The dashed lines in the calculated stick spectra at the bottom indicate the experimental absorption spectra of the corresponding porphyrins in DMF.

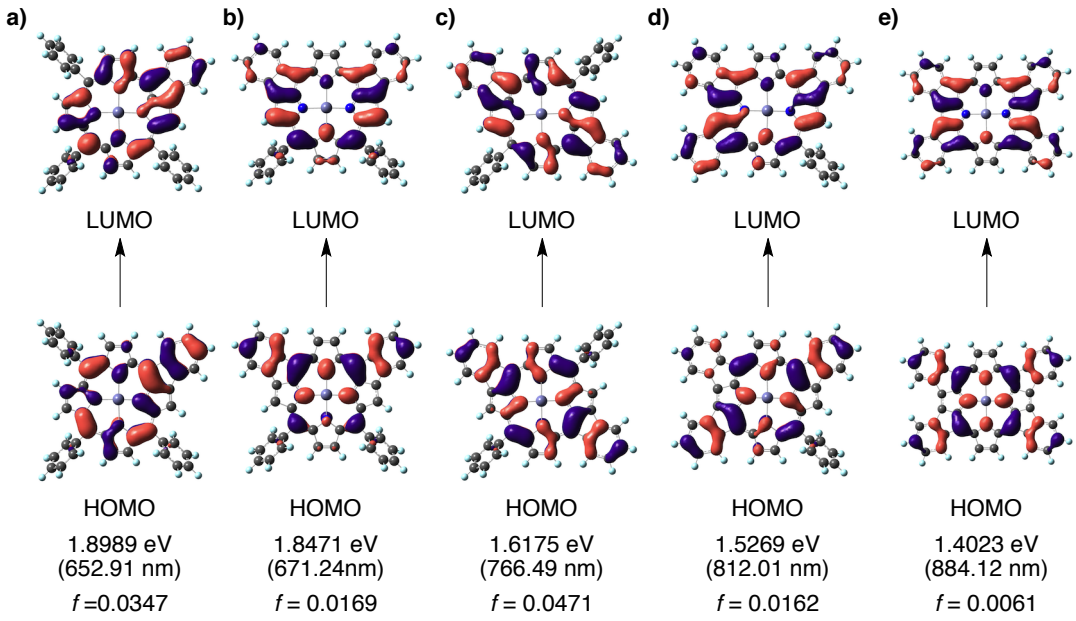

Figure 2-18. The frontier orbitals related to the lowest-energy absorption bands with the transition energies and oscillator strengths (f) for **1** (a), **2**-*cis* (b), **2**-*trans* (c), **3** (d) and **4a** (e), obtained from TD-DFT calculations at the B3LYP/6-31G(d) level of theory.

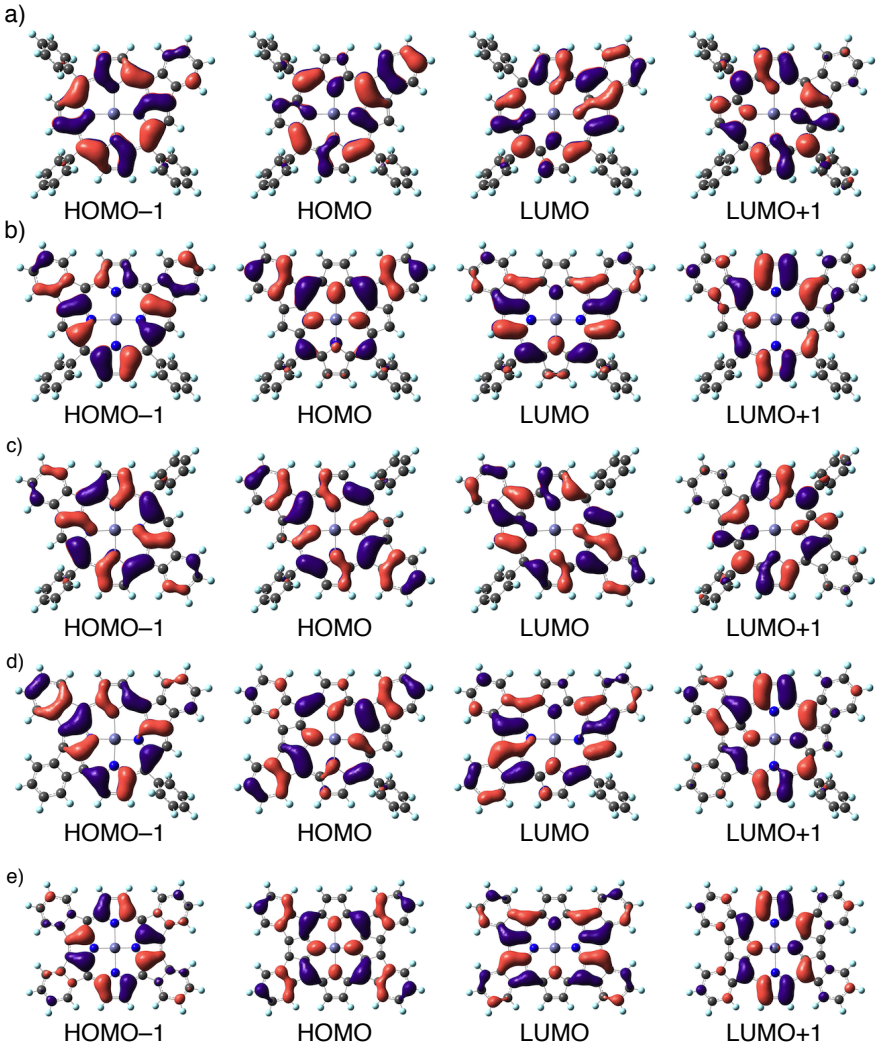

Figure 2-19. The frontier four orbitals of **1** (a), **2**-*cis* (b), **2**-*trans* (c), **3** (d) and **4a** (d), obtained from DFT calculations at the B3LYP/6-31G(d) level of theory.

of the four frontier orbitals and implied that the increase of ΔLUMO is caused by stabilization of the LUMO by the ring fusion (Figure 2-20).

2-6. Oxidation and reduction of ring-fused porphyrins

To confirm the electronic effects of the ring-fusion on the porphyrin π-conjugation, the author has measured the electronic absorption spectra and cyclic and differential-pulse voltammograms (CV and DPV) of the fused porphyrins

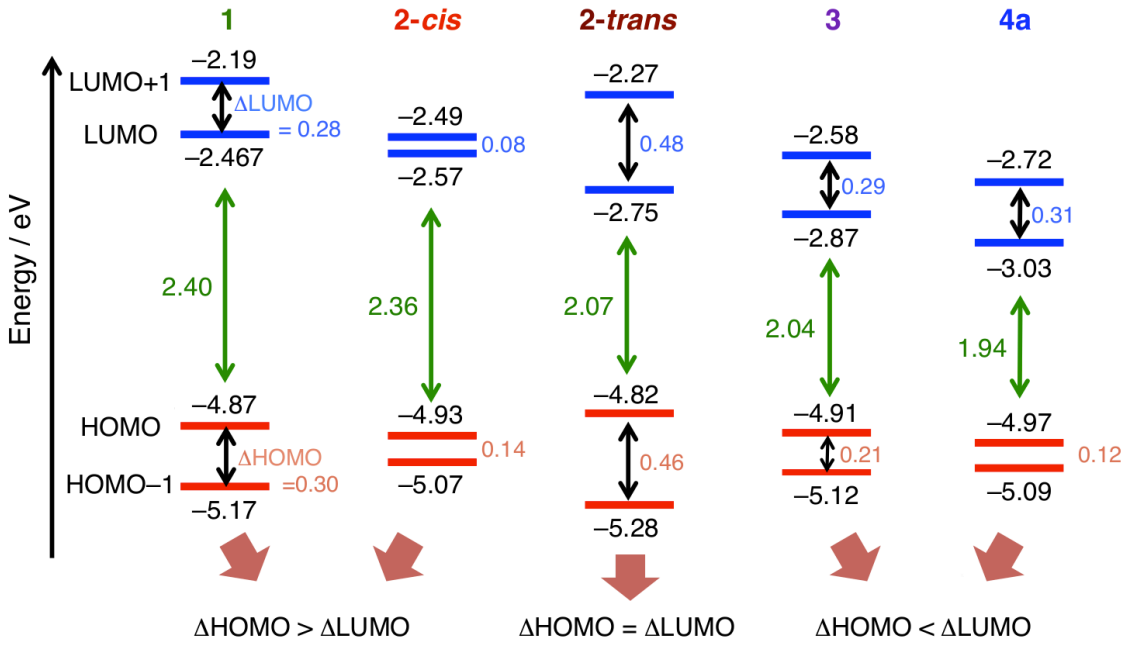

Figure 2-20. Illustrations of the MCD band sign patterns predicted by the Michl's perimeter model for the separations of the energy levels of the frontier orbitals obtained for **1** – **4a**. Energy levels given in the figure were obtained by DFT calculations at the B3LYP/6-31G(d) level of theory.

(Figure 2-17). Due to the low solubility of **3** and **4a** into CH_2Cl_2 and $CHCl_3$that are typical good solvents for porphyrins, dimethylformamide (DMF) was employed as the solvent for absorption spectroscopy and electrochemical measurements. All the fused porphyrins exhibited reversible first-oxidation and first-reduction waves in DMF, and reversible or pseudo-reversible second-oxidation and second-reduction waves (Figure 2-21). HOMO-LUMO gaps obtained from the first oxidation and the first reduction potentials become narrower with increasing the number of fused rings. It should be noted that the lowering of the LUMO level by ring-fusion was more remarkable than the rise of the HOMO level; for instance, the difference of the first reduction potentials between **4a** (–0.67 V) and ZnTPP (–1.36 V) was 0.69 V, whereas that of the first oxidation potentials of **4a** (+0.65 V) and ZnTPP (+0.83 V) was 0.18 V (Table 2-7).

To confirm the large effect of the ring-fusion on the LUMO level, the author conducted DFT calculations on **4a**. As a result, it was indicated that the HOMO was delocalized mainly on the porphyrin core, whereas the LUMO was expanded to the ring-fused moieties (Figure 2-19). Therefore, the energy level of LUMO is strongly affected by the degree of ring-fusion, compared to that of HOMO. To elucidate the electronic structures of ZnQFP in detail,

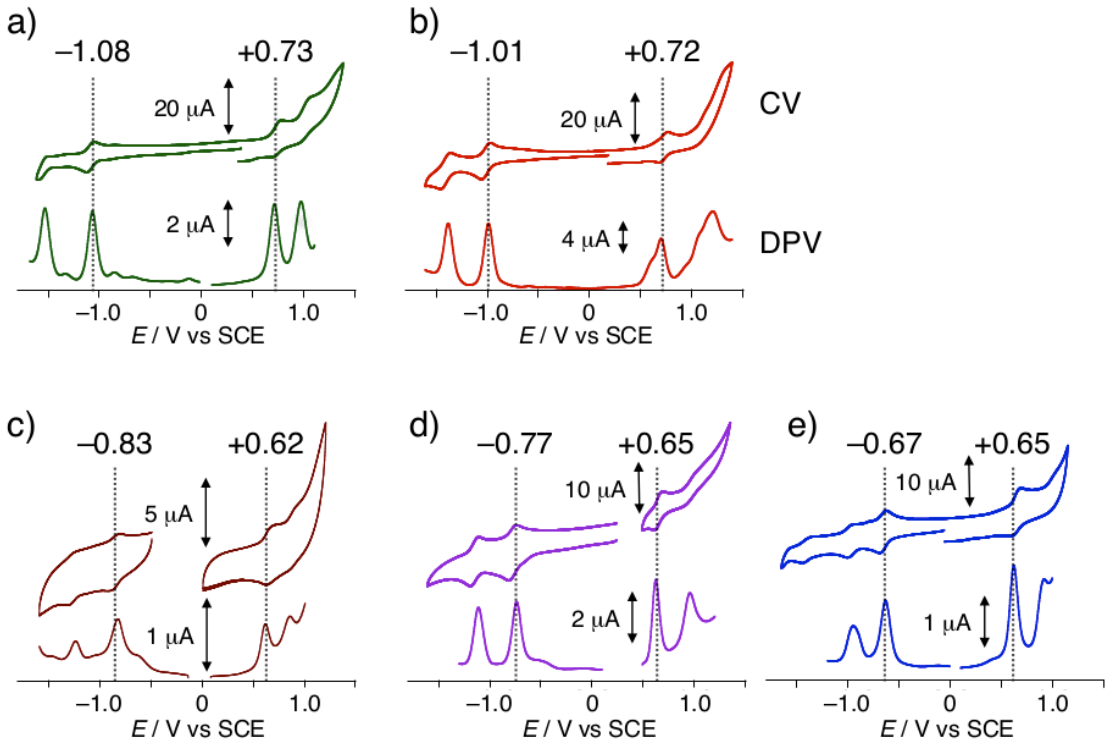

Figure 2-21. Cyclic (above) and differential-pulse (below) voltammograms of the fused porphyrins in DMF containing 0.1 M $TBAPF_6$ as an electrolyte at room temperature: (a) **1**, (b) **2**-*cis*, (c) **2**-*trans*, (d) **3**, and (e) **4a**.

Table 2-7. Summary for optical and electrochemical data for the fused porphyrins.

	λ_{max} (B)[a]	λ_{max} (Q)[b]	Red2[c]	Red1[c,d]	Ox1[c,d]	Ox2[c]	Ox1 – Red1
1	471	773	–1.53	–1.08	+0.73	+0.97	1.81
2-*cis*	532	889	–1.40	–1.01	+0.72	+1.08	1.73
2-*trans*	489	895	–1.23	–0.83	+0.62	+0.86	1.45
3	580	955	–1.11	–0.77	+0.65	+0.96	1.42
4a	592	1021	–0.94	–0.67	+0.65	+0.96	1.32
ZnTPP	425	599	–1.77	–1.36	+0.83	+1.03	2.19

[a] Wavelengths (nm) of the largest Soret-like bands in DMF. [b] Wavelengths (nm) of the longest Q-like bands in DMF. [c] Redox potentials (V vs SCE) were determined with the peak potentials in DPV. [d] Half-wave potentials.

electron-spin resonance (ESR) spectra of the $1e^-$-oxidized and $1e^-$-reduced species of ZnQFP were measured in THF (Figure 2-22). As a ZnQFP derivative, mesityl-substituted **4b**, was employed for the ESR studies to ensure the solubility in THF and to preclude the association among the radical species. The cyclic and differential-pulse voltammograms (CV and DPV) of **4b** measured in THF indicated the rest potential to be +0.13 V vs SCE and exhibited four reversible redox couples at –0.98, –0.60, +0.86, and +1.23 V vs SCE (Figure 2-23), and all of the four redox waves were considered to be $1e^-$ processes. Thus, the first oxidation and reduction potentials of **4b** are +0.86 and –0.60 V vs

SCE, respectively. The 1e$^-$-oxidized species of **4b** (**4b**$^{\bullet+}$) was formed by the addition of 1 equiv of tris(4-bromophenyl)aminium hexachloroantimonate (TBPAH; E_{red} = +1.31 V vs SCE)[31] as an oxidant to the solution of **4b** in THF in an ESR tube. The ESR spectrum of **4b**$^{\bullet+}$ at 298 K exhibited no hyperfine structure due to the nitrogen nuclei. This result is in stark contrast to that of ZnTPP;[32] the ESR signal of 1e$^-$-oxidized ZnTPP in CH_2Cl_2 at 298 K was split into nine lines due to the hyperfine coupling of the four nitrogen nuclei (A_N = 1.55 G). The ESR spectrum of **4b**$^{\bullet+}$ was simulated and the signal broadening can be elucidated by the hyperfine couplings of the peripheral hydrogen nuclei (A_H = 0.98 G). On the other hand, the ESR signal of 1e$^-$-reduced species of **4b** (**4b**$^{\bullet-}$), which was formed using 1 equiv of decamethyl-cobaltocene (Co(Cp*)$_2$; E_{ox} = –1.30 V vs SCE)[33] as a reductant in THF at 222 K, exhibited a five-peaked hyperfine splitting pattern due to the coupling of two of the nitrogen nuclei (Figure 2-22). The simulation of the ESR signal was performed to indicate that the hyperfine coupling constants, A_N and A_H, are 1.43 and 0.77 G, respectively. The hyperfine splitting patterns are quite different between the reduced species of ZnQFP and ZnTPP. In the ESR spectrum of 1e$^-$-reduced ZnTPP (ZnTPP$^{\bullet-}$) in THF at room temperature, a relatively broadened and isotropic signal was observed without any hyperfine splitting due to the nitrogen nuclei.[33] The difference in the hyperfine splitting patterns between ZnQFP and ZnTPP can be accounted for on the basis of the distribution of the SOMOs obtained by DFT calculations. The SOMO of ZnTPP$^{\bullet+}$ shows a_{2u} symmetry and has a large spin density on the inner four nitrogen

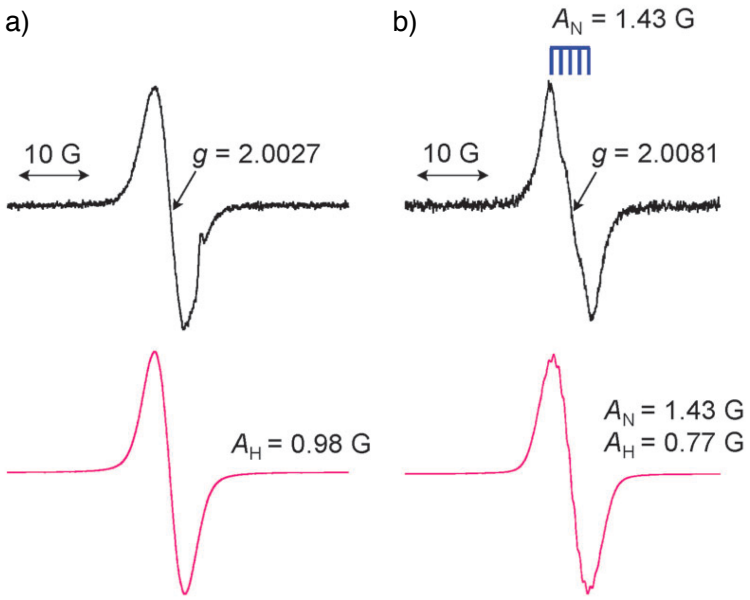

Figure 2-22. Experimental (top) and simulated (bottom) ESR spectra of the π-radical cation (a) and anion (b) obtained from the chemical oxidation and reduction of **4b** in THF. The former was formed with TBPAH as the oxidant and the latter with Co(Cp*)$_2$ as the reductant.

atoms,[35] whereas that of ZnQFP$^{\bullet+}$ has a_{1u} symmetry, expanding to the fused phenyl rings, and shows no spin density on the four nitrogen atoms (Figure 2-24). Therefore, the ESR signal of ZnQFP$^{\bullet+}$ does not exhibit hyperfine splitting due to the nitrogen nuclei. On the other hand, calculations on ZnTPP$^{\bullet-}$ afforded the b_{1g} symmetric SOMO without electron density on the four nitrogen atoms.[36] In contrast, the SOMO of ZnQFP in the b_{1g} symmetry possesses electron density

on the two nitrogen atoms of the non-fused pyrroles (Figure 2-24b). Thus, the ESR signal of ZnQFP shows hyperfine splitting due to the two nitrogen nuclei.

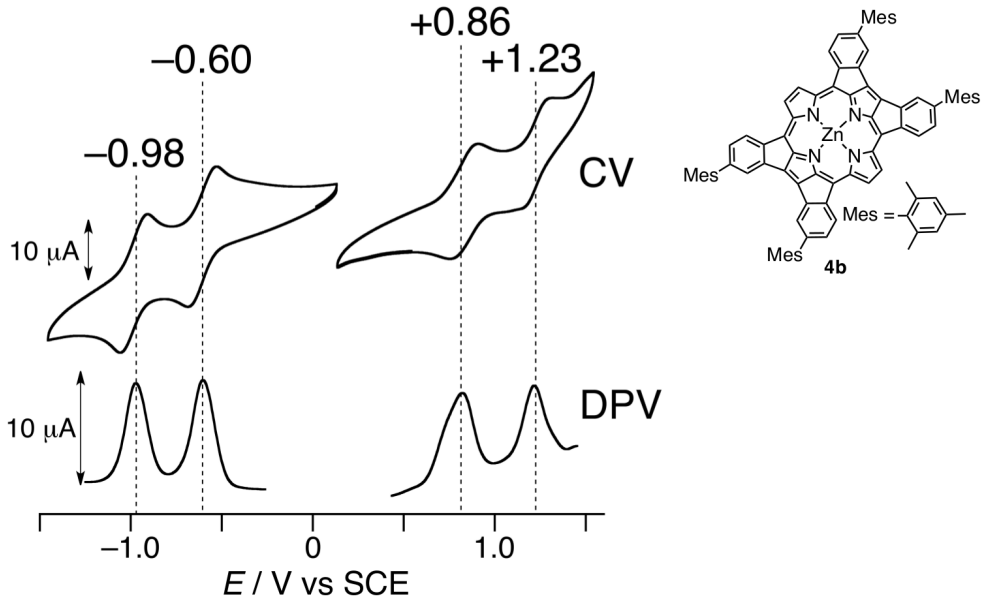

Figure 2-23. Cyclic (above) and differential-pulse (below) voltammograms of **4b** in THF at room temperature in the presence of $[(n\text{-Bu})_4N](PF_6)$ (0.1 M) as an electrolyte.

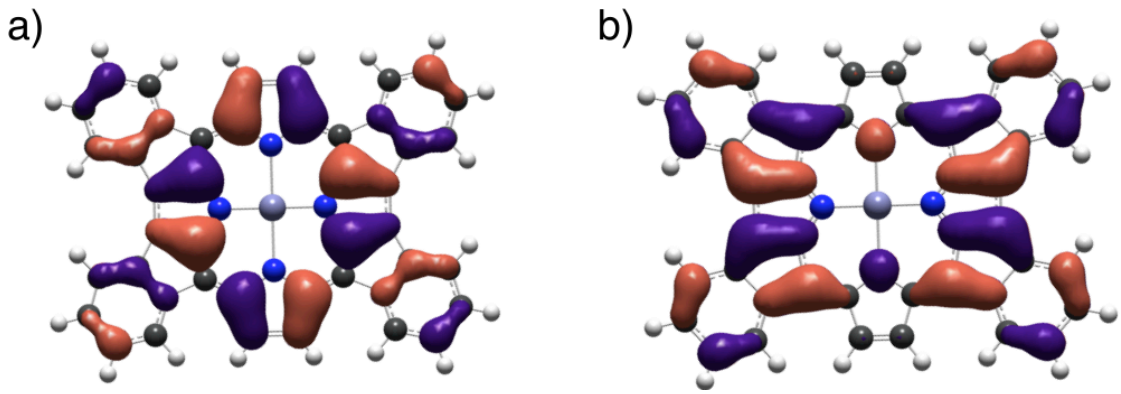

Figure 2-24. SOMOs of $1e^-$-oxidized (a) and $1e^-$-reduced species (b) of **4a** calculated at the B3LYP/6-31G(d) level of theory.

2-7. Summary

The author has synthesized a novel quadruply-fused porphyrin with a facilely prepared precursor in a high yield. In addition, partly-ring-fused porphyrin derivatives have been isolated and fully characterized by spectroscopic and X-ray diffraction analysis. The crystal structures revealed the expansion of the π-conjugation circuits to the fused *meso*-phenyl groups as evidenced by the bond lengths between the *ipso*-carbon and the *ortho*-carbon bonded to the *β*-pyrrole carbon. In the crystal packing, the fused porphyrins exhibited strong intermolecular π-π stacking, reflecting the highly planar structures. The author has clarified the significant effects of the ring fusion on the electronic structures of the porphyrin derivatives due to the expansion of the π-conjugated aromatic circuits to the fused *meso*-aryl groups.

The expansion of the π-conjugated circuits also results in the unique aromatic and magnetic properties of the porphyrin derivatives, and causes not only the remarkable red shifts of the absorption bands derived from the narrowed HOMO-LUMO gaps, but also the contribution of antiaromatic resonance forms to the magnetic properties as observed in the ^{1}H NMR spectra.

2-8. Experimental section

General.

Chemicals and solvents were used as received from commercial sources unless otherwise mentioned. 1,4-dioxane for the synthesis was distilled over Na/benzophenone. DMF for the electrochemical measurements was distilled before use. Tetarabuthylammmonium Acetate (TBAOAc) was recrystallized from CH_2Cl_2/hexane. Zinc(II) 2,3,12,13,-tetrabromo-5,10,15,20-tetraphenyl- porpyrinate (**5a**) was synthesized in accordance with the reported procedure.[15] ^{1}H NMR measurements were performed on a Bruker AVANCE400 spectrometer. UV-vis absorption spectra were measured at room temperature in DMF on a Shimadzu UV-3600 spectrophotometer. MALDI-TOF- MS spectrometry was performed on an AB SCIEX TOF/TOF 5800 spectrometer by using dithranol as a matrix. Electrochemical measurements were performed on ALS/CH instruments electrochemical analyzer model 710D.

Synthesis.

Procedure of Pd-catalyzed fused reactions using Pd-nanoclusters with [Pd(η^3-C_3H_5)Cl]$_2$. A solution of TBAOAc (627 mg, 2.08 mmol), [Pd(η^3-C_3H_5)Cl]$_2$ (3.53 mg, 9.65 μmol), molecular sieves 4A (70 mg), and potassium carbonate (279 mg, 2.03 mmol) in 1,4-dioxane (1.0 mL) was heated at 110 ºC for 3 min. After the color of the solution changed to black, **5a** (49.8 mg, 50 μmol) was quickly added to the solution. After stirring for 11 h, the reaction mixture was cooled to ambient temperature. The volatiles were removed under vacuum and the residual solid was washed with water. The solid was dissolved in pyridine and the precipitate including the palladium catalyst was filtered off. The filtrate was dried under vacuum to give black powder. The black powder was recrystallized from the THF solution in the presence of one drop of pyridine by depositing EtOH vapor as a poor solvent. The crystals obtained was filtered and washed with THF to give a red-purple filtrate. The remaining dark red solid mainly involved **4a** and the further recrystallization by vapor deposition of EtOH to the THF solution in the presence of one drop of pyridine to give pure **4a** (29.9 mg, 40 μmol, 79%). In addition, the major component of the red-purple filtrate in THF was **3** and further purification by preparative thin-layer chromatography on silica gel (PLC Silica gel 60 F254, 1 mm) using THF/toluene (1:10, v/v) as an eluent. The recrystallization from THF/hexane gave dark violet powder of **3** (3.86 mg, 5.7 μmol, 11%).

Procedure of Pd-catalyzed fused reactions using Pd-nanoclusters with Pd(OAc)$_2$. A solution of TBAOAc (627 mg, 2.08 mmol), palladium acetate (4.81 mg, 21 μmol), triphenylphosphine (10.5 mg, 40 μmol), molecular sieves 4A (70 mg), potassium carbonate (280 mg, 2.03 mmol), and **5a** (50.2 mg, 51 μmol) in 1,4-dioxane (1.0 mL) was stirred at 110 ºC for 16 h. The reaction mixture was cooled to ambient temperature, and filtered, then washed with water. The red-brown powder was chromatographed on a silica gel column by using CH_2Cl_2/hexane (1:1, v/v) as an eluent to give

ZnTPP (3.3 mg, 18 μmol, 10%), **1** (8.7 mg, 13 μmol, 25%), **2** and the isomers (13 mg, 20 μmol, 40%), and **3** (5.0 mg, 7.4 μmol, 15%).

Zinc(II) singly-fused porphyrinate (1).[14a] ^{1}H NMR (DMSO-d_6): δ 9.31 (d, J = 4.8 Hz, 1H, 3-β-H), 8.47 (d, J = 4.8 Hz, 1H, 2-β-H) , 8.35 (d, J = 4.4 Hz, 1H, β-H), 8.31 – 8.30 (m, 2H, β-H), 8.23 (d, J = 4.4 Hz, 1H, β-H), 8.20 (d, J = 7.7 Hz, 1H, 26-phenyl-H), 8.07 – 8.00 (m, 6H, *o*-Ph-H), 7.83 (s, 1H, 8-β-H), 7.81 – 7.67 (m, 9H, *m*, *p*-Ph-H), 7.42 (d, J = 7.7 Hz, 1H, 23-Ph-H), 7.04 (t, J = 7.7 Hz, 1H, 25-Ph-H), 6.91 (t, J = 7.7 Hz, 1H, 24-Ph-H). UV-vis (DMF): λ_{max} [nm] (log (ε, M^{-1} cm^{-1})) = 408 (4.67), 451 (4.82), 471 (5.15), 514 (4.43), 562 (3.48), 602 (3.89), 654 (3.56), 704 (3.59), 773 (3.43). MS (MALDI, dithranol matrix): *m/z* = 676.2 (calcd. for $[M]^+$: 676.1).

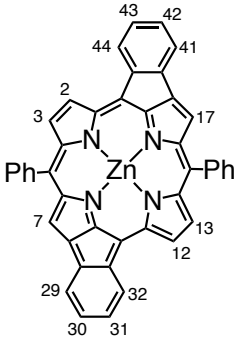

Zinc(II) *cis*-Doubly-fused porphyrinate (2-*cis*).[14c] ^{1}H NMR (DMSO-d_6): δ 9.16 (s, 2H, 2,3-β-H), 8.18 (d, J = 7.4 Hz, 2H, 26,44-Ph-H), 7.92 – 7.89 (m, 4H, *o*-Ph-H), 7.78 (s, 2H, 12,13-β-H), 7.74 – 7.65 (m, 6H, m, *p*-Ph-H), 7.52 (s, 2H, 8,17-β-H), 7.41 (d, 2H, J = 7.4 Hz, 23,41-Ph-H), 7.07 (t, J = 7.4 Hz, 2H, 25,43-Ph-H), 6.94 (t, J = 7.4 Hz, 2H, 24,42-Ph-H). UV-vis (DMF): λ_{max} [nm] (log (ε, M^{-1} cm^{-1})) = 360 (4.43), 408 (4.67), 454 (4.51), 500 (4.70), 532 (5.04), 580 (4.18), 667 (3.85), 795 (3.32), 889 (2.46). MS (MALDI, dithranol matrix): *m/z* = 674.1 (calcd. for $[M]^+$: 674.1).

Zinc(II) *trans*-doubly-fused porphyrinate (2-*trans*).[14c] ^{1}H NMR (DMSO-d_6): δ 8.99 (d, J = 4.2 Hz, 2H, 12-β-H), 8.17 (d, J = 4.2 Hz, 2H, 13-β-H), 8.11 (d, J = 7.7 Hz, 2H, 29,41-Ph-H), 8.00 – 7.90 (m, 4H, *o*-Ph-H), 7.75 – 7.66 (m, 6H, *m*, *p*-Ph-H), 7.56 (s, 2H, 7,17-β-H), 7.36 (d, 2H, J = 7.7 Hz, 32,44-Ph-H), 7.02 (t, J = 7.7 Hz, 2H, 30,42-Ph-H), 6.91 (t, J = 7.7 Hz, 2H, 31,43-Ph-H). UV-vis (DMF): λ_{max} [nm] (log (ε, M^{-1} cm^{-1})) = 432 (4.58), 489 (5.08), 522 (4.69), 643 (3.97), 799 (3.71), 895 (3.75). MS (MALDI-TOF, *dithranol* matrix): *m/z* = 674.1 (calcd. for $[M]^+$: 674.1).

Zinc(II) triply-fused porphyrinate (3). ^{1}H NMR (DMSO-d_6): δ 8.81 (d, J = 4.8 Hz, 1H, 3-β-H), 8.67 (d, J = 4.8 Hz, 1H, 2-β-H), 8.38 (d, J = 4.6 Hz, 1H, 12-β-H), 8.06 (d, J = 7.4 Hz, 1H, 44-Ph-H), 7.82 (dd, J = 9.4, 3.7 Hz, 2H, *o*-Ph-H), 7.76 (d, J = 7.1 Hz, 1H, 32-Ph-H), 7.69 – 7.66 (m, 3H, m, *p*-Ph-H), 7.65 – 7.64 (m, 2H, 13- β-H, 26-Ph-H), 7.35 (d, J = 7.4 Hz, 1H, 41-Ph-H), 7.28 (s, 1H, 17-β-H), 7.15 (d, J = 7.1 Hz, 1H, 29-Ph-H), 7.10 (d, J = 6.4 Hz, 1H, 23-Ph-H), 7.04 (t, J = 7.4 Hz, 1H, 43-Ph-H), 6.95 – 6.75 (m, 5H, 24,25,30,31,42-Ph-H). UV-vis (DMF): λ_{max} [nm] (log (ε, M^{-1} cm^{-1})) = 320 (4.43), 374 (4.32), 447 (4.45), 580 (4.62), 721 (3.68), 846 (3.41), 955 (3.20). MS (MALDI, dithranol matrix): *m/z* = 672.1 (calcd. for $[M]^+$: 672.1). Anal. calcd. for $C_{44}H_{22}N_4Zn \cdot 0.5H_2O \cdot 1.5THF \cdot 1.5DMSO$: C 70.23, H 4.89, N 6.18; found: C 69.96, H 4.68, N 5.98.

Zinc(II) quadruply-fused porphyrinate (4a). ^{1}H NMR (DMSO-d_6): δ 8.34 (s, 4H, 2, 3,12,13-β-H), 7.70 (d, J = 7.4 Hz, 4H, 26,32,38,44-Ph-H), 7.14 (d, J = 7.4 Hz, 4H, 23,29,35,41-Ph-H), 6.89 (t, J = 7.4 Hz, 4H, 25,31,37,43-Ph-H), 6.82 (t, J = 7.4 Hz, 4H, 24,30,36,42-Ph-H). UV-vis (DMF): λ_{max} [nm] (log (ε, M^{-1} cm^{-1})) = 323 (4.34), 406 (4.38), 489 (4.20), 592 (4.65), 770 (3.51), 867 (3.26), 1021 (3.00). MS (MALDI, dithranol matrix): *m/z* = 670.0 (calcd. for $[M]^+$: 670.0). Anal. calcd. for $C_{44}H_{20}N_4Zn \cdot 3H_2O \cdot$ 0.25pyridine$\cdot$0.5DMF: C 71.95, H 3.97, N 8.53; found: C 71.92, H 3.71, N 8.32.

Zinc(II) 24,30,36,42-tetramesityl-quadruply-fused porphyrin (4b). A ring-fusion reaction according to the general procedure mentioned above was performed utilizing **5b** (73 mg, 50 μmol) as a starting material to obtain **4b**. After

filtration, the precipitate obtained was chromatographed on a bio-beads S-X1 gel using THF as an eluent. The second moving fraction was collected and the solvent was removed under vacuum. The residual solid was recrystallized from

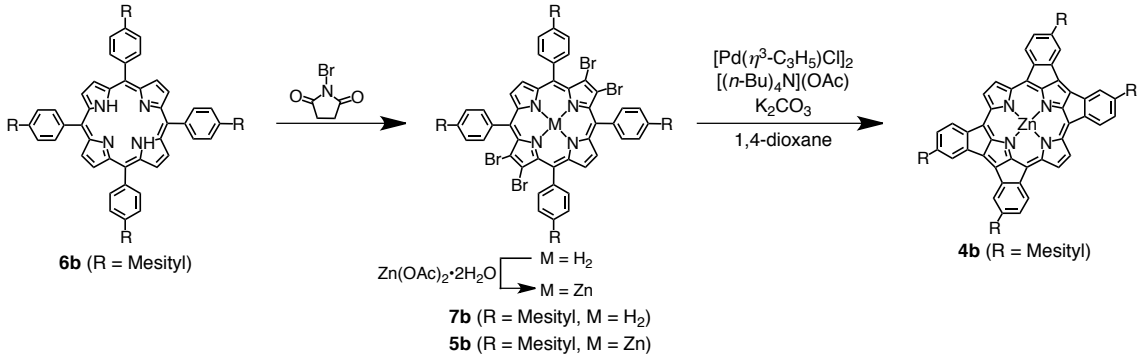

Scheme 2-2. Synthesis of quadruplly fused porphyrin derivative, **4b**.

THF/ethanol (1:3, v/v) and dried under vacuum to give pure **4b** (42 mg, 37 μmol, 74%). m.p.: >300 ºC. ^{1}H NMR (DMSO-d_6): δ 8.35 (s, 4H, 2, 3,12,13-β-H), 7.71 (d, J = 7.6 Hz, 4H, 26,32,38,44-Ph-H), 6.95 (s, 4H, 23,29,35,41-Ph-H), 6.90 (s, 8H, *m*-mesityl-H), 6.54 (d, J = 7.6 Hz, 4H, 25,31,37,43-Ph-H), 2.23 (s, 12H, mesityl-*p*-CH_3), 2.11 (s, 24H, mesityl-*o*-CH_3). UV-vis (THF): λ_{max} [nm] (log (ε, M^{-1} cm^{-1})) = 320 (4.61), 412 (4.65), 437 (4.62), 598 (4.98), 616 (4.97), 775 (3.80), 918 (3.38), 1046 (3.15). MS (MALDI-TOF, *dithranol matrix*): *m/z* = 1140.4 (calcd. for $[M]^+$: 1140.8). Anal. calcd. for $C_{80}H_{60}N_4Zn \cdot 5H_2O \cdot CH_2Cl_2$: C 73.83, H 5.51, N 4.25; found: C 73.64, H 5.70, N, 3.98.

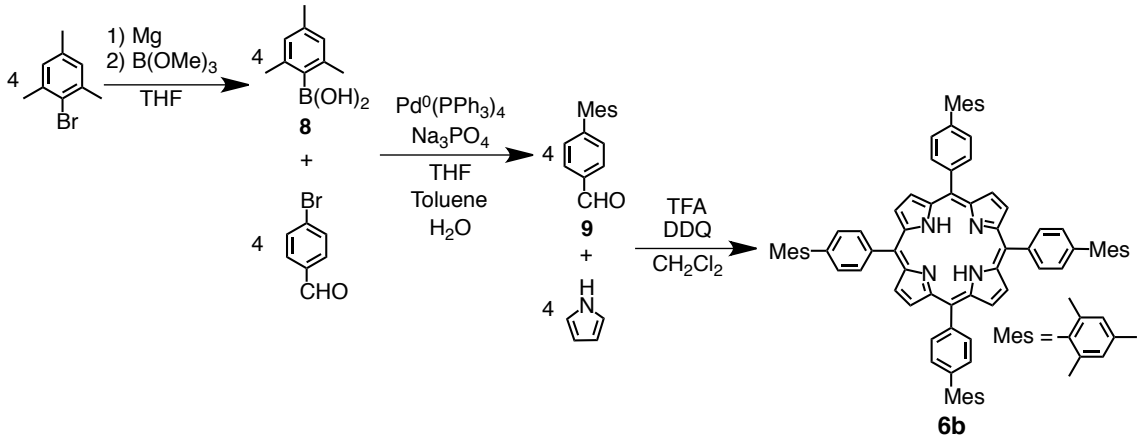

Scheme 2-3. Synthesis of a precursor of the porphyrin derivative, **5b**.

5,10,15,20-Tetrakis(4-mesitylphenyl)porphyrin (**6b**).[37] To the solution of **9** (3.15 g, 15 mmol) in CH_2Cl_2 (1.5 L) was added pyrrole (1.04 mL, 15 mmol), and subsequently, trifluoroacetic acid (2.24 mL, 30 mmol), and the reaction mixture was stirred at room temperature for 3 h. To the resultant solution was added DDQ (= 2,3-dichloro-5,6-dicyanobenzoquinone; 1.71 g, 7.5 mmol) and the reaction mixture was further stirred at room temperature for 1 h. The reaction mixture was poured onto an alumina pad and eluted with CH_2Cl_2 until the eluting solution became pale brown. The solvent was removed under vacuum to give a purple solid. The resulting purple

powder was chromatographed on a silica gel column using CH_2Cl_2/hexane (3:4, v/v) as an eluent. The red purple fraction was collected and the solvent was removed under vacuum. The residual solid was recrystallized from CH_2Cl_2/CH_3OH (1:3, v/v) and dried under vacuum to yield **6b** (843 mg, 0.77 mmol, 21%). ^{1}H NMR ($CDCl_3$): δ 8.99 (s, 8H, β-H), 8.30 (dd, J = 6.3, 1.9 Hz, 4H, *o*-phenyl-H), 7.54 (dd, J = 6.3, 1.9 Hz, 8H, *m*, *p*-phenyl-H), 7.12 (s, 8H, *m*-mesityl-H), 2.44 (s, 12H, mesityl-*p*-CH_3), 2.36 (s, 24H, mesityl-*o*-CH_3), –2.65 (br s, 2H, inner N*H*). UV-vis ($CHCl_3$): λ_{max} [nm] = 648, 593, 553, 518, 421. MS (MALDI-TOF, dithranol matrix): *m/z* = 1150.85 (calcd. for $[M]^+$: 1150.84).

2,3,12,13-Tetrabromo-5,10,15,20-tetrakis(4-mesitylphenyl)porphyrin (7b). To a solution of **6b** (799 mg, 0.74 mmol) in $ClCH_2CH_2Cl$ (160 mL) was added recrystallized *N*-bromosuccinimide (NBS) (768 mg, 4.4 mmol) and the reaction mixture was refluxed for 4 h. After cooling to room temperature, the reaction mixture was washed with water to remove any soluble succinimide impurities. The brown-colored solid was chromatographed on a silica gel column using toluene/hexane (3:2, v/v) as an eluent. The second moving fraction was collected and the solvent was removed under vacuum. The residual solid was recrystallized from CH_2Cl_2/CH_3OH (1:3, v/v) and dried under vacuum to yield **7b** (567 mg, 0.40 mmol, 54%). ^{1}H NMR ($CDCl_3$): δ 8.87 (s, 4H, β-H), 8.26 (d, J = 8.0 Hz, 4H, *o*-phenyl-H), 7.57 (d, J = 8.0 Hz, 8H, *m*-phenyl-H), 7.11 (s, 8H, *m*-mesityl-H), 2.43 (s, 12H, mesityl-*p*-CH_3), 2.33 (s, 24H, mesityl-*o*-CH_3), –2.70 (br s, 2H, inner N*H*). UV-vis ($CHCl_3$): λ_{max} [nm]= 690, 539, 442. MS (MALDI-TOF, dithranol matrix): *m/z* = 1403.2 (calcd. for $[M + H]^+$: 1403.2).

Zinc(II) 2,3,12,13-tetrabromo-5,10,15,20-tetrakis(4-mesitylphenyl)porphyrinate (5b). To a solution of **7b** (301 mg, 0.21 mmol) in $CHCl_3$ (50 mL), was added a suspension of $Zn(OAc)_2{\cdot}2H_2O$ (230 mg, 1.1 mmol) in CH_3OH (20 mL) and the reaction mixture was refluxed for 3 h. The reaction mixture was poured into water and the organic phase was separated and then dried over Na_2SO_4. After removing the solvent, the resulting red-purple powder was chromatographed on a silica gel column by using $CHCl_3$/ hexane (3:1, v/v) as an eluent. The second moving fraction was collected and the solvent was removed under vacuum. The residual solid was recrystall **5b** (297 mg, 0.20 mmol, 95%). ^{1}H NMR ($CDCl_3$): δ 8.95 (s, 4H, β-H), 8.13 (d, J = 7.8 Hz, 4H, *o*-phenyl-H), 7.51 (d, J = 7.8 Hz, 8H, *m*-phenyl-H), 7.11 (s, 8H, *m*-mesityl-H), 2.43 (s, 12H, mesityl-*p*-CH_3), 2.35 (s, 24H, mesityl-*o*-CH_3). UV-vis ($CHCl_3$): λ_{max} [nm] = 610, 568, 437. MS (MALDI-TOF, dithranol matrix): *m/z* = 1466.6 (calcd. for $[M + 2H]^+$: 1466.2).

2,4,6-Trimethylphenylboronic Acid (8). This compound was synthesized according to the literature procedure.[38] ^{1}H NMR (DMSO-d_6): δ 8.05 (s, 2H, OH-H), 6.73 (s, 2H, *m*-mesityl-H), 2.22 (s, 6H, mesityl-*o*-CH_3), 2.19 (s, 3H, mesityl-*p*-CH_3).

Mesityl-benzaldehyde (9). This compound was synthesized according to the literature procedure of a similar compound.[39] Into a 500 mL three-necked flask equipped with a teflon magnetic stirring bar were charged **8** (10.1 g, 61.6 mmol), 4-bromobanzaldehyde (6.75 g, 36.5 mmol), Na_3PO_4 (25 g, 153 mmol) and $Pd(PPh_3)_4$ (624 mg, 0.546 mmol). Then, THF (100 mL), toluene (100 mL) and H_2O (32 mL) were added and the reaction mixture was refluxed for 8 d. The solvent was removed to give a white solid and the residual solid was dissolved in EtOAc. The reaction mixture was washed with water and dried over Na_2SO_4, and the solvent was evaporated. The white solid obtained was chromatographed on a silica gel column using EtOAc/hexane (1:6, v/v) as an eluent. The second moving fraction was

collected and the solvent was removed under vacuum to yield **9** (8.04 g, 35.8 mmol, 98%). ^{1}H NMR ($CDCl_3$): δ 10.07 (s, 1H, C*H*O), 7.95 (d, J = 6.6 Hz, 2H, *o*-phenyl-H), 7.33 (d, J = 6.6 Hz, 2H, *m*-phenyl-H), 6.96 (s, 2H, mesityl-*m*-H), 2.34 (s, 3H, mesityl-*p*-CH_3), 1.99 (s, 6H, mesityl-*o*-CH_3).

X-ray diffraction analysis for 1 – 4a.

The single crystals were mounted on mounting loops. All diffraction data were collected by using a Bruker APEXII diffractometer at 120 K equipped with graphite-monochromated Mo $K\alpha$ (λ = 0.71073 Å) by the ω-2θ scan.

Table 2-8. Crystallographic data for the fused porphyrin derivatives.

compound	**1**-THF	**2**-*cis*	**3**	**4a**-py
crystal system	triclinic	monoclinic	monoclinic	monoclinic
space group	$P\ \bar{1}$	$P2_1/n$	$P2_1/c$	$P2_1/c$
T / K	120	120	120	120
formula	$C_{44}H_{26}N_4Zn{\cdot}C_4H_8O$	$C_{44}H_{24}N_4Zn$	$C_{44}H_{22}N_4Zn$	$C_{44}H_{20}N_4Zn{\cdot}C_5H_5N$
FW	748.16	674.04	672.03	749.11
a / Å	10.995(3)	13.9576(14)	8.010(4)	13.6200(15)
b / Å	13.281(4)	8.0178(8)	13.436(6)	16.3270(18)
c / Å	13.404(4)	25.842(3)	26.359(11)	16.8358(19)
α / °	92.598(4)	90	90	90
β / °	108.215(4)	98.1530(10)	97.647(6)	94.124(2)
γ / °	99.610(4)	90	90	90
V / Å^3	1823.3(9)	2862.7(5)	2812(2)	3734.1(7)
Z	2	4	4	4
λ(MoKα) / Å	0.71073			
D_c / g cm^{-3}	1.363	1.564	1.587	1.332
reflns measured	9815	15619	14366	19936
reflns unique	7626	6456	6011	8104
$R1$ ($I > 2\sigma(I)$)	0.0825	0.0356	0.0814	0.0498
$wR2$ (all)	0.2244	0.0986	0.1762	0.1228
GOF	1.072	1.055	1.032	1.008

The structures were solved by direct methods by using SIR97 and SHELX-97.[40] Crystallographic data for these compounds are summarized in Table 2-8. In the structure refinements for **1**-THF and **4a**-py, the author could not determine the exact positions of the solvent molecules of crystallization because of their severe disorder. Their contribution was thus subtracted from the diffraction pattern by the "Squeeze" program.[41] These data can be obtained free of charge from the Cambridge Crystallographic Data Center: CCDC-929175 (**1**-THF), -929176 (**2**), -929177 (**3**),

and -929178 (**4a**-py).

Reference and notes

1 (a) J. Wu, W. Pisula, K. Müllen, *Chem. Rev.* **2007**, *107*, 718. (b) T. Aida, E. W. Meijer, S. I. Stupp, *Science* **2012**, *335*, 813. (c) D. Görl, X. Zhang, F. Würthner, *Angew. Chem. Int. Ed.* **2012**, *51*, 6328.

2 (a) L. Schmidt-Mende, A. Fechtenkötter, K. Müllen, E. Moons, R. H. Friend, J. D. MacKenzie, *Science* **2001**, *293*, 1119. (b) X. Feng, V. Marcon, W. Pisula, M. R. Hansen, J. Kirkpatrick, F. Grozema, D. Andrienko, K. Kremer, K. Müllen, *Nat. Mater.* **2009**, *8*, 421.

3 Y. Yamamoto, T. Fukushima, Y. Suna, N. Ishii, A. Saeki, S. Seki, S. Tagawa, M. Taniguchi, T. Kawai, T. Aida, *Science* **2006**, *314*, 1761.

4 (a) *The Porphyrin Handbook*, *Vol. 1* (eds.: K. M. Kadish, K. M. Smith, R. Guilard), Academic Press, New York, **2000**. (b) M. O. Senge, M. Fazekas, E. G. A. Notaras, W. J. Blau, M. Zawadzka, O. B. Locos, E. M. N. Mhuircheartaigh, *Adv. Mater.* **2007**, *19*, 2737.

5 (a) P. Rothemund, *J. Am. Chem. Soc.* **1936**, *58*, 625. (b) A. D. Adler, F. R. Longo, J. D. Finarelli, J. Goldmacher, J. Assour, L. Korsakoff, *J. Org. Chem.* **1967**, *32*, 476. (c) J. S. Lindsey, I. C. Schreiman, H. C. Hsu, P. C. Kearney, A. M. Marguerettaz, *J. Org. Chem.* **1987**, *52*, 827.

6 M. P. Byrn, C. J. Curtis, Y. Hsiou, S. I. Khan, P. A. Sawin, S. K. Tendick, A. Terzis, C. E. Strouse, *J. Am. Chem. Soc.* **1993**, *115*, 9480.

7 (a) S. Bhosale, A. L. Sisson, P. Talukdar, A. Fürstenberg, N. Banerji, E. Vauthey, G. Bollot, J. Mareda, C. Röger, F. Würthner, N. Sakai, S. Matile, *Science* **2006**, *313*, 84. (b) Y. Matsuo, Y. Sato, T. Niinomi, I. Soga, H. Tanaka, E. Nakamura, *J. Am. Chem. Soc.* **2009**, *131*, 16048. (c) A. W. Hains, Z. Liang, M. A. Woodhouse, B. A. Gregg, *Chem. Rev.* **2010**, *110*, 6689.

8 (a) S. Fox, R. W. Boyle, *Tetrahedron* **2006**, *62*, 10039. (b) J. P. Lewtak, D. T. Gryko, *Chem. Commun.* **2012**, *48*, 10069. (c) H. Mori, T. Tanaka, A. Osuka, *J. Mater. Chem. C* **2013**, *1*, 2500. (d) M. Stępień, E. Gońka, M. Żyła, N. Sprutta, *Chem. Rev.* **2016**, ASAP (DOI: 10.1021/acs.chemrev.6b00076).

9 D. Myśliwiec, B. Donnio, P. J. Chmielewski, B. Heinrich, M. Stepień, *J. Am. Chem. Soc.* **2012**, *134*, 4822. (b) H. Boedigheimer, G. M. Ferrence, T. D. Lash, *J. Org. Chem.* **2010**, *75*, 2518. (c) L. Jiang, J. T. Engle, L. Sirk, C. S. Hartley, C. J. Ziegler, H. Wang, *Org. Lett.* **2011**, *13*, 3020.

10 (a) H. Aihara, L. Jaquinod, D. J. Nurco, K. M. Smith, *Angew. Chem. Int. Ed.* **2001**, *40*, 3439. (b) M. Nath, J. C. Huffman, J. M. Zaleski, *J. Am. Chem. Soc.* **2003**, *125*, 11484. (c) L. J. K. Boerner, S. Mazumder, M. Pink, M.-H. Baik, J. M. Zaleski, *Chem. Eur. J.* **2011**, *17*, 14539.

11 (a) K. Kurotobi, K. S. Kim, S. B. Noh, D. Kim, A. Osuka, *Angew. Chem. Int. Ed.* **2006**, *45*, 3944. (b) H. S. Gill, M. Harmjanz, J. Santamaria, I. Finger, M. J. Scott, *Angew. Chem. Int. Ed*. **2004**, *43*, 485. (c) C. Maeda, T. Yoneda, N. Aratani, M.-C. Yoon, J. M. Lim, D. Kim, N. Yoshioka, A. Osuka, *Angew. Chem. Int. Ed.* **2011**, *50*, 5691. (d) S. Nakamura, S. Hiroto, H. Shinokubo, *Chem. Sci.* **2012**, *3*, 524.

12 (a) N. K. S. Davis, A. L. Thompson, H. L. Anderson, *J. Am. Chem. Soc.* **2011**, *133*, 30. (b) N. K. S. Davis, A. L. Thompson, H. L. Anderson, *Org. Lett.* **2010**, *12*, 2124. (c) A. N. Cammidge, P. J. Scaife, G. Berber, D. L. Hughes, *Org. Lett.* **2005**, *7*, 3413.

13 (a) A. Tsuda, A. Osuka, *Science* **2001**, *293*, 79. (b) Y. Nakamura, N. Aratani, H. Shinokubo, A. Takagi, T. Kawai, T. Matsumoto, Z. S. Yoon, D. Y. Kim, T. K. Ahn, D. Kim, A. Muranaka, N. Kobayashi, A. Osuka, *J. Am. Chem. Soc.* **2006**, *128*, 4119.

14 (a) S. Fox, R. W. Boyle, *Chem. Commun.* **2004**, 1322. (b) D.-M. Shen, C. Liu, Q.-Y. Chen, *Chem. Commun.* **2005**, 4982. (c) D.-M. Shen, C. Liu, Q.-Y. Chen, *J. Org. Chem.* **2006**, *71*, 6508. (d) S. Hayashi, Y. Matsubara, S. Eu, H. Hayashi, T. Umeyama, Y. Matano, H. Imahori, *Chem. Lett.* **2008**, 846. (e) T. D. Lash, B. E. Smith, M. J. Melquist, B. A. Godfrey, *J. Org. Chem.* **2011**, *76*, 5335.

15 P. K. Kumar, P. Bhyrappa, B. Varghese, *Tetrahedron Lett.* **2003**, *44*, 4849.

16 B. D. Steinberg, E. A. Jackson, A. S. Filatov, A. Wakamiya, M. A. Petrukhina, L. T. Scott, *J. Am. Chem. Soc.* **2009**, *131*, 10537.

17 S. Higashibayashi, H. Sakurai, *Chem. Lett.* **2007**, *36*, 18.

18 The pyridine molecule was originally ligated on the central Zn^{II} of **4** during the recrystallization. Judging from the chemical shifts observed, the pyridine molecule dissociates from the Zn^{II} center upon dissolving into DMSO-d_6.

19 The crystal structure of **2** having THF as the axial ligand has been reported by Shen *et al.* (ref 14c).

20 (a) Y. Mitsushige, S. Yamaguchi, B. S. Lee, Y. M. Sung, S. Kuhri, C. A. Schierl, D. M. Guldi, D. Kim, Y. Matsuo, *J. Am. Chem. Soc.* **2012**, *134*, 16540. (b) H. Fliegl, N. Özcan, R. Mera-Adasme, F. Pichierri, J. Jusélius, D. Sundholm, *Mol. Phys.* **2013**, *111*, 1364.

21 (a) A. Nakano, N. Aratani, H. Furuta, A. Osuka, *Chem. Commun.* **2001**, 1920. (b) A. K. Sahoo, S. Mori, H. Shinokubo, A. Osuka, *Angew. Chem. Int. Ed.* **2006**, *45*, 7972. (c) N. Fukui, H. Yorimitsu, J. M. Lim, D. Kim, A. Osuka, *Angew. Chem. Int. Ed.* **2014**, *53*, 4395.

22 (a) N. Fukui, W.-Y. Cha, S. Lee, S. Tokuji, D. Kim, H. Yorimitsu, A. Osuka, *Angew. Chem. Int. Ed.* **2013**, *52*, 9728. (b) K. Ota, T. Tanaka, A. Osuka, *Org. Lett.* **2014**, *16*, 2974.

23 The symbol of (1) represents that the NICS values are estimated at 1 Å above from the π-conjugated planes: (a) P. von Ragué Schleyer, C. Maerker, A. Dransfeld, H. Jiao, N. J. R. van Eikema Hommes, *J. Am. Chem. Soc.* **1996**, *118*, 6317. (b) J. A. N. F. Gomes, R. B. Mallion, *Chem. Rev.* **2001**, *101*, 1349.

24 (a) T. Ito, Y. Hayashi, S. Shimizu, J.-Y. Shin, N. Kobayashi, H. Shinokubo, *Angew. Chem. Int. Ed.* **2012**, *51*, 8542. (b) S. Mori, A. Osuka, *J. Am. Chem. Soc.* **2005**, *127*, 8030.

25 As shown in Table 2-6, the main contribution to the lowest-energy absorption band stems from the HOMO to LUMO π-π* transition commonly for all the ring-fused porphyrins; however, other π-π* transitions also contribute to the lowest-energy absorptions of the fused porphyrins as minor components.

26 (a) J. Michl, *J. Am. Chem. Soc.* **1978**, *100*, 6801. (b) A. Ceulemans, W. Oldenhof, C. Gorller-Walrand, L. G. Vanquickenborne, *J. Am. Chem. Soc.* **1986**, *108*, 1155.

27 (a) J. Mack, M. J. Stillman, N. Kobayashi, *Coord. Chem. Rev.* **2007**, *251*, 429. (b) J. Mack, M. J. Stillman, *Coord. Chem. Rev.* **2001**, *219-221*, 993.

28 (a) A. Muranaka, M. Yokoyama, Y. Matsumoto, M. Uchiyama, A. Tsuda, A. Osuka, N. Kobayashi, *ChemPhysChem* **2005**, *6*, 171. (b) J. Mack, Y. Asano, N. Kobayashi, M. J. Stillman, *J. Am. Chem. Soc.* **2005**, *127*, 17697. (c) S. Sripothongnak, C. J. Ziegler, M. R. Dahlby, V. N. Nemykin, *Inorg. Chem.* **2011**, *50*, 6902.

29 (a) J. Michl, *J. Am. Chem. Soc.* **1978**, *100*, 6812. (b) J. Michl, *J. Am. Chem. Soc.* **1978**, *100*, 6819. (c) J. Michl, *Pure Appl. Chem.* **1980**, *52*, 1549.

30 J. D. Keegan, A. M. Stolzenberg, Y.-C. Lu, R. E. Linder, G. Barth, A. Moscowitz, E. Bunnenberg, C. Djerassi, *J. Am. Chem. Soc.* **1982**, *104*, 4317.

31 The reduction potential of TBPAH was determined by the cyclic voltammogram in THF containing 0.1 M $TBAPF_6$ as an electrolyte at 298 K.

32 K. Ichimori, H. Ohya-Nishiguchi, N. Hirota, *Bull. Chem. Soc. Jpn.* **1988**, *61*, 2753.

33 J. Ruiz, D. C. Astruc, *C. R. Acad. Sci. Paris, Chimie* **1998**, *1*, 21.

34 (a) R. H. Felton, H. Linschitz, *J. Am. Chem. Soc.* **1966**, *88*, 1113. (b) G. L. Closs, L. E. Closs, *J. Am. Chem. Soc.* **1963**, *85*, 818. (c) J. Seth, D. F. Bocian, *J. Am. Chem. Soc.* **1994**, *116*, 143. (d) J. Pawlik, G. Lileta, S. Karabunarliev, M. Baugmgarten, *Chem. Phys.* **1997**, *221*, 121.

35 T. Vangberg, R. Lie, A. Ghosh, *J. Am. Chem. Soc.* **2002**, *124*, 8122.

36 K. Yoshizawa, T. Nakayama, T. Kamachi, P. M. Kozlowski, *J. Phys. Chem. A* **2007**, *111*, 852.

37 J. S. Lindsey, R. W. Wagner, *J. Org. Chem.* **1989**, *54*, 828.

38 T. Leermann, F. R. Leroux, F. Colobert, *Org. Lett.* **2011**, *13*, 4479.

39 Y. Nakayama, Y. Baba, H. Yasuda, K. Kawakita, N. Ueyama, *Macromolecules* **2003**, *36*, 7953.

40 G. M. Sheldrick, SIR97 and SHELX97, Programs for Crystal Structure Refinement, University of Göttingen, Göttingen (Germany), 1997.

41 P. V. D. Sluis, A. L. Spek, *Acta Crystallogr.* **1990**, *A46*, 194.

Chapter 3

Substituent effects of Zn^{II} complexes of quadruply fused-porphyrins

3-1. Introduction

Porphyrin and its derivatives have been well studied as a representative compound having a large π-conjugated aromatic circuit with a planar structure.[1] Porphyrin and its derivatives exhibit strong absorption bands so-called as Soret and Q bands in the visible region, and, utilizing the strong absorption, porphyrins exhibit light-harvesting properties in the natural photosynthesis[2] and artificial photovoltaic cells.[3] To enhance the characteristic optical properties of porphyrins, introduction of substituents to porphyrin derivatives have been intensively performed so far;[4] as a result, substituents at the *β*- and *meso*-positions of porphyrins induced large shifts of redox potentials and absorption bands;[5] for instance, the differences between the mono *β*-nitro-substituted and non-substituted porphyrin derivatives in the redox potentials for the first reduction process have been reported to be 0.35 V.[5c] However, the substituents effect at the *meso*-aryl groups of tetraphenylporphyrin derivatives is not so significant, because of the cleavage of the π-conjugation between the porphyrin core and the *meso*-aryl groups.[5b]

In recent years, introduction of fused rings at the periphery of a porphyrin aromatic circuit has been intensively studied,[6-19] because of the characteristic physical properties derived from the narrowed HOMO-LUMO gaps. Due to such unique properties, porphyrins having exocyclic fused rings are considered to be attractive candidates as components to construct optoelectronic devices such as dye-sensitized solar cells.[15] However, synthesis of precursors to obtain the porphyrins bearing fused aromatic moieties at the periphery is generally difficult, since it requires complicated processes.[16,17] For example, ring-fusing reactions by an oxidative process has been reported to require activation of the aryl moieties, to be fused with the porphyrin core, by introduction of electron-donating groups; otherwise, ring-fusion of non-activated aryl moieties with the porphyrin core did not proceed under similar conditions.[16,18] Therefore, substituents possible to be introduced to the ring-fused porphyrins to finely control the physical properties are highly limited and the process is time-consuming.[17] In consequence, substituent effects on the optical and electrochemical properties of ring-fused porphyrins have yet to be systematically investigated so far.[18,19a]

In Chapter 2 of this thesis, the author has described the synthesis of a novel ring-fused porphyrin, quadruply-fused porphyrin (QFP, **4a**) with a facile and efficient procedure using direct C-H activation catalyzed by Pd clusters derived from $[Pd^{II}(\eta^3\text{-}C_3H_5)Cl]_2$.[20] The precursor of **4a**, zinc(II) 2,3,12,13-tetrabromo-tetraphenylporphyrinate ($ZnTPPBr_4$, **5a**), can be easily prepared with a two-step procedure starting from TPP.[21] Therefore, QFP derivatives can be synthesized using tetraarylporphyrin precursors having various substituents, which can be easily obtained. In this chapter, significant substituent effects at the *para*-positions of the fused *meso*-aryl groups of the ZnQFP derivatives have been clarified on their optical and electrochemical properties and the crystal structures; the sensitiveness to the

electronic properties of the substituents is based on the expansion of the π-conjugated circuits to the fused *meso*-aryl groups.

3-2. Synthesis

To elucidate the impact of substituents on the electronic characteristics of QFP, various functional groups has introduced at the *para*-positions of the four *meso*-phenyl groups of the $ZnTPPBr_4$ precursor, $ZnT(Ar)PBr_4$ (**5x**; **x** = **a**, **c** – **f**), as precursors of Zn^{II}QFP derivatives (**4x**; **x** = **a**, **c** – **f**) (Scheme 3-1). Syntheses of the derivatives, **5x**, were done as follows: the tetra-*meso*-aryl porphyrins (**6x**; **x** = **a**, **c** – **f**) were brominated with *N*-bromosuccinimide (NBS) at the four *β*-carbons. As for the syntheses of **4x**, the C-C bond formation was performed on **5x** with Pd clusters derived from $[Pd(\eta^3\text{-}C_3H_5)Cl]_2$[22] as the catalyst in 1,4-dioxane. The yields of the derivatives are 72% for **4c** with *tert*-butyl groups, 65% for **4d** with methoxy groups, 22% for **4e** with methoxycarbonyl groups and 22% for **4f** with trifluoromethyl groups. The low yields of **4e** and **4f** are not caused by the low reaction efficiency but by the low solubility of the products to cause difficulty in the isolation. The characterization of the derivatives was done by ^{1}H NMR spectroscopy, MALDI-TOF-MS spectrometry, and elemental analysis.

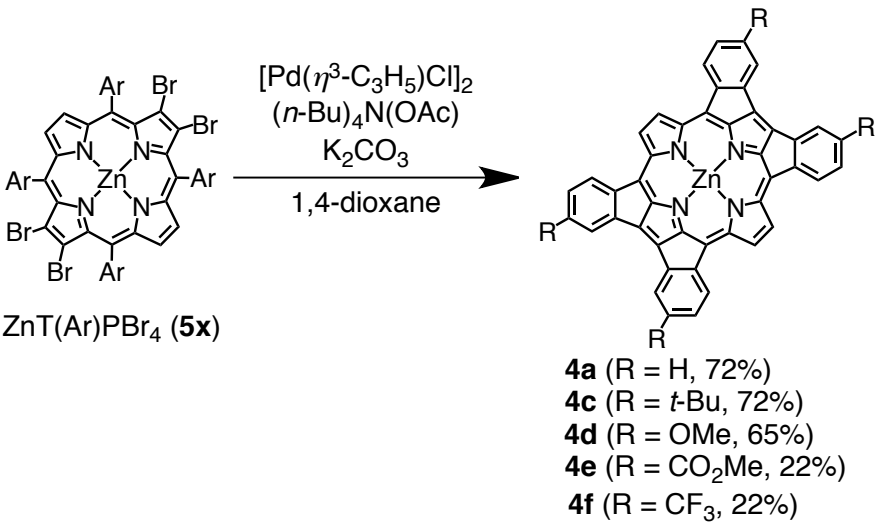

Scheme 3-1. Syntheses of quadruply-fused porphyrin derivatives having substituents at the fused *meso*-aryl groups.

3-3. Substituents effects on crystal structures

In Chapter 2 of this thesis,[20] the crystal structure of **4a**-py has been described (the molecule mentioned after hyphen indicates the axial ligand on the central Zn^{II} ion). In this section, the author clarifies crystal structures of QFP derivatives, **4c**-py, **4c**-dox (dox = 1,4-dioxane), **4d**-py and **4f**-py (Figure 3-1). The representative bond lengths and other structural parameters of the crystal structures are summarized in Table 3-1. One of the most important structural characteristics of QFP is elongation of the C_{ipso}-C_{ortho} bonds of the fused rings; the elongation derives from the expansion of the π-conjugation circuits to the fused benzene rings. As a result of the π-expansion, not only 18π, the

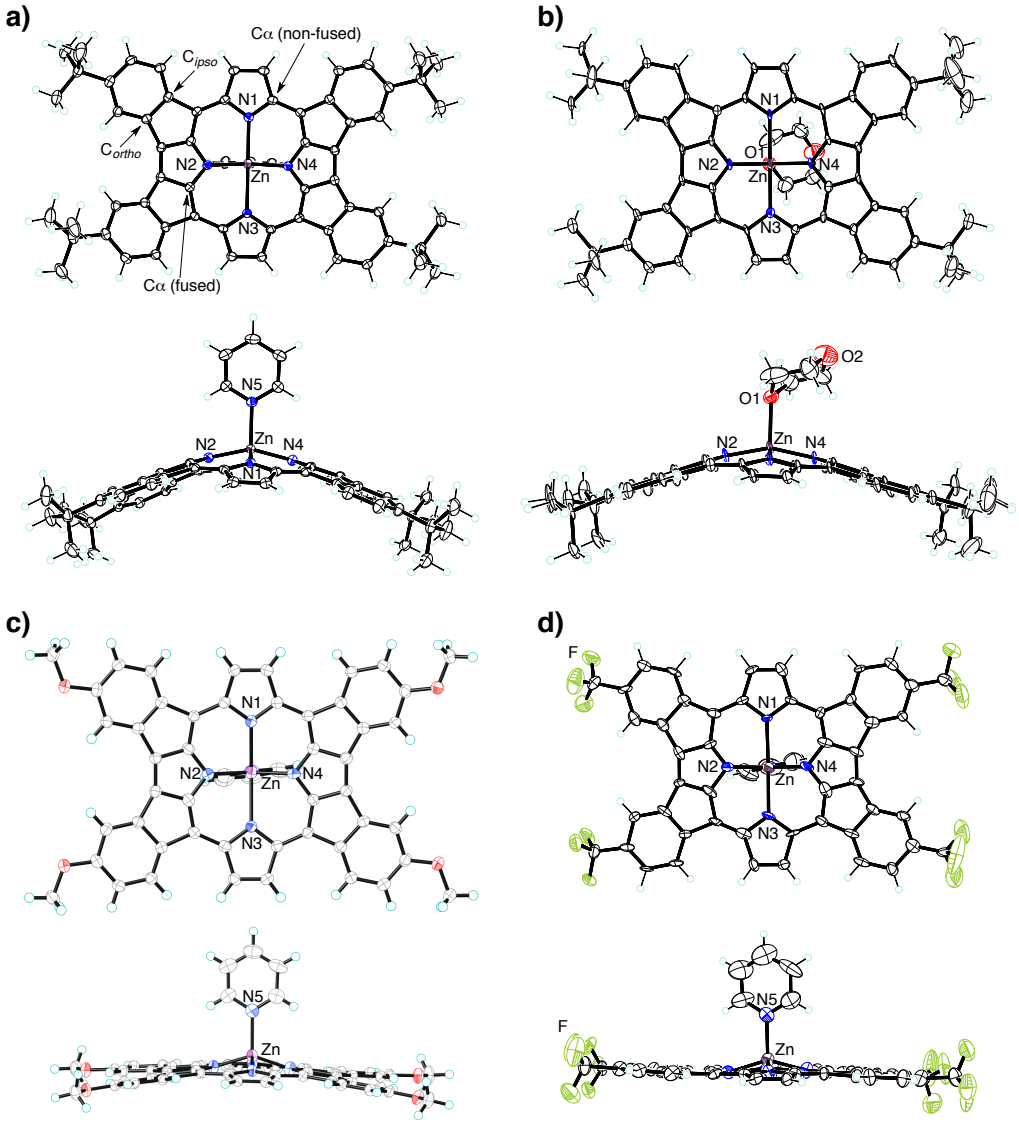

Figure 3-1. Top and side views of crystal structures of **4c**-py (a), **4c**-dox (b), **4d**-py (c) and **4f**-py (d). The thermal ellipsoids are drawn with 50% probability. Green-colored atoms in (c) indicate fluorine atoms.

most typical number of π-electrons accompanying the aromatic circuit for porphyrins, but also 20π, 22π, 24π, 26π, and 30π aromatic circuits can be drawn and the contribution of each aromatic circuit significantly affects the magnetic properties of QFP (see Chapter 2).[20] The characteristic elongation of the C_{ipso}-C_{ortho} bond distances is also observed for **4c**-py, **4c**-dox, **4d**-py and **4f**-py; the mean values of the C_{ipso}-C_{ortho} bond distances are 1.43, 1.43, 1.44 and 1.44 Å for **4c**-py, **4c**-dox, **4d**-py and **4f**-py, respectively, and they are significantly longer than that of the typical C-C bond in a benzene ring (*ca.* 1.38 Å)[23] and comparable to the value for **4a**-py (1.44 Å).[20] Bond lengths and angles are very similar to each other among **4a**-py, **4c**-X (X = py or dox), **4d**-py and **4f**-py; however, there are significant differences found in the degree of conformational distortion of the porphyrin cores among **4a**-py, **4c**-X, **4d**-py and **4f**-py. The molecules of **4a**-py and **4c**-X showed a dome-type distortion[24] and the mean deviations of the 48 core atoms of the porphyrin

mean-plane are 0.212, 0.501 and 0.390 Å for **4a**-py, **4c**-py and **4c**-dox, respectively (Figure 3-2a, b, c). In contrast, **4d**-py and **4f**-py are almost planar and the mean deviations are 0.151 Å and 0.056 Å for **4d**-py and **4f**-py, respectively (Figure 3-2d and e). On the other hand, the deviations of the zinc ions from the porphyrin mean-planes are 0.937, 1.452, 1.181 0.879 and 0.586 Å for **4a**-py, **4c**-py, **4c**-dox, **4d**-py and **4f**-py (mean value for the two independent zinc centers), respectively. In addition, the porphyrin plane of **4c**-X forms a bowl-like shape including the central zinc ion and the resulting smooth curvature was observed, whereas the zinc center deviates from the flat porphyrin plane in **4d**-py and **4f**-py (Figure 3-2). The bond lengths are very similar for **4a**-py, **4c**-X, **4d**-py and **4f**-py as mentioned above and

Table 3-2. Selected bond lengths and other structural data for **4a**-py, **4c**-X, **4d**-py and **4f**-py

	4a-py	**4c**-py	**4c**-dox	**4d**-py	**4f**-py
Meso-substituent	H	*t*-Bu	*t*-Bu	OMe	CF_3
Zn-N1 / Å	2.277(2)	2.1959(12)	2.280(4)	2.304(3)	2.313(7), 2.206(8)
Zn-N2 / Å	1.900(2)	1.9301(12)	1.892(4)	1.884(3)	1.86(1), 1.883(9)
Zn-N3 / Å	2.268(2)	2.4340(12)	2.276(3)	2.236(3)	2.23(1), 2.272(9)
Zn-N4 / Å	1.894(2)	1.9284(12)	1.897(4)	1.887(3)	1.90(1), 1.840(9)
Zn-X(axial) / Å	2.079(2) (X = N)	2.0999(12) (X = N)	2.135(4) (X = O)	2.095(4) (X = N)	2.10(1), 2.078(7) (X = N)
N-Cα (fused, av) / Å	1.356	1.359	1.358	1.350	1.36
N-Cα (non-fused, av) / Å	1.371	1.376	1.377	1.369	1.38
C_{ipso}-C_{ortho} (fused, av) / Å	1.436	1.431	1.431	1.439	1.43, 1.44
C-C (por core, total) / Å	28.229	28.285	28.235	28.125	28.18, 28.26
N1···N3 / Å	4.423(3)	4.460(2)	4.462(5)	4.411(5)	4.44(1), 4.41(1)
N2···N4 / Å	3.361(3)	3.748(2)	3.714(5)	3.592(5)	3.59(1), 3.59(1)
Mean deviation / Å	0.212	0.501	0.390	0.151	0.070, 0.061
Zn from the plane / Å	0.937	1.452	1.181	0.879	0.594, 0.578

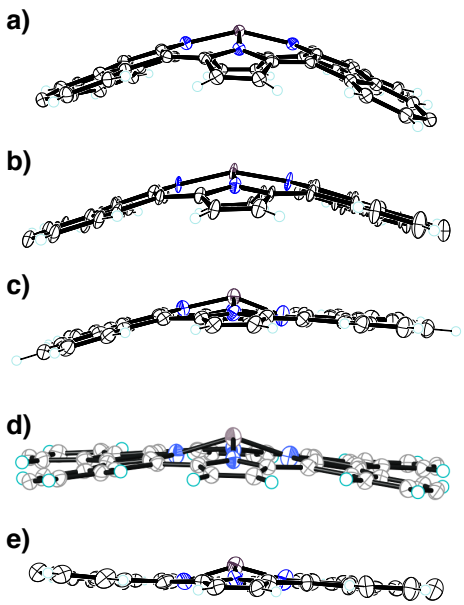

Figure 3-2. Side views of porphyrin cores consisting of 48 atoms of **4c**-py (a), **4c**-dox (b), **4a**-py (c), **4d**-py (d) and **4f**-py. The thermal ellipsoids are drawn with 50% probability. The axial ligands and the substituents at the *para*-positions are omitted for clarity.

the only difference found was in the atom distance between the nitrogen atoms of the fused pyrrole ring (N2···N4) (Table 3-2). Therefore, the substituents at the fused phenyl rings do not affect the size of the porphyrin core so significantly. These results indicate that the dome-like distortion do not depend on the electronic properties of substituents at the fused *meso*-aryl groups, and the clear reason of this substituents effect on the QFP structure has yet to be elucidated.

3-4. Substituent effects on optical and electrochemical properties

The optical and electrochemical properties of ZnQFP are largely affected by the substituents at the *para*-position of the fused *meso*-aryl groups. The introduction of substituents at the *para*-positions of the fused aryl groups caused bathochromic shifts of the absorption bands for all the four derivatives, **4c** – **4f**, relative to those of **4a** (Table 3-3 and Figure 3-3). Comparing the shift widths in an energy unit (cm^{-1}) with those of ZnTPP and the derivatives, the absorption bands of ZnQFP derivatives are 10 times more affected by the substituents than those of ZnTPP; for instance, the methoxy-substituted ZnQFP, **4d**, exhibits the longest Q-band at 1200 nm (8330 cm^{-1}) in *N*,*N*-dimethylformamide (DMF) and the shift width relative to that of **4a** is 1460 cm^{-1}, whereas the shift width of the Q-band for ZnT(*p*-OMe)PP to that of ZnTPP is only 110 cm^{-1}. As mentioned above, the absorption bands of the ZnQFP derivatives are highly affected by the *meso*-aryl substituents, whereas the direction and width of the shifts is not correlated with the electronic properties of the substituents. Both the electron-withdrawing and -donating groups cause red shifts of the absorption bands. To shed light on the substituent effects for the influence of the energy levels of the frontier orbitals that most

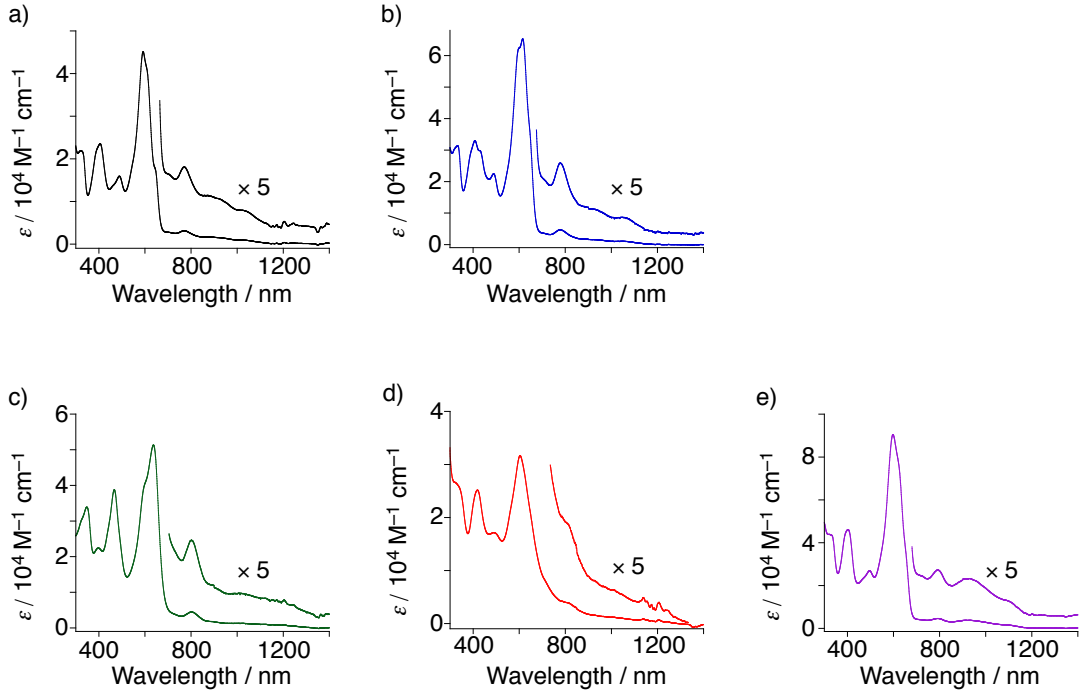

Figure 3-3. UV-Vis spectra of the ZnQFP derivative in DMF at 298 K; (a) **4a**, (b) **4c**, (c) **4d**, (d) **4e** and (e) **4f**.

directly relate to the π-π* transitions,[25] electrochemical studies were performed on the ZnQFP derivatives to determine the redox potentials of the ZnQFP and ZnTPP derivatives (Figure 3-4). The redox potentials are also summarized in Table 3-3. Both the potentials for the first reduction and first oxidation processes, E_{Red1} and E_{Ox1}, of the ZnQFP derivatives were positively shifted upon introducing electron-withdrawing groups (Figure 3-4). E_{Ox1} of the ZnQFP derivatives is more sensitive to the substituents than E_{Red1}; the differences in the potentials between the most electron-donating methoxy derivative, **4d**, and the most electron-withdrawing trifluoromethyl one, **4f**, are 0.51 V for E_{Ox1} (+0.37 V for **4d** and +0.88 V vs SCE for **4f**), whereas that for E_{Red1} is only 0.05 V (–0.71 V for **4d** and –0.66 V vs SCE for **4f**). On the other hand, the redox potentials of the ZnTPP derivatives are less sensitive to the substituents of the *meso*-aryl groups. To confirm this tendency in the substituent effects on the redox potentials, Hammett plots were provided (Figure 3-5). A Hammett parameter, σ_p^+,[26] was the best fit for the present studies. Consequently, the plots of the redox potentials against σ_p^+ exhibited good linearity and the coefficients, ρ, were obtained to be +0.098 and +0.009 for E_{Ox1} and E_{Red1} of ZnQFPs, respectively, and +0.039 and +0.035 for E_{Ox1} and E_{Red1} of ZnTPPs, respectively. As indicated by the ρ values, E_{Ox1} of ZnQFP is sensitive to the substituents than the E_{Red1}, and the redox potentials of ZnQFP are more significantly affected by the substituents than those of ZnTPP.[27] This sensitiveness can be accounted for by the distribution of the electron densities in the frontier orbitals (Figure 3-6). The DFT-calculated HOMO and LUMO show large distribution on the *meso*-aryl groups due to the ring-fusion and resultant expansion of the

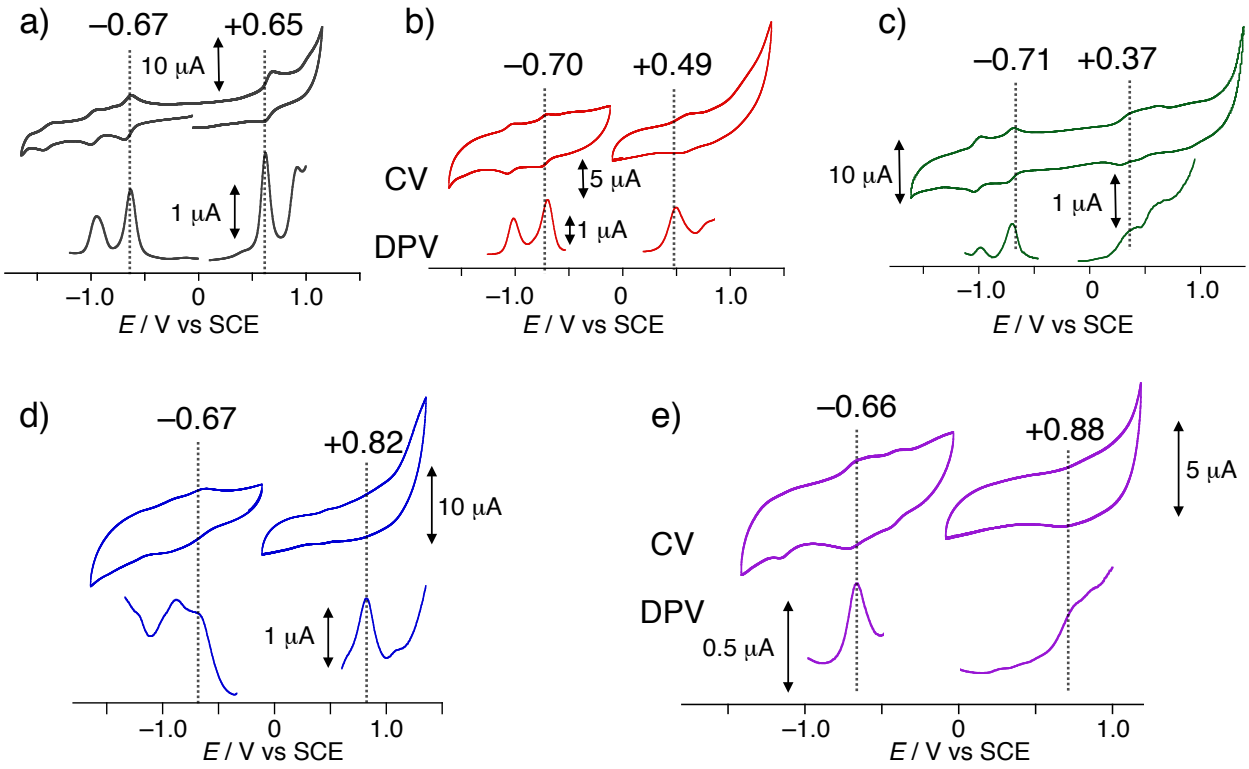

Figure 3-4. Cyclic (above) and differential-pulse (below) voltammograms of the ZnQFP derivatives in DMF containing 0.1 M $TBAPF_6$ as an electrolyte at room temperature; (a) **4a**, (b) **4c**, (c) **4d**, (d) **4e** and (e) **4f**.

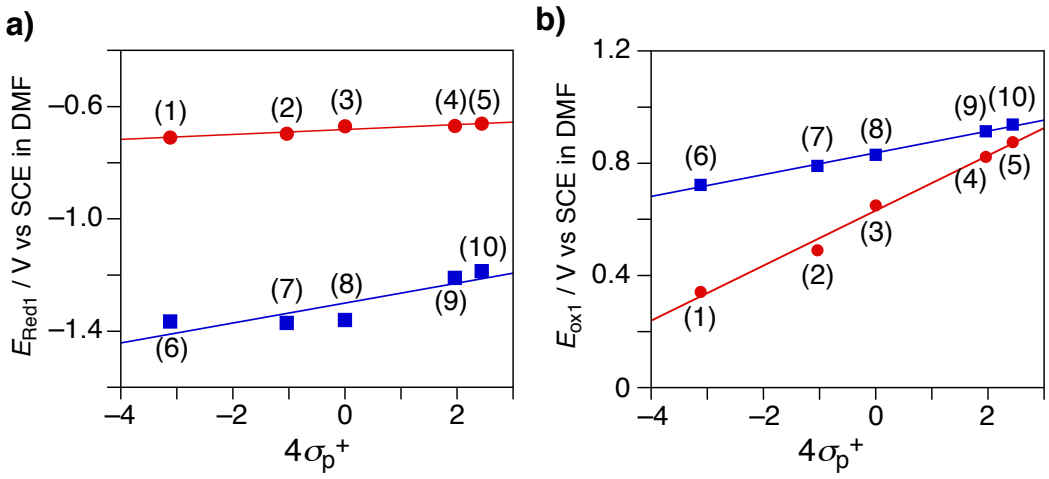

Figure 3-5. Hammett plots of E_{Red1} (a) and E_{Ox1} (b) of the ZnQFP and ZnTPP derivatives ((1) **4d**, (2) **4c**, (3) **4a**, (4) **4e**, (5) **4f**, (6) ZnT(*p*-OMe)PP, (7) ZnT(*p*-*t*Bu)PP, (8) ZnTPP, (9) ZnT(*p*-CO_2Me)PP, and (10) ZnT(*p*-CF_3)PP) against $4\sigma_p^+$. Solvent: DMF containing 0.1 M $TBAPF_6$ (TBA = tetra(*n*-butyl)ammonium). Values of σ_p^+ are taken from ref. 26.

Table 3-3. Absorption maxima and redox potentials of QFP and ZnTPP derivatives in DMF

	λ_{max}(B)[a]	ν(B)[b]	$\Delta\nu$(B)[b]	λ_{max}(Q)[a]	ν(Q)[b]	$\Delta\nu$(Q)[b]	E_{Red1}[c]	E_{Ox1}[c]	$E_{Ox1} - E_{Red1}$[d]
4a (R = H)	592	16900	—	1021	9790	—	–0.67	+0.65	1.32
4c (R = *t*-Bu)	616	16230	–670	1060	9430	–360	–0.70	+0.49	1.19
4d (R = OMe)	637	15700	–1200	1200	8330	–1460	–0.71	+0.37	1.08
4e (R = CO_2Me)	616	16230	–670	1046	9560	–230	–0.67	+0.82	1.49
4f (R = CF_3)	598	16840	–60	1104	9060	–730	–0.66	+0.88	1.54
ZnTPP	425	23530	0	599	16690	0	–1.36	+0.83	2.19
ZnT(*p*-*t*Bu)PP	427	23420	–110	601	16640	–50	–1.37	+0.79	2.16
ZnT(*p*-OMe)PP	429	23310	–220	603	16580	–110	–1.36	+0.74	2.10
ZnT(*p*-CO_2Me)PP	429	23310	–220	600	16660	–30	–1.21	+0.91	2.12
ZnT(*p*-CF_3)PP	426	23 470	–60	597	16750	60	–1.19	+0.94	2.13

[a] in nm, [b] in cm^{-1}, [c] in vs SCE, [d] in V.

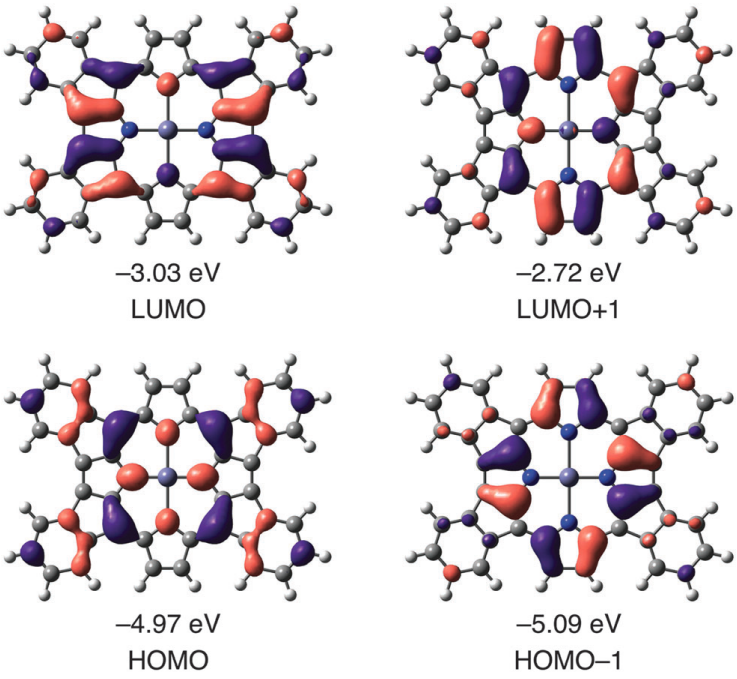

Figure 3-6. The frontier orbitals of **4a** calculated at the B3LYP/6-31G(d) level of theory.

π-conjugation. In particular, the *para*-position of the fused *meso*-aryl groups has large electron density in the HOMO, but no distribution of the LUMO, which causes high sensitivity of the HOMO-related E_{Ox1} and low sensitivity of LUMO-related E_{Red1} to the substituents.

3-5. Summary

Novel quadruply-fused porphyrin derivatives having substituents at the *para*-positions of fused *meso*-aryl groups have been synthesized and characterized by spectroscopic and electrochemical measurements and X-ray crystallography. The author has revealed the substituent effects at the fused *meso*-aryl groups of QFP on the crystal structures, absorption spectra and redox potentials. The introduction of substituents at the *para*-positions of the fused aryl groups caused large bathochromic shifts of the absorption bands for all the four derivatives. Direct introduction of substituents to the aromatic circuit of QFPs significantly affect the first oxidation potentials than that of *meso*-aryl substituted Zn^{II}TPPs, although the first reduction potential is not so influenced by the substitution. Thus, the HOMO level is more strongly affected by the introduction of the substituents at the *para*-porisition of the fused *meso*-aryl groups than the LUMO level.

3-6. Experimental section

General.

Chemicals and solvents were used as received from commercial sources unless otherwise mentioned. 1,4-Dioxane for the synthesis was distilled over Na/benzophenone before use. DMF for the electrochemical measurements was distilled before use. Synthesis of Zn^{II} tetrabromo-porphyrinate derivatives, **5a**, was performed with

the reported procedures.[21] ^{1}H NMR measurements were performed on a Bruker AVANCE400 spectrometer operating at 400 MHz for ^{1}H nuclei. UV-Vis absorption spectra were measured at room temperature in DMF on a Shimadzu UV-3600 spectrophotometer. MALDI-TOF- MS spectrometry was performed on an AB SCIEX TOF/TOF 5800 spectrometer by using dithranol as a matrix. Electrochemical experiments were done under an atmospheric pressure of Ar at 298 K with an ALS/CH electrochemical analyzer model 710D.

Synthesis.

A general procedure of Pd-catalyzed ring-fusing reactions using Pd-nanoclusters with [Pd(η^3- C_3H_5)Cl]$_2$.[20, 22] A solution of TBA·OAc (TBA = tetra(*n*-butyl)ammonium, 627 mg, 2.08 mmol), allyl palladium(II) chloride dimer (3.53 mg, 9.65 μmol), and potassium carbonate (279 mg, 2.03 mmol) in 1,4-dioxane (1.0 mL) was heated at 110 ºC for 3 min.

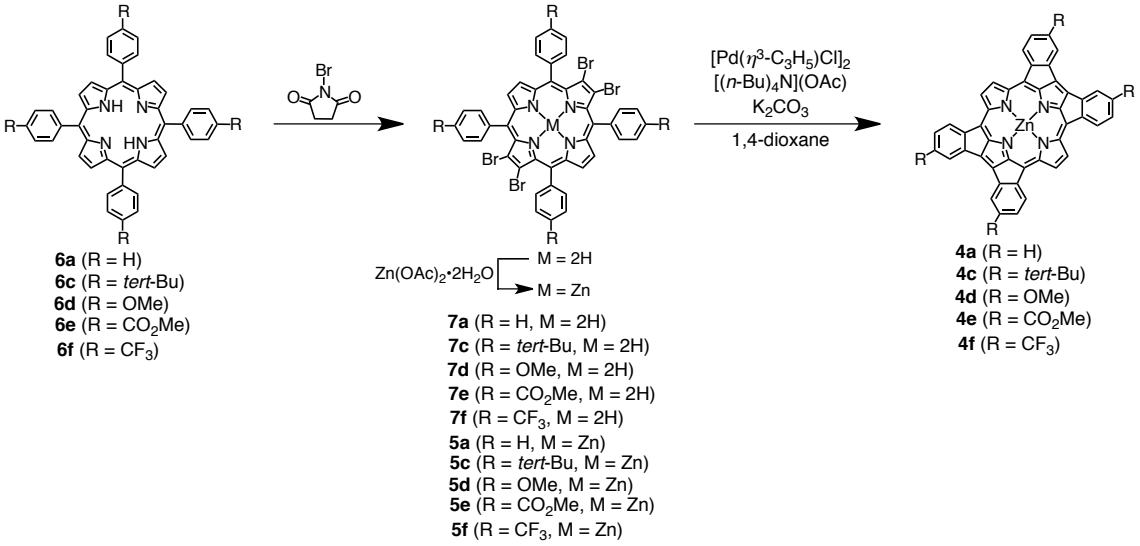

Scheme 3-2. Synthetic route of quadruply-fused porphyrins.

After the color of the solution changed to black, a tetrabromo-derivative of porphyrin **5x** (50 μmol) was quickly added to the solution. After stirring for 11 h, the reaction mixture was cooled to ambient temperature. The volatiles were removed under vacuum and the residual solid was washed with water. The solid was dissolved in pyridine and the precipitate including the palladium catalyst was filtered off. The filtrate was dried under vacuum to give black powder and the black powder was recrystallized from the THF solution in the presence of one drop of pyridine by depositing ethanol vapor as a poor solvent. The crystals obtained was filtered and washed with THF to give a red-purple filtrate. The remaining dark red solid mainly involved the quadruply-fused derivative and the further recrystallization by vapor deposition of ethanol to the THF solution in the presence of one drop of pyridine to give pure QFP derivative.

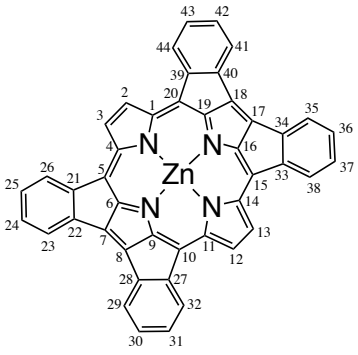

Zinc(II) 24,30,36,42-tetrakis(*tert*-butyl)-quadruply-fused porphyrinato (4c). A ring-fusion reaction was performed utilizing **5c** (130.3 mg, 107 μmol) as a starting

material to obtain **4c**, using the aforementioned general procedure. After filtration, the precipitate obtained was chromatographed on a bio-beads S-X1 gel using THF as an eluent. The second fraction was collected and the solvent was removed under vacuum. The residual solid was recrystallized from THF/ethanol (1:3, v/v) and dried under vacuum to give **4c** (69.0 mg, 77.1 μmol, 72%). m.p.: > 300 ºC. ^{1}H NMR (DMSO-d_6): δ 7.89 (s, 4H, 2, 3,12,13-β-H), 7.20 (d, J = 8.0 Hz, 4H, 26,32,38,44-Ph-H), 6.87 (s, 4H, 23,29,35,41-Ph-H), 6.74 (m, 4H, 25,31,37,43-Ph-H), 1.32 (s, 36H, *tert*-Bu-H). UV-vis (DMF): λ_{max} [nm] (log (ε, M^{-1} cm^{-1})) = 334 (4.49), 408 (4.52), 489 (4.34), 616 (4.81), 778 (3.72), 934 (3.38), 1060 (3.26). MS (MALDI-TOF, *dithranol matrix*): *m/z* = 892.4 (calcd. for $[M]^+$: 892.4). Anal. calcd. for $C_{60}H_{52}N_4Zn\cdot H_2O\cdot C_5H_5N$: C 78.73, H 6.00, N 7.06; found: C 78.66, H 5.82, N 6.98.

Zinc(II) 24,30,36,42-tetramethoxy-quadruply-fused porphyrinato (4d). A ring-fusion reaction using the above-mentioned general procedure was performed utilizing **5d** (59.7 mg, 53.6 μmol) as a starting material to obtain **4d**. After filtration, the precipitate obtained was chromatographed on a bio-beads S-X1 gel using THF as an eluent. The second fraction was collected and the solvent was removed under vacuum. The residual solid was recrystallized from THF/ethanol (1:3, v/v) and dried under vacuum to give **4d** (27.8 mg, 35.3 μmol, 65%). m.p.: > 300 ºC. ^{1}H NMR (DMSO-d_6): δ 8.09 (s, 4H, 2, 3,12,13-β-H), 7.41 (d, J = 7.4 Hz, 4H, 26,32,38,44-Ph-H), 6.70 (s, 4H, 23,29,35,41-Ph-H), 6.37 (m, 4H, 25,31,37,43- Ph-H), 3.81 (s, 12H, methoxy-H). UV-vis (DMF): λ_{max} [nm] (log (ε, M^{-1} cm^{-1})) = 347 (4.52), 399 (4.34), 467 (4.59), 637 (4.71), 803 (3.66), 913 (3.26), 1026 (3.11), 1200 (2.99). MS (MALDI-TOF, *dithranol matrix*): *m/z* = 788.5 (calcd. for $[M]^+$: 788.1). Anal. calcd. for $C_{48}H_{28}N_4O_4Zn\cdot 0.5H_2O\cdot 0.25THF\cdot 0.5CH_2Cl_2$: C 69.16, H 3.75, N 6.52; found: C 68.99, H 3.79, N 6.29.

Zinc(II) 24,30,36,42-tetra(methoxycarbonyl)-quadruply-fused porphyrinato (4e). A ring-fusion reaction using the general procedure mentioned above was performed utilizing **5e** (61.5 mg, 50.2 μmol) as a starting material to obtain **4e**. After filtration, the collected solid was recrystallized from pyridine/ethanol (1:3, v/v) and dried under vacuum to give pure **4e** (10.4 mg, 11.0 μmol, 22%). m.p.: > 300 ºC. ^{1}H NMR (DMSO-d_6): δ 8.28 (s, 4H, 2, 3,12,13-β-H), 7.74 (m, 4H, 26,32,38,44-Ph-H), 7.52 – 7.42 (m, 8H, 23,25,29,31,35,37,41,43-Ph-H). UV-vis (DMF): λ_{max} [nm] (log (ε, M^{-1} cm^{-1})) = 420 (4.40), 491 (4.23), 604 (4.50), 721 (3.91), 815 (3.61), 1028 (3.13). MS (MALDI-TOF, *dithranol matrix*): *m/z* = 1161.6 (calcd. for $[M + dithranol - 2H + K]^+$: 1162.1). Anal. calcd. for $C_{52}H_{28}N_4O_8Zn\cdot 3H_2O$: C 65.31, H 3.58, N 5.86; found: C 65.11, H 3.68, N 5.60.

Zinc(II) 24,30,36,42-tetrakis(trifluoromethyl)-quadruply-fused porphyrinato (4f). A ring-fusion reaction using the aforementioned general procedure was performed utilizing **5f** (62.6 mg, 49.3 μmol) as a starting material to obtain **4f**. After filtration, the remaining dark red solid mainly including **4f** was recrystallized by vapor deposition of ethanol as a poor solvent to the THF solution in the presence of one drop of pyridine to give pure **4f** (10.2 mg, 10.8 μmol, 22%). m.p.: > 300 ºC. ^{1}H NMR (DMSO-d_6): δ 8.17 (s, 4H, 2,3,12,13-β-H), 7.68 (d, J = 7.4 Hz, 4H, 26,32,38,44-Ph-H), 7.25 – 7.15 (m, 8H, 23,25,29,31,35, 37,41,43-Ph-H). UV-vis (DMF): λ_{max} [nm] (log (ε, M^{-1} cm^{-1})) = 320 (4.64), 403 (4.66), 497 (4.43), 598 (4.95), 793 (4.66), 929 (3.57), 1104 (3.18). MS (MALDI-TOF, *dithranol matrix*): *m/z* = 940.3 (calcd. for $[M]^+$: 940.1). Anal. calcd. for $C_{48}H_{16}N_4F_{12}Zn\cdot H_2O\cdot C_2H_5OH$: C 59.69, H 2.40, N 5.57; found: C 59.82, H 2.46, N 5.55.

5,10,15,20-Tetraphenylporphyrin (6a). This compound was synthesized according to the literature procedure[28] to yield a purple solid of **6a** (787 mg, 1.3 mmol, 19%). ^{1}H NMR ($CDCl_3$): δ 8.84 (s, 8H, β-H), 8.22 (dd, J = 8.0, 1.6 Hz, 4H, *o*-phenyl-H), 7.72-7.78 (m, 12H, *m*, *p*-phenyl-H), –2.77 (br s, 2H, inner N*H*). UV-vis ($CHCl_3$): λ_{max} [nm] = 647, 591, 550, 512, 418. Fluorescence (λ_{ex} = 418 nm, $CHCl_3$): λ_{max} [nm] = 714, 649. MS (MALDI-TOF, dithranol matrix): *m/z* = 613.9 (calcd. for $[M]^+$: 614.3).

5,10,15,20-Tetrakis(4-*tert*-butylphenyl)porphyrin (6c).[29] A condensation of pyrrole (2.79 mL, 40.2 mmol) and 4-*tert*-butylbenzaldehyde (6.72 mL, 40.1 mmol) was performed with a similar procedure of **6a** to obtain **6c** (2.03 g, 2.4 mmol, 24%). ^{1}H NMR ($CDCl_3$): δ 8.97 (s, 8H, β-H), 8.15 (d, J = 8.3 Hz, 4H, *o*-phenyl-H), 7.76 (d, J = 8.3 Hz, 4H, *m*-phenyl-H), –2.77 (br s, 2H, inner N*H*). UV-vis ($CHCl_3$): λ_{max} [nm] = 648, 592, 554, 518, 421. MS (MALDI-TOF, dithranol matrix): *m/z* = 841.1 (calcd. for $[M]^+$: 841.5).

5,10,15,20-Tetrakis(4-methoxyphenyl)porphyrin (6d).[30] A condensation of pyrrole (2.78 mL, 40.2 mmol) and 4-methoxyphenylbenzaldehyde (4.88 mL, 40.2 mmol) was performed with a similar procedure of **6a** to obtain **6d** (1.38 g, 1.9 mmol, 19%). ^{1}H NMR ($CDCl_3$): δ 8.86 (s, 8H, β-H), 8.12 (d, J = 8.6 Hz, 4H, *o*-phenyl-H), 7.29 (d, J = 8.6 Hz, 8H, *m*-phenyl-H), 4.10 (s, 12H, methoxy-H), –2.74 (br s, 2H, inner N*H*). UV-vis ($CHCl_3$): λ_{max} [nm] = 651, 594, 556, 520, 422. MS (MALDI-TOF, dithranol matrix): *m/z* = 798.3 (calcd. for $[M]^+$: 798.2).

5,10,15,20-Tetrakis(4-methoxycarbonylphenyl)porphyrin (6e).[31] A condensation of pyrrole (2.79 g, 40.2 mmol) and 4-methoxycarbonylbenzaldehyde (6.62 g, 40.2 mmol) was performed with a similar procedure of **6a** to obtain **6e** (2.35 g, 2.8 mmol, 28%). ^{1}H NMR ($CDCl_3$): δ 8.82 (s, 8H, β-H), 8.45 (d, J = 6.5 Hz, 8H, *o*-phenyl-H), 8.30 (d, J = 6.5 Hz, 8H, *m*-phenyl-H), 4.12 (s, 12H, CO_2CH_3), –2.81 (br s, 2H, inner N*H*). UV-vis ($CHCl_3$): λ_{max} [nm] = 648, 589, 550, 517, 421. MS (MALDI-TOF, dithranol matrix): *m/z* = 846.1 (calcd. for $[M]^+$: 846.3).

5,10,15,20-Tetrakis(4-trifluoromethylphenyl)porphyrin (6f).[32] A condensation of pyrrole (2.09 mL, 30.2 mmol) and 4-trifluoromethylbenzaldehyde (4.05 mL, 30.2 mmol) was performed with a similar procedure of **6a** to obtain **6f** (1.06 g, 1.20 mmol, 16%). ^{1}H NMR ($CDCl_3$): δ 8.81 (s, 8H, β-H), 8.34 (d, J = 8.0 Hz, 4H, *o*-phenyl-H), 8.05 (d, J = 8.0 Hz, 8H, *m*-phenyl-H), –2.84 (br s, 2H, inner N*H*). UV-vis ($CHCl_3$): λ_{max} [nm] = 645, 589, 548, 513, 418. MS (MALDI-TOF, dithranol matrix): *m/z* = 885.7 (calcd. for $[M]^+$: 885.2).

2,3,12,13-Tetrabromo-5,10,15,20-tetraphenylporphyrin (7a).[21,33] To a solution of **6a** (303.2 mg, 0.49 mmol) in $CHCl_3$ (60 mL) was added recrystallized NBS (532 mg, 2.99 mmol) and the reaction mixture was refluxed for 4 h. After cooling to room temperature, the reaction mixture was washed with water to remove any soluble succinimide impurities. The brown-colored solid was chromatographed on a silica gel column using $CHCl_3$/hexane (1:3, v/v) as an eluent. The first fraction was collected and the solvent was removed under vacuum. The residual solid was recrystallized from CH_2Cl_2/CH_3OH (1:3, v/v) and dried under vacuum to yield **7a** (280 mg, 0.30 mmol, 61%). ^{1}H NMR ($CDCl_3$): δ 8.70 (s, 4H, β-H), 8.17 (d, J = 8.0 Hz, 8H, *o*-phenyl-H), 7.75-7.81 (m, 12H, *m*, *p*-phenyl-H), –2.82 (br s, 2H, inner N*H*). UV-vis ($CHCl_3$): λ_{max} [nm] = 684, 536, 438. MS (MALDI-TOF, dithranol matrix): *m/z* = 927.1 (calcd. for $[M + H]^+$: 926.9).

2,3,12,13-Tetrabromo-5,10,15,20-tetrakis(4-*tert*-butylphenyl)porphyrin (7c).[34] A bromination reaction was performed utilizing **6c** (1.00 g, 1.19 mmol) as a starting material and NBS (1.74 g, 9.76 mmol) to obtain **7c** (758 mg, 0.65 mmol, 55%) with a method as described in the synthesis of **7a**. ^{1}H NMR ($CDCl_3$): δ 8.84 (s, 8H, β-H), 8.22 (dd, J = 8.0, 1.6 Hz, 4H, *o*-phenyl-H), 7.72 – 7.78 (m, 12H, *m*, *p*-phenyl-H), –2.77 (br s, 2H, inner N*H*). UV-vis ($CHCl_3$): λ_{max} [nm] = 699, 543, 444. MS (MALDI-TOF, dithranol matrix): *m/z* = 1154.7 (calcd. for $[M + 4H]^+$: 1154.2).

2,3,12,13-Tetrabromo-5,10,15,20-tetrakis(4-methoxyphenyl)porphyrin (7d).[34] A bromination reaction with a similar procedure of **7c** was performed utilizing **6d** (507 mg, 0.68 mmol) and NBS (564 mg, 3.26 μmol) as starting materials to obtain **7d** (544 mg, 0.52 mmol, 76%). ^{1}H NMR ($CDCl_3$): δ 8.69 (s, 4H, β-H), 8.10 (d, J = 8.6 Hz, 4H, *o*-phenyl-H), 732 (d, J = 8.6 Hz, 8H, *m*-phenyl-H), 4.10 (s, 12H, methoxy-H), –2.71 (br s, 2H, inner N*H*). UV-vis ($CHCl_3$): λ_{max} [nm] = 699, 590, 543, 446. MS (MALDI- TOF, dithranol matrix): *m/z* = 1051.2 (calcd. for $[M + H]^+$: 1050.9).

2,3,12,13-Tetrabromo-5,10,15,20-tetrakis(4-methoxycarbonylphenyl)porphyrin (7e).[34] A bromination reaction with a similar procedure of **7c** was performed utilizing **6e** (600 mg, 0.71 mmol) and NBS (745 mg, 4.3 μmol) as a starting material in 1,2-dichloroethane (150 mL) to obtain **7e**. After washing with H_2O and removal of the solvent, the reaction mixture was chromatographed on a silica gel column by using $CH_2Cl_2/CH_3OH/Et_3N$ (100:3:0.5, v/v/v) as an eluent. The second fraction was collected and the solvent was removed under vacuum. The residual solid was recrystallized from CH_2Cl_2/CH_3OH (1:3, v/v) and the crystalline solid obtained was dried under vacuum to yield **7e** (389 mg, 0.33 mmol, 47%). ^{1}H NMR ($CDCl_3$): δ 8.65 (s, 4H, β-H), 8.46 (d, J = 8.0 Hz, 8H, *o*-phenyl-H), 8.25 (d, J = 8.0 Hz, 8H, *m*-phenyl-H), 4.11 (s, 12H, CO_2CH_3), –2.85 (br s, 2H, inner N*H*). UV-vis ($CHCl_3$): λ_{max} [nm] = 681, 615, 535, 439. MS (MALDI-TOF, dithranol matrix): *m/z* = 1162.9 (calcd. for $[M]^+$: 1162.9).

Zinc(II) 2,3,12,13-tetrabromo-5,10,15,20-tetraphenylporphyrinato (5a).[34,35] To a solution of **7a** (260 mg, 0.262 mmol) in $CHCl_3$ (50 mL) was added a suspension of $Zn(OAc)_2 \cdot 2H_2O$ (311 mg, 1.42 mmol) in CH_3OH (20 mL) and the reaction mixture was refluxed for 5 h. The reaction mixture was poured into water and the organic phase was separated and then dried over Na_2SO_4. After removing the solvent, the resulting red-purple powder was chromatographed on a silica gel column using $CHCl_3$/hexane (3:1, v/v) as an eluent. The second fraction was collected and the solvent was removed under vacuum. The residual solid was recrystallized from CH_2Cl_2/hexane (1:3, v/v) and the crystalline solid obtained was dried under vacuum to yield **5a** (217 mg, 0.22 mmol, 83%). ^{1}H NMR ($CDCl_3$): δ 8.65 (s, 4H, β-H), 8.02 (d, J = 8.0 Hz, 8H, *o*-phenyl-H), 7.66-7.77 (m, 12H, *m*, *p*-phenyl-H). UV-vis ($CHCl_3$): λ_{max} [nm] = 597, 557, 431. MS (MALDI-TOF, dithranol matrix): *m/z* = 988.3 (calcd. for $[M + H]^+$: 988.8).

Zinc(II) 2,3,12,13-tetrabromo-5,10,15,20-tetrakis(4-*tert*-butylphenyl)porphyrinato (5c).[36] Metalation of **7c** with a similar procedure of **5c** was performed utilizing **7c** (385 mg, 0.33 mmol) and $Zn(OAc)_2 \cdot 2H_2O$ (362 mg, 1.65 mmol) as starting materials to obtain **5c** (310 mg, 0.25 mmol, 76%). ^{1}H NMR ($CDCl_3$): δ 8.65 (s, 4H, β-H), 8.02 (d, J = 8.0 Hz, 8H, *o*-phenyl-H), 7.66 – 7.77 (m, 12H, *m*, *p*-phenyl-H). UV-vis ($CHCl_3$): λ_{max} [nm] = 611, 598, 437. MS (MALDI-TOF, dithranol matrix): *m/z* = 1221.7 (calcd. for $[M + 3H]^+$: 1221.2).

Zinc(II) 2,3,12,13-tetrabromo-5,10,15,20-tetrakis(4-methoxyphenyl)porphyrinato (5d). Metalation of **7d** with a similar procedure of **5a** was performed utilizing **7d** (396 mg, 0.38 mmol) and $Zn(OAc)_2 \cdot 2H_2O$ (417 mg, 1.9 mmol) as

starting materials to obtain **5d** (378 mg, 0.34 mmol, 89%). ^{1}H NMR ($CDCl_3$): δ 8.57 (s, 4H, β-H), 7.92 (d, J = 8.2 Hz, 8H, *o*-phenyl-H), 7.23 (d, J = 8.2 Hz, 8H, *m*-phenyl-H), 4.07 (s, 12H, OCH_3). UV-vis ($CHCl_3$): λ_{max} [nm] = 613, 568, 439. MS (MALDI-TOF, dithranol matrix): *m/z* = 1114.9 (calcd. for $[M + H]^+$: 1114.8).

Zinc(II) 2,3,12,13-tetrabromo-5,10,15,20-tetrakis(4-methoxycarbonylphenyl)porphyrinato (5e).[36] Metalation of **7e** with a similar procedure of **5a** was performed utilizing **7e** (352 mg, 0.30 mmol) and $Zn(OAc)_2 \cdot 2H_2O$ (329 mg, 1.5 mmol) as starting materials to obtain **5e** (217 mg, 0.18 mmol, 68%). ^{1}H NMR ($CDCl_3$): δ 8.57 (s, 4H, β-H), 8.36 (d, J = 7.9 Hz, 8H, *o*-phenyl-H), 8.11 (d, J = 7.9 Hz, 8H, *m*-phenyl-H), 4.08 (s, 12H, CO_2CH_3). UV-vis ($CHCl_3$): λ_{max} [nm] = 681, 567, 436. MS (MALDI-TOF, dithranol matrix): *m/z* = 1227.6 (calcd. for $[M + H]^+$: 1226.8).

Zinc(II) 2,3,12,13-tetrabromo-5,10,15,20-tetrakis(4-trifluoromethylphenyl)porphyrinato (5f). To a solution of **6f** (203 mg, 0.23 mmol) in 1,2-dichloroethane (50 mL) was added recrystallized NBS (234 mg, 1.35 mmol) and the reaction mixture was refluxed for 24 h. The solvent was removed under vacuum, and the residual solid was washed with H_2O and dried under vacuum to obtain crude **7f**. To the solution of the crude **7f** (273 mg, 0.23 mmol) in $CHCl_3$ (45 mL) was added a suspension of $Zn(OAc)_2 \cdot 2H_2O$ (359 mg, 1.1 mmol) in CH_3OH (16 mL) and the reaction mixture was refluxed for 3 h. The reaction mixture was poured into water and the organic phase was separated and then dried over Na_2SO_4. After removing the solvent, the resulting red-purple powder was chromatographed on a silica gel column by using $CHCl_3$/hexane (2:1, v/v) as an eluent. The second fraction was collected and the solvent was removed under vacuum. The residual solid was recrystallized from CH_2Cl_2/hexane (1:3, v/v) and dried under vacuum to yield **5f** (85 mg, 67 μmol, 30% (2 step)). ^{1}H NMR ($CDCl_3$): δ 8.65 (s, 4H, β-H), 8.02 (d, J = 8.0 Hz, 8H, *o*-phenyl-H), 7.66-7.77 (m, 12H, *m*, *p*-phenyl-H). UV-vis ($CHCl_3$): λ_{max} [nm] = 605, 565, 434. MS (MALDI-TOF, dithranol matrix, negative mode): *m/z* = 1226.8 (calcd. for $[M + H]^-$: 1226.7).

X-ray diffraction analysis.

The single crystals were mounted on mounting loops. All diffraction data were collected using a Bruker APEXII diffractometer at –153 °C (120 K) equipped with graphite- monochromated Mo $K\alpha$ (λ = 0.71073 Å) by the ω-2θ scan. The structures were solved by direct methods by using SIR97 and SHELX97.[37] Crystallographic data are summarized in Table 3-4. Recrystallization of the *t*-Bu derivative **4c** from the solution in chlorobenzene in the presence of one drop of pyridine by slow concentration afforded single crystals of **4c**-py. On the other hand, recrystallization of **4c** from the 1,4-dioxane solution by deposition of 2-propanol vapor as a poor solvent gave single crystals of **4c**-dox. One molecule of **4c**-py and two co-crystallized chlorobenzene molecules were involved in the asymmetric unit, whereas the asymmetric unit of the crystal of **4c**-dox contained one molecule of **4c**-dox and two co-crystallized dox molecules and one 2-propanol molecule. One of the two co-crystallized dox molecules in the crystal of **4c**-dox was severely disordered and deleted using the SQUEEZE program.[38] Recrystallization of the methoxy derivative **4d** from the solution in pyridine by deposition of 1,2-dichlorobenzene vapor as a poor solvent gave single crystals of **4d**-py. One molecule of **4d**-py and one co-crystallized 1,2-dichlorobenzene molecules were involved in the asymmetric unit. A single crystal of

Table 3-4. Crystallographic data for QFP Derivatives.

compound	**4c**-py	**4c**-dox	**4d**-py	**4f**-py
crystal system	monoclinic	monoclinic	monoclinic	triclinic
space group	$P2_1/a$	$P2_1/a$	$P2_1/c$	$P\ \bar{1}$
T / K	120			
Formula	$C_{60}H_{52}N_4Zn{\cdot}C_5H_5N{\cdot}2$ C_6H_5Cl	$C_{60}H_{52}N_4Zn{\cdot}$ $C_4H_8O_2$	$C_{48}H_{28}N_4O_4Zn{\cdot}$ C_5H_5N	$C_{48}H_{16}N_4F_{12}Zn{\cdot}$ C_5H_5N
FW	1198.62	1130.72	1016.20	1021.12
a / Å	17.737(2)	19.126(2)	16.247(6)	16.724(13)
b / Å	18.295(3)	17.2247(18)	14.572(5)	16.971(14)
c / Å	19.069(3)	19.215 (2)	18.789(7)	20.045(16)
a / °	90	90	90	107.054(11)
b / °	92.168(2)	93.303(2)	91.671(5)	107.580(10)
g / °	90	90	90	105.011(12)
V / Å^3	6183.5(15)	6319.6(11)	4446(3)	4793(7)
Z	4	4	4	4
λ / Å	0.71073 (Mo $K\alpha$)			
D_c / g cm^{-3}	1.288	1.188	1.518	1.415
reflns measured	34682	33306	23940	18428
reflns unique	13927	13857	10244	12549
$R1$ ($I > 2s(I)$)	0.0331	0.1176	0.0644	0.0835
$wR2$ (all)	0.0916	0.3252	0.2089	0.2096
GOF	1.038	1.137	1.024	0.838

4f-py was obtained by recrystallization from the pyridine solution with a vapor deposition method using MeCN as a poor solvent.Two independent molecules of **4f**-py and one MeCN molecule as a co-crystallized solvent molecule were found in the asymmetric unit. The co-crystallized MeCN molecule was highly disordered and treated with the SQUEEZE program to be deleted.[38]

Computational method.

The structures of porphyrin derivatives were optimized by using the B3LYP functional.[39] The 6-31G(d) basis set[40,41] was used for all atoms. The program used was Gaussian 09.[42] Time-dependent density functional theory (TD-DFT)[43] has been applied to calculate the excited-state energies.

Reference and notes

1 (a) *The Porphyrin Handbook, Vol. 1–10* (Eds.: K. M. Kadish, K. M. Smith, R. Guilard), Academic Press, New York, **2000**. (b) *The Porphyrin Handbook*, *Vol. 11-20* (Eds.: K. M. Kadish, K. M. Smith, R. Guilard), Academic Press, San Diego, **2003**. (c) *The Porphyrins* (Eds.: D. Dolphin), Academic Press, New York, 1979.

2 (a) J. J. Warren, J. R. Winkler, H. B. Gray, *Coord. Chem. Rev.* **2013**, *257*, 165. (b) H. Michel, J. Deisenhofer, *Biochemistry* **1988**, *27*, 1. (c) J. P. Allen, G. Feher, T. O. Yeates, H. Komiya, D. C. Rees, *Proc. Natl. Acad. Sci.*

USA **1987**, *84*, 5730. (d) S. G. Boxer, *Biochim. Biophys. Acta* **1983**, *726*, 265.

3 (a) H. Imahori, S. Fukuzumi, *Adv. Funct. Mater.* **2004**, *14*, 525. (b) M. V. Martínez-Díaz, G. de la Torre, T. Torres, *Chem. Commun.* **2010**, *46*, 7090.

4 M. O. Senge, M. Fazekas, E. G. A. Notaras, W. J. Blau, M. Zawadzka, O. B. Locos, E. M. N. Mhuircheartaigh, *Adv. Mater.* **2007**, *19*, 2737.

5 A. Giraudeau, H. J. Callot, M. Gross, *Inorg. Chem.* **1979**, *18*, 201. (b) K. M. Kadish, M. M. Morrison, *J. Am. Chem. Soc.* **1976**, *98*, 3326. (c) A. Giraudeau, H. J. Callot J. Jordan, I. Ezhar, M. Gross, *J. Am. Chem. Soc.* **1979**, *101*, 3857.

6 Reviews on this topic: (a) S. Fox, R. W. Boyle, *Tetrahedron* **2006**, *62*, 10039. (b) J. P. Lewtak, D. T. Gryko, *Chem. Commun.* **2012**, *48*, 10069. (c) H. Mori, T. Tanaka, A. Osuka, *J. Mater. Chem. C* **2013**, *1*, 2500. (d) M. Stępień, E. Gońka, M. Żyła, N. Sprutta, *Chem. Rev.* **2017**, ASAP (DOI: 10.1021/acs.chemrev.6b00076).

7 (a) L. Edwards, M. Gouterman, C. B. Rose, *J. Am. Chem. Soc.* **1976**, *98*, 7638. (b) T. D. Lash, B. H. Novak, A*ngew. Chem., Int. Ed. Engl.* **1995**, *34*, 683. (c) S. Ito, T. Murashima, H. Uno, N. Ono, *Chem. Commun.* **1998**, 1661.

8 (a) R. Deshpande, L. Jiang, G. Schmidt, J. Rakovan, X. Wang, K. Wheeler, H. Wang, *Org. Lett.* **2009**, *11*, 4251. (b) L. Jinag, J. T. Engle, L. Sirk, C. S. Hartley, C. J. Ziegler, H. Wang, *Org. Lett.* **2011**, *13*, 3020. (c) S. Banala, T. Rühl, K. Wurst, B. Kräutler, *Angew. Chem. Int. Ed.* **2009**, *48*, 599.

9 (a) H. Aihara, L. Jaquinod, D. J. Nurco, K. M. Smith, *Angew. Chem. Int. Ed.* **2001**, *40*, 3439. (b) M. Nath, J. C. Huffman, J. M. Zaleski, *J. Am. Chem. Soc.* **2003**, *125*, 11484. (c) M. Nath, M. Pink, J. M. Zaleski, *J. Am. Chem. Soc.* **2005**, *127*, 478.

10 (a) A. N. Cammidge, P. J. Scaife, G. Berber, D. L. Hughes, *Org. Lett.* **2005**, *7*, 3413. (b) M. Tanaka, S. Hayashi, S. Eu, T. Umeyama, Y. Matano, H. Imahori, *Chem. Commun.* **2007**, 2069. (c) C. Jiao, K.-W. Huang, Z. Guan, Q.-H. Xu, J. Wu, *Org. Lett.* **2010**, *12*, 4046.

11 (a) H. S. Gill, M. Harmjanz, J. Santamaría, I. Finger, M. J. Scott, *Angew. Chem. Int. Ed.* **2004**, *43*, 485. (b) K. Kurotobi, K. S. Kim, S. B. Noh, D. Kim, A. Osuka, *Angew. Chem. Int. Ed.*, **2006**, *45*, 3944.

12 C. Jiao, L. Zhu, J. Wu, *Chem. Eur. J.* **2011**, *17*, 6610.

13 (a) K. Sendt, L. A. Johnston, W. A. Hough, M. J. Crossley, N. S. Hush, J. R. Reimers, *J. Am. Chem. Soc.* **2002**, *124*, 9299. (b) R. Paolesse, L. Jaquinod, F. S. Della, D. J. Nurco, L. Prodi, M. Montalti, C. D. Natale, A. D'Amico, A. D. Carlo, P. Lugli, K. M. Smith, *J. Am. Chem. Soc.* **2000**, *122*, 11295. (c) H. Uno, A. Masumoto, N. Ono, *J. Am. Chem. Soc.* **2003**, *125*, 12082. (d) M. Akita, S. Hiroto, H. Shinokubo, *Angew. Chem. Int. Ed.* **2012**, *51*, 2894.

14 (a) A. Tsuda, A. Nakano, H. Furuta, H. Yamochi, A. Osuka, *Angew. Chem. Int. Ed.* **2000**, *39*, 558. (b) A. Tsuda, H. Furuta, A. Osuka, *Angew. Chem. Int. Ed.* **2000**, *39*, 2549. (c) A. Tsuda, H. Furuta, A. Osuka, *J. Am. Chem. Soc.* **2001**, *123*, 10304. (d) A. Tsuda, A. Osuka, *Science* **2001**, *293*, 79. (e) Y. Nakamura, N. Aratani, H. Shinokubo, A. Takagi, T. Kawai, T. Matsumoto, Z. S. Yoon, D. Y. Kim, T. K. Ahn, D. Kim, A. Muranaka, N. Kobayashi, A. Osuka, *J. Am. Chem. Soc.* **2006**, *128*, 4119.

15 (a) S. Hayashi, Y. Matsubara, S. Eu, H. Hayashi, T. Umeyama, Y. Matano, H, Imahori, *Chem. Lett.* **2008**, *37*, 846. (b) S. Hayashi, M. Tanaka, H. Hayashi, S. Eu, T. Umeyama, Y. Matano, Y. Araki, H. Imahori, *J. Phys. Chem. C* **2008**, *112*, 15576. (c) J. M. Ball, N. K. S. Davis, J. D. Wilkinson, J. Kirkpatrick, J. Teuscher, R. Gunning, H. L. Anderson, H. J. Snaith, *RSC Adv.* **2012**, *2*, 6846.

16 N. Fukui, W.-Y. Cha, S. Lee, S. Tokuji, D. Kim, H. Yorimitsu, A. Osuka, *Angew. Chem. Int. Ed.* **2013**, *52*, 9728.

17 (a) N. K. S. Davis, M. Pawlicki, H. L. Anderson, *Org. Lett.*, **2008**, *10*, 3945. (b) N. K. S. Davis, A. L. Thompson, H. L. Anderson, *Org. Lett.* **2010**, *12*, 2124. (c) N. K. S. Davis, A. L. Thompson, H. L. Anderson, *J. Am. Chem. Soc.* **2011**, *133*, 30.

18 C.-M. Feng, Y.-Z. Zhu, S.-C. Zhang, J.-Y. Zheng, *Org. Biomol. Chem.* **2015**, *13*, 2566.

19 (a) Y. Mitsushige, S. Yamaguchi, B. S. Lee, Y. M. Sung, S. Kuhri, C. A. Schierl, D. M. Guldi, D. Kim, Y. Matsuo, *J. Am. Chem. Soc.* **2012**, *134*, 16540. (b) H. Fliegl, N. Özcan, R. Mera-Adasme, F. Pichierri, J. Jusélius, D. Sundholm, *Mol. Phys.* **2013**, *111*, 1364.

20 (a) T. Ishizuka, Y. Saegusa, Y. Shiota, K. Ohtake, K. Yoshizawa, T. Kojima, *Chem. Commun.* **2013**, *49*, 5939. (b) Y. Saegusa, T. Ishizuka, K. Komamura, S. Shimizu, H. Kotani, N. Kobayashi, T. Kojima, *Phys. Chem. Chem. Phys.* **2015**, *17*, 15001. (c) Y. Saegusa, T. Ishizuka, T. Kojima, S. Mori, M. Kawano, T. Kojima, *Chem. Eur. J.* **2015**, *21*, 5302.

21 P. K. Kumar, P. Bhyrappa, B. Varghese, *Tetrahedron Lett.* **2003**, *44*, 4849.

22 S. Higashibayashi, H. Sakurai, *Chem. Lett.* **2007**, *36*, 18.

23 Typical C-C bond lengths of phenyl rings are *ca.* 1.38 Å for porphyrin derivatives: (a) C. K. Schauer, O. P. Anderson, S. S. Eaton, G. R. Eaton, *Inorg. Chem.* **1985**, *24*, 4082. (b) M. P. Byrn, C. J. Curtis, I. Goldberg, Y. Hsiou, S. I. Khan, P. A. Sawin, S. K. Tendick, C. E. Strouse, *J. Am. Chem. Soc.* **1991**, *113*, 6549. (c) E. B. Fleischer, C. K. Miller, L. E. Webb, *J. Am. Chem. Soc.* **1964**, *86*, 2342. (d) W. R. Scheidt, J. U.Mondal, C. W. Eigenbrot, A. Adler, L. J. Radonovich, J. L. Hoard, *Inorg. Chem.* **1986**, *25*, 795.

24 (a) D. J. Nurco, C. J. Medforth, T. P. Forsyth, M. M. Olmstead, K. M. Smith, *J. Am. Chem. Soc.* **1996**, *118*, 10918. (b) C. J. Medforth, M. O. Senge, K. M. Smith, L. D. Sparks, J. A. Shelnutt, *J. Am. Chem. Soc.* **1992**, *114*, 9859.

25 (a) A. D. Bond, N. Feeder, J. E. Redman, S. J. Teat, J. K. M. Sanders, *Cryst. Growth Des.* **2002**, *2*, 27. (b) Y. Inokuma, Z. S. Yoon, D. Kim, A. Osuka, *J. Am. Chem. Soc.* **2007**, *129*, 4747.

26 C. Hansch, A. Leo, R. W. Taft, *Chem. Rev.* **1991**, *91*, 165.

27 Similar sensitiveness to the substituents has been also reported to the redox potentials of TPP derivatives with the *β*-substituents. (a) A. Giraudeau, H. J. Callot, M. Gross, *Inorg. Chem.* **1979**, *18*, 201. (b) K. M. Kadish, M. M. Morrison, *J. Am. Chem. Soc.* **1976**, *98*, 3326.

28 A. D. Adler, F. R. Longo, J. D. Finarelli, J. Goldmacher, J. Assour, L. Korsakoff, *J. Org. Chem.* **1967**, *32*, 476.

29 J. Arnold, D. Y. Dawson, C. C. Hoffman, *J. Am. Chem. Soc.* **1993**, *115*, 2707.

30 M. O'Rourke, C. Curran, *J. Am. Chem. Soc.* **1970**, *92*, 1501.

31 K. M. Kadish, M. M. Morrison, *J. Am. Chem. Soc.* **1976**, *98*, 3326.

32 S. S. Eaton, G. R. Eaton, *J. Am. Chem. Soc.* **1975**, *97*, 3660.

33 M. J. Crossley, P. L. Burn, S. S. Chew, F. B. Cuttance, I. A. Newsom, *J. Chem. Soc., Chem. Commun.* **1991**, 1564.

34 P. Bhyrappa, V. Velkannan, K. Karunanithi, B. Varghese, Harikrishna, *Bull. Chem. Soc. Jpn.* **2008**, *81*, 995.

35 Y. Terazono, B. O. Patrick, D. H. Dolphin, *Inorg. Chem.* **2002**, *41*, 6703.

36 P. Bhyrappa, V. Velkannan, *J. Porphyrin Phthalocyanine* **2011**, *15*, 883.

37 G. M. Sheldrick, SIR97 and SHELX97, Programs for Crystal Structure Refinement, University of Göttingen, Göttingen (Germany), 1997.

38 P. V. D. Sluis, A. L. Spek, *Acta Crystallogr.* **1990**, *A46*, 194.

39 (a) A. D. Becke, *Phys. Rev. A* **1988**, *38*, 3098. (b) C. Lee, W. Yang, R. G. Parr, *Phys. Rev. B* **1988**, *37*, 785; (c) A. D. Becke, *J. Chem. Phys.* **1993**, *98*, 5648.

40 M. M. Francl, W. J. Petro, W. J. Hehre, J. S. Binkley, M. S. Gordon, D. J. DeFrees, J. A. Pople, *J. Chem. Phys.* **1982**, *77*, 3654.

41 V. Rassolov, J. A. Pople, M. Ratner, T. L. Windus, *J. Chem. Phys.* **1998**, *109*, 1223.

42 Gaussian 09 (Revision D.01), M. J. Frisch, G. W. Trucks, H. B. Schlegel, G. E. Scuseria, M. A. Robb, J. R. Cheeseman, G. Scalmani, V. Barone, B. Mennucci, G. A. Petersson, H. Nakatsuji, M. Caricato, X. Li, H. P. Hratchian, A. F. Izmaylov, J. Bloino, G. Zheng, J. L. Sonnenberg, M. Hada, M. Ehara, K. Toyota, R. Fukuda, J. Hasegawa, M. Ishida, T. Nakajima, Y. Honda, O. Kitao, H. Nakai, T. Vreven, J. A. Montgomery, Jr., J. E. Peralta, F. Ogliaro, M. Bearpark, J. J. Heyd, E. Brothers, K. N. Kudin, V. N. Staroverov, R. obayashi, J. Normand, K. Raghavachari, A. Rendell, J. C. Burant, S. S. Iyengar, J. Tomasi, M. Cossi, N. Rega, M. J. Millam, M. Klene, J. E. Knox, J. B. Cross, V. Bakken, C. Adamo, J. Jaramillo, R. Gomperts, R. E. Stratmann, O. Yazyev, A. J. Austin, R. Cammi, C. Pomelli, J. W. Ochterski, R. L. Martin, K. Morokuma, V. G. Zakrzewski, G. A. Voth, P. Salvador, J. J. Dannenberg, S. Dapprich, A. D. Daniels, Ö. Farkas, J. B. Foresman, J. V. Ortiz, J. Cioslowski, D. J. Fox, Gaussian, Inc., Wallingford CT, 2009.

43 (a) *Density Functional Theory* (Ed.: R. F. Nalewajski), Springer: Heidelberg, **1996**. (b) *Recent Advances in Density Functional Methods Vol. 1* (Ed.: D. P. Chong), World Scientific: Singapore, **1995**, pp 155−193.

Chapter 4

Functionalization of QFP at the *β*-positions of the non-fused pyrroles

4-1. Introduction

Porphyrin and its derivatives have attracted much interest of scientists in various fields because of the strong absorption bands in the visible region and multi-redox processes.[1] Based on the π-conjugated nature of the porphyrin ring system, electron-donating or -withdrawing substituents at the periphery of porphyrins can affect the basicity of the porphyrin nitrogen atoms,[1b] and also can control the absorption bands and redox potentials.[2] In addition, porphyrin derivatives can form metal complexes with various metal ions, and the electronic properties of the metal center can be finely tuned by introduction of substituents to the porphyrin ligands.[3]

The characteristics of porphyrins such as optical properties including strong absorption in the visible region can be controlled not only by introduction of substituents, as mentioned above, but also by formation of ring-fused structures at the periphery.[4] The unique physical properties of the ring-fused derivatives of porphyrins are derived from expansion of the π-conjugation due to coplanarity of the porphyrin plane and the peripheral fused aromatic moieties.[4] Recently, modification methods of porphyrins by direct introduction of fused rings on the aromatic circuit have been intensively developed.[5] The author also has reported a facile and efficient procedure of a quadruply ring-fused porphyrins (QFP, **4a**) with a easily accessible precursor (Chapters 2 and 3):[6] The four *meso*-aryl groups of QFP are covalently bonded to the *β*-carbons of the pyrrole rings at the *ortho*-positions. In this chapter, direct functionalization of QFPs with bromination at the non-fused pyrroles is described and further modification of the Br groups with Pd-catalyzed coupling reactions is also presented.

4-2. Synthesis

To elucidate substituent effects of functional groups at the *β*-positions of QFP on the electronic properties, bromination at the *β*-positions of the non-fused pyrrole has been performed with *N*-bromosuccinimide (NBS); 5 equiv of NBS was reacted with **4c** at 60 °C in $CHCl_3$ and chromato- graphed on a bio-beads S-X1 gel column using THF as an eluent. The collected fraction was dried under vacuum and recrystallized from THF/EtOH to give dark-green powder of the tetrabromo-derivative, **10c**, in 37% yield. Formation of **10c** was confirmed by disappearance of the *β*-proton signal, observed for **4c**, in the ^{1}H NMR spectrum of **10c** in DMSO-d_6 (Figure 4-1). In the MALDI-TOF-MS spectrum of **10c**, a peak cluster was observed at m/z = 1211.6, which matches to the simulated pattern of the target tetrabromo-derivative, **10c**. A peak cluster was also observed at m/z = 2418.2, which matches to the simulated pattern of the dimeric species of **10c** (see below).

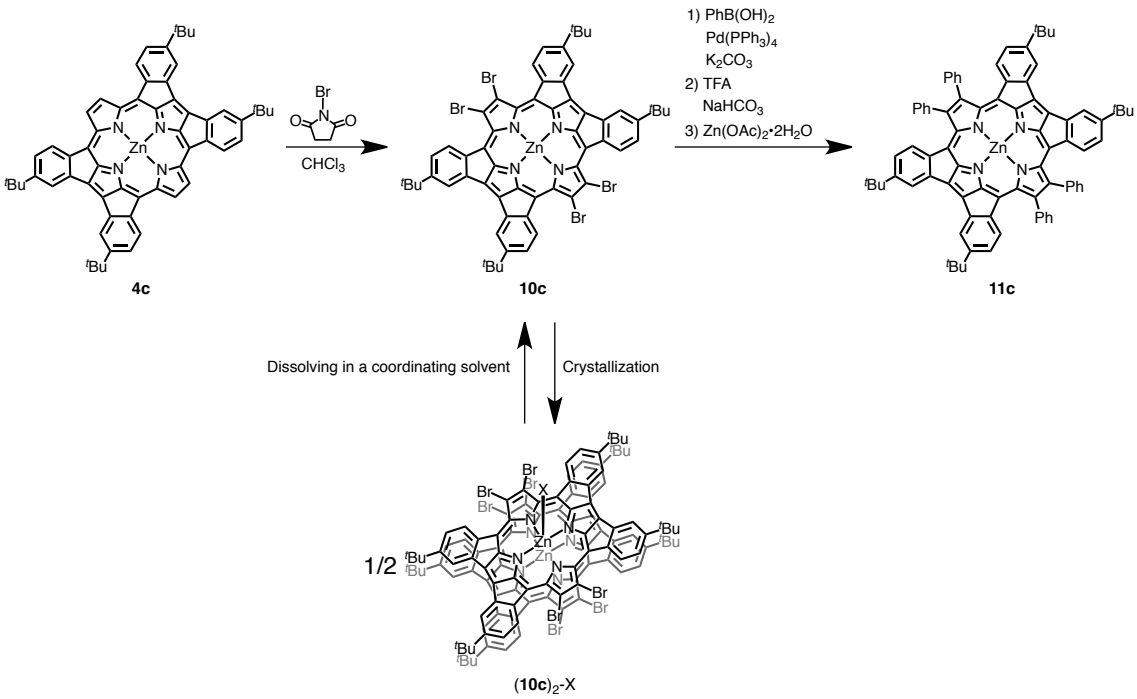

Scheme 4-1. Synthesis of *β*-substituted QFP derivatives.

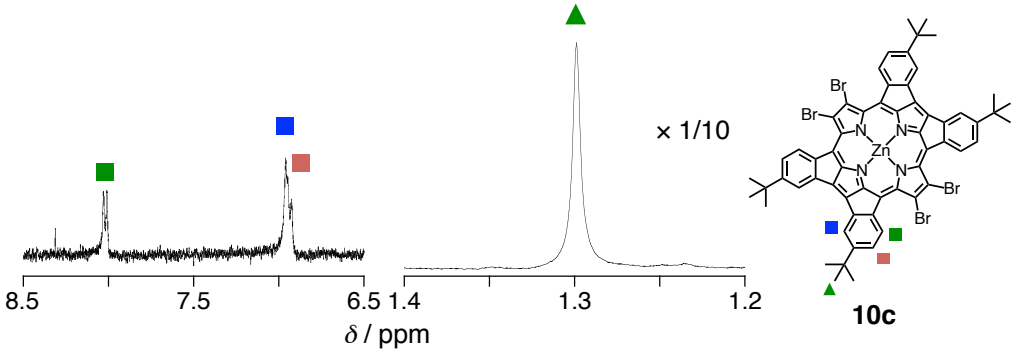

Figure 4-1. ^{1}H NMR spectrum of **10c** in DMSO-d_6.

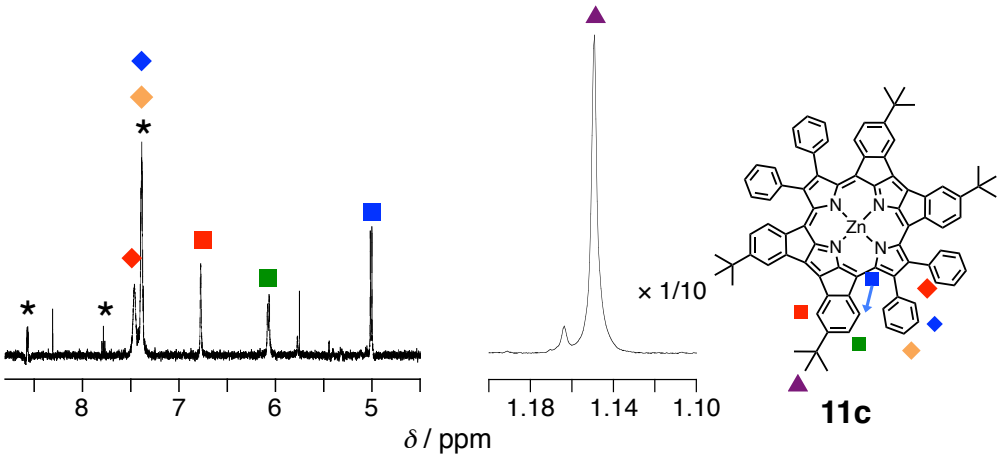

Figure 4-2. ^{1}H NMR spectrum of **11c** in DMSO-d_6. Asterisks (*) denote the free pyridine from recrystallization solvent.

Phenyl groups were subsequently introduced at the *β*-positions of ZnQFP using **10c** as a precursor under Pd-catalyzed cross-coupling conditions (Scheme 4-1). To confirm the formation of **11c**, the ^{1}H NMR spectrum of **11c** was measured in DMSO-d_6 (Figure 4-2); signals of the fused aryl moieties of **11c** were highly upfield shifted in comparison to those of **4c**, due to strong ring current effects caused by the phenyl groups introduced. Supporting this, the distance from the center of the introduced phenyl groups to the nearest *ortho*-carbon at the fused aryl groups, which are represented by a blue square in Figure 4-2, is calculated to be 3.43 Å in the DFT-optimized structure of **11c** (Figure 4-3). The distance is close enough to form edge-to-face π-π interaction between them and to exert the ring-current effect on the *o*-H of the fused phenyl groups, causing the upfield shift mentioned above. According to the DFT-optimized structure of **11c**, the non-fused pyrroles are tilted against the porphyrin plane by 14° (the mean value of the two pyrrole moieties), due to steric congestion between phenyl groups and the fused aromatic rings.

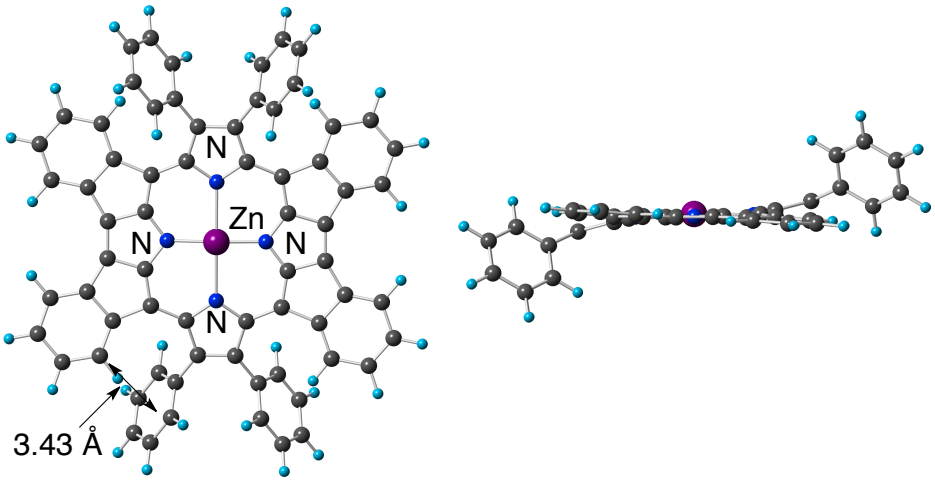

Figure 4-3. Top and side views of DFT-optimized structure of **11c** at the B3LYP/6-31G* level of theory. The *t*-Bu groups are replaced with hydrogen atoms for computational costs.

4-3. Substituent effects at the *β*-positions on crystal structures

The tetra-brominated **10c** was recrystallized from the solution in chloroform by vapor deposition of ethanol as a poor solvent and the crystal structure was determined by single-crystal X-ray diffraction analysis. Contrary to the expectation from the ^{1}H NMR spectrum of **10c** in DMSO-d_6 (Figure 4-1), the compound obtained was revealed to be in an unexpected dimeric structure as shown in Figure 4-4. The representative bond distances and interatomic distances are summarized in Table 4-1. In the structure, an ethanol molecule, which is axially coordinated to the zinc center, exhibited a crystallographic disorder. In the crystal, the non-fused pyrroles of **10c** are tilted relative to the porphyrin plane by 26° (the mean value of the independent four pyrrole moieties), due to steric repulsion between the Br groups and the fused aromatic rings. As a result, the lone pair of a pyrrolic nitrogen (N1) did not direct to the Zn center, and instead, the nitrogen atom of the non-fused pyrrole coordinates to the Zn center of the other molecule of **10c** to form a

dimeric structure, (**10c**)$_2$-EtOH. In addition, one of the non-fused pyrrolic nitrogen (N5) of the other molecule forming the dimeric structure dissociates from the Zn center (Zn2) and forms a hydrogen bond with the hydroxyl group of a cocrystallized EtOH molecule (Figure 4-4). The atom separations of Zn1···N1 and Zn2···N5 in the crystal structure of (**10c**)$_2$-EtOH are found to be 2.786(4) Å and 2.730(4) Å, respectively, which are too long to recognize coordination

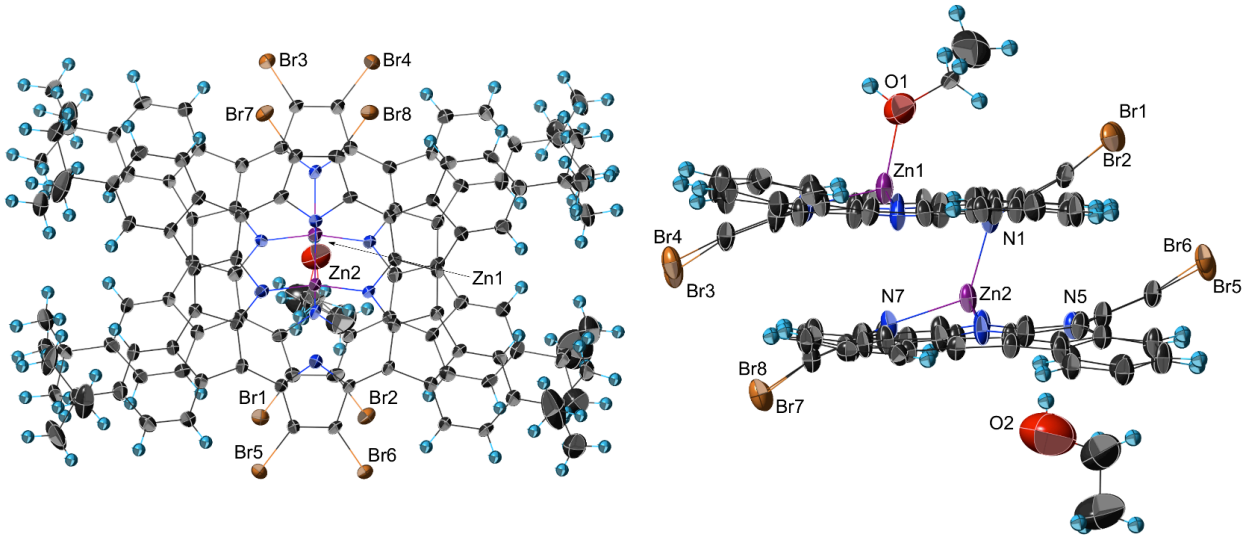

Figure 4-4. Top and side views of crystal structure of (**10c**)$_2$-EtOH. The thermal ellipsoids are drawn at the 50% probability level. One of the two disordered conformers of ethanol as the axial ligand is not shown for clarity.

Table 4-1. Selected bond length and other structural data of (**10c**)$_2$-EtOH

Zn1···N1 / Å	2.786(4)	Zn2···N5 / Å	2.730(4)	N5···O2 / Å	2.83(1)
Zn1-N2 / Å	1.882(4)	Zn2-N6 / Å	1.924(4)	N1···N3 / Å	4.673(5)
Zn1-N3 / Å	2.034(4)	Zn2-N7 / Å	2.103(4)	N2···N4 / Å	3.516(5)
Zn1-N4 / Å	1.893(4)	Zn2-N8 / Å	1.926(4)	N5···N7 / Å	4.636(5)
Zn1-O1(axial) / Å	2.049(5)	Zn2-N1(axial) / Å	2.090(5)	N6···N8 / Å	3.482(5)
N-Ca (fused, av) / Å	1.906	C_{ipso}-C_{ortho} (fused, av) / Å	1.43	Mean deviation / Å	0.225 [a] 0.295 [b]
N-Ca (non-fused, av) / Å	2.069			Zn from the plane / Å	0.406 [a] 1.058 [b]

[a] determined to the porphyrin plane containing N1, N2, N3, N4 atoms. [b] determined to the porphyrin plane containing N5, N6, N7, N8 atoms.

bonds between them. The bond distance of Zn2-N1 and the atom separation of N5···O2 are 2.090(5) Å and 2.83(1) Å, respectively, the former of which is in the typical range of Zn-N bonds[7] and the latter is short enough to form the hydrogen bond.[8] The Zn1-O1 bond distance was 2.049(5) Å, which was shorter than those observed for ZnTPP-alcohol complexes.[9] The short distance of the Zn1-O1 bond indicates the strong Lewis acidity of the Zn center in (**10c**)$_2$-EtOH, since the Zn1 center was tetra-coordinated by three QFP nitrogen atoms and O1 of the coordinated EtOH, whereas the Zn centers of the ZnTPP complexes were penta-coordinated by the four nitrogen atoms of TPP and one oxygen atom of the coordinated alcohols. Supporting this, Zn^{II} complexes having a tridentate *N*-confused porphyrin and monodentate isopropanol as ligands of the Zn center, showed a comparable Zn-O distance, 2.047(7) Å, to that of (**10c**)$_2$-EtOH.[10] Together with the distortion causes by the steric repulsion between the Br group and the fused phenyl protons, the introduction of the electron-withdrawing Br groups reduces the basicity of the pyrrole nitrogen atoms to weaken the Zn-N bond; the less donating character can cause the dissociation in the course of the crystallization using EtOH, which can also stabilize the dissociated structure by the hydrogen-bond formation.

The crystal structure of (**10c**)$_2$-EtOH is not consistent with the structure assumed on the basis of the ^{1}H NMR spectrum in DMSO-d_6 (Figure 4-1). To reexamine the solution structure of (**10c**)$_2$-EtOH, the ^{1}H NMR spectrum of (**10c**)$_2$-EtOH was measured in non-coordinating CD_2Cl_2 instead of strongly coordinating DMSO-d_6 and a relatively complicated spectral pattern was observed due to low symmetric structures (Figure 4-5). For instance, the ^{1}H NMR signals of the *t*-Bu groups were observed as two singlet signals at 1.32 and 1.34 ppm, whereas that in DMSO-d_6 was observed as a singlet at 1.30 ppm. In addition, the ^{1}H NMR signals of the aromatic protons in CD_2Cl_2 also exhibited complicated splitting, compared to those in DMSO-d_6. This difference between the ^{1}H NMR spectrum in DMSO-d_6 (Figure 4-1) and that in CD_2Cl_2 indicates that the dimeric structure of (**10c**)$_2$-X, similar to that observed in the crystal structure (Figure 4-4), is maintained in non-coordinating CD_2Cl_2, whereas the dimeric structure is collapsed into the monomeric one (**10c**) in DMSO-d_6 due to its strong coordinating ability. Unfortunately, the ^{1}H NMR signals of the axial ligand were not observed in CD_2Cl_2 probably due to the ligand substitution by water molecules contained in the solvent CD_2Cl_2.

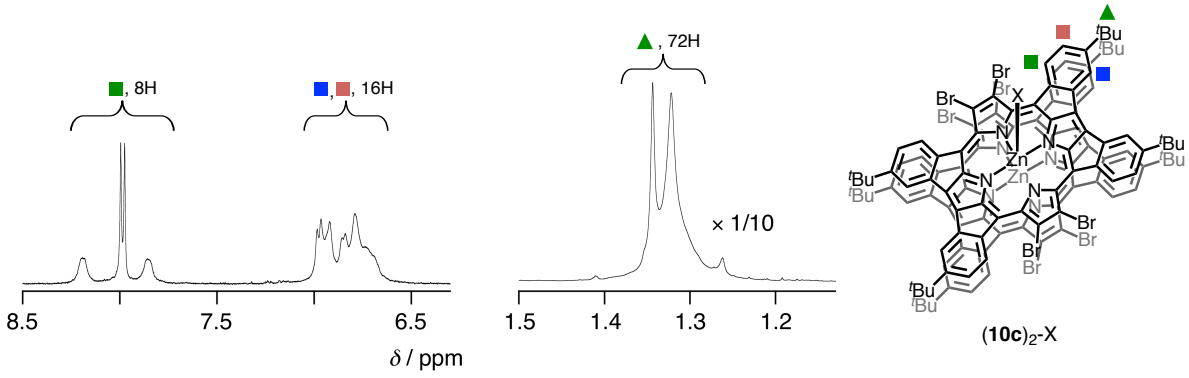

Figure 4-5. ^{1}H NMR spectrum of (**10c**)$_2$-X in CD_2Cl_2. X denotes the axial ligand at one of the Zn^{II} centers.

4-4. Substituent effects at the β-positions of QFP on the optical and electrochemical properties

The optical and electrochemical properties of ZnQFP are largely affected by the substituents at the β-position of the pyrrole moieties. Both of the introduction of phenyl and bromo groups at the β-positions of the pyrrole moieties of QFP caused red shifts of the Soret-like bands relative to those of **4c**; the absorption maximum of the Soret-like band appears at 616 nm for **4c**, 656 nm for **10c**, and 637 nm for **11c** in DMF, in which the dimeric (**10c**)$_2$-X should exist as a monomer, such as **10c**-DMF, due to the strong coordination ability. The bromo-substituted ZnQFP, **10c**, exhibited the

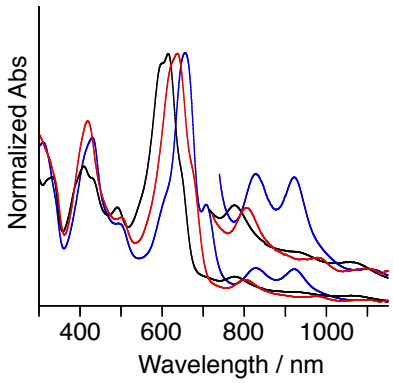

Figure 4-6. UV-vis spectra of β-substituted ZnQFPs, **4c** (black), **10c** (blue), and **11c** (red) in DMF.

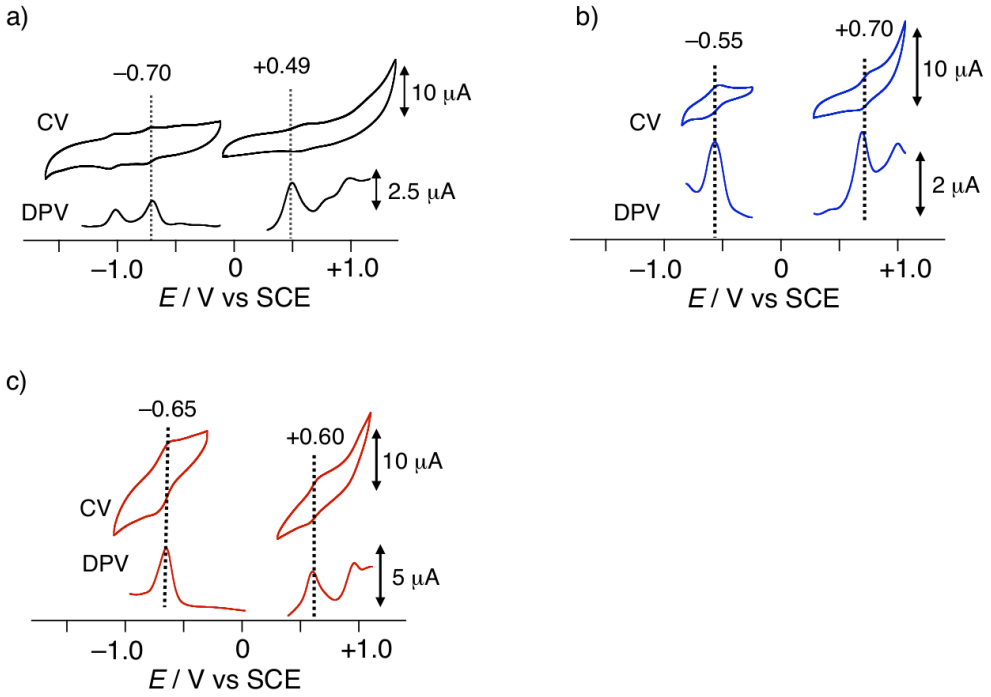

Figure 4-7. Cyclic (above) and differential-pulse (below) voltammograms of the ZnQFP derivatives in DMF containing 0.1 M $TBAPF_6$ as an electrolyte at room temperature; (a) **4c**, (b) **10c** and (c) **11c**.

longest Q-band at 1109 nm in DMF and the shift width relative to that of **4c** is 49 nm (Figure 4-6). It should be noted that the Q bands of **10c** showed intense two peaks at 919 and 826 nm ($\varepsilon \sim 12000$), whereas compounds **4c** and **11c** did not show such intense peaks but exhibited Q-like bands with weak three peaks around 790, 950, and 1080 nm ($\varepsilon \sim 5200$, 2400, and 1800, respectively).

The voltammograms of **4c**, **10c**, and **11c** measured in DMF are shown in Figure 4-7 and the redox potentials are summarized in Table 4-2. Both of the redox potentials for the first reduction and first oxidation processes, E_{Red1} and E_{Ox1}, of the ZnQFP derivatives were positively shifted upon introducing electron-withdrawing groups such as Br and Ph

Table 4-2. Absorption maxima and redox potentials of QFP derivatives in DMF

	l_{max}(B)[a]	n(B)[b]	Dn(B)[b]	l_{max}(Q)[a]	n(Q)[b]	Dn(Q)[b]	E_{Red1}[c]	E_{Ox1}[c]	$E_{Ox1} - E_{Red1}$[d]
4c	616	16230	—	1060	9430	—	–0.70	+0.49	1.19
10c	656	15240	–990	1109	9020	–410	–0.55	+0.70	1.25
11c	637	15670	–560	1092	9160	–270	–0.65	+0.60	1.25

[a] in nm, [b] in cm^{-1}, [c] in V vs SCE. [d] in V.

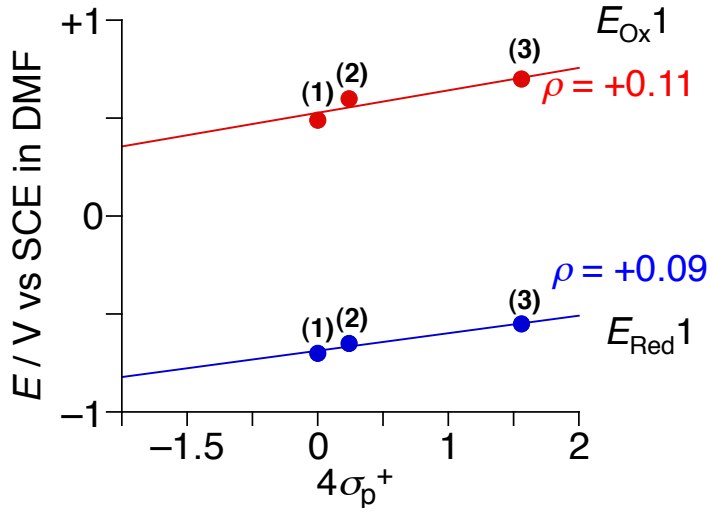

Figure 4-8. Hammett plots of $E_{Red}1$ and $E_{Ox}1$ of the β-substituted ZnQFP derivatives, **4c** (1), **11c** (2) and **10c** (3), against $4\sigma_p^+$. Solvent: DMF containing 0.1 M $TBAPF_6$ (TBA = tetra(*n*-butyl)ammonium). Values of σ_p^+ are taken from ref. 11.

groups (Figure 4-7). To confirm the substituent effects on the redox potentials, the Hammett plots were provided as depicted in Figure 4-8, where a Hammett parameter, σ_p^+,[11] was the best fit for the present studies. The plots of the redox potentials against σ_p^+ exhibited good linearity and the coefficients, ρ, for E_{Ox1} and E_{Red1} of the β-substituted ZnQFPs were determined to be +0.11 and + 0.09, respectively. On the other hand, the ρ values for E_{Ox1} and E_{Red1} of ZnQFPs having substituents at the *para*-positions of the fused aryl group were reported to be +0.098 and +0.009 (See Chapter 3).[6b] As indicated by the ρ values, the redox potentials of ZnQFP are more affected by the substituents at the β-positions of the non-fused pyrrole moiety than those at the *para*-positions of the fused aryl groups. In addition, the ρ values

indicate that the substituents at the *para*-positions affect the first oxidation potentials more than the first reduction potential (See Chapter 3);[6b] however, the substituents at the β-positions affect both of the first oxidation and the first reduction potentials to the same extent.

4-5. Determination of the Lewis acidity of the central Zn^{II} ion in QFP

One of the structural features of ZnQFP complexes is the rhombic distortion around the Zn^{II} centers;[6] that is, the Zn-N distances for the nitrogen atoms of the pyrroles (Zn-N2 and Zn-N4) are shorter by *ca.* 0.27 Å than those of the non-fused pyrroles (Zn-N1 and Zn-N3) and the mean Zn-N distance of the ZnQFP complexes (*ca.* 2.11 Å) is longer than that of ZnTPP (*ca.* 2.04 Å).[7,12] This remarkable elongation suggests weak overall σ-donation from the nitrogen atoms of the QFP ligand to the central Zn^{II} ion, which enhances the Lewis acidity of the central Zn^{II} ion.[6b] The Lewis acidity of the Zn center of QFPs can be further improved by introduction of substituents at the β-positions of the non-fused pyrroles in light of the aforementioned strong impact on the electron-donating ability of the pyrrole nitrogen atoms. To elucidate substituent effects on the Lewis acidity, the association constants (K_{assoc}) of the ZnQFP derivatives, **4c**, **10c** or **11c**, with pyridine in CH_2Cl_2 have been determined by UV-vis titration experiments (Scheme 4-2). The solution of pyridine in CH_2Cl_2 was added dropwise to that of a ZnQFP derivative, **4c**, in CH_2Cl_2 and the UV-Vis spectral change was observed at 298 K (Figure 4-9). The absorbance changes of **4c** at 618 nm upon the titration experiments were analyzed using eq (1) to obtain the K_{assoc} values, and the K_{assoc}

$$\mathrm{Abs} = \varepsilon_p[P]_0L + (\varepsilon_{PyP} / (2 \times K)) \times (1 + K \times [py] + K \times [P]_0) - ((1+K \times [py] + K \times [P]_0)^2 - 4 \times K^2 \times [py] \times [P]_0)^{1/2} \quad (1)$$

values obtained are summarized in Table 4-3. Here, ε_p, [P], [py], ε_{PyP}, and K, refer to the absorption coefficient of the porphyrin derivative at a certain wavelength, the concentration of the porphyrin derivative, the concentration of pyridine, the absorption coefficient of the associated complex between the porphyrin derivative and pyridine at the corresponding wavelength, and the association constant, respectively. In comparison with the K_{assoc} values of Zn^{II} complexes of other porphyrin derivatives,[6c] compound **4c** exhibits larger K_{assoc} values than that of ZnTPP and ZnOPP (OPP = 2,3,5,10,12,13, 15,20-octaphenyl- porphyrin);[13] the K_{assoc} of **4c** for py ($(3.5 \pm 0.1) \times 10^4$ M^{-1}) is *ca.* 3 times larger than that of ZnTPP ($(1.1 \pm 0.1) \times 10^4$ M^{-1})[13c] and as large as even that of the Zn^{II} complex of dodecaphenylporphyrin (DPP), which has been known to exhibit relatively higher Lewis acidity due to the conformational distortion to a saddle form and the resultant weak σ-donation from the nitrogen atoms to the central metal ions.[13c] Therefore, the structural expansion of the core of the QFP ligand can exert a remarkable impact on the enhancement of the Lewis acidity of the central metal ions due to the deformation of the core structure.[14] The mesityl-substituted Zn^{II}QFP derivative, **4b**,[6b] exhibited a larger K_{assoc} value than that of **4c**, which is probably attributed to the electron-withdrawing character of the mesityl groups in **4b** relative to that of the *t*-Bu group in **4c**.[15]

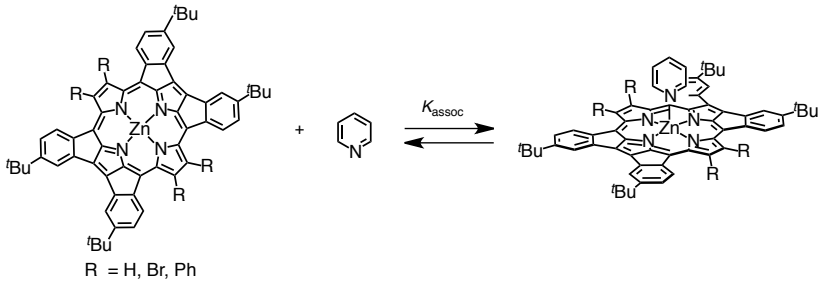

Scheme 4-2. Coordination of pyridine on the Zn center of a QFP derivative.

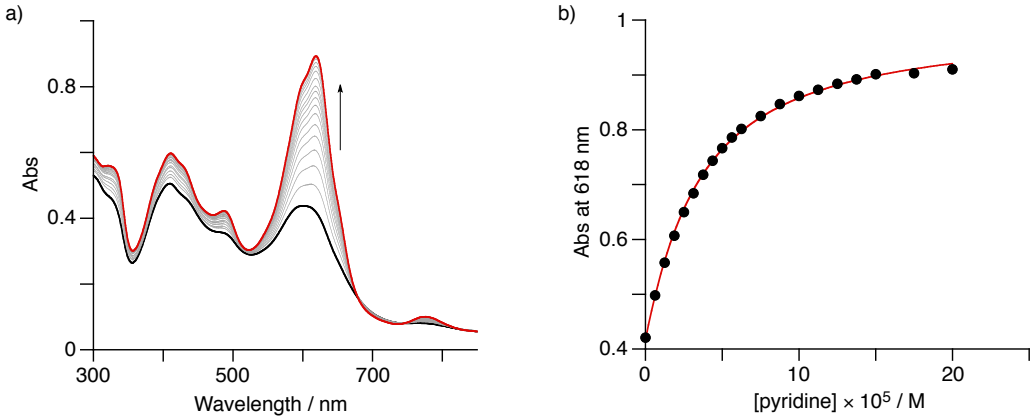

Figure 4-9. UV-Vis spectral changes of **4c** upon titration with pyridine (a) in CH_2Cl_2 at 298 K; (b) the absorbance changes at 618 nm fitted with eq 1. The concentration of **4c** was 1.25×10^{-5} M.

Table 4-3. Association constants of Zn^{II} complexes of porphyrin derivatives with pyridine in CH_2Cl_2

	4c	(**10c**)$_2$-X	**11c**	**4b**	ZnTPP	ZnOPP	ZnDPP
K_{assoc} / 10^4 M^{-1}	3.5 ± 0.1	2.2 ± 0.1	—	76 ± 5[a]	1.1 ± 0.1[b]	1.4 ± 0.1[b]	4.6 ± 0.1[b]

[a] Ref. 6b. [b] Ref. 13c.

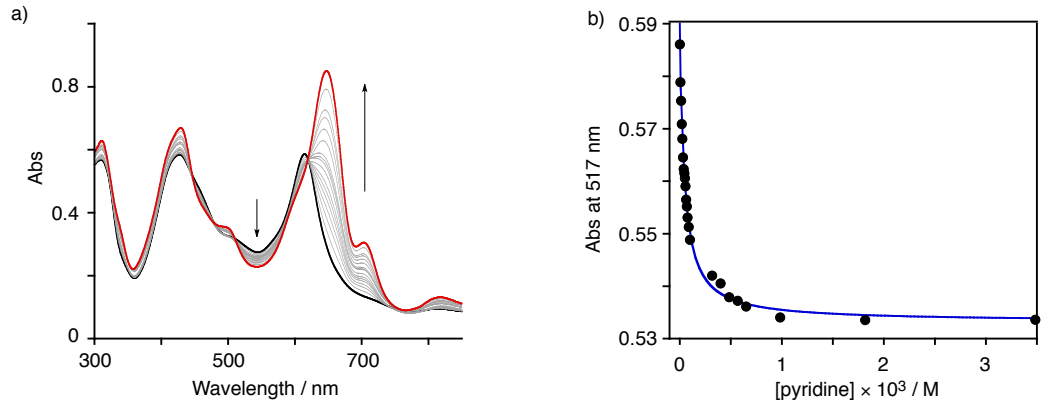

Figure 4-10. UV-Vis spectral changes of (**10c**)$_2$-X upon titration with pyridine (a) in CH_2Cl_2 at 298 K; (b) the absorbance changes at 517 nm fitted with eq 1. The concentration of (**10c**)$_2$-X was 1.16×10^{-5} M.

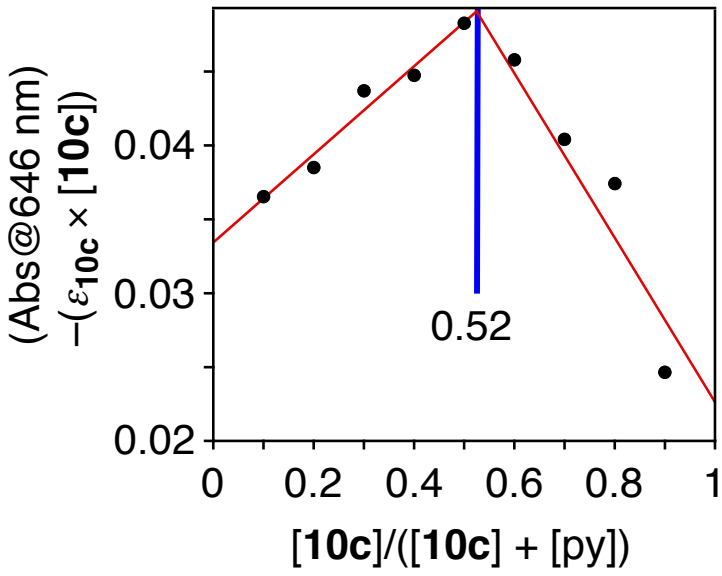

Figure 4-11. A Job's plot for (**10c**)$_2$-X and pyridine in CH_2Cl_2 at 298 K. The plot was made by setting the total concentration of **10c**, which was calculated to be two-fold of the concentration of (**10c**)$_2$-X, and the pyridine as 1.32×10^{-4} M. [**10c**] and [py] refer to the concentrations of **10c** and pyridine, where [**10c**] = 1/2[(**10c**)$_2$-X].

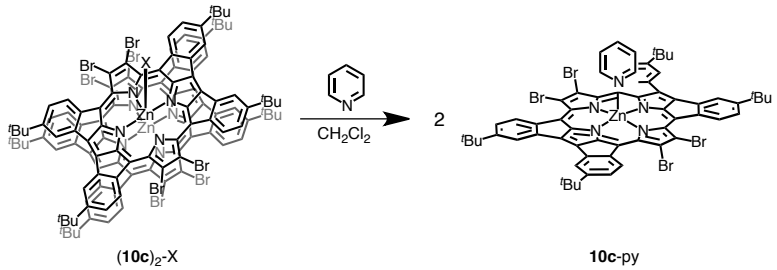

Scheme 4-3. Coordination process of pyridine on the Zn center of (**10c**)$_2$-X.

The K_{assoc} value of β-substituted ZnQFPs, **10c**, were also determined by UV-vis titration experiments (Figure 4-10); addition of pyridine up to 3.5×10^{-3} M caused strengthening of the Soret-like band, accompanying an isosbestic point at 620 nm, and the K_{assoc} value is determined to be $(2.2 \pm 0.1) \times 10^4$ M^{-1}. It is expected that introduction of electron-withdrawing groups such as Br groups of **10c** causes suppression of the electron donation from the porphyrin ligand to the Zn^{II} center, and thus, the Lewis acidity of the Zn^{II} center would increase. The K_{assoc} value of **10c** experimentally determined, however, was comparable to that of **4c**. This lower K_{assoc} value than expected can be explained by the fact that the dimeric structure of **10c** observed in the crystal structure (Figure 4-4) is maintained even in CH_2Cl_2 as supported by the ^{1}H NMR spectrum of **10c** in CD_2Cl_2 showing relatively complicated pattern due to the dimeric structure (Figure 4-5). In the dimeric structure, one of the non-fused pyrrole nitrogen atoms of **10c** coordinates to the Zn^{II} center of the other molecule of **10c** with X; the tridentate QFP ligand should enhances the Lewis acidity of the Zn center to thermodynamically stabilize the dimeric structure involving strong coordination of a solvent molecule

such as EtOH and the pyrrole nitrogen of the other molecule as in Figure 4-4. The considerable stability of the dimer can be competitive with that of the five-coordinated pyridine complex, **10c**-py, affording a smaller ΔG value of the equilibrium. Therefore, the K_{assoc} value of (**10c**)$_2$-X was smaller than that expected for simple ligand binding to vacant

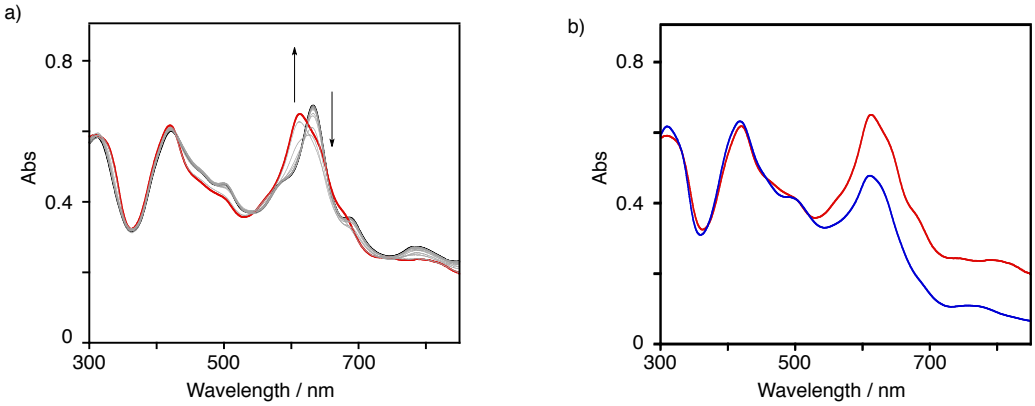

Figure 4-12. (a) UV-Vis spectral changes of **11c** upon titration with pyridine in CH_2Cl_2 at 298 K; (b) UV-Vis spectra of **11c** with pyridine (1.09×10^{-2} M; red) and **11c** with AcOH (1.75 M; blue) in CH_2Cl_2 at 298 K. The concentration of **11c** was set to be 1.47×10^{-5} M both for (a) and (b).

site of square square-planer and four-coordinate **4c**. To examine the molecular ratio between (**10c**)$_2$-X and pyridine in the associated complex, a Job's plot for the association of (**10c**)$_2$-X with pyridine was made under relatively concentrated conditions at 298 K (total concentration of **10c**, which was calculated to be two-fold of the concentration of (**10c**)$_2$-X, and pyridine: 1.32×10^{-4} M) (Figure 4-11). The Job's plot exhibited the peak at 0.52, indicating that the monomer **10c** associates with one pyridine molecule. Combining the fact that the spectral change showed isosbestic points (Figure 4-10), the dimer (**10c**)$_2$-X dissociates into the monomer **10c** upon addition of strongly coordinating pyridine to form a 1:1 complex of **10c** and pyridine in a one-step process (Scheme 4-3).

On the other hand, addition of pyridine to the solution of **11c** in CH_2Cl_2 brought a blue shift of the Soret-like band with showing a peak top at 613 nm (Figure 4-12a). To confirm the cause of this blue shift, acetic acid, which is acidic enough to demetalate ZnQFP but not enough to protonate H_2QFP (See Chapter 5), was added to the solution of **11c** in CH_2Cl_2 (Figure 4-12b); as a result, the spectrum of **11c** upon addition of acetic acid showed a similar spectral change to that upon addition of pyridine: The absorption maximum of the Soret-like band was observed at 611 nm upon addition of acetic acid, which was comparable to that observed upon addition of pyridine. In addition, in the MALDI-TOF-MS spectrum of the solution of **11c** after addition of pyridine, a peak cluster was observed at m/z = 1135.7, which was consistent with the simulated pattern to the demetalated **11c**. Thus, the spectral change observed upon addition of pyridine is probably derived from the demetalation process of **11c**.

4-6. Summary

The author has performed the functionalization at the β-positions of ZnQFP and has revealed the substituent effects at the β-positions of QFP on the absorption spectra and redox potentials. The substituents at the β-positions

more intensively affect the redox potentials of ZnQFP than those at the fused *meso*-aryl groups. The introduction of bromo and phenyl groups at the *β*-positions of the non-fused pyrroles of ZnQFP induced the tilting of the non-fused pyrroles against the porphyrin core plane, together with weakening of the coordination bond between the pyrrolic nitrogen atoms of the non-fused pyrroles and the Zn center. In fact, dissociation of a non-fused pyrrole from the Zn center was observed in the crystal structure of the tetrabromo-derivative, **10c**, and the dissociated pyrrolic nitrogen atoms coordinated to the Zn center of the other ZnQFP complex to form the dimeric structure, (**10c**)$_2$-EtOH, which was stable even in a CH_2Cl_2 solution as evidenced by the ^{1}H NMR spectrum.

4-7. Experimental section

General.

Chemicals and solvents were used as received from commercial sources unless otherwise mentioned. CH_2Cl_2 used for the UV-vis spectral measurements was distilled over CaH_2 before use. DMF for electrochemical studies and *N*,*N*-dimethylacetamide (DMA) for the synthesis were distilled before use.

^{1}H NMR measurements were performed on a Bruker AVANCE 400, 500 and 600 MHz spectrometers. UV-vis absorption spectra were measured in CH_2Cl_2 on a Shimadzu UV-3600 spectro- photometer. MALDI-TOF-MS spectrometry was performed on an AB SCIEX TOF/TOF 5800 spectrometer using dithranol as a matrix. Electrochemical experiments were done in DMF under an atmospheric pressure of Ar at 298 K on ALS/CH electrochemical analyzer model 710D.

Synthesis.

Zinc(II) 2,3,12,13-tetrabromo-24,30,36,42-tetrakis(*tert*-butyl)-quadruply-fused porphyrinato (10c). To a solution of **4c** (24 mg, 28 μmol) in $CHCl_3$ (50 mL) was added recrystallized NBS (24 mg, 140 μmol) and the reaction mixture was refluxed for 4 h. After cooling to room temperature, the reaction mixture was washed with water to remove any soluble succinimide-derived impurities. The brown-colored solid was chromatographed on a bio-beads S-X1 gel column using THF as an eluent. The second fraction was collected and the solvent was removed under vacuum. The residual solid was recrystallized from THF/EtOH (1:3, v/v) and dried under vacuum to yield (**10c**)$_2$-EtOH (12 mg, 10 μmol, 37%). ^{1}H NMR (DMSO-d_6, where **10c** is in the monomeric form): δ 8.02 (d, J = 8.0 Hz, 4H, 26,32,38,44-Ph-H), 7.06 – 6.86 (m, 8H, 23,25,29,31,35,37,41, 43-Ph-H), 1.30 (s, 36H, *t*-Bu-H). ^{1}H NMR (CD_2Cl_2, where **10c** is in the dimeric form, (**10c**)$_2$-X): δ 8.20 – 8.19 (m, 2H, *o*-Ph(fus)-H), 7.99 (d, J = 8.0 Hz, 4H, *o*-Ph(fus)-H) 7.88 – 7.86 (m, 2H, *o*-Ph(fus)-H), 6.99 – 6.60 (m, 16H, *m*-Ph(fus)-H), 1.34 (s, 18H, *t*-Bu-H), 1,32 (s, 54H, *t*-Bu-H). UV-vis (DMF): λ_{max} [nm] = 1109, 921, 827, 708, 657, 496, 428. MS (MALDI-TOF, dithranol matrix): *m/z* = 1211.6 (calcd. for $[M + H]^+$: 1211.0), 2418.2 (calcd. for $[(M)_2 + H]^+$: 2418.0).

Zinc(II) 2,3,12,13-tetrakisphenyl-24,30,36,42-tetrakis(*tert*-butyl)-quadruply-fused porphyrinato (11c). To a solution of the crude mixture of tetrabrominated (**10c**)$_2$-EtOH (10 mg, 4.2 μmol) in DMA (1 mL) was added phenylboronic acid (43 mg, 330 μmol), K_2CO_3 (150 mg, 660 μmol), and $Pd(PPh_3)_4$ (12 mg, 10 μmol).[16] The reaction

mixture was stirred at 130 °C for 10 h and the solvent was removed under vacuum. The residual solid was dissolved in $CHCl_3$ (30 mL) and filtered. To the filtrate was added TFA (3 mL) and the reaction mixture was stirred for 1 h at room temperature. The mixture was washed with Na_2CO_3 aq and water, and dried over Na_2SO_4. The solvent was removed under vacuum and the black solid obtained was chromatographed on a silica gel column using CH_2Cl_2/hexane (1:1, v/v) as an eluent. The second fraction was collected and the solvent was removed under vacuum. To a solution of black powder in $CHCl_3$ (10 mL) was added a suspension of $Zn(OAc)_2 \cdot 2H_2O$ (7.4 mg, 34 μmol) in CH_3OH (2 mL) and the reaction mixture was refluxed for 2 h. The reaction mixture was poured into water and the organic phase was separated and then dried over Na_2SO_4. The residual solid was recrystallized from THF/hexane (1:3, v/v) and the crystalline solid obtained was dried under vacuum to yield **11c** (5.8 mg, 4.8 μmol, 58% (2 steps)). ^{1}H NMR (DMSO-d_6): δ 7.46 (m, 8H, β-*o*-Ph-H), 7.39 (m, 12H, β-*m,p*-Ph-H), 6.78 (s, 4H, 23,29,35,41-Ph-H), 6.07 (d, J = 7.9 Hz, 4H, 25,31,37,43-Ph-H), 5.01 (d, J = 7.9 Hz, 4H, 26,32,38,44-Ph-H), 1.15 (s, 36H, *t*-Bu-H). UV-vis (DMF): λ_{max} [nm] = 418, 500, 637, 802, 977, 1092. MS (MALDI-TOF, *dithranol matrix*): *m/z* = 1198.6 (calcd. for $[M]^+$: 1198.9).

X-ray diffraction analysis.

A single crystal of (**10c**)$_2$-EtOH was obtained by recrystallization from the THF solution with vapor deposition method using EtOH as a poor solvent. The single crystal was mounted on a mounting loop. All diffraction data were collected at 120 K by using a Bruker APEXII diffractometer equipped with graphite-monochromated Mo $K\alpha$ (λ = 0.71073 Å) by the ω-2θ scan. The structure was solved by direct methods using SIR97 and SHELX97.[17]

Table 4-4. Crystallographic data for (**10c**)$_2$-EtOH.

crystal system	triclinic
space group	$P\ \bar{1}$
T / K	120
formula	$C_{132}H_{124}N_8O_4Br_8Zn_2$
FW	2656.40
a / Å	11.751(5)
b /Å	20.751(5)
c /Å	82.420(5)
a / °	82.470(5)
b / °	89.413(5)
g / °	74.957(5)
V / Å^3	6277(3)
Z	2
l / Å	0.71073 (Mo Ka)
D_c / g cm^{-3}	1.405
reflns measured	34492
reflns unique	14312
$R1$ ($I > 2s(I)$)	0.0564
$wR2$ (all)	0.1603
GOF	0.976

Crystallographic data for (**10c**)$_2$-EtOH are summarized in Table 4-4. The co-crystallized four EtOH molecules and a THF molecule in the crystal of (**10c**)$_2$-EtOH were severely disordered and thus deleted by using the SQUEEZE program.[18]

Computational method.

DFT calculations were performed with optimized local minima using the B3LYP method[19,20] combined with the 6-31G(d) basis set.[21,22] The Gaussian 09 program package[23] was used for all DFT calculations.

Reference and notes

1 (a) *The Porphyrin Handbook*, *Vol. 1-10* (eds.: K. M. Kadish, K. M. Smith, R. Guilard), Academic Press, New York, **2000**. (b) K. M. Kadish, M. M. Morison, *J. Am. Chem. Soc.* **1976**, *98*, 3326.

2 (a) A. Giraudeau, H. J. Callot, M. Gross, *Inorg. Chem.* **1979**, *18*, 201. (b) A. Giraudeau, H. J. Callot, J. Jordan, I. Ezhar, M. Gross, *J. Am. Chem. Soc.* **1979**, *101*, 3857.

3 (a) K. M. Kadish, M. M. Morrison, *Bioinorg. Chem.* **1977**, *7*, 107. (b) F. A. Walker, D. Beroiz, K. M. Kadish, *J. Am. Chem. Soc.* **1976**, *98*, 3484. (c) K. M. Kadish, M. M. Morrison, L. A. Constant, L. Dickens, D. G. Davis, *J. Am. Chem. Soc.* **1976**, *98*, 8387.

4 Reviews on this topic: (a) S. Fox, R. W. Boyle, *Tetrahedron* **2006**, *62*, 10039. (b) J. P. Lewtak, D. T. Gryko, *Chem. Commun.* **2012**, *48*, 10069. (c) H. Mori, T. Tanaka, A. Osuka, *J. Mater. Chem. C* **2013**, *1*, 2500. (d) M. Stępień, E. Gońka, M. Żyła, N. Sprutta, *Chem. Rev.* **2017**, ASAP (DOI: 10.1021/acs.chemrev.6b00076).

5 (a) N. K. S. Davis, A. L. Thompson, H. L. Anderson, *J. Am. Chem. Soc.* **2011**, *133*, 30. (b) N. K. S. Davis, A. L. Thompson, H. L. Anderson, *Org. Lett.* **2010**, *12*, 2124. (c) A. N. Cammidge, P. J. Scaife, G. Berber, D. L. Hughes, *Org. Lett.* **2005**, *7*, 3413.

6 (a) T. Ishizuka, Y. Saegusa, Y. Shiota, K. Ohtake, K. Yoshizawa, T. Kojima, *Chem. Commun.* **2013**, *49*, 5939. (b) Y. Saegusa, T. Ishizuka, K. Komamura, S. Shimizu, H. Kotani, N. Kobayashi, T. Kojima, *Phys. Chem. Chem. Phys.* **2015**, *17*, 15001. (c) Y. Saegusa, T. Ishizuka, T. Kojima, S. Mori, M. Kawano, T. Kojima, *Chem. Eur. J.* **2015**, *21*, 5302.

7 M. P. Byrn, C. J. Curtis, Y. Hsiou, S. I. Khan, P. A. Sawin, S. K. Tendick, A. Terzis, C. E. Strouse, *J. Am. Chem. Soc.* **1993**, *115*, 9480.

8 *The Hydrogen Bond* (Eds.: P. Schuster, G. Zundel, C. Sandorfy), North-Holland Publ. Co., Amsterdam, **1976**.

9 J. Nakazawa, M. Mizuki, J. Hagiwara, Y. Shimazaki, F. Tani, Y. Naruta, *Bull. Chem. Soc. Jpn.* **2006**, *79*, 1431.

10 H. Furuta, T. Ishizuka, A. Osuka, *Inorg. Chem. Commun.* **2003**, *6*, 398.

11 C. Hansch, A. Leo, R. W. Taft, *Chem. Rev.* **1991**, *91*, 165.

12 Rhombic distortions were also found in other porphyrin derivatives. (a) A. N. Kozyrev, V. Suresh, S. Das, M. O. Senge, M. Shibata, T. J. Dougherty, R. K. Pandey, *Tetrahedron* **2000**, *56*, 3353. (b) M. O. Senge, W. W. Kalisch,

S. Runge, *Tetrahedron* **1998**, *54*, 3781. (c) M. O. Senge, Y. M. Shaker, M. Pintea, C. Ryppa, S. S. Hatscher, A. Ryan, Y. Sergeeva, *Eur. J. Org. Chem.* **2010**, 237.

13 (a) C. H. Kirksey, P. Hambright, C. B. Storm, *Inorg. Chem.* **1969**, *8*, 2141. (b) T. Mizutani, K. Wada, S. Kitagawa, *J. Am. Chem. Soc.* **1999**, *121*, 11425. (c) T. Kojima, T. Nakanishi, T. Honda, R. Harada, M. Shiro, S. Fukuzumi, *Eur. J. Inorg. Chem.* **2009**, 727.

14 As a preliminary experiment, compound **4b** catalyzed hydrolysis of DMF into dimethylamine and formic acid in water, using its strong Lewis acidity.

15 A. Levens, F. An, M. Breugst, H. Mayr, D. W. Lupton, *Org. Lett.* **2016**, *18*, 3566.

16 (a) A. Suzuki, *Chem. Commun.* **2005**, 4759. (b) L. Yin, J. Liebscher, *Chem. Rev.* **2007**, *107*, 133. (c) S. Chamoin, S. Houldsworth, C. G. Kruse, W. Iwema Bakker, V. Snieckus, *Tetrahedron Lett.* **1998**, *39*, 4179.

17 G. M. Sheldrick, SIR97 and SHELX97, Programs for Crystal Structure Refinement, University of Göttingen, Göttingen (Germany), 1997.

18 P. V. D. Sluis, A. L. Spek, *Acta Crystallogr.* **1990**, *A46*, 194.

19 A. D. Becke, *Phys. Rev. A* **1988**, *38*, 3098.

20 C. Lee, W. Yang, R. G. Parr, *Phys. Rev. B* **1988**, *37*, 785.

21 R. Ditchfield, W. J. Hehre, J. A. Pople, *J. Chem. Phys.* **1971**, *54*, 724.

22 W. J. Hehre, R. Ditchfield, J. A. Pople, *J. Chem. Phys.* **1972**, *56*, 2257.

23 Gaussian 09, Revision D.01, M. J. Frisch, G. W. Trucks, H. B. Schlegel, G. E. Scuseria, M. A. Robb, J. R. Cheeseman, G. Scalmani, V. Barone, B. Mennucci, G. A. Petersson, H. Nakatsuji, M. Caricato, X. Li, H. P. Hratchian, A. F. Izmaylov, J. Bloino, G. Zheng, J. L. Sonnenberg, M. Hada, M. Ehara, K. Toyota, R. Fukuda, J. Hasegawa, M. Ishida, T. Nakajima, Y. Honda, O. Kitao, H. Nakai, T. Vreven, J. A. Montgomery, Jr., J. E. Peralta, F. Ogliaro, M. Bearpark, J. J. Heyd, E. Brothers, K. N. Kudin, V. N. Staroverov, R. Kobayashi, J. Normand, K. Raghavachari, A. Rendell, J. C. Burant, S. S. Iyengar, J. Tomasi, M. Cossi, N. Rega, J. M. Millam, M. Klene, J. E. Knox, J. B. Cross, V. Bakken, C. Adamo, J. Jaramillo, R. Gomperts, R. E. Stratmann, O. Yazyev, A. J. Austin, R. Cammi, C. Pomelli, J. W. Ochterski, R. L. Martin, K. Morokuma, V. G. Zakrzewski, G. A. Voth, P. Salvador, J. J. Dannenberg, S. Dapprich, A. D. Daniels, Ö. Farkas, J. B. Foresman, J. V. Ortiz, J. Cioslowski, D. J. Fox, Gaussian, Inc., Wallingford CT, 2009.

Chapter 5

Acid-Base properties of a freebase form of ring-fused porphyrins

5-1. Introduction

Freebase porphyrins have attracted much attention not only for versatile utility as ligands for various metal ions,[1] but also due to the interest in the unique electrochemical properties.[2] For instance, inspired by the fact that pheophytin, the freebase form of chlorophyll, is utilized as the first electron acceptor from the photo-excited special pair in the reaction center of photosystem II,[3] freebase porphyrins have been used as an electron acceptor in photoinduced electron-transfer systems with use of zinc(II)-porphyrinato complexes as electron donors.[4] Freebase porphyrins also can function as weak bases (pK_a = ~4),[5] whereas they can inversely behave as weak acids to release one proton.[6] Porphyrins are known to selectively undergo diprotonation and thus the intermediate monoprotonated state is difficult to be detected.[5, 7-9] Protonation of a freebase porphyrin has been known to exert strong impacts on shape and

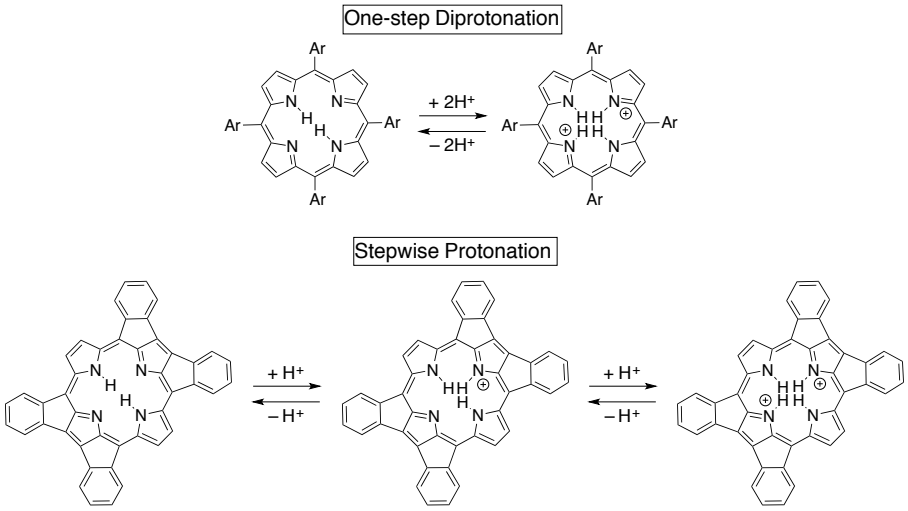

Scheme 5-1. Acid-base properties of tetraphenylporphyrin and quadruply-fsed porphyrin.

electronic structure of the π-conjugated system, as represented by conformational deformation of the ring structure,[5c,10] red shifts of the absorption bands,[11,12] and elevation of the redox potentials.[2c,13] Diprotonated porphyrins also have attracted interest due to their self-aggregation induced by protonation.[14,15] In addition, the elevated reduction potentials of diprotonated porphyrins enable them to act as efficient electron acceptors in photoinduced electron transfer.[16]

Recently, a lot of efforts have been dedicated to synthesis and characterization of novel π-expanded porphyrins having ring-fused structures at the periphery.[17-32] Among them, the derivatives having fused five-membered rings have attracted attention due to the interest in their unique aromaticity.[30] However, effects of the ring fusion on properties of

the freebase derivatives of ring-fused porphyrins, such as acid-base properties, have yet to be explored. The synthesis of a zinc(II) complex of a quadruply-fused porphyrin (Zn^{II}QFP), and the characteristics and supramolecular interaction with fullerenes have been reported.[33] The QFP ligand in Zn^{II}QFP shows a rhombically distorted structure; that is, the interatomic distance between the two inner nitrogen atoms of the fused pyrroles is shortened, whereas that between the two inner nitrogen atoms of the non-fused pyrroles is elongated, relative to those of Zn^{II}TPP (TPP = tetraphenylporphyrin).[33a] Consequently, the mean bond distance between the nitrogen atoms and the central Zn^{II} ion is elongated in comparison with that of Zn^{II}TPP; as a result of the elongation, the Lewis acidity of the central Zn^{II} ion is enhanced.[33b,c] Additionally, the π-conjugation circuit of QFP expands to the fused *meso*-aryl groups and the properties of QFP such as redox potentials are highly sensitive to the substituents at the fused aryl groups.[33b] The expansion of the π-conjugation circuit causes contribution of antiaromatic circuits to the magnetic properties of QFP.[33b] Concerning the protonation of freebase ring-fused porphyrins, however, no detailed investigation has been made to elucidate impacts of the protonation on the characteristics including electronic structures and redox potentials. Herein, the author describes synthesis and characterization of a novel freebase QFP derivative, together with the stepwise protonation behavior (Scheme 5-1). Furthermore, the unsymmetrical structure of the monoprotonated QFP derivative has been elucidated by an ESR spectrum of its electrochemically $1e^-$-reduced species.

5-2. Synthesis and spectroscopic characterization of the freebase form of a quadruply fused porphyrin

Syntheses of freebase QFP derivatives can be performed by treatment of the Zn^{II} complex (**4c**)[33] with TFA (= trifluoroacetic acid) in $CHCl_3$ (Scheme 5-2). Herein, the author chose the *tert*-butyl *(t*-Bu) derivative of QFP, which has four *t*-Bu groups at the *para*-position of the fused *meso*-aryl groups, because the freebase form of the *t*-Bu-QFP, **12c**, is exceptionally soluble in $CHCl_3$ among the QFP derivatives synthesized so far. Characterization of **12c** was performed by ^{1}H NMR and UV-Vis spectroscopies, MALDI-TOF-MS spectrometry, elemental analysis, and single-crystal X-ray crystallography (See below).

In the ^{1}H NMR spectrum of **12c** in $CDCl_3$, only six signals were observed, reflecting the D_{2h} symmetry (Figure 5-1a). Four signals observed in the range of δ 6.7 – 7.6 ppm were derived from the pyrrole β-Hs and the hydrogen atoms of the fused aryl groups. A broad signal observed at 4.98 ppm was assigned to the inner NH protons. To confirm the exchangeability of the NH protons, an aliquot of D_2O was added to the solution. Then the ^{1}H NMR signal at 4.98 ppm gradually diminished, and simultaneously, the doublet signal at 7.53 ppm (J = 1.6 Hz; Figure 5-1a, Inset) became a singlet (Figure 5-1b). This indicates that the signal at 7.55 ppm is ascribable to the pyrrole-β protons, coupled with the inner NH protons observed at 4.98 ppm. Therefore, the inner NH protons were revealed to localize at the non-fused pyrroles (see below).[34] Even at low temperature, the ^{1}H NMR signal of the inner NH protons did not show splitting due to formation of the other NH tautomer having the NH protons at the fused pyrroles (Figure 5-2). Additionally, the inner NH signal was highly downfield shifted in comparison to that of the corresponding TPP derivative, tetrakis(*p*-*t*-Bu-phenyl)-porphyrin (**6c**; Chart 5-1):[35] δ_{NH} –2.77 ppm. The downfield shift observed for the

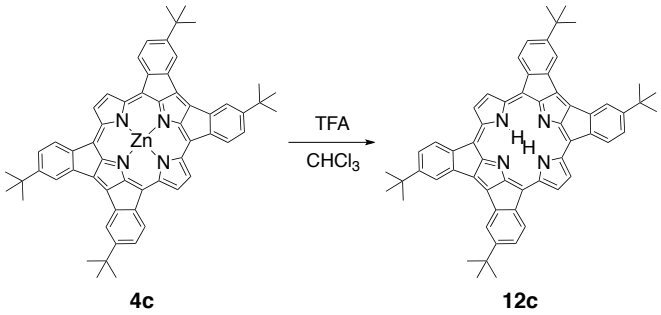

Scheme 5-2. Synthesis of a freebase QFP derivative, **12c**.

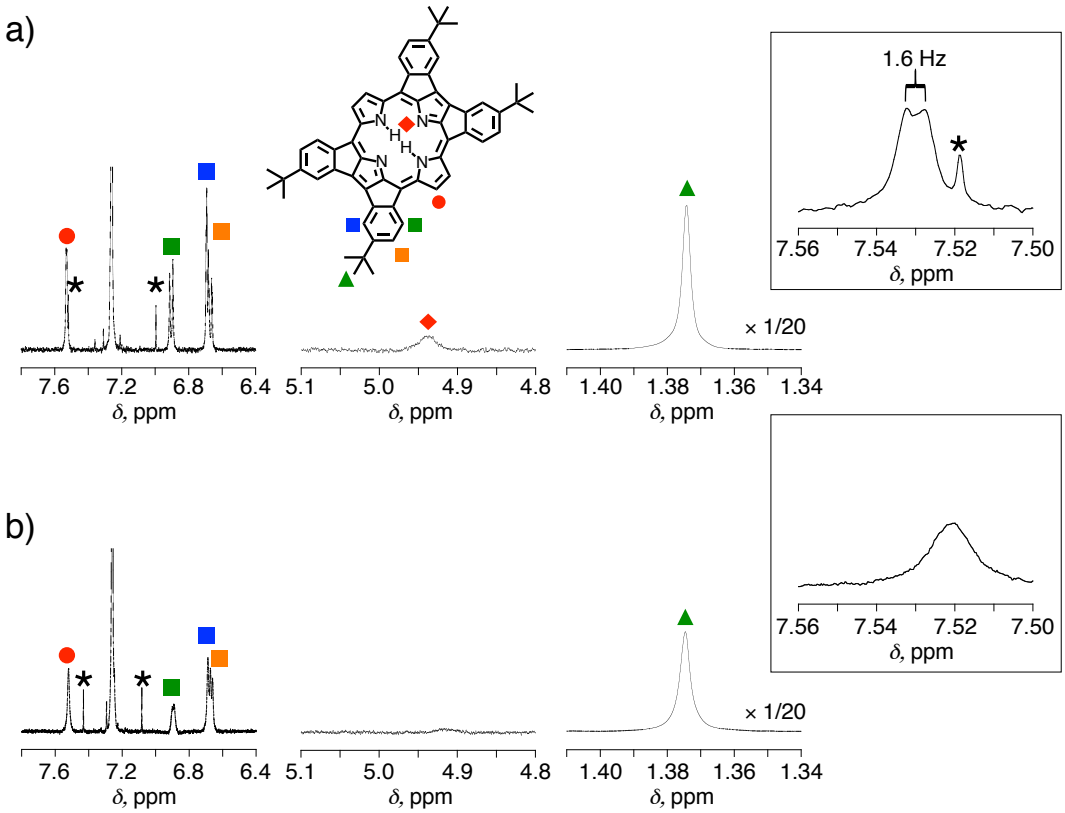

Figure 5-1. ^{1}H NMR spectra of **12c** in $CDCl_3$ at 298 K before (a) and after addition of an aliquot of D_2O (b). Insets: Magnified spectra in the range of 7.52 – 7.58 ppm. Asterisks (*) denote the satellite signal of chloroform.

NH signal of **12c** can be accounted for by the weak aromatic currents of **12c** and strong hydrogen bonding of the inner NH protons with the vicinal imine nitrogen atoms in **12c**. As described previously,[30a, 33b] the shielding effect on the inside of QFP is weak due to contribution of the antiaromatic ring currents. In fact, the NICS(1) value[36] of **12c** (–5.9) is more positive than that of **6c** (NICS(1): –13). On the other hand, the interatomic distances between adjacent nitrogen atoms of **12c** are shorter than those of **6c** (See below). As a result of the short distances, strong hydrogen bonding should be formed between inner NH protons and imine nitrogen atoms in **12c**. Supporting this assumption, the stretching band of the inner N-H bonds (ν_{NH}) for **12c** was observed at 3134 cm^{-1} in the IR spectrum, which was low-energy shifted relative to that for **6c** (ν_{NH} = 3315 cm^{-1}).[37] The low-energy shift of the stretching band derives from

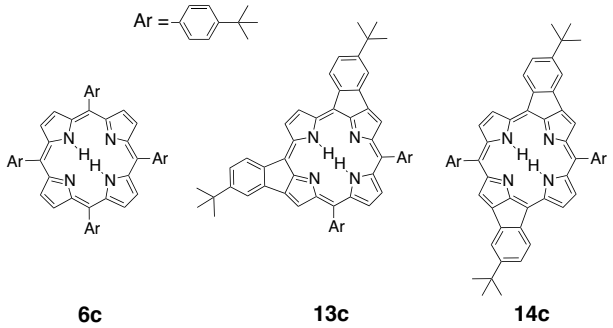

Chart 5-1. Molecular structures of compounds **6c**, **13c** and **14c**.

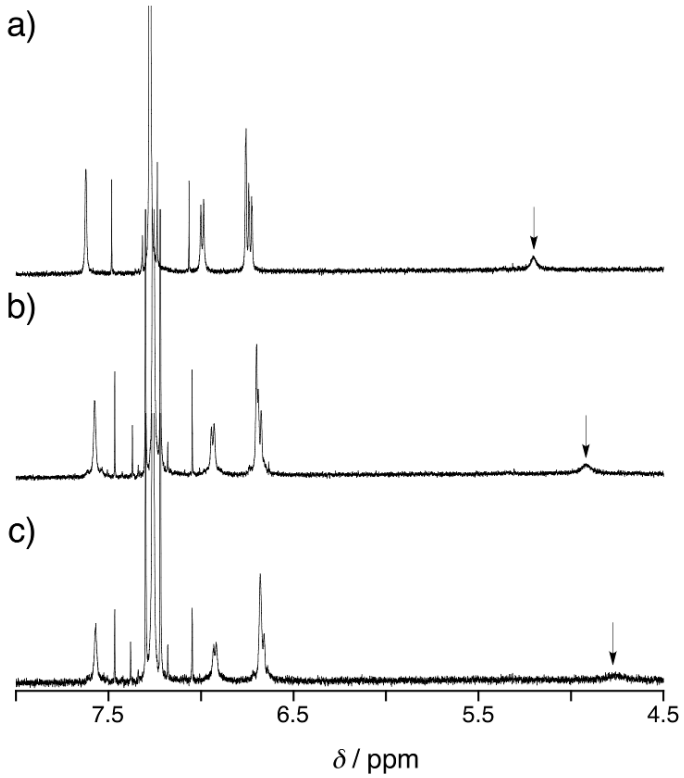

Figure 5-2. ^{1}H NMR spectra of **12c** (*ca.* 0.16 mM) in $CDCl_3$ at 298 K (a), 278 K (b) and 258 K (c). The signals indicated by arrows can be assigned to those of the inner NH protons.

the strong hydrogen bonding of the inner NH protons with the imine-nitrogen atoms in **12c**.[38] As mentioned above, the strong hydrogen bonding of **12c** also contributes to the downfield shift of the ^{1}H NMR signal of the inner NH protons.

5-3. Crystal structure of a freebase QFP

A single crystal of **12c** suitable for X-ray diffraction analysis was obtained with recrystallization from the solution in $CHCl_3$ with vapor diffusion of CH_3CN as a poor solvent. The crystal system is monoclinic with the space group of $P2_1/n$ and the asymmetric unit includes three and a half molecules of **12c** and four molecules of $CHCl_3$ as co-crystallized solvent molecules, which are highly disordered and thus deleted with the SQUEEZE program.[39] The

ORTEP drawings of one of the independent molecules of **12c** are shown in Figure 5-3. Compound **12c** is almost planar and the mean deviation from the least-square plane consisting of 48 atoms including the fused *meso*-aryl groups is 0.089 Å. Reflecting the planarity, the molecules of **12c** formed a π-π stacking pentamer (Figure 5-4) and the pentamer was surrounded by another molecule of **12c** due to the CH/π interaction between the *t*-Bu groups and the porphyrin π-plane. The porphyrin core of **12c** was rhombically distorted due to the ring-fusion, similarly to Zn^{II}QFP derivatives.[33]

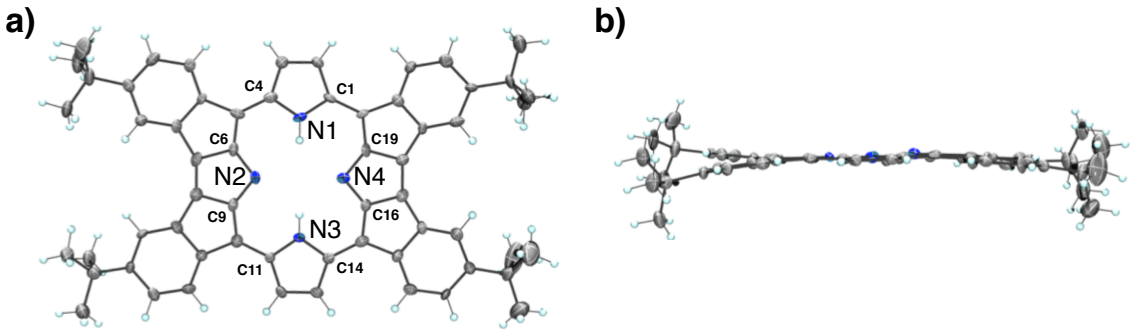

Figure 5-3. ORTEP drawings of the crystal structure of **12c**: (a) top and (b) side views with the thermal ellipsoids of 40% probability.

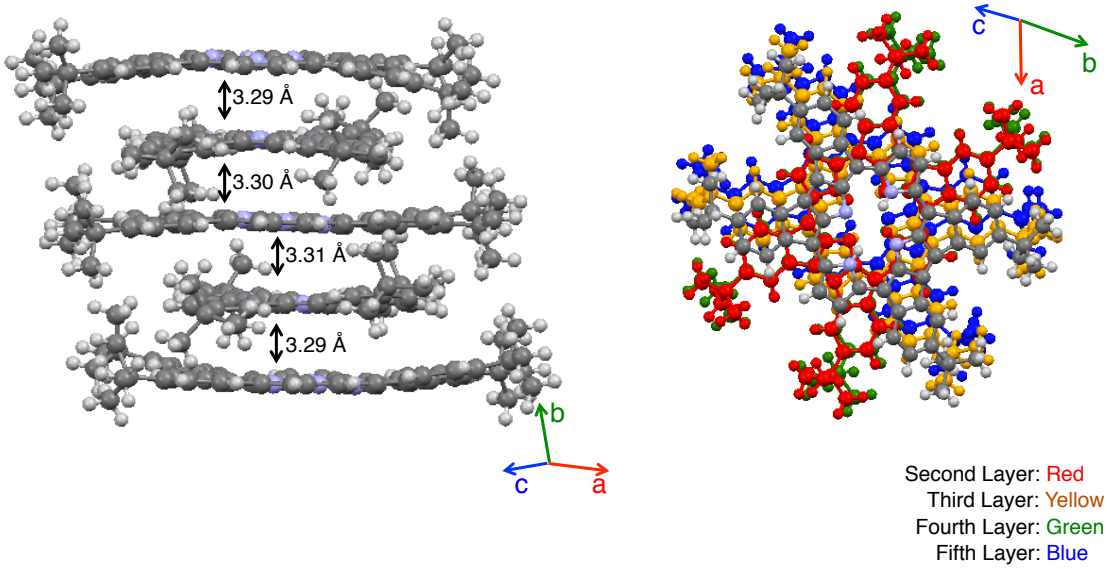

Figure 5-4. Crystal packing diagrams of **12c**.

The interatomic distances between two nitrogen atoms diagonally positioned are 4.615(9) Å for N1···N3 and 3.374(7) Å for N2···N4; that is, contracted between the fused pyrroles, whereas expanded between the non-fused pyrroles. Additionally, the bond angles of Cα-N-Cα of pyrroles showed characteristic difference between the fused and non-fused pyrroles; that is, those of non-fused pyrroles (∠C1-N1-C4 = 111.9(7)° and ∠C11-N3-C14 = 112.3(7)°) were wider than those of fused ones (∠C6-N2-C9 = 100.3(6)° and ∠C16-N4-C19 = 100.8(7)°). The wider bond angle of Cα-N-Cα over 109° in porphyrin pyrrole rings generally indicates that the inner NH proton localizes on the pyrrole,

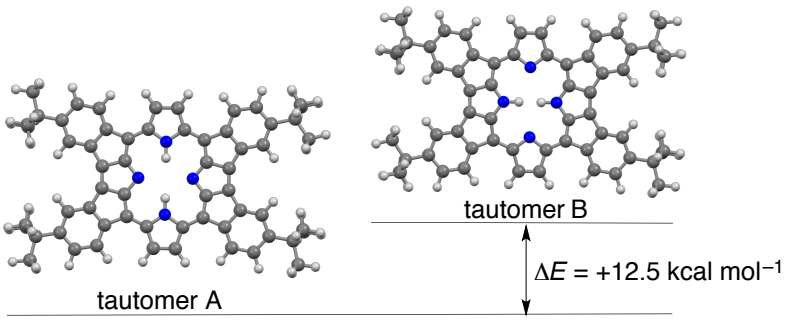

Figure 5-5. DFT-optimized structures of the two tautomers A (left) and B (right) at the B3LYP/6-31G** level of theory.

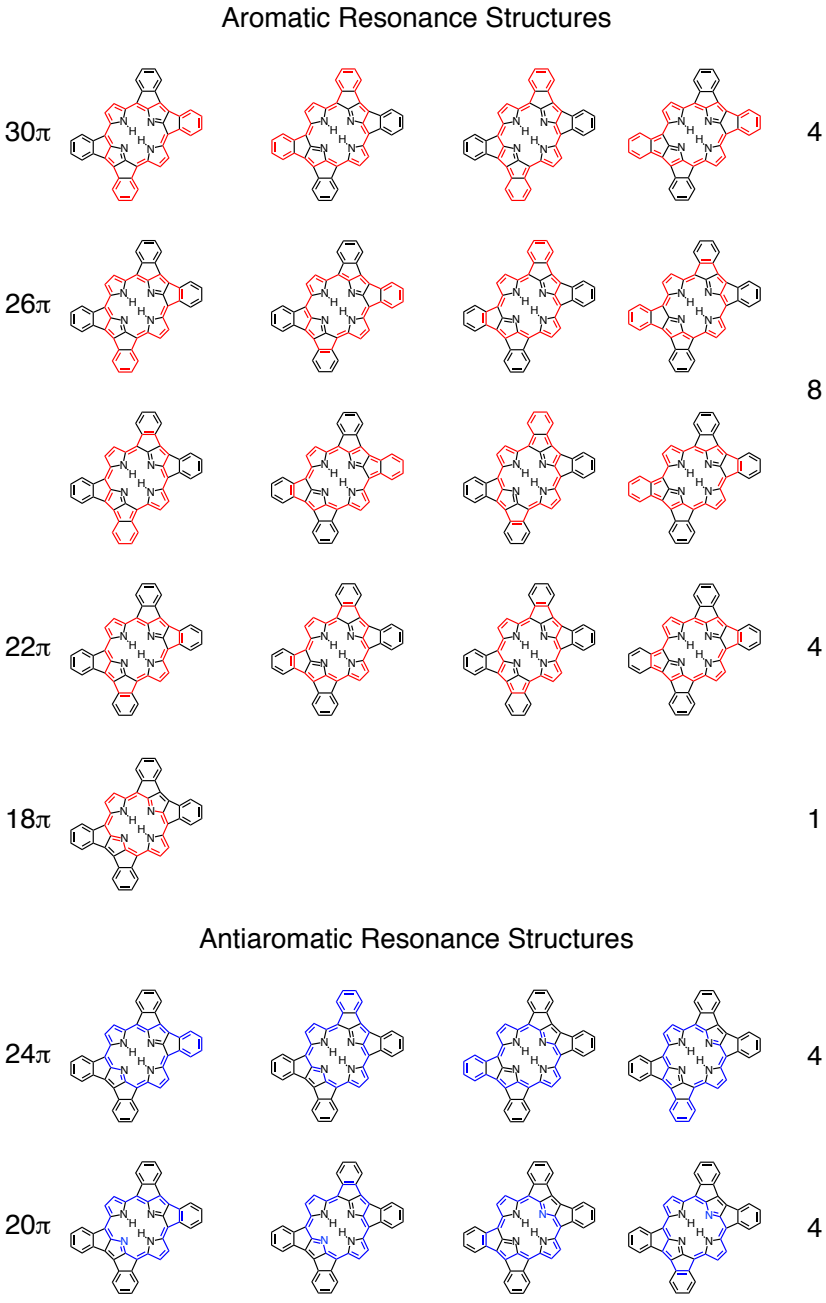

Figure 5-6. Possible resonance structures of tautomer A for **12c**.

whereas the narrower one below 105° does that the pyrrole is in the imino form.[40,41] Therefore, consistent with the results of the ^{1}H NMR spectroscopy (see above), the two inner NH protons localize at the non-fused pyrroles in the solid state as well as in solution.

5-4. DFT calculations on H_2QFP

To elucidate the difference in stability between two NH tautomers of **12c**, DFT calculations on them (Figure 5-5) was performed at the B3LYP/6-31G** level of theory. As a result, the tautomer A, which has the two inner NH protons on the non-fused pyrroles, is more stable by 12.5 kcal mol^{-1} than the tautomer B, in which the two inner NH protons are located on the fused pyrroles. The large difference in stability is probably derived from the two factors: the steric repulsion between the two closely located inner NH protons in tautomer B and the resonance stabilization in tautomer A. The N2···N4 distance (3.374(7) Å), observed in the crystal structure, is significantly shorter than the sum of two N-H bond lengths (*ca.* 1.0 Å)[42] and van der Waals radii of two hydrogen atoms (*ca.* 1.2 Å);[43] that is, 2 × 1.0 + 2 × 1.2 = 4.4 Å. Actually, the DFT-optimized structure of tautomer B exhibits deviation of the two inner NH protons from the QFP mean plane to avoid steric repulsion. In addition, for tautomer B, only 18π aromatic circuits can be drawn, whereas tautomer A has 25 kinds of resonance structures of 18π – 30π circuits including 20π and 24π antiaromatic circuits (Figure 5-6). The possible contribution of various resonance structures also assists the stability of the tautomer A.

5-5. Basicities of ring-fused porphyrins

The basicity of the imino-nitrogen atoms of the fused pyrroles in **12c** was explored by UV-Vis titration with TFA as an acid in CH_2Cl_2 at 298 K (Figure 5-7). The absorption spectrum of **12c** (1.5×10^{-5} M) in CH_2Cl_2 exhibited a Soret-like band at 604 nm and Q-like bands at 865, 817, and 744 nm; addition of TFA up to 1.5×10^{-4} M caused weakening and broadening of the Soret-like band, accompanying an isosbestic point at 428 nm (Figure 5-7a). Further addition of TFA brought rise and red-shift of the Soret-like band with showing an isosbestic point at 415 nm (Figure 5-7b). Therefore, it is clarified that **12c** undergoes two-step protonation (Scheme 5-3). Analysis of the absorbance change at 601 nm for the first step and that at 631 nm for the second step allowed us to determine the equilibrium constant of each step (insets of Figure 5-7): $K_1 = (1.3 \pm 0.1) \times 10^5$ M^{-1} and $K_2 = 7.3 \pm 0.3$ M^{-1}.

Table 5-1. Equilibrium Constants for Protonation of **12c**, **6c**, **13c** and **14c** with TFA in CH_2Cl_2 at 298 K

Compound	**12c**	**6c**	**13c**	**14c**
K_1, 10^5 M^{-1}	1.3 ± 0.1	—	1.1 ± 0.3	2.1 ± 0.2
K_2, M^{-1}	7.3 ± 0.3	—	$(1.9 \pm 0.3) \times 10^2$	$(1.4 \pm 0.2) \times 10^2$
β,[a] M^{-2}	$(9.5 \pm 1.1) \times 10^5$	$(1.0 \pm 0.3) \times 10^{10}$	$(2.1 \pm 1.0) \times 10^6$	$(2.9 \pm 0.7) \times 10^7$

[a] $\beta = K_1 \times K_2$.

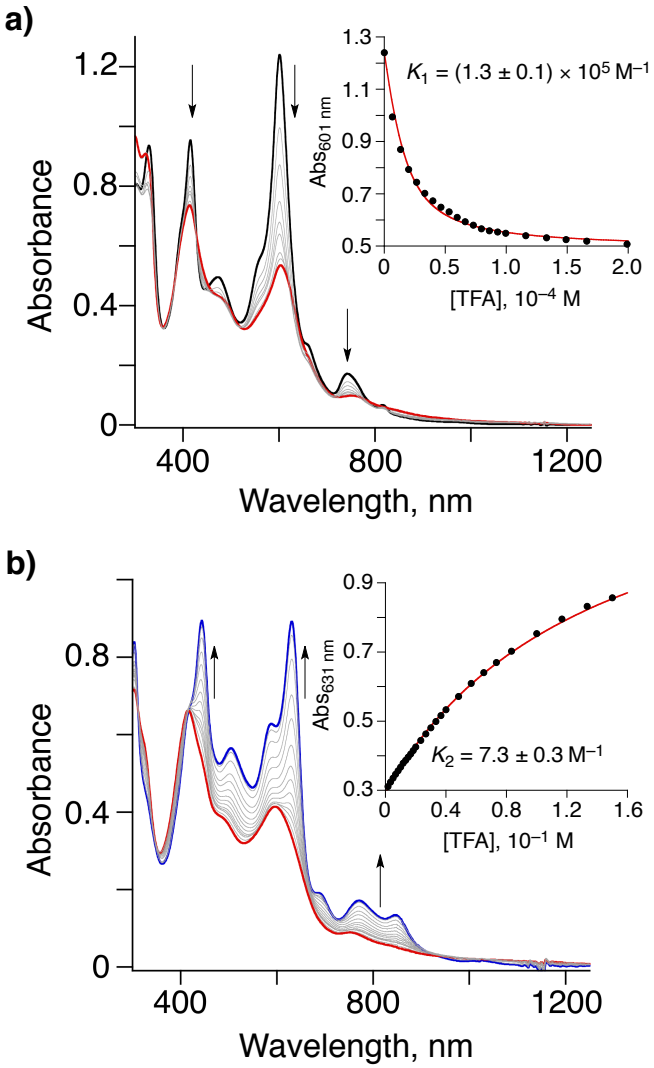

Figure 5-7. UV-Vis spectral changes of **12c** (1.5×10^{-5} M) in CH_2Cl_2 upon addition of TFA at 298 K. The concentration ranges of TFA are 0 – 1.5×10^{-4} M (a) and 5.0×10^{-3} – 0.15 M (b). The red traces in both (a) and (b) indicate the spectrum of the monoprotonated form. Insets: the absorbance changes at 601 nm for (a) and 631 nm for (b) and the fitting curves to obtain the equilibrium constants.

$$H_2P + H^+ \overset{K_1}{\rightleftharpoons} H_3P^+ \qquad K_1 = \frac{[H_3P^+]}{[H_2P][H^+]}$$

$$H_3P^+ + H^+ \overset{K_2}{\rightleftharpoons} H_4P^{2+} \qquad K_2 = \frac{[H_4P^{2+}]}{[H_3P^+][H^+]}$$

Scheme 5-3. Stepwise protonation equilibrium of porphyrin. H_2P, H_3P^+ and H_4P^{2+} denote neutral, monoprotonated and diprotonatd porphyrins, respectively.

As the equilibrium constants indicate, the second protonation is very difficult relative to the first protonation. As a piece of evidence to support that the first equilibrium process observed in the UV-Vis titration was monoprotonation of **12c**, a Job's plot was made with changing the concentration of **12c** and TFA (Figure 5-8). The Job's plot clearly

indicates that the binding process between **12c** and TFA is a 1:1 process, *i.e.* monoprotonation. To compare the equilibrium constants of the protonation, UV-Vis titrations of the TPP derivative, **6c**, and *cis*- and *trans*-doubly fused porphyrins (**13c** and **14c**; Chart 5-1) with TFA in CH_2Cl_2 were also performed (Figure 5-9 to 5-11). The equilibrium constants obtained are summarized in Table 5-1. Compound **6c** exhibited one-step diprotonation, as previously reported,[5] and the overall formation constant, β (= $K_1 \times K_2$), was determined to be $(1.0 \pm 0.3) \times 10^{10}$ M^{-2}. Doubly-fused

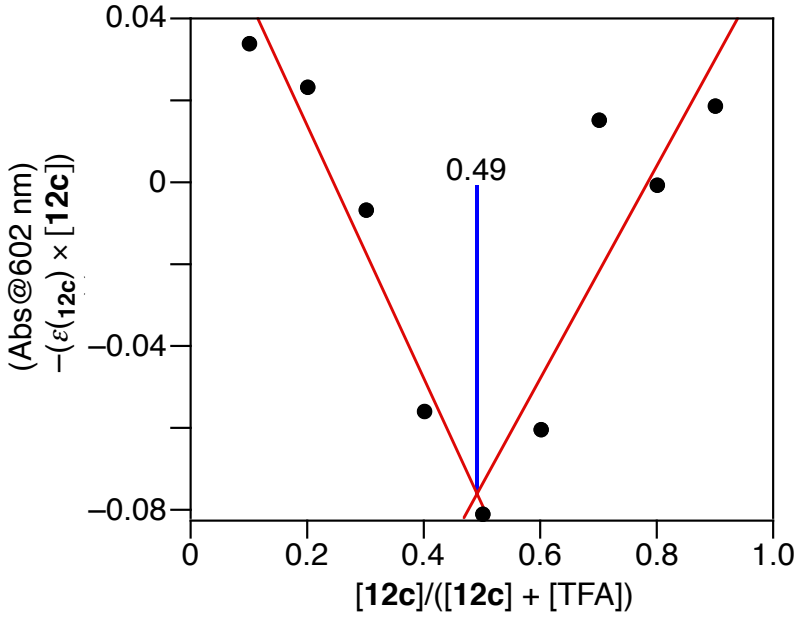

Figure 5-8. A Job's plot for **12c** with TFA in CH_2Cl_2 at 298 K. The total concentration of **12c** and TFA was set to be 2.9×10^{-5} M.

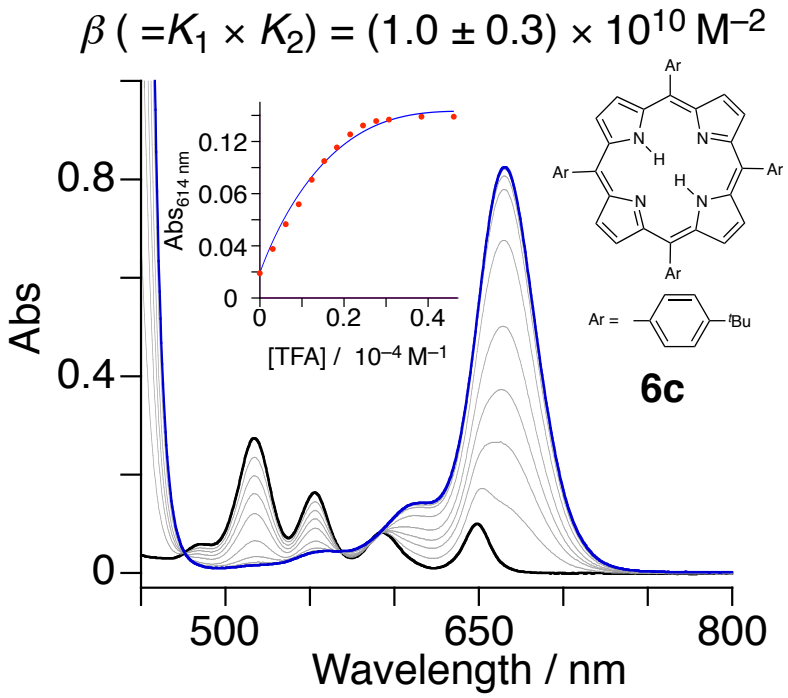

Figure 5-9. UV-Vis spectral change of **6c** (1.5×10^{-5} M) in CH_2Cl_2 upon addition of TFA. The concentration range of TFA is 0 – 4.6 $\times 10^{-5}$ M. Inset: the absorbance changes at 614 nm and the fitting curve to obtain the equilibrium constant.

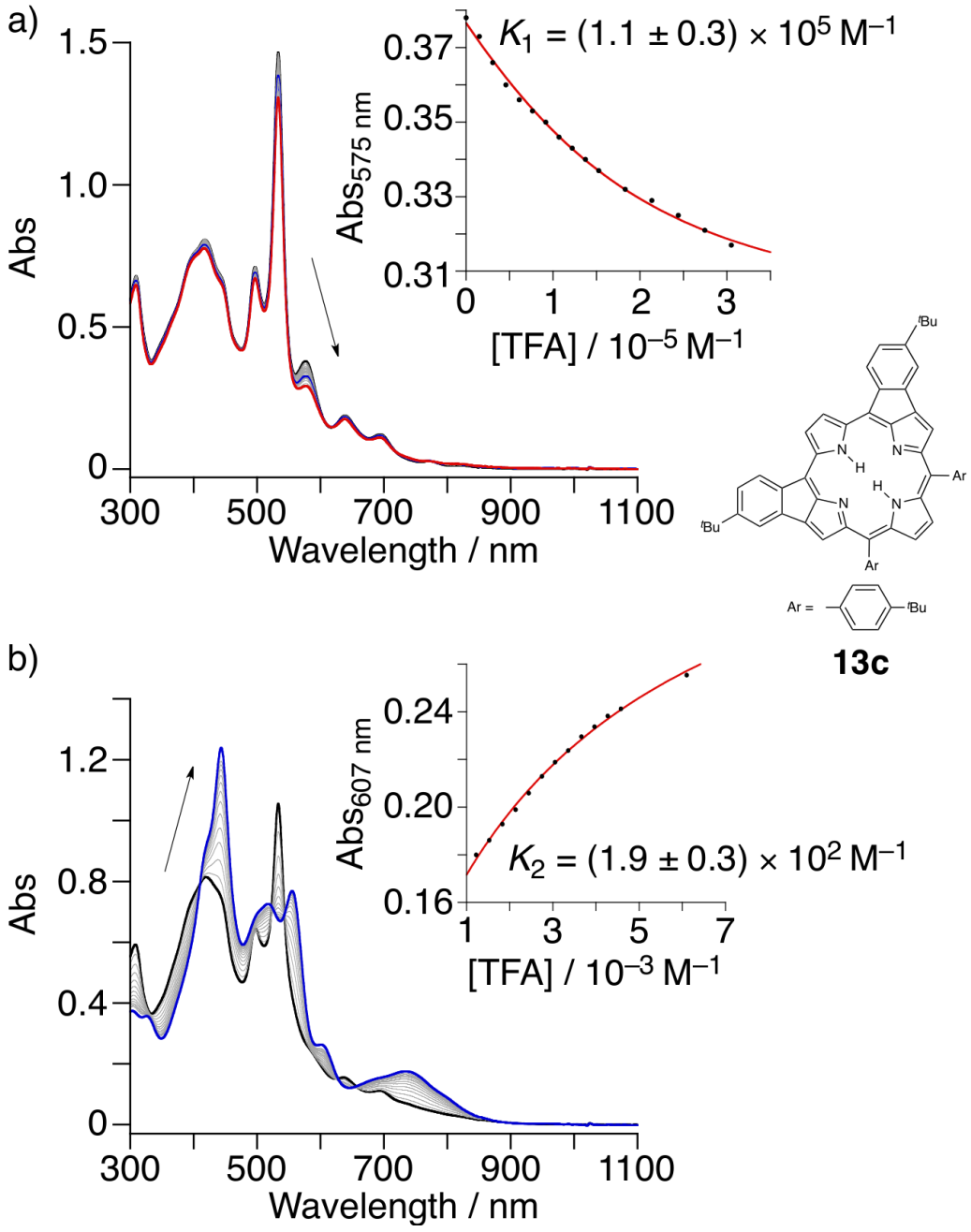

Figure 5-10. UV-Vis spectral changes of **13c** (1.5×10^{-5} M) in CH_2Cl_2 upon addition of TFA. The concentration ranges of TFA are $0 - 3.0 \times 10^{-5}$ M for (a) and $1.2 - 6.1 \times 10^{-3}$ M for (b). Inset: the absorbance changes at 575 nm for (a) and 607 nm for (b) and the fitting curves to obtain the equilibrium constants.

13c and **14c** exhibited two-step protonation, similarly to **12c**, and the Job's plots suggested that the first equilibrium processes were also based on the mono-protonation (Figure 5-12). The first protonation constants, K_1, of **12c**, **13c** and **14c** are in the same order of 10^5 M^{-1}, which corresponds to the square root of β for **6c** (1×10^5). Therefore, the first protonation is not significantly affected by ring-fusion. In sharp contrast, the

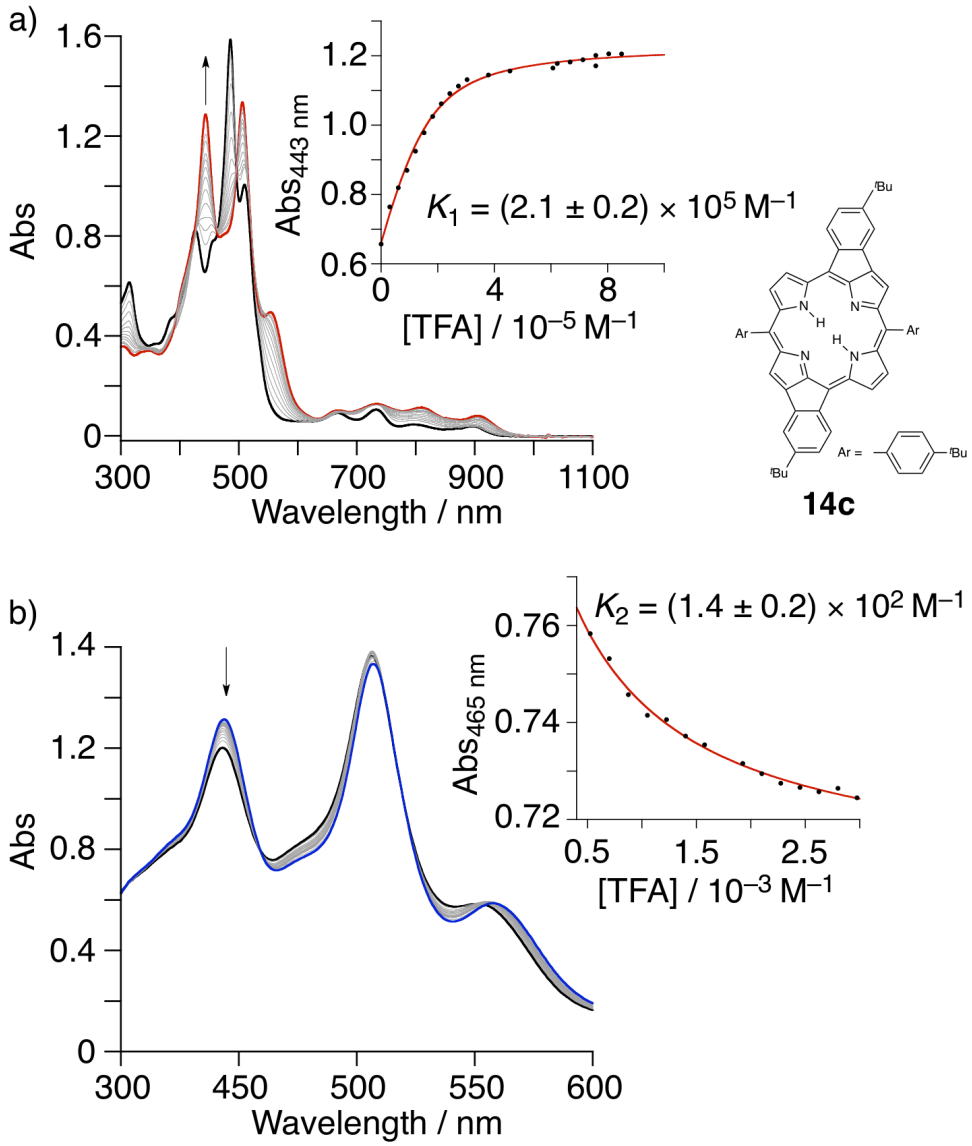

Figure 5-11. UV-Vis spectral changes of **14c** (1.5×10^{-5} M) in CH_2Cl_2 upon addition of TFA. The concentration ranges of TFA are $0 - 8.5 \times 10^{-5}$ M for (a) and $3.5 \times 10^{-3} - 3.0 \times 10^{-2}$ M for (b). Inset: the absorbance changes at 443 nm for (a) and 465 nm for (b) and the fitting curves to obtain the equilibrium constants.

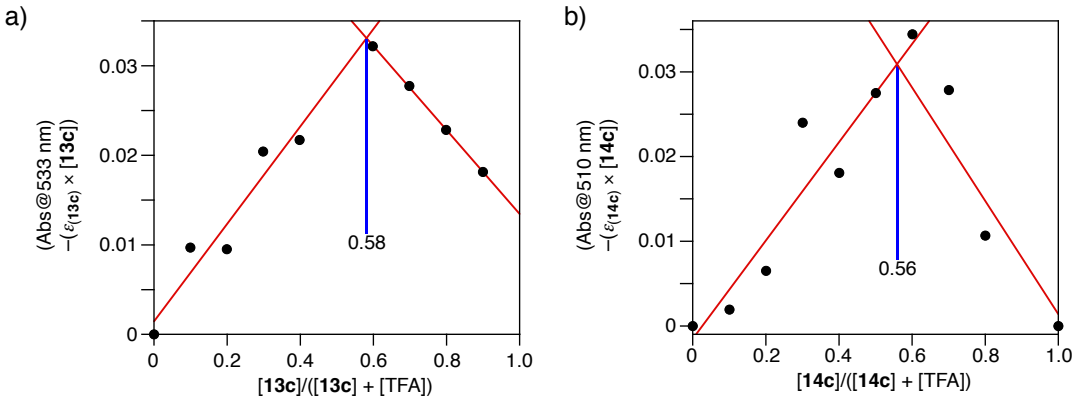

Figure 5-12. Job's plots for **13c** (a) and **14c** (b) with TFA in CH_2Cl_2 at 298 K. The total concentration of a doubly-fused porphyrin and TFA was set to be 2.9×10^{-5} M.

second protonation constants, K_2, of **12c**, **13c** and **14c** decrease with increase in the number of fused rings. Stepwise protonation behavior is relatively rare for porphyrins,[7-9] because the first protonation of a porphyrin causes loss of planarity of the skeletal conformation, making the second protonation more feasible. On the other hand, the difficulty in the second protonation of the fused porphyrins can be explained by the rigidity of the porphyrin skeleton caused by the ring-fusion, which makes it harder to avoid the steric repulsion among the inner protons.

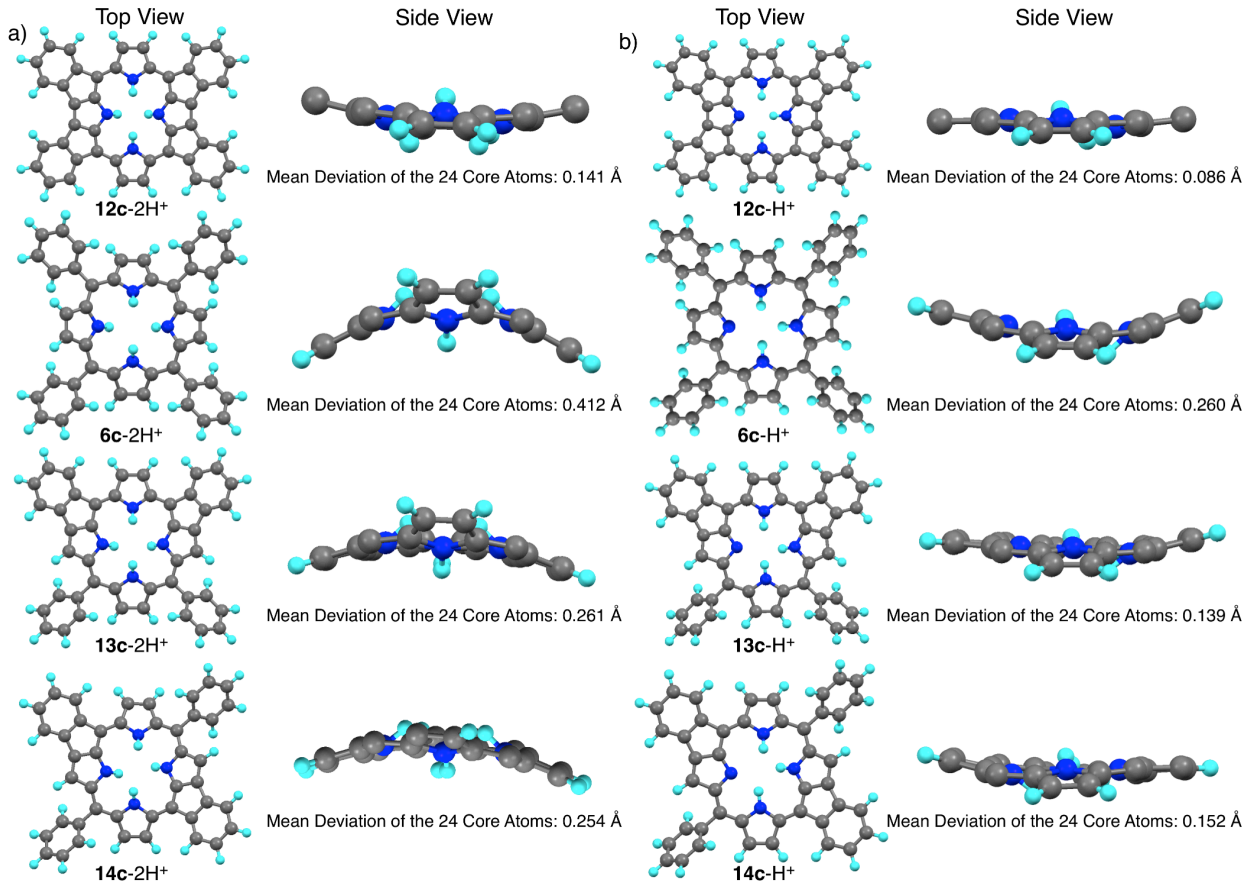

Figure 5-13. DFT-optimized structures of the diprotonatedand (a) and monoprotonated forms (b) of **12c**, **6c**, **13c**, and **14c** at the B3LYP/6-31G** level of theory. The *t*-Bu groups were replaced with hydrogen atoms for computational costs. In the side views, the fused-phenyl moieties and phenyl groups at the *meso*-positions are omitted for clarity.

As noted above, when normal porphyrins including **6c** are diprotonated, the steric repulsion among the inner four protons results in saddle-type distortion of the porphyrin core using the structural flexibility.[5c, 10c] On the other hand, the ring-fused porphyrins cannot strain enough to evade the steric repulsion among the inner protons, due to the structural rigidity gained by the ring-fusion. In fact, the DFT-optimized structures of the diprotonated forms for **12c**, **13c** and **14c** do not exhibit severe distortion of the porphyrin skeletons, compared to the structure of the diprotonated **6c** (Figure 5-13a). Instead of distortion of the porphyrin core, the N-H bonds are warped to opposite directions to avoid the steric repulsion among the inner protons as observed in the optimized structures, which causes the instability of the diprotonated forms. For the monoprotonated forms of **12c**, **13c** and **14c**, the three inner protons are placed in the inner space of the porphyrin core without distortion of the porphyrin core and severe warp of the N-H bonds to suppress the

steric repulsion (Figure 5-13b). Therefore, the first protonation constants for **12c**, **13c**, and **14c** do not become significantly small due to the ring fusion.[44]

5-6. Redox properties of protonated QFPs

To elucidate impacts of the protonation on redox potentials of freebase QFP, electrochemical studies of **12c** were performed in the presence of TFA (Figure 5-14 and Table 5-2). The solubility of monoprotonated **12c** (**12c**-H^+) is low in CH_2Cl_2 containing 0.1 M tetrabutylammonium hexafluoro- phosphate as an electrolyte for electrochemical measurements, and thus, 0.1 M tetrabutylammonium tetraphenylborate ($TBABPh_4$) was used as an electrolyte. Due to utilization of $TBABPh_4$, the potential window of electrochemical measurements was narrowed on the anodic side. Thus, only reduction waves of the QFP derivatives are discussed in this study. A cyclic voltammogram of **12c** in CH_2Cl_2 in the absence of acids exhibited quasi-reversible waves at –1.24 and –1.50 V vs Fc/Fc^+ (Figure 5-14a and d), which were assigned to the first and second reduction processes of **12c**, respectively.

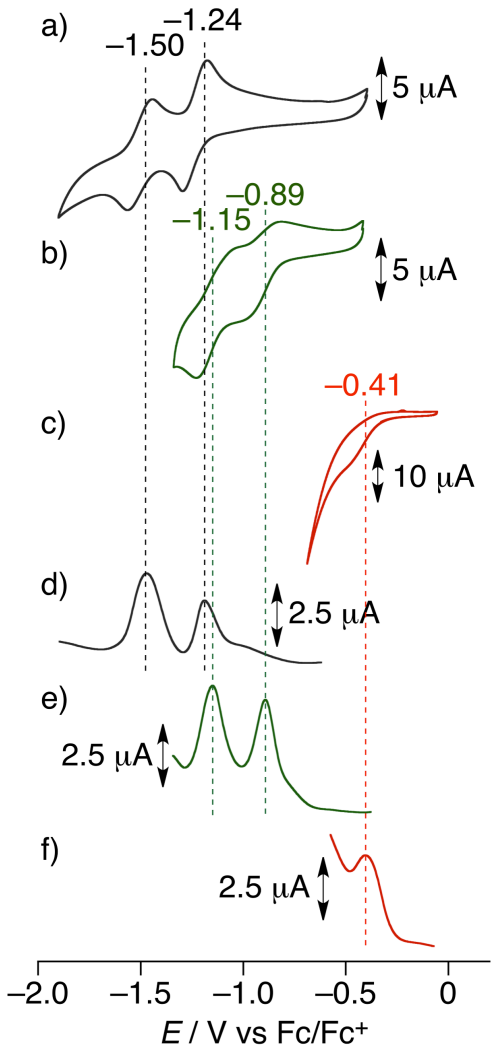

Figure 5-14. Cyclic (a, b and c) and differential-pulse voltammograms (d, e and f) of **12c** (a and d), **12c**-H^+ (b and e), and **12c**-$2H^+$ (c and f) in CH_2Cl_2 in the presence of $TBABPh_4$ (0.1 M) at 298 K. The detailed procedures to form protonated species of **12c** are described in the experimental section.

Table 5-2. Redox potentials of **12c** in its various protonated states in CH_2Cl_2 in the presence of 0.1 M $TBABPh_4$ at 298 K.

	E / V vs Fc/Fc^+	
	$P/P^{\bullet-}$	$P^{\bullet-}/P^{2-}$
12c	–1.24	–1.50
12c-H^+	–0.89	–1.15
12c-$2H^+$	–0.41	—

When the concentration of TFA was adjusted to be 1.3 mM in the solution of **12c** (0.61 mM) in CH_2Cl_2, 99% of **12c** in the solution was monoprotonated on the basis of the equilibrium constant described above and resultantly a positive shift of the reduction potentials was observed; the first and second quasi-reversible waves of **12c**-H^+ were observed at –0.89 and –1.15 V vs Fc/Fc^+ (Figure 5-14b and e). The potential shifts of the first and second redox processes were both +0.35 V, relative to those of **12c**. Upon further addition of TFA to reach the concentration of 1 M, 87% of **12c** in the solution was diprotonated; the first reduction potential was more positively shifted to –0.41 V vs Fc/Fc^+ (Figure 5-13c and f). The second reduction wave was not observed due to the fact that the potential window of the solution was narrowed by addition of excess TFA.

To elucidate the electronic structure of $1e^-$-reduced species of **12c**-H^+, an ESR spectrum of electrochemically $1e^-$-reduced **12c**-H^+ was measured in CH_2Cl_2 at 223 K (Figure 5-15). Controlled- potential bulk electrolysis of the CH_2Cl_2 solution of **12c**-H^+ in the presence of $TBABPh_4$ (0.1 M) was performed at –1.0 V vs Ag/AgCl at 223 K. As a result, a clear ESR signal was observed at g = 2.003 with

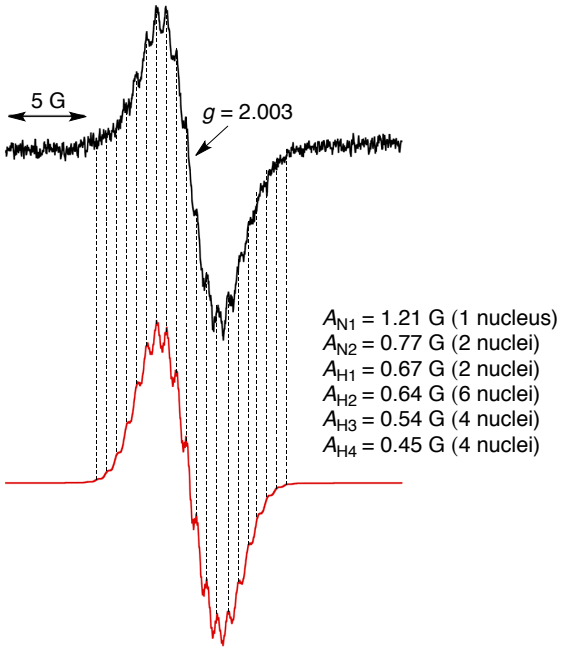

Figure 5-15. ESR spectrum (black line) of electrochemically $1e^-$-reduced **12c**-H^+ in CH_2Cl_2 at 223 K in the presence of $TBABPh_4$ (0.1 M) and the simulated one (red line) with the hyperfine coupling constants.

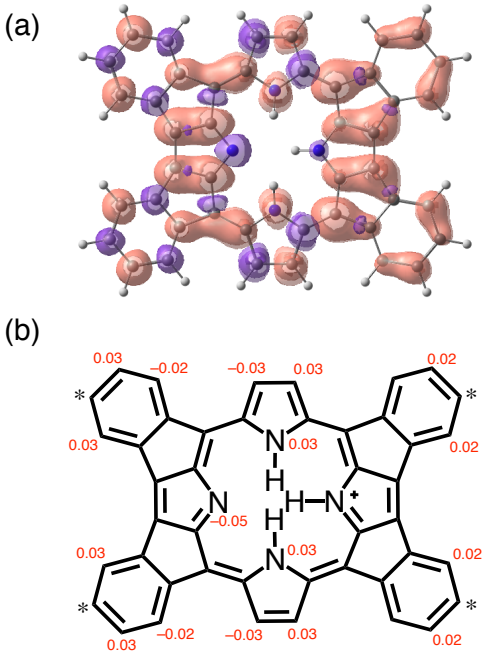

Figure 5-16. Spin density distribution (a) and schematic description of its spin densities (b) of the 1e$^-$-reduced species of **12c**-H$^+$ obtained by DFT calculations at the UB3LYP/6-31+G** level of theory. The *t*-Bu groups of **12c**-H$^+$ at the positions noted by asterisks (*) are replaced with hydrogen atoms for computational costs.

well-resolved hyperfine splitting in the ESR spectrum (black trace in Figure 5-15). To investigate the spin distributions of the 1e$^-$-reduced species of **12c**-H$^+$, DFT calculations were performed at the UB3LYP/6-31+G** level of theory. The spin-density distribution indicates that the unpaired electron localizes on three inner nitrogen atoms except the protonated fused pyrrole nitrogen atom (Figure 5-16). ESR simulation was performed (red trace in Figure 5-15) by considering contribution from hyperfine coupling with the three inner nitrogen nuclei and 16 protons attached to the two inner nitrogen, four pyrrole-β, and ten fused *meso*-aryl positions (Figure 5-16b). The simulated spectrum well reproduces the experimental result (Figure 5-15), and thus, the unsymmetrical electronic structure induced by the monoprotonation has been confirmed by the ESR measurement.

5-7. Summary

The author has synthesized and characterized a freebase derivative of QFP, **12c**. Particularly, the basicity of the inner imine nitrogen atoms in **12c** was investigated by UV-Vis titration in CH_2Cl_2 with TFA as an acid. As a result, the first protonation of **12c** proceeds similarly to TPP derivatives, whereas the second protonation is hard to occur unless a large excess amount of TFA is added. This difference stems from the fact that the monoprotonated form of **12c** maintains a stable planar structure; on the contrary, the diprotonated structure is unstable due to the severe repulsion among the four inner protons in the rigid planar framework of H_2QFP. The stepwise protonation also causes stepwise positive shifts of the reduction potentials of the H_2QFP derivatives. In addition, unsymmetrical electronic structure of the monoprotonated QFP has been revealed by the ESR spectrum of its 1e$^-$-reduced species, which was formed by electrochemical reduction.

5-8. Experimental section

General.

Chemicals and solvents were used as received from commercial sources unless otherwise mentioned. CH_2Cl_2 used for the UV-vis spectral measurements was distilled over CaH_2 before use. Compounds **4c**,[33b] **6c**[45] and 2,3,12,13-tetrabromo-tetrakis(*p*-*t*-Bu-phenyl)-porphyrin (**5c**)[33b] were synthesized according to the literature procedure.

^{1}H NMR measurements were performed on a Bruker AVANCE 400, 500 and 600 MHz spectrometers. UV-vis absorption spectra were measured in CH_2Cl_2 on a Shimadzu UV-3600 spectrophotometer. MALDI-TOF-MS spectrometry was performed on an AB SCIEX TOF/TOF 5800 spectrometer using dithranol as a matrix. ESR spectroscopy was performed on a Bruker EMXPlus9.5/2.7 spectrometer. Electrochemical experiments were done under an atmospheric pressure of Ar on an ALS/CH instruments electrochemical analyzer model 710D at 298 K with a CH_2Cl_2 solution of **12c** (0.61 mM), with that of **12c** (0.61 mM) including TFA (1.3 mM), in which 99% of **12c** were monoprotonated, and with that of **12c** (0.61 mM) including TFA (1 M), in which 87% of **12c** were diprotonated. The aforementioned three solutions of **12c** used for the electrochemical measurements contained $TBABPh_4$ (0.1 M) as an electrolyte. A small three-electrode cell (2.0 mL) was used with a gold-disk working electrode and a platinum wire as the counter electrode for the electrochemical measurements. The potentials were measured with respect to the Ag/AgCl reference electrode. Before the measurements, CV of ferrocene was measured to convert all of the potentials to values vs that of the ferrocene/ferrocenium redox couple. X-band ESR spectra were obtained on a spectrometer equipped with a temperature controller. To measure ESR spectra of the 1e$^-$-reduced species of **12c**-H$^+$, electrochemical reduction of **12c**-H$^+$ was performed in an ESR cell containing a CH_2Cl_2 solution of **12c** (0.53 mM), TFA (1.0 mM) as an acid and $TBABPh_4$ (0.1 M) as an electrolyte. The ESR cell was equipped with helix gold working electrode, gold wire as a counter electrode, and an Ag wire covered with AgCl as a reference electrode. The applied voltage was –1.0 V vs Ag/AgCl. The simulation of the ESR spectrum was carried out with use of the WinSIM software.[46]

Synthesis.

24,30,36,42-Tetrakis(*tert*-butyl)-quadruply-fused porphyrin (12c). To a solution of **4c** (32.6 mg, 36.4 μmol) in $CHCl_3$ (50 mL), was added TFA (6.0 mL, 78 mmol) and the reaction mixture was stirred for 1 h at room temperature. The reaction mixture was washed with Na_2CO_3 aq and water, and dried over Na_2SO_4. The solvent was removed under vacuum and the residual solid was recrystallized from CH_2Cl_2/EtOH (1:3, v/v) to give dark blue crystals of **12c** (25.2 mg, 30.4 mmol, 83%). ^{1}H NMR ($CDCl_3$): δ 7.51 (d, J = 1.6 Hz, 4H, 2,3,12,13-β-H), 6.88 (d, J = 7.4 Hz, 4H, 26,32,38,44-Ph-H), 6.68 – 6.65 (m, 8H, 23,29,35,41- Ph-H), 4.91 (br s, 2H, inner NH), 1.37 (s, 36H, *t*-Bu-CH_3). UV-vis (CH_2Cl_2): λ_{max} [nm] (log ε) = 817 (3.62), 742 (4.03), 663 (4.21), 604 (4.88), 478 (4.49), 416 (4.77), 331 (4.76). MS (MALDI-TOF, dithranol matrix): *m/z* = 831.9 (calcd. for [M]$^+$: 831.4). Anal. calcd. for $C_{60}H_{54}N_4 \cdot 0.5H_2O$: C 85.78, H 6.60, N 6.67; found: C 85.83, H 6.71, N 6.47. m.p. > 300 °C.

24,30,36,42-Tetrakis(*tert*-butyl)-doubly-fused porphyrins (13c and 14c). A solution of tetra(*n*-butyl)- ammonium acetate (TBA·OAc, 500 mg, 1.65 mmol), palladium acetate (10.5 mg, 46.6 μmol), triphenylphosphine (20.8 mg, 79.1

μmol), molecular sieves 4A (70 mg), potassium carbonate (552 mg, 3.99 mmol), and **5c** (112 mg, 92 μmol) in 1,4-dioxane (2 mL) was stirred at 110 °C for 16 h.[47] The reaction mixture was cooled to ambient temperature, filtered, and washed with water. The residual solid was dissolved in $CHCl_3$ (30 mL) and then filtered. To the filtrate was added TFA (3 mL, 39 mmol) and the reaction mixture was stirred for 3 h at room temperature. The reaction mixture was washed with Na_2CO_3 aq and water, and dried over Na_2SO_4. The solvent was removed under vacuum and the red-brown powder obtained was chromatographed on a silica gel column by using toluene/hexane (1:2, v/v) as an eluent and three fractions were obtained. Recrystallization of solids obtained from the second fraction from CH_2Cl_2/MeOH gave light-red powder of **13c** (5.3 mg, 6.4 μmol, 7%). Solids obtained from the first and the third fractions were recrystallized from the same solvent to give red powder of **14c** (8.7 mg, 10.4 mmol, 11%) and red powder of triply-fused **15c** (36.7 mg, 44.1 μmol, 48%), respectively.

24,30,36,42-Tetrakis(*tert*-butyl)-*cis*-doubly-fused porphyrin (13c). ^{1}H NMR ($CDCl_3$, 298 K): δ 8.61 (d, J = 1.6 Hz, 2H, 12,13-β-H), 7.78 (d, J = 8.3 Hz, 4H, 26,44-Ph-H), 7.66 (d, J = 1.9 Hz, 2H, 23,41-Ph-H), 7.63 – 7.59 (m, 6H, 2,3-β-H, m-Ph-H), 7.20 (s, 2H, 8,17-β-H), 7.04 (dd, J = 7.9, 1.9 Hz, 2H, 25,43-Ph-H), 5.30 (s, 1H, inner NH), 2.86 (s, 1H, inner NH), 1.52 (s, 18H, t-Bu-CH_3), 1.35 (s, 18H, 24,42-t-Bu-CH_3). UV-vis (CH_2Cl_2): λ_{max} [nm] (log ε) = 309 (4.64), 417 (4.71), 496 (4.66), 534 (4.97), 577 (4.39), 693 (3.89), 771 (3.25). MS (MALDI-TOF, dithranol matrix): m/z = 835.1 (calcd. for $[M + H]^+$: 835.5). Anal. calcd. for $C_{60}H_{58}N_4 \cdot 1.5H_2O \cdot 0.5CH_2Cl_2$: C 80.33, H 6.91, N 6.19; found: C 80.36, H 6.99, N 5.93. m.p. > 300 °C.

24,30,36,42-Tetrakis(*tert*-Butyl)-*trans*-doubly-fused porphyrin (14c). ^{1}H NMR ($CDCl_3$, 298 K): δ 8.69 (dd, J = 4.8, 2.0 Hz, 2H, 3,13-β-H), 8.26 (dd, J = 4.8, 2.0 Hz, 4H, 2,12-β-H), 7.87 (d, J = 8.2 Hz, 4H, o-Ph-H), 7.77 (d, J = 8.0 Hz, 2H, 32,44-Ph-H), 7.68 (d, J = 8.2 Hz, 4H, m-Ph-H), 7.38 (s, 2H, 7,17-β-H), 7.20 (d, J = 1.7 Hz, 2H, 29,41-Ph-H), 6.99 (dd, J = 8.0, 1.7 Hz, 2H, 31,43-Ph-H), 2.64 (s, 1H, inner NH), 1.34 (s, 36H, t-Bu-CH_3). UV-vis (CH_2Cl_2): λ_{max} [nm] (log ε) = 316 (4.69), 381 (4.43), 429 (4.74), 454 (4.69), 487 (5.10), 513 (3.71), 668 (4.91), 733 (3.97), 798 (3.64), 898 (3.60). MS (MALDI-TOF, dithranol matrix): m/z = 835.0 (calcd. for $[M + H]^+$: 835.5). Anal. calcd. for $C_{60}H_{58}N_4 \cdot 1.5H_2O \cdot CH_2Cl_2$: C 77.36, H 6.70, N 5.92; found: C 77.19, H 6.61, N 5.74. m.p. > 300 ºC.

X-ray diffraction analysis.

Recrystallization of **12c** from the solution in chloroform with vapor deposition of acetonitrile as a poor solvent gave single crystals of **12c**. A single crystal of **12c** was mounted on a mounting loop. All diffraction data were collected at 120 K equipped with graphite-monochromated Mo $K\alpha$ (λ = 0.71073 Å) by the ω-2θ scan. The structures were solved by direct methods using SIR97 and SHELX97.[48] Crystallographic data for **12c** are summarized in Table 5-3. CCDC-1434621 contains the supplementary crystallographic data. The co-crystallized chloroform molecules in the crystal of **12c** was severely disordered and thus deleted by using the SQUEEZE program.[39] The disorder of co-crystallized solvent molecules caused weak diffraction in the high angle region, which resulted in the low value of sin2θ/λ (0.4674) relative to the IUCr criteria.

Table 5-3. Crystallographic data for **12c**

compound	**12c**
crystal system	monoclinic
space group	$P2_1/n$
T / K	120
formula	$C_{60}H_{54}N_4$
FW	831.07
a / Å	20.774(5)
b / Å	29.800(8)
c / Å	30.233(8)
a / °	90
b / °	108.120(4)
g / °	90
V / Å^3	17788(8)
Z	14
λ / Å	0.71073 (Mo $K\alpha$)
D_c / g cm^{-3}	1.086
reflns measured	97443
reflns unique	15178
$R1$ ($I > 2s(I)$)	0.0911
$wR2$ (all)	0.2331
GOF	1.081

Determination of equilibrium constants of protonation of the fused porphyrin derivatives.

A solution of a freebase porphyrin derivative was titrated with that of TFA in CH_2Cl_2 at 298 K and the absorbance change at an appropriate wavelength was fitted on the basis of eq 1 (Figure 5-7, 9, 10, and 11).

$$\mathrm{Abs} = \varepsilon_P[P]_0 + \{(\varepsilon_{HP} - \varepsilon_P) / (2 \times K)\} \times [(1 + K \times [TFA] + K \times [P]_0) - \{(1+K \times [TFA] + K \times [P]_0)_2 - 4 \times K^2 \times [TFA] \times [P]_0\}^{1/2}] \quad (1)$$

Here, ε_P, $[P]_0$, [TFA], ε_{HP}, and K refer to the absorption coefficient of the porphyrin derivative at a certain wavelength, the concentration of the porphyrin derivative, the concentration of TFA added, the absorption coefficient of the associated complex between the porphyrin derivative and TFA at the corresponding wavelength, and the binding constant, respectively.

Reference and notes

1 (a) *The Porphyrin Handbook, Vol. 1–10* (Eds.: K. M. Kadish, K. M. Smith, R. Guilard), Academic Press, New York, **2000**. (b) J. W. Buchler in *The Porphyrins, Vol. 1* (Ed.: D. Dolphin), Academic Press, New York, **1979**. (c) *Porphyrins and Metalloporphyrins* (Ed.: K. M. Smith), Elsevier, Amsterdam-Oxford, New York, **1975**.

2 (a) K. M. Kadish, N. Guo, E. Van Caemelbecke, A. Froiio, R. Paolesse, D. Monti, P. Tagliatesta, T. Boschi, L. Prodi, F. Bolletta, N. Zaccheroni, *Inorg. Chem.* **1998**, 37, 2358. (b) P. Bhyrappa, V. Krishnan, *Inorg. Chem.* **1991**, *30*, 239. (c) J. Shen, J. Shao, Z. Ou, W. E. B. Koszarna, D. T. Gryko, K. M. Kadish, *Inorg. Chem.* **2006**, *45*, 2251.

(d) Y. Fang, P. Bhyrappa, Z. Ou, K. M. Kadish, *Chem. Eur. J.* **2014**, *20*, 524. (e) Y. Fang, Y. G. Gorbunova, P. Chen, X. Jiang, M. Manowong, A. A. Sinelshchikova, Y. Y. Enakieva, A. G. Martynov, A. Y. Tsivadze, A. Bessmertnykh-Lemeune, C. Stern, R. Guilard, K. M. Kadish, *Inorg. Chem.* **2015**, *54*, 3501. (f) A. Rananaware, R. S. Bhosale, K. Ohkubo, H. Patil, L. A. Jones, S. L. Jackson, S. Fukuzumi, S. V. Bhosale, S. V. Bhosale, *J. Org. Chem.* **2015**, *80*, 3832.

3 (a) J. J. Warren, J. R. Winkler, H. B. Gray, *Coord. Chem. Rev.* **2013**, *257*, 165. (b) H. Michel, J. Deisenhofer, *Biochemistry* **1988**, *27*, 1. (c) J. P. Allen, G. Feher, T. O. Yeates, H. Komiya, D. C. Rees, *Proc. Natl. Acad. Sci. USA* **1987**, *84*, 5730. (d) S. G. Boxer, *Biochim. Biophys. Acta* **1983**, *726*, 265.

4 (a) M. R. Wasielewski, *Chem. Rev.* **1992**, *92*, 435. (b) D. Gust, T. A. Moore, A. L. Moore, *Acc. Chem. Res.* **1993**, *26*, 198. (c) D. M. Guldi, *Chem. Soc. Rev.* **2002**, *31*, 22. (d) A. Osuka, S. Marumo, N. Mataga, S. Taniguchi, T. Okada, I. Yamazaki, Y. Nishimura, T. Ohno, K. Nozaki, *J. Am. Chem. Soc.* **1996**, *118*, 155. (e) A. Osuka, G. Noya, S. Taniguchi, T. Okada, Y. Nishimura, I. Yamazaki, N. Mataga, *Chem. Eur. J.* **2000**, *6*, 33. (f) M. M. A. Kelson, R. S. Bhosale, K. Ohkubo, L. A. Jones, S. V. Bhosale, A. Gupta, S. Fukuzumi, S. V. Bhosale, *Dyes and Pigments* **2015**, *120*, 340.

5 (a) P. Hambright, *Coord. Chem. Rev.* **1971**, *6*, 247. (b) S. Aronoff, *J. Phys. Chem.* **1958**, *62*, 428. (c) A. Stone, E. B. Fleischer, *J. Am. Chem. Soc.* **1968**, *90*, 2735. (d) R. Karaman, T. C. Bruice, *Inorg. Chem.* **1992**, *31*, 2455. (e) T. P. C. Sutter, P. Hambright, *Inorg. Chem.* **1992**, *31*, 5089.

6 (a) J. Braun, C. Hasenfratz, R. Schwesinger, H.-H. Limbach, *Angew. Chem. Int. Ed. Engl.* **1994**, *33*, 2215. (b) A. J. Bonnell, J. C. Kennedy, R. A. Jones, P. Nadeau, R. Pottier, *J. Photochem. Photobiol. B* **1990**, *6*, 309.

7 (a) C. P. Hrung, M. Tsutsui, D. L. Cullen, E. F. Meyer, Jr., *J. Am. Chem. Soc.* **1976**, *98*, 7878. (b) C. P. Hrung, M. Tsutsui, D. L. Cullen, E. F. Meyer, Jr., C. N. Morimoto, *J. Am. Chem. Soc*. **1978**, *100*, 6068.

8 (a) H. Ogoshi, E. Watanabe, Z. Yoshida, *Tetrahedron* **1973**, *29*, 3241. (b) Ö. Almarsson, A. Blasko, T. C. Bruice, *Tetrahedron* **1993**, *49*, 10239.

9 (a) G. De Luca, A. Romeo, L. Monsù Scolaro, G. Ricciardi, A. Rosa, *Inorg. Chem.* **2007**, *46*, 5979. (b) S. Thyagarajan, T. Leiding, S. Peterson Årsköld, A. V. Cheprakov, S. A. Vinogradov, *Inorg. Chem.* **2010**, *49*, 9909. (c) T. Honda, T. Kojima, S. Fukuzumi, *Chem. Commun.* **2009**, 4994. (d) A. B. Rudine, B. D. Del Fatti, C. C. Wamser, *J. Org. Chem.* **2013**, *78*, 6040.

10 (a) M. O. Senge, T. P. Forsyth, L. T. Nguyen, K. M. Smith, *Angew. Chem. Int. Ed. Engl.* **1994**, *33*, 2485. (b) M. Meot-Ner, A. D. Adler, *J. Am. Chem. Soc.* **1975**, *97*, 5107. (c) B. Cheng, O. Q. Munro, H. M. Marques, W. R. Scheidt, *J. Am. Chem. Soc.* **1997**, *119*, 10732.

11 (a) P. Stepanek, V. Andrushchenko, K. Ruud, P. Bour, *J. Phys. Chem. A* **2012**, *116*, 778. (b) A. B. Rudine, B. D. DelFatti, C. C. Wamser, *J. Org. Chem.* **2013**, *78*, 6040. (c) A. Rosa, G. Ricciardi, E. Jan Baerends, A. Romeo, L. Monsù Scolaro, *J. Phys. Chem. A* **2003**, *107*, 11468.

12 (a) V. S. Chirvony, A. van Hoek, V. A. Galievsky, I. V. Sazanovich, T. J. Schaafsma, D. Holten, *J. Phys. Chem. B* **2000**, *104*, 9909. (b) P. Stepánek, V. Andrushchenko, K. Ruud, P. Bour, *J. Phys. Chem. A* **2012**, *116*, 778.

13 (a) D. L. Langhus, G. S. Wilson, *Anal. Chem.* **1979**, *51*, 1139. (b) E. C. A. Ojadi, H. Linschitz, M. Gouterman, R. I. Walter, J. S. Lindsey, R. W. Wagner, P. R. Droupadi, W. Wang, *J. Phys. Chem.* **1993**, *97*, 13192.

14 (a) R. F. Pasternack, P. R. Huber, P. Boyd, G. Engasser, L. Francesconi, E. Gibbs, P. Fasella, G. Cerio Venturo, L. deC. Hinds, *J. Am. Chem. Soc.* **1972**, *94*, 4511. (b) K. M. Kadish, G. B. Maiya, C. Araullo, R. Guilard, *Inorg. Chem.* **1989**, *28*, 2125. (c) D. C. Barber, R. A. Freitag-Beeston, D. G. Whitten, *J. Phys. Chem.* **1991**, *95*, 4074.

15 (a) G. De Luca, A. Romeo, L. Monsù Scolaro, *J. Phys. Chem. B* **2005**, *109*, 7149. (b) G. De Luca, A. Romeo, L. Monsù Scolaro, *J. Phys. Chem. B* **2006**, *110*, 7309. (c) G. De Luca, A. Romeo, L. Monsù Scolaro, *J. Phys. Chem. B* **2006**, *110*, 14135.

16 (a) S. Fukuzumi, T. Honda, T. Kojima, *Coord. Chem. Rev.* **2012**, *256*, 2488 and references therein. (b) T. Kojima, T. Honda, K. Ohkubo, M. Shiro, T. Kusukawa, T. Fukuda, N. Kobayashi, S. Fukuzumi, *Angew. Chem. Int. Ed.* **2008**, *47*, 6712. (c) T. Nakanishi, K. Ohkubo, T. Kojima, S. Fukuzumi, *J. Am. Chem. Soc.* **2009**, *131*, 577.

17 Reviews on this topic: (a) S. Fox, R. W. Boyle, *Tetrahedron* **2006**, *62*, 10039. (b) J. P. Lewtak, D. T. Gryko, *Chem. Commun.* **2012**, *48*, 10069. (c) H. Mori, T. Tanaka, A. Osuka, *J. Mater. Chem. C* **2013**, *1*, 2500. (d) M. Stępień, E. Gońka, M. Żyła, N. Sprutta, *Chem. Rev.* **2017**, ASAP (DOI: 10.1021/acs.chemrev.6b00076).

18 (a) L. Edwards, M. Gouterman, C. B. Rose, *J. Am. Chem. Soc.* **1976**, *98*, 7638. (b) T. D. Lash, B. H. Novak, *Angew. Chem. Int. Ed. Engl.* **1995**, *34*, 683. (c) S. Ito, T. Murashima, H. Uno, N. Ono, *Chem. Commun.* **1998**, 1661.

19 (a) R. Deshpande, L. Jiang, G. Schmidt, J. Rakovan, X. Wang, K. Wheeler, H. Wang, *Org. Lett.* **2009**, *11*, 4251. (b) L. Jiang, J. T. Engle, L. Sirk, C. S. Hartley, C. J. Ziegler, H. Wang, *Org. Lett.* **2011**, *13*, 3020. (c) S. Banala, T. Rühl, K. Wurst, B. Kräutler, *Angew. Chem. Int. Ed.* **2009**, *48*, 599.

20 (a) H. Aihara, L. Jaquinod, D. J. Nurco, K. M. Smith, *Angew. Chem. Int. Ed.* **2001**, *40*, 3439. (b) M. Nath, J. C. Huffman, J. M. Zaleski, *J. Am. Chem. Soc.* **2003**, *125*, 11484. (c) M. Nath, M. Pink, J. M. Zaleski, *J. Am. Chem. Soc.* **2005**, *127*, 478.

21 (a) N. Cammidge, P. J. Scaife, G. Berber, D. L. Hughes, *Org. Lett.* **2005**, *7*, 3413. (b) M. Tanaka, S. Hayashi, S. Eu, T. Umeyama, Y. Matano, H. Imahori, *Chem. Commun.* **2007**, 2069. (c) C. Jiao, K.-W. Huang, Z. Guan, Q.-H. Xu, J. Wu, *Org. Lett.* **2010**, *12*, 4046.

22 (a) H. S. Gill, M. Harmjanz, J. Santamaría, I. Finger, M. J. Scott, *Angew. Chem. Int. Ed.* **2004**, *43*, 485. (b) K. Kurotobi, K. S. Kim, S. B. Noh, D. Kim, A. Osuka, *Angew. Chem. Int. Ed.* **2006**, *45*, 3944.

23 Jiao, L. Zhu, J. Wu, *Chem. Eur. J.* **2011**, *17*, 6610.

24 (a) N. K. S. Davis, M. Pawlicki, H. L. Anderson, *Org. Lett.* **2008**, *10*, 3945. (b) N. K. S. Davis, A. L. Thompson, H. L. Anderson, *Org. Lett.* **2010**, *12*, 2124. (c) N. K. S. Davis, A. L. Thompson, H. L. Anderson, *J. Am. Chem. Soc.* **2011**, *133*, 30.

25 (a) K. Sendt, L. A. Johnston, W. A. Hough, M. J. Crossley, N. S. Hush, J. R. Reimers, *J. Am. Chem. Soc.* **2002**, *124*, 9299. (b) R. Paolesse, L. Jaquinod, F. Della Sala, D. J. Nurco, L. Prodi, M. Montalti, C. Di Natale, A. D'Amico, A. Di Carlo, P. Lugli, K. M. Smith, *J. Am. Chem. Soc.* **2000**, *122*, 11295. (c) H. Uno, A. Masumoto, N.

Ono, *J. Am. Chem. Soc.* **2003**, *125*, 12082. (d) M. Akita, S. Hiroto, H. Shinokubo, *Angew. Chem. Int. Ed.* **2012**, *51*, 2894.

26 (a) Tsuda, A. Nakano, H. Furuta, H. Yamochi, A. Osuka, *Angew. Chem. Int. Ed.* **2000**, *39*, 558. (b) A. Tsuda, H. Furuta, A. Osuka, *Angew. Chem. Int. Ed.* **2000**, *39*, 2549. (c) A. Tsuda, H. Furuta, A. Osuka, *J. Am. Chem. Soc.* **2001**, *123*, 10304. (d) A. Tsuda, A. Osuka, *Science* **2001**, *293*, 79. (e) Y. Nakamura, N. Aratani, H. Shinokubo, A. Takagi, T. Kawai, T. Matsumoto, Z. S. Yoon, D. Y. Kim, T. K. Ahn, D. Kim, A. Muranaka, N. Kobayashi, A. Osuka, *J. Am. Chem. Soc.* **2006**, *128*, 4119.

27 (a) R. B. Woodward, W. A. Ayer, J. M. Beaton, F. Bickelhaupt, R. Bonnet, P. Buchschacher, G. L. Closs, H. Dutler, J. Hannah, F. P. Hauck, S. Ito, A. Langemann, E. Le Goff, W. Leimgruber, W. Lwowski, J. Sauer, Z. Valenta, H. Volz, *J. Am. Chem. Soc.* **1960**, *82*, 3800. (b) R. B. Woodward, W. A. Ayer, J. M. Beaton, F. Bickelhaupt, R. Bonnet, P. Buchschacher, G. L. Closs, H. Dutler, J. Hannah, F. P. Hauck, S. Ito, A. Langemann, E. Le Goff, W. Leimgruber, W. Lwowski, J. Sauer, Z. Valenta, H. Volz, *Tetrahedron* **1990**, *46*, 7599.

28 (a) S. Fox, R. W. Boyle, *Chem. Commun.* **2004**, 1322. (b) D.-M. Shen, C. Liu, Q.-Y. Chen, *Chem. Commun.* **2005**, 4982. (c) D.-M. Shen, C. Liu, Q.-Y. Chen, *J. Org. Chem.* **2006**, *71*, 6508.

29 (a) S. Hayashi, Y. Matsubara, S. Eu, H. Hayashi, T. Umeyama, Y. Matano, H. Imahori, *Chem. Lett.* **2008**, *37*, 846. (b) T. D. Lash, B. E. Smith, M. J. Melquist, B. A. Godfrey, *J. Org. Chem.* **2011**, *76*, 5335. (c) A. M. V. M. Pereira, M. G. P. M. S. Neves, J. A. S. Cavaleiro, C. Jeandon, J.-P. Gisselbrecht, S. Choua, R. Ruppert, *Org. Lett.* **2011**, *13*, 4742.

30 (a) Y. Mitsushige, S. Yamaguchi, B. S. Lee, Y. M. Sung, S. Kuhri, C. A. Schierl, D. M. Guldi, D. Kim, Y. Matsuo, *J. Am. Chem. Soc.* **2012**, *134*, 16540. (b) H. Fliegl, N. Özcan, R. Mera-Adasme, F. Pichierri, J. Jusélius, D. Sundholm, *Mol. Phys.* **2013**, *111*, 1364.

31 (a) Nakano, N. Aratani, H. Furuta, A. Osuka, *Chem. Commun.* **2001**, 1920. (b) A. K. Sahoo, S. Mori, H. Shinokubo, A. Osuka, *Angew. Chem. Int. Ed.* **2006**, *45*, 7972. (c) N. Fukui, H. Yorimitsu, J. M. Lim, D. Kim, A. Osuka, *Angew. Chem. Int. Ed.* **2014**, *53*, 4395.

32 (a) N. Fukui, W.-Y. Cha, S. Lee, S. Tokuji, D. Kim, H. Yorimitsu, A. Osuka, *Angew. Chem. Int. Ed.* **2013**, *52*, 9728. (b) K. Ota, T. Tanaka, A. Osuka, *Org. Lett.* **2014**, *16*, 2974.

33 Please see other chapters of this thesis. See also: (a) T. Ishizuka, Y. Saegusa, Y. Shiota, K. Ohtake, K. Yoshizawa, T. Kojima, *Chem. Commun.* **2013**, *49*, 5939. (b) Y. Saegusa, T. Ishizuka, K. Komamura, S. Shimizu, H. Kotani, N. Kobayashi, T. Kojima, *Phys. Chem. Chem. Phys.* **2015**, *17*, 15001. (c) Y. Saegusa, T. Ishizuka, T. Kojima, S. Mori, M. Kawano, T. Kojima, *Chem. Eur. J.* **2015**, *21*, 5302.

34 In the case of TPP, only when the ^{1}H NMR spectrum was measured at very low temperature, where the inner NH protons localized at two pyrroles among four at the NMR timescale, splitting of the ^{1}H NMR signal assigned to the inner NH protons was observed due to the coupling of the ^{1}H NMR signal of the pyrrole β-protons (C. B. Storm, Y. Teklu, *J. Am. Chem. Soc.* **1972**, *94*, 1745). Therefore, the splitting of the ^{1}H NMR signal due to the inner NH protons of **12c** is a strong evidence to support that the inner NH protons localize at the non-fused pyrroles.

35 G. Zhang, X. Lu, X. Cai, Y. Fang, M. Zhu, W. Zhu, Z. Ou, K. M. Kadish, *J. Porphyrins Phthalocyanines* **2013**, *17*, 941.

36 The symbol of (1) represents that the nucleus-independent chemical shift (NICS) values are estimated at 1 Å above from the π-conjugated planes. (a) P. von Ragué Schleyer, C. Maerker, A. Dransfeld, H. Jiao, N. J. R. van Eikema Hommes, *J. Am. Chem. Soc.* **1996**, *118*, 6317. (b) J. A. N. F. Gomes, R. B. Mallion, *Chem. Rev.* **2001**, *101*, 1349.

37 Downfield shifts of the inner NH signals due to the strong hydrogen bonds were also observed for porphycene (ν_{NH} = 3099 cm^{-1}), and the ^1H NMR signal of the inner NHs for porphycene appeared at 3.24 ppm in $CDCl_3$. See: E. Vogel, M. Kocher, H. Schmickler, J. Lex, *Angew. Chem. Int. Ed. Engl.* **1986**, *25*, 257.

38 J. Braun, M. Schlabach, B. Wehrle, M. Köcher, E. Vogel, H.-H. Limbach, *J. Am. Chem. Soc.* **1994**, *116*, 6593.

39 P. V. D. Sluis, A. L. Spek, *Acta Crystallogr.* **1990**, *A46*, 194.

40 (a) S. J. Silvers, A. Tulinski, *J. Am. Chem. Soc.* **1967**, *89*, 3331. (b) G. B. Jameson, J. A. Ibers, *J. Am. Chem. Soc.* **1980**, *102*, 2823.

41 One might consider that this difference in Cα-N-Cα bond angles between the fused and non-fused pyrroles derives from the structural requirement by the ring fusion; however, the Cα-N-Cα bond angles of the fused and non-fused pyrroles are almost the same in the QFP metal complexes (see ref. 33). Therefore, the difference in the Cα-N-Cα bond angles is probably ascribable to the presence or absence of a proton at the pyrrole nitrogen atom.

42 S. H. Pine, *Organic Chemistry, 5th Ed, McGraw-Hill*, New York, **1987**.

43 P. Atkins, J. de Paula, *Physical Chemistry, 8th Ed*, Oxford University Press, Oxford, **2006**.

44 M. S. R. Bobe, M. Al Kobaisi, S. V. Bhosale, S. V. Bhosale, *ChemistryOpen* **2015**, *4*, 516. (b) S. V. Bhosale, S. V. Nalage, J. M. Booth, A. Gupta, S. K. Bhargava, S. V. Bhosale, *Supramolecular Chem.* **2012**, *24*, 779.

45 S. Richeter, A. Hadj-Aïssa, C. Taffin, A. van der Lee, D. Leclercq, *Chem. Commun.* **2007**, 2148.

46 The WinSIM program is developed at the NIEHS by Duling (URL: http://www.niehs.nih.gov/ research/ resources/software/tools/index.)

47 S. Higashibayashi, H. Sakurai, *Chem. Lett.* **2007**, *36*, 18.

48 G. M. Sheldrick, SIR97 and SHELX97, Programs for Crystal Structure Refinement, University of Göttingen, Göttingen (Germany), 1997.

Chapter 6

NH tautomerism of a freebase form of QFP

6-1. Introduction

Intramolecular hydrogen-bonding plays important roles to regulate molecular structures and to control physical properties of organic compounds.[1-3] For example, an oligo-peptide, called as a foldamer, forms a folding structure by virtue of intramolecular hydrogen bonding among amino-acid residues.[4] Intramolecular hydrogen bonding also contributes to structural planarization of an oligoarene having hydrogen-bonding substituents to induce bathochromic shifts of the absorption bands by extension of the π-conjugation.[5] In addition, NH tautomerism induced by proton transfer between the intramolecular hydrogen-bonded pair has attracted much attention because of interests in amino-acid functions[6] and in controlling the electronic structure in the excited state.[7]

Intramolecular hydrogen bonding is also found between the inner pyrrolic NH protons and imino nitrogen atoms of freebase porphyrins[8] and the analogues,[9] and the hydrogen bonding contributes to stabilization of the planar structures of porphyrins and their analogues and controls their physical properties.[10]

Related to the aforementioned intramolecular hydrogen bonding found in freebase porphyrins, NH tautomerism of freebase porphyrins, in which two inner pyrrolic NH protons move very fast among the four nitrogen atoms, has been

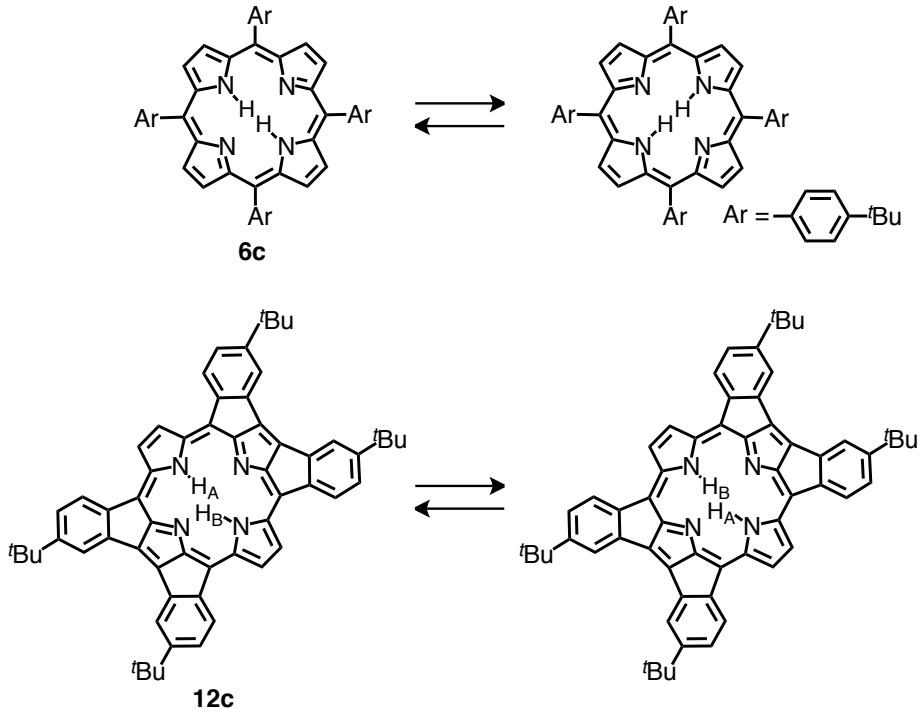

Scheme 6-1. NH tautomerism of tetraarylporphyrin (above) and quadruply-fused porphyrin (below).

intensively studied due to the interest for proton-transfer reactions of strongly hydrogen-bonded protons locating inside of an aromatic current.[11-23] Structural anisotropy caused by the positions of the inner NH protons in freebase porphyrins and the dynamics of the NH tautomerism significantly affect physical and chemical properties of porphyrins.[19f] Furthermore, thermally and vibrationally induced proton transfer in the inner cavity of a porphyrin analogue has been utilized for applications to a single-molecule switch, which is an essential component in single-molecule-based devices.[20] Therefore, the NH tautomerism of porphyrins has been well investigated experimentally[11-20] and theoretically and has been regarded as an important issue in porphyrin chemistry toward development of porphyrin-based molecular devices.[21-23]

In recent years, remarkable efforts have been dedicated to synthesis and characterization of novel π-expanded porphyrins having ring-fused structures at the periphery.[24-34] Among them, the derivatives having fused five-membered rings have attracted considerable attention due to the interest in their unique aromaticity.[35-39] However, the effects of the ring fusion on the properties of the freebase derivatives of the ring-fused porphyrins, such as NH tautomerism, have yet to be well explored. As mentioned in Chapter 2, the author has developed the synthesis of a zinc(II) complex of a quadruply-fused porphyrin (Zn^{II}QFP).[40] A freebase derivative of the quadruply-fused porphyrin has been also synthesized from Zn^{II}QFP and characterized (See Chapter 5 of this thesis);[40d] the imino-nitrogen atoms of the fused pyrroles in H_2QFP exhibit high proton acceptability.[40d] Thus, the NH tautomerism of H_2QFP, which involves intermediates having a proton on the imino nitrogen atoms of the fused pyrroles, can be expected to be observed. In this chapter, the author describes the NH tautomerism of a freebase QFP derivative (Scheme 6-1).

6-2. Introduction of a mesityl group at the *β*-position

For exploration of the NH tautomerism of a freebase QFP, a substituent was introduced at the *β*-position of a non-fused pyrrole to break the structural symmetry; since compound **12a** has a symmetric structure to make the two inner NH atoms identical in the ^{1}H NMR spectrum, the NH tautomerism cannot be clarified. To introduce the substituent, bromination of one of the *β*-positions of the non-fused pyrrole was performed with *N*-bromosuccinimide (NBS) in $CHCl_3$ (Scheme 6-2). When 1.9 equiv of NBS was used to brominate **4c**, a mixture of mono-brominated (Br)

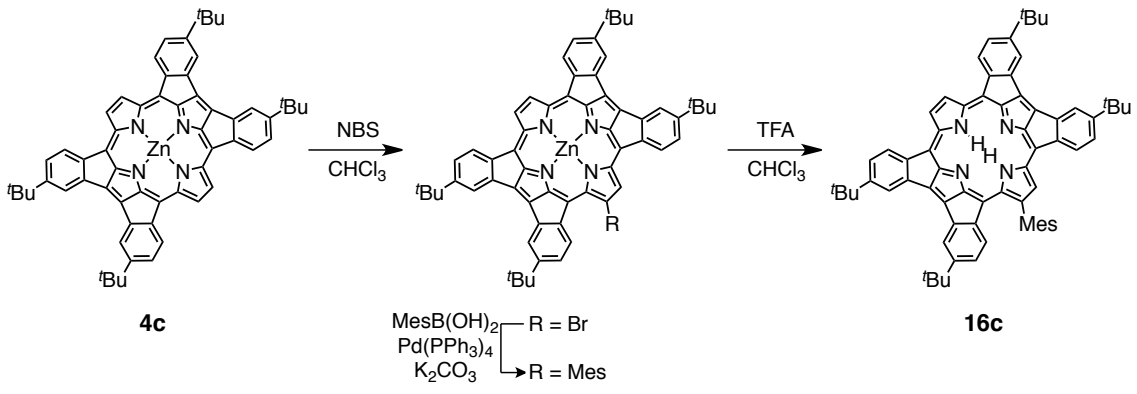

Scheme 6-2. Synthesis of mesityl-QFP, **16c**.

and di-brominated (Br_2) derivatives was obtained, together with unreacted **4c**. The ratio of the three species obtained from the GPC (gel permeation chromatography)-HPLC analysis was determined to be Br : Br_2 : **4c** = 7 : 1 : 2. Without isolation of the mono-brominated species, a Suzuki-cross-coupling reaction was performed with use of mesitylboronic acid in the presence of $Pd(PPh_3)_4$ as a catalyst and K_2CO_3 as a base in dimethylacetamide (DMA).[41] The reaction mixture was separated with column chromatography on silica gel and subsequent demetallation with TFA in $CHCl_3$ gave the target mono-mesityl derivative, **16c**. The ^{1}H NMR spectrum of **16c** in $CDCl_3$ exhibited a larger number of independent signals in comparison to that of **12c**,[40d] due to the lower symmetry of **16c** (Figure 6-1). The ^{1}H NMR signals of the methyl protons of the mesityl group appeared at 2.10 and 2.47 ppm for the *o*- and *p*-methyl groups, respectively, and that of the *m*-protons of the mesityl group was observed at 7.11 ppm. For another feature of the ^{1}H NMR spectrum of **16c**, the fused *meso*-aryl groups nearest to the mesityl group showed the signals in a relatively high-field region due to the ring-current effect of the mesityl group; *i.e.* the signal for the *o*-C-H remaining after the ring fusion appeared at 5.20 ppm as a doublet and that for the *m*-C-H adjacent to the *o*-carbon was observed at 6.19 ppm as a double-doublet. The ^{1}H NMR signal of the inner NHs was observed at 6.02 ppm as a broad singlet at 298 K.

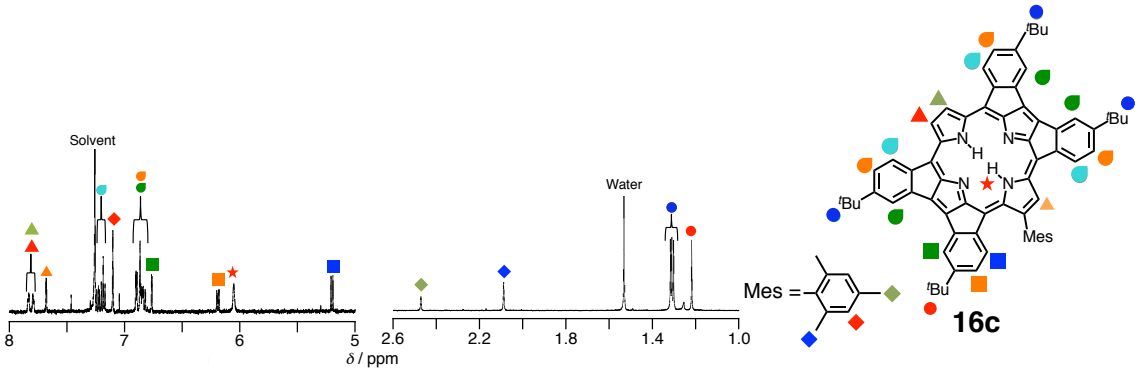

Figure 6-1. ^{1}H NMR spectrum of **16c** (1.1×10^{-4} M) in $CDCl_3$ at 298 K.

6-3. Crystal structure of mono-substituted H_2QFP.

Introduction of the mesityl group at one of the *β*-positions of the non-fused pyrroles in **16c** was explicitly confirmed by the X-ray diffraction analysis. In the triclinic lattice with the space group of $P\bar{1}$, two independent molecules of **16c** were included in the unit cell. ORTEP drawings of one of the molecules are shown in Figure 6-2a and b. The mesityl group was almost perpendicular to the porphyrin plane; the dihedral angle between the mean plane of the porphyrin core consisting of 48 atoms and the benzene ring of the mesityl group was 82°. One of the fused *meso*-aryl groups, nearest to the mesityl group, formed edge-to-face π-π interaction with the mesityl group and the distance of one of the *o*-carbon (C56) from the benzene ring of the mesityl group was 3.19 Å. Due to the overlap, the *o*-C-H proton exhibited a large upfield shift in the ^{1}H NMR spectrum (See above).

Reflecting the planar and expanded π-conjugated plane of **16c**, in the crystal packing, two

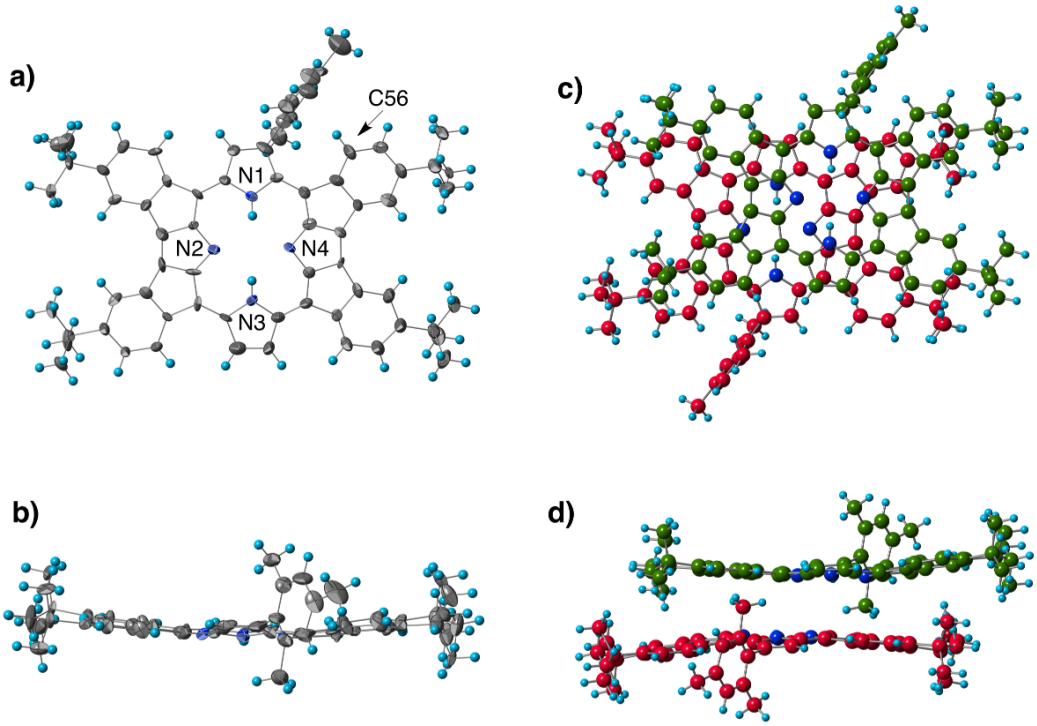

Figure 6-2. Top (a) and side views (b) for ORTEP drawings for the crystal structure of **16c** and top (c) and side (d) views for the π-π stacked dimer of **16c**. Thermal ellipsoids are depicted with the 40% probability in (a) and (b). The carbon atoms of the first layer were colored with green, those in the second layer were with red, and nitrogen atoms were with blue in (c) and (d).

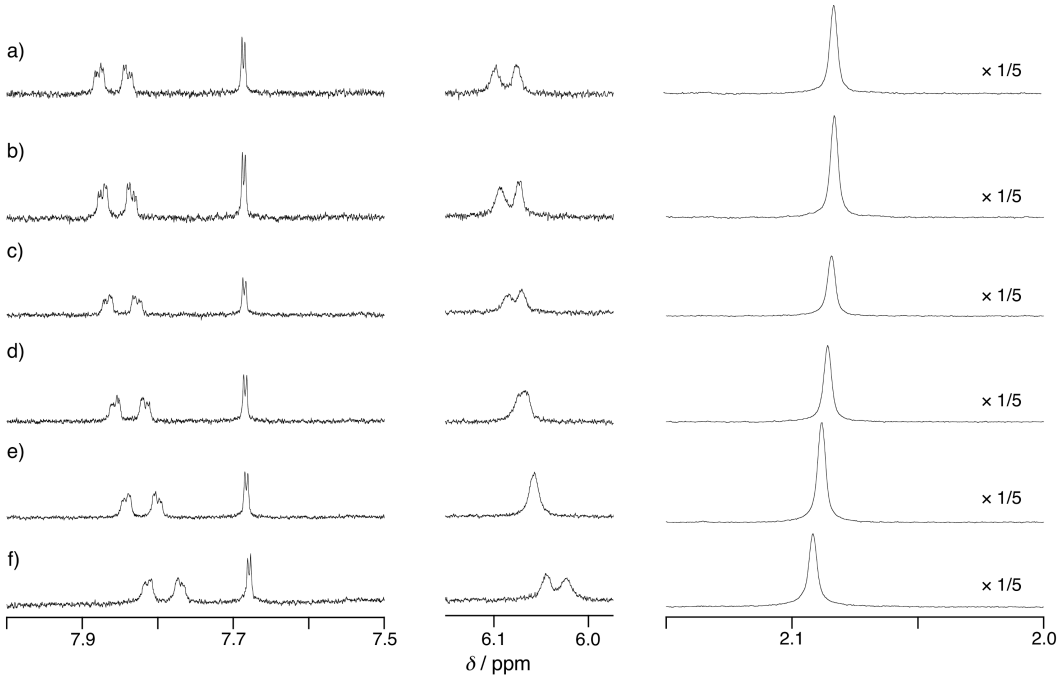

Figure 6-3. ^{1}H NMR spectra of **16c** at various concentrations in $CDCl_3$ at 298 K. The concentrations of **16c** are 4.89×10^{-4} (a), 5.71×10^{-4} (b), 6.85×10^{-4} (c), 8.56×10^{-4} (d), 1.14×10^{-3} (e), and 1.71×10^{-3} M (f), respectively.

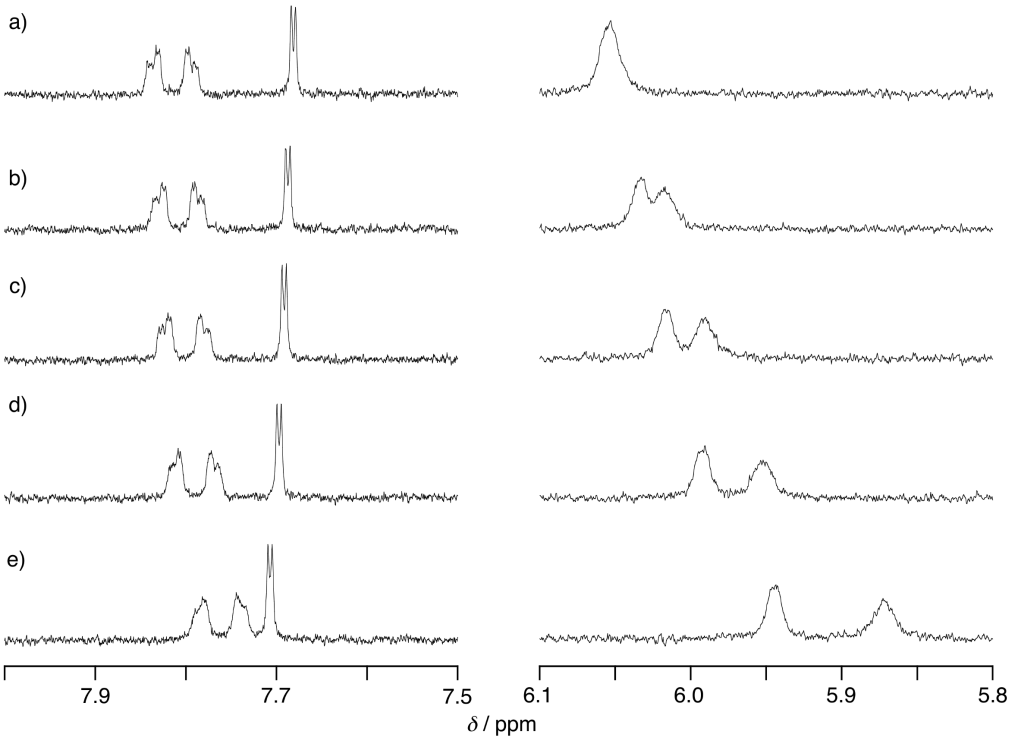

Figure 6-4. ^{1}H NMR spectral changes of **16c** (1.14 mM) in $CDCl_3$ at various temperatures. The temperatures were 298 K (a), 293 K (b), 288 K (c), 283 K (d), and 273 K (e), respectively.

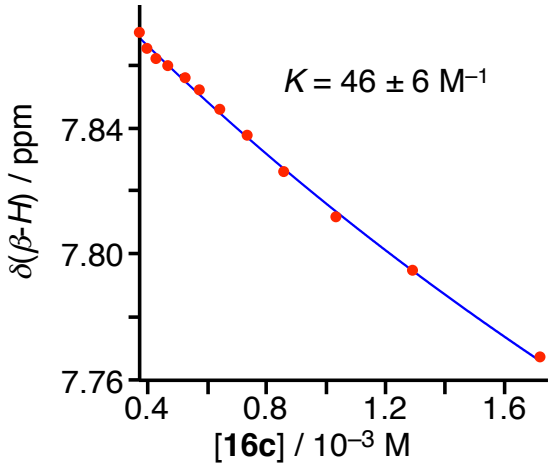

Figure 6-5. Concentration-dependent change of the chemical shift of the β-H signal for **16c** in $CDCl_3$ at 298 K and the fitting curve based on eq 1.

molecules of **16c** formed a π-π stacking dimer in a head-to-tail manner to avoid steric repulsion caused by the mesityl group (Figure 6-2c and d) with the interplane distance of 3.43 Å in the dimer. This π-stacked dimer can be observed even in the solution. Upon increasing the concentration of **16c** in $CDCl_3$ from 4.89×10^{-4} to 1.71×10^{-3} M at 298 K, the ^{1}H NMR signals of the inner NH protons and the β-protons of N3-pyrrole showed upfield shifts from 6.1 to 6.0 ppm and from 7.8 to 7.7 ppm, respectively (Figure 6-3).[42] In addition, with lowering the temperature,

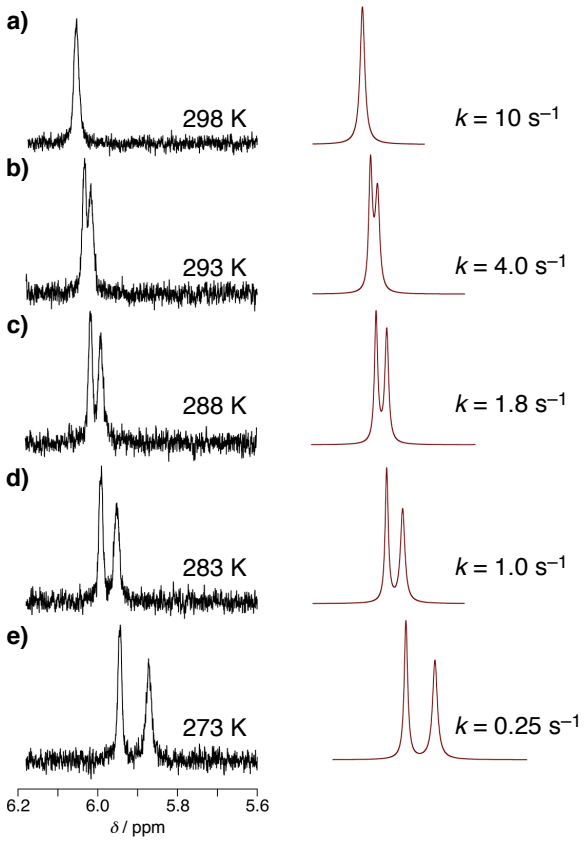

Figure 6-6. Experimental (left, black) and simulated ^{1}H NMR spectra (right, red) of **16c** in $CDCl_3$.

Table 6-1. Activation parameters of the NH tautomerism of **16c** in various solvents.

solvent	$CDCl_3$	50%C_6D_6 [d]	10%CD_3CN [d]	10%$(CD_3)_2CO$ [d]	25%$(CD_3)_2CO$ [d]
ε [a]	4.9	3.7	8.0	6.5	9.0
$\Delta G^{\ddagger}_{298}$ [b]	68 ± 3	79 ± 1	70 ± 2	73 ± 4	75 ± 2
$\Delta H^{\ddagger}$ [b]	95 ± 2	121 ± 1	52 ± 1	108 ± 3	50 ± 1
$\Delta S^{\ddagger}$ [c]	89 ± 2	144 ± 1	–64 ± 1	120 ± 3	–83 ± 2

[a] Static permittivity (ε) was calculated with the following equation: $\varepsilon = x_1\varepsilon_1 + x_2\varepsilon_2$; x_n: mole fraction of solvent n, ε_n: permittivity of solvent n. [b] In kJ mol^{-1}. [c] In J mol^{-1} K^{-1}. [d] The symbol indicates the percentage of the solvent in a mixed solvent with $CDCl_3$.

the ^{1}H NMR signals of the inner NH protons and the β-protons of N3-pyrrole also exhibited upfield shifts (Figure 6-4). The upfield shifts by increasing concentration and lowering temperature are probably due to ring-current effects induced by the formation of the π-π stacking dimer. Actually, the signals showing significant shifts are assigned to the proton covered by the other molecule in the dimer as observed in the crystal packing. Based on the shifts of the signals for the β-protons by increasing the concentration, the equilibrium constant of the dimerization of **16c** (K) was obtained to be 46 ± 6 M^{-1} in $CDCl_3$ at 298 K (Figure 6-5).

6-4. Kinetics of the NH tautomerism of mono-substituted H_2QFP in $CDCl_3$

The ^{1}H NMR signal of the inner NH protons for **16c** was observed as a broad singlet in $CDCl_3$ at 298 K (Figure 6-1), indicating that the exchange process of the two inner NH protons (*i.e.* NH tautomerism) is too fast for the two protons to be distinguished in the NMR timescale. Thus, to observe the NH tautomeric behavior of **16c**, the ^{1}H NMR spectra of **16c** were measured at lower temperatures (Figure 6-6). At 293 K, the signal of the inner NH protons was observed as a slightly split signal, which indicates that the exchange process of the two inner NH protons (*i.e.* NH tautomerism) is slow enough to be distinguished in the NMR timescale; the two inner NH protons show different signals, reflecting the different magnetic circumstances. Upon cooling the sample below 293 K, the split of the signal became evident. Line-shape analysis[43] of the ^{1}H NMR signals was adopted to obtain rate constants of the inner-NH exchange at various temperatures (Figure 6-6). Based on the rate constants, Eyring plot for the NH tautomerism of **16c** was made (Figure 6-6) and the activation parameters were obtained (Table 6-1).

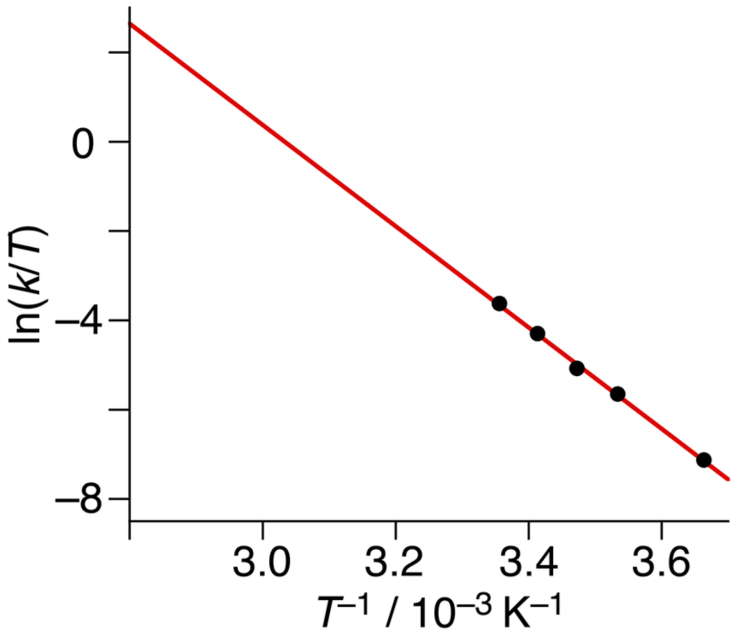

Figure 6-7. An Eyring plot for the NH tautomerism of **16c** in $CDCl_3$.

On the basis of the Eyring plot, the activation enthalpy, $\Delta H^{\ddagger}$, and activation entropy, $\Delta S^{\ddagger}$, were determined to be 95 kJ mol^{-1} and 89 J mol^{-1} K^{-1}, respectively. In comparison with the activation parameters for the NH tautomerism of TPP in $CDCl_3$ ($\Delta H^{\ddagger}$ = 38.6 kJ mol^{-1} and $\Delta S^{\ddagger}$ = –42 J mol^{-1} K^{-1}),[12b] the $\Delta H^{\ddagger}$ value for **16c** was 2.5 times larger, indicating that the proton transfer reaction in **16c** is energetically hard to occur relative to TPP, despite the fact that the inter-nitrogen distances are shorter in **16c** than those in TPP (see below). The large $\Delta H^{\ddagger}$ for **16c** is probably derived from the steric repulsion between the two protons in an intermediate for the NH tautomerism, which has an inner NH proton at a non-fused pyrrole and the other at a fused pyrrole. DFT calculations suggested that the steric repulsion of the two inner NH protons in the *cis*-intermediate resulted in distortion of the core structure of **16c** from the original rhombic structure into a parallelogram-shaped structure (see below). It should be noted that the $\Delta S^{\ddagger}$ value was positively large for **16c**,

whereas that for TPP was negative. The positively large $\Delta S^{\ddagger}$ value for the NH tautomerism of **16c** in $CDCl_3$ should derive from dissociation of the π-stacked dimer structure observed even in the solution (see above). The π-stacked

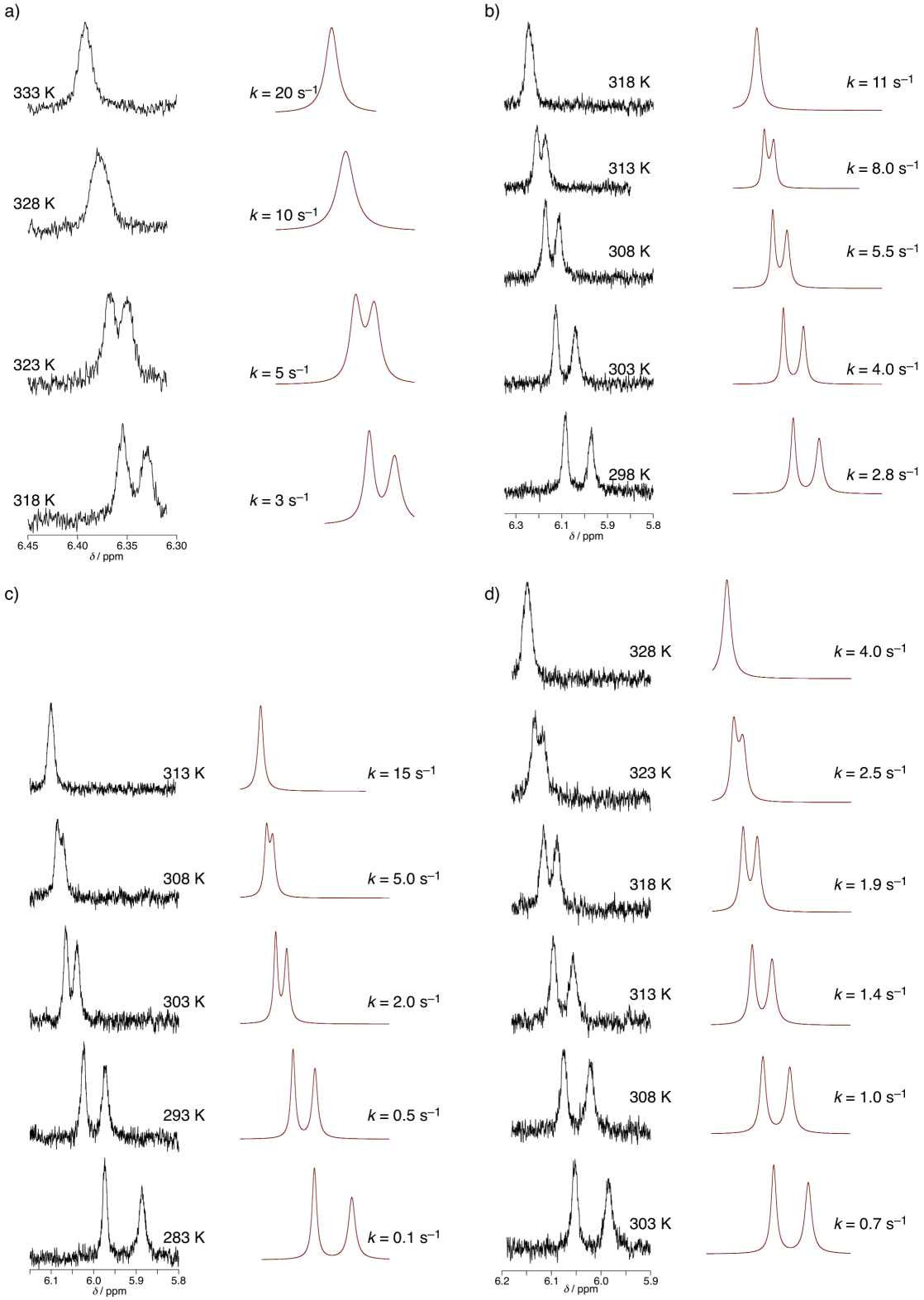

Figure 6-8. Experimental (left, black) and simulated ^{1}H NMR spectra (right, red) of **16c** in 50% $C_6D_6/CDCl_3$ (a), 10% $CD_3CN/CDCl_3$ (b), 10% $(CD_3)_2CO/CDCl_3$ (c), 25% $(CD_3)_2CO/CDCl_3$ (d).

dimer structure observed in the ground state is assumed to be broken in the transition state to afford the positively large $\Delta S^{\ddagger}$ value.

6-5. Solvent Effects on the NH tautomerism of mono-substituted H_2QFP in $CDCl_3$

Solvent effects of the NH tautomerism of **16c** were investigated using four kinds of mixture of deuterated solvents, 50%C_6D_6/$CDCl_3$, 10%CD_3CN/$CDCl_3$, 10%$(CD_3)_2CO$/$CDCl_3$, and 25%$(CD_3)_2CO$/$CDCl_3$, by ^{1}H NMR spectroscopy. Selection of the solvents is highly limited, because the ^{1}H NMR signals of the inner NH protons need to coalesce between the melting and boiling points of the solvent. The four kinds of the mixed solvents used satisfied the criteria. The rate constants of the NH tautomerism were determined at various temperatures in each of the four mixed solvents (Figure 6-8). Based on the temperature dependence of the rate constants, an Eyring plot for **16c** in each solvent was provided (Figure 6-9); the activation parameters and the activation free-energies at 298 K, $\Delta H^{\ddagger}$, $\Delta S^{\ddagger}$, and $\Delta G^{\ddagger}_{298}$, were obtained for the NH tautomerism as listed in Table 6-1. To elucidate the solvent effects in the NH tautomersim, the author focused on static permittivity, ε, as a solvent parameter; the permittivity values of the four solvents employed

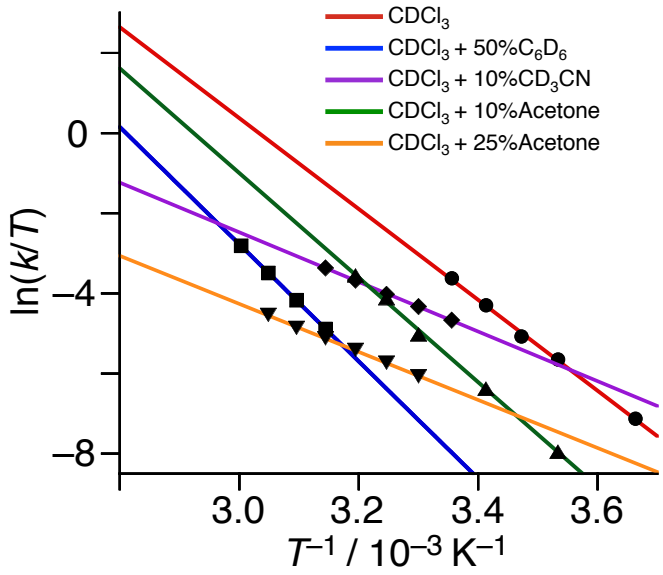

Figure 6-9. Overlaid Eyring plots for the NH tautomerism of **16c** in various solvents.

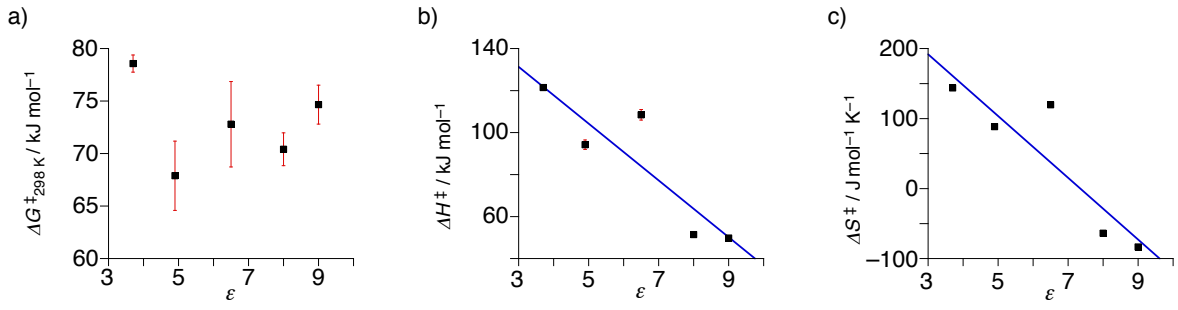

Figure 6-10. Plots of $\Delta G^{\ddagger}_{298}$ (a), $\Delta H^{\ddagger}$ (b) and $\Delta S^{\ddagger}$ (c) against ε.

in this study are not so different (chloroform = 4.9, benzene = 2.4, acetonitrile = 36, acetone = 21). Here, the additivity of the permittivity of each solvent was assumed in the mixed solvents.[44] Then, the activation parameters, $\Delta G^{\ddagger}_{298}$, $\Delta H^{\ddagger}$ and $\Delta S^{\ddagger}$, were plotted against the calculated ε of the mixed solvent (Figure 6-10). As a result, $\Delta H^{\ddagger}$ and $\Delta S^{\ddagger}$ exhibited linearity in the plots against ε (Figure 6-10b and c), and upon increasing the solvent polarity, both $\Delta H^{\ddagger}$ and $\Delta S^{\ddagger}$ decreased. In contrast, $\Delta G^{\ddagger}_{298}$ seems independent of the solvent polarity (Figure 6-10a). The negative proportion of $\Delta H^{\ddagger}$ to ε indicates that the transition state of the NH tautomerism of **16c** is stabilized in a polar solvent, and thus, is relatively more polar than the ground state. On the other hand, the $\Delta S^{\ddagger}$ was also negatively proportional to ε; that is, the polar transition state induces stronger solvation in a polar solvent, which results in the stabilization in the aspect of $\Delta H^{\ddagger}$ and simultaneously in destabilization in the aspect of $\Delta S^{\ddagger}$. Therefore, the solvation mechanism can explain the independency of $\Delta G^{\ddagger}$ on the solvent polarity with reversed effects of solvation on$\Delta H^{\ddagger}$ and $\Delta S^{\ddagger}$;[45] the $\Delta H^{\ddagger}$ value becomes more negative (stabilized) and the $\Delta S^{\ddagger}$ value also becomes more negative (destabilized) with increasing the solvent polarity.

6-6. DFT calculations on the transition state of the NH tautomerism

Two kinds of reaction mechanisms have been proposed for the NH tautomerism of porphyrins: Stepwise mechanism,[12a,13a,22b] which involves an asynchronous transfer of the two N-H atoms through a *cis*-type tautomer, and concerted one, in which the two N-H atoms transfer synchronously.[12b] Long-term debates have been given to answer the question; which is the mechanism plausible in the NH tautomerism on the basis of experiments and theoretical studies? The stepwise mechanism is now generally accepted to be the true mechanism for the NH tautomersim of porphyrins.[15b, 18d]

Structures and stabilities of intermediates and the transition states of the NH tautomerism of non-substituted **12c** were calculated with DFT methods at the B3LYP/6-31G** level of theory (Figure 6-11). As mentioned above,

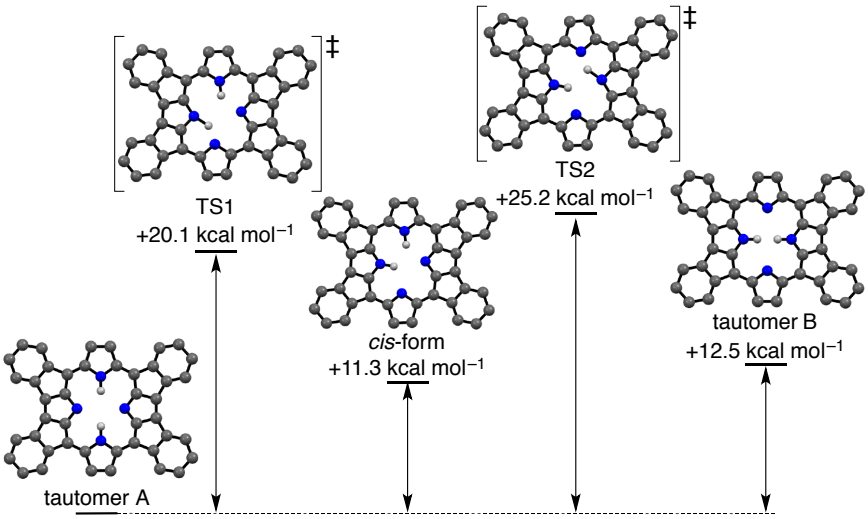

Figure 6-11. Energy diagram of the NH tautomerism of **12c** obtained by DFT calculations. The peripheral *t*Bu groups are omitted for clarity.

one of the intermediates (tautomer B), having the two inner NHs at the two fused pyrroles, is less stable by 12.5 kcal mol^{-1} than the structurally characterized tautomer A (see also Figure 5-5). The other intermediate (*cis*-form; Figure 6-11), having one inner NH proton at one of the non-fused pyrrole and the other NH proton at one of the fused pyrrole, is less stable by 11.3 kcal mol^{-1} than the tautomer A. The reason why the tautomer B is less stable than the *cis*-form is probably severe steric repulsion between the two inner NH protons in the tautomer B. Transition states obtained from DFT calculations have a transferring inner NH proton at the midpoint between the two adjacent nitrogen atoms; one is the nitrogen atom at which the proton is originally located, and another is the nitrogen atom, by which the NH proton is accepted. One of the transition states (TS1), intervened between the ground state and the *cis*-form, is less stable by 20.1 kcal mol^{-1} than the tautomer A. The other transition state (TS2), intervened between the *cis*-form and the tautomer B, is less stable by 25.2 kcal mol^{-1} than the tautomer A. Additionally, the calculated dipole moments in debye were 0.0748 for tautomer A, 0.0186 for tautomer B, 1.2451 for the *cis*-form, 0.6282 for TS1, and 0.6216 for TS2, respectively (Figure 6-12). Therefore, the TS states bear more polar characters than the tautomer A, which is consistent with the smaller $\Delta H^{\ddagger}$ in polar solvents. In addition, the more negative $\Delta S^{\ddagger}$ values in more polar solvents reflect the dissociation of the π-stacked dimer that should be more stabilized due to unfavorable solvation of **16c** in polar solvents.

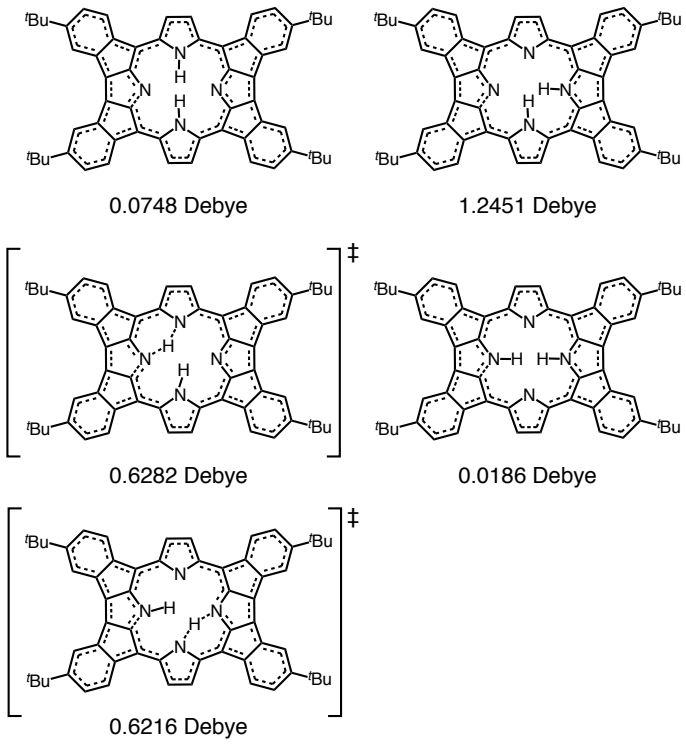

Figure 6-12. Dipole moments, noted below the structures, of NH tautomers of **12c** and the transition states of the NH tautomerism obtained from DFT calculations.

6-7. Conclusion

A freebase derivative of a symmetry-broken QFP having a mesityl group, **16c**, has been synthesized and characterized by crystallographic and spectroscopic methods. The NH tautomerism of **16c** was kinetically investigated

to reveal solvent effects on the activation parameters. Based on the kinetic analysis, the author concludes that the NH tautomerism of **16c** proceeds through dissociation of a π-stacked dimer of **16c** and subsequent polar transition states bearing larger dipole moments than that of **16c**. Additionally, the $\Delta G^{\ddagger}_{298}$ value for the NH tautomerism of **16c** was larger than that of tetraphenylporphyrin due to severer steric congestion of the NH protons in the deformed QFP core. The activation parameters obtained indicate that the NH tautomerism for H_2QFP is deactivated by the rigid ring-fused structure in comparison to that of tetraphenylporphyrin. Finally, the present study provides a strong support for a generally accepted stepwise mechanism of NH tautomerism of the porphyrin core.

6-8. Experimental Section

General.

Chemicals and solvents were used as received from commercial sources unless otherwise mentioned. CH_2Cl_2 used for the UV-vis spectral measurements was distilled over CaH_2 before use. DMA for the synthesis was distilled before use.

^{1}H NMR measurements were performed on Bruker AVANCE-400, -500 and -600 spectrometers. UV-vis absorption spectra were measured in CH_2Cl_2 on a Shimadzu UV-3600 spectrophotometer. MALDI-TOF-MS spectrometry was performed on an AB SCIEX TOF/TOF 5800 spectrometer by using dithranol as a matrix. Gel permeation chromatography (GPC) was performed in 0.5% triethylamine/ $CHCl_3$ utilizing a LC-9110 NEXT Liquid Chromatography system equipped with two JAIGEL-40 columns.

Synthesis.

2-Mesityl-24,30,36,42-tetrakis(*tert*-butyl)-quadruply-fused porphyrin (16c). To a solution of **4c** (27.8 mg, 33.4 μmol) in $CHCl_3$ (50 mL) was added recrystallized NBS (11.2 mg, 64.7 μmol) and the reaction mixture was refluxed for 10 h. After cooling to room temperature, the solvent was removed under vacuum and the residual solid was washed with H_2O and dried under vacuum to obtain black powder. The black powder was recrystallized from THF/MeOH (1:3, v/v) and dried under vacuum to give crude mono-brominated **4c**. To a solution of crude mono-brominated **4c** (26 mg) in DMA (1 mL) was added mesitylboronic acid (**8**)[46] (47.3 mg, 288 μmol), K_2CO_3 (172 mg, 1.24 mmol), and $Pd(PPh_3)_4$ (2.0 mg, 1.73 μmol). The reaction mixture was stirred at 130 °C for 9.5 h and the solvent was removed under vacuum. The residual solid was dissolved in $CHCl_3$ (50 mL) and filtered. To the filtrate was added TFA (5 mL, 65 mmol) and the reaction mixture was stirred for 1 h at room temperature. The mixture was washed with Na_2CO_3 aq and water, and dried over Na_2SO_4. The solvent was removed under vacuum and the black solid obtained was chromatographed on a silica gel column using toluene/hexane (1:2, v/v) as an eluent. The second fraction was collected and the solvent was removed under vacuum. The residual solid was recrystallized from CH_2Cl_2/MeOH (1:3, v/v) to give black crystals of **16c** (1.6 mg, 1.7 μmol, 5% (3 steps)). ^{1}H NMR ($CDCl_3$, 298 K): δ 7.80 (dd, J = 4.7, 2.1 Hz, 1H, β-H), 7.75 (dd, J = 4.7, 2.0 Hz, 1H, β-H), 7.68 (d, J = 2.4 Hz, 1H, 3-β-H), 7.20 – 7.14 (m, 3H, 26,32,38-Ph-H), 7.11 (s, 2H, *m*-mesityl-H), 6.90 – 6.81 (m, 6H, 23,25,29,31,35,37-Ph-H), 6.76 (d, J = 2.0 Hz, 1H, 41-Ph-H), 6.19 (dd, J = 8.2, 2.0 Hz 1H, 43-Ph-H),

6.06 (br s, 1H, inner N*H*), 5.99 (br s, 1H, inner N*H*), 5.20 (d, *J* = 8.2 Hz, 1H, 44-Ph-H), 2.47 (s, 3H, mesityl-*p*-CH_3), 2.10 (s, 6H, mesityl-*o*-CH_3), 1.32 (s, 9H, *t*-Bu-CH_3), 1.31 (s, 9H, *t*-Bu-CH_3), 1.30 (s, 9H, *t*-Bu-CH_3), 1.22 (s, 9H, *t*-Bu-CH_3). UV-vis ($CHCl_3$): λ [nm] (log ε) = 820 (3.52), 745 (4.00), 667 (4.10), 605 (4.84), 478 (4.34), 417 (4.60), 331 (4.56). MS (MALDI-TOF, dithranol matrix): *m/z* = 949.5 (calcd. for $[M]^+$: 949.3). Anal. calcd. for $C_{60}H_{54}N_4 \cdot 0.5H_2O \cdot 2CH_2Cl_2 \cdot 1.5C_6H_{14}$: C 76.42, H 7.21, N 4.46; found: C 76.64, H 7.46, N 4.24.

X-ray diffraction analysis.

A single crystal of **16c** was obtained by recrystallization from the chloroform solution with vapor diffusion method using acetonitrile as a poor solvent. A single crystal was mounted on a mounting loop. All diffraction data were collected at 120 K using a Bruker APEXII diffractometer equipped with graphite-monochromated Mo $K\alpha$ (λ = 0.71073 Å) by the ω-2θ scan. The structures were solved by direct methods using SIR97 and SHELX97.[47] The co-crystallized MeCN molecule in the crystal of **16c** were severely disordered and deleted by using the SQUEEZE program.[48] Crystallographic data for these compounds are summarized in Table 6-2. CCDC-1434622 contains the supplementary crystallographic data.

Table 6-2. Crystallographic data for **16c**.

crystal system	triclinic
space group	*P*`1
T / K	120
formula	$C_{69}H_{64}N_4$
FW	949.24
a / Å	17.432(14)
b /Å	17.593(14)
c /Å	21.576(17)
a / °	73.384(12)
b / °	86.348(13)
g / °	70.488(11)
V / Å^3	5973(8)
Z	4
λ / Å	0.71073 (Mo $K\alpha$)
D_c / g cm^{-3}	1.056
reflns measured	15426
reflns unique	9425
*R*1 (*I* > 2s(*I*))	0.1044
*wR*2 (all)	0.3037
GOF	0.934

Computational method.

To calculate activation energies for the NH tautomerism of H_2QFP, DFT calculations were performed with optimized local minima and transition states on the potential energy surfaces using the B3LYP method[49,50] combined

with the 6-31G(d,p) basis set.[51,52] The Gaussian 09 program package[53] was used for all DFT calculations.

Determination of the dimerization constant of 16c.

Concentration of **16c** was changed in various solvents at 298 K and the ^{1}H NMR spectral changes at an appropriate chemical shifts was fitted with eq 1 (Figure 6-5).

$$\delta_{obs} = \frac{(\delta_{monomer} - \delta_{dimer})(1 + \sqrt{1 + 8K[P]}}{4K[P]} + \delta_{dimer} \qquad (1)$$

Here, δ_{obs}, $\delta_{monomer}$, δ_{dimer}, K, and [P] refer to the observed chemical shift, the chemical shift of the monomer of **16c**, the chemical shift of the dimer of **16c**, the dimerization constant, and the concentration of the porphyrin derivative, respectively.

Kinetic studies of the NH tautomerism.

Determination of the rate constants, k (s^{-1}), for the NH tautomerism of **16c** was performed on a Bruker AVANCE-500 spectrometer at various temperatures. Porphyrin **16c** (1.1 mM) was dissolved in $CDCl_3$ or one of four kinds of mixed deuterated solvents, 50%C_6D_6/$CDCl_3$, 10%CD_3CN/$CDCl_3$, 10%$(CD_3)_2CO$/$CDCl_3$, and 25%$(CD_3)_2CO$/$CDCl_3$. The k values determined at various temperatures were used to provide the corresponding Eyring plots.

Reference and notes

1 (a) *The Hydrogen Bond* (Eds.: P. Schuster, G. Zundel, C. Sandorfy), North-Holland Publ. Co., Amsterdam, **1976**. (b) G. A. Jeffrey, W. Saenger, *Hydrogen Bonding in Biological Structures*, Springer-Verlag, Berlin, **1991**.

2 (a) A. Kovács, A. Szabó, I. Hargittai, *Acc. Chem. Res.* **2002**, *35*, 887. (b) H. Fu, Y. Liu, H. Zeng, *Chem. Commun.* **2013**, *49*, 4127. (c) G.-J. Zhao, K.-L. Han, *Acc. Chem. Res.* **2012**, *45*, 404.

3 (a) M. Itoh, Y. Fujiwara, *J. Am. Chem. Soc.* **1985**, *107*, 1561. (b) M. Chan-Huot, A. Dos, R. Zander, S. Sharif, P. M. Tolstoy, S. Compton, E. Fogle, M. D. Toney, I. Shenderovich, G. S. Denisov, H.-H. Limbach, *J. Am. Chem. Soc.* **2013**, *135*, 18160. (c) B. Qin, C. L. Ren, R. J. Ye, C. Sun, K. Chiad, X. Y. Chen, Z. Li, F. Xue, H. B. Su, G. A. Chass, H. Q. Zeng, *J. Am. Chem. Soc.* **2010**, *132*, 9564.

4 (a) D. J. Hill, M. J. Mio, R. B. Prince, T. S. Hughes, J. S. Moore, *Chem. Rev.* **2001**, *101*, 3893. (b) G. P. Dado, S. H. Gellman, *J. Am. Chem. Soc.* **1994**, *116*, 1054. (c) D.-W. Zhang, X. Zhao, J.-L. Hou, Z.-T. Li, *Chem. Rev.* **2012**, *112*, 5271.

5 (a) G. Hughes, M. R. Bryce, *J. Mater. Chem.* **2005**, *15*, 94. (b) A. P. Monkman, L.-O. Pålsson, R. W. T. Higgins, C. Wang, M. R. Bryce, A. S. Batsanov, J. A. K. Howard, *J. Am. Chem. Soc.* **2002**, *124*, 6049.

6 (a) S. Sharif, G. S. Denisov, M. D. Toney, H.-H. Limbach, *J. Am. Chem. Soc.* **2006**, *128*, 3375. (b) J. M. L. del Amo, U. Langer, V. Torres, G. Buntkowsky, H.-M. Vieth, M. Pérez-Torralba, D. Sanz, R. M. Claramunt, J. Elguero, H.-H. Limbach, *J. Am. Chem. Soc.* **2008**, *130*, 8620.

7 (a) M. Obi, H. Sakuragi, T. Arai, *Chem. Lett*. **1998**, *27*, 169. (b) S. Park, O.-H. Kwon, S. Kim, S. Park, M.-G. Choi, M. Cha, S. Y. Park, D.-J. Jang, *J. Am. Chem. Soc.* **2005**, *127*, 10070. (c) T. Iijima, A. Momotake, Y. Shinohara, T. Sato, Y. Nishimura, T. Arai, *J. Phys. Chem. A* **2010**, *114*, 1603.

8 (a) J. W. Weigl, R. Livingston, *J. Am. Chem. Soc.* **1953**, *75*, 2173. (b) M. S. Somma, C. J. Medforth, N. Y. Nelson, M. M. Olmstead, R. G. Khoury, K. M. Smith, *Chem Commun.* **1999**, 1221. (c) N. V. Ivashin, O. P. Parkhots, S. Larsson, *J. Appl. Spectroscopy* **2002**, *69*, 659.

9 E. Vogel, M. Köcher, H. Schmickler, J. Lex, *Angew. Chem. Int. Ed. Engl.* **1986**, *25*, 257.

10 (a) P. Bhyrappa, C. Arunkumar, B. Varghese, *Inorg. Chem.* **2009**, *48*, 3954. (b) K. M. Barkigia, D. J. Nurco, M. W. Renner, D. Melamed, K. M. Smith, J. Fajer, *J. Phys. Chem. B* **1998**, *102*, 322. (c) A. Osuka, S. Saito, *Chem. Commun.* **2011**, *47*, 4330.

11 C. B. Storm, Y. Teklu, *J. Am. Chem. Soc.* **1972**, *94,* 1745.

12 (a) R. J. Abraham, G. E. Hawkes, K. M. Smith, *Tetrahedron Lett.* **1974**, *15,* 1483. (b) S. S. Eaton, G. R. Eaton, *J. Am. Chem. Soc.* **1977**, *99,* 1601. (c) D. Gust, J. D. Roberts, *J. Am. Chem. Soc.* **1977**, *99,* 3637. (d) R. J. Butcher, G. B. Jameson, C. B. Storm, *J. Am. Chem. Soc.* **1985**, *107*, 2978.

13 (a) J. Hennig, H.-H. Limbach, *J. Chem. Soc., Faraday Trans. 2* **1979**, *75,* 752. (b) H.-H. Limbach, J. Hennig, D. Gerritzen, H. Rumpel, *Faraday Discuss. Chem. Soc.* **1982**, *74,* 229. (c) J. Hennig, H.-H. Limbach, *J. Am. Chem. Soc.* **1984**, *106,* 292. (d) H.-H. Limbach, J. Hennig, R. Kendrick, C. S. Yannoni, *J. Am. Chem. Soc.* **1984**, *106*, 4059. (e) J. Braun, M. Schlabach, B. Wehrle, M. Köcher, E. Vogel, H.-H. Limbach, *J. Am. Chem. Soc.* **1994**, *116*, 6593. (f) J. Braun, H.-H. Limbach, P. G. Williams, H. Morimoto, D. E. Wemmer, *J. Am. Chem. Soc.* **1996**, *118,* 7231.

14 (a) M. Schlbach, B. Wehrle, H.-H. Limbach, E. Bunnenberg, A. Knierzinger, A. Y. L. Shu, B. R. Tolf, C. Djerassi, *J. Am. Chem. Soc.* **1986**, *108,* 3856. (b) M. Schlabach, H. Rumpel, H.-H. Limbach, *Angew. Chem. Int. Ed. Engl.* **1989**, *28*, 76. (c) M. Schlabach, G. Scherer, H.-H. Limbach, *J. Am. Chem. Soc.* **1991**, *113*, 3550. (d) M. Schlbach, H.-H. Limbach, E. Bunenberg, A. Y. L. Shu, B. R. Tolf, C. Djerassi, *J. Am. Chem. Soc.* **1993**, *115,* 4554. (e) M. S. Somma, C. J. Medforth, N. Y. Nelson, M. M. Olmstead, R. G. Khoury, K. M. Smith, *Chem. Commun.* **1999**, 1221.

15 (a) J. R. Reimers, T. X. Lü, M. J. Crossley, N. S. Hash, *J. Am. Chem. Soc.* **1995**, *117*, 2855. (b) D. K. Maity, R. L. Bell, T. N. Truong, *J. Am. Chem. Soc.* **2000**, *122*, 897.

16 J. Braun, R. Schwesinger, P. G. Williams, H. Morimoto, D. E. Wemmer, H.-H. Limbach, *J. Am. Chem. Soc.* **1996**, *118*, 11101.

17 (a) M. J. Crossley, M. M. Harding, S. Sternhell, *J. Am. Chem. Soc.* **1986**, *108*, 3608. (b) M. J. Crossley, L. D. Field, M. M. Harding, S. Sternhell, *J. Am. Chem. Soc.* **1987**, *109*, 2335. (c) P. Wacker, K. Dahms, M. O. Senge, E. Kleinpeter, *J. Org. Chem.* **2008**, *73*, 2182. (d) E. A. Ermilov, B. Büge, S. Jasinski, N. Jux, B. Röder, *J. Chem.*

Phys. **2009**, *130*, 134509. (e) M. Urbani, T. Torres, *Chem. Eur. J.* **2014**, *20*, 16337. (e) H. García-Ortega, J. Crusats, M. Feliz, J. M. Ribo, *J. Org. Chem.* **2002**, *67*, 4170.

18 (a) K. Kawano, Y. Ozaki, Y. Kyogoku, H. Ogoshi, H. Sugimoto, Z.-I. Yoshida, *J. Chem. Soc., Chem. Commun.* **1977**, 226. (b) C. S. Irving, A. Lapidot, *J. Chem. Soc., Chem. Commun.* **1977**, 184. (c) K. Kawano, Y. Ozaki, Y. Kyogoku, H. Ogoshi, H. Sugimoto, Z.-I. Yoshida, *J. Chem. Soc., Perkin 2* **1978**, 1319. (d) M. J. Crossley, M. M. Harding, S. Sternhell, *J. Org. Chem.* **1992**, 57, 1833. (e) J. Helaja, F.-P. Montforts, I. Kilpeläinen, P. H. Hynninen, *J. Org. Chem.* **1999**, *64*, 432. (f) J. Helaja, M. Stapelbroek-Möllmann, I. Kilpeläinen, P. H. Hynninen, *J. Org. Chem.* **2000**, *65*, 3700.

19 NH tautomerisms of porphyrin analogues have been also studied: a) B. H. Meier, C. B. Storm, W. L. Earl, *J. Am. Chem. Soc.* **1986**, *108*, 6072. (b) B. Wehrle, H.-H. Limbach, M. Köchner, O. Ermer, E. Vogel, *Angew. Chem., Int. Ed. Engl.* **1987**, *26*, 934. (c) B. Frydman, C. O. Fernandez, E. Vogel, *J. Org. Chem.* **1998**, *63,* 9385. (d) U. Langer, C. Hoelger, B. Wehrle, L. Latanowicz, E. Vogel, H.-H. Limbach, *J. Phys. Org. Chem.* **2000**, *13*, 23. (e) K. Rachlewicz, L. Latos-Grażyński, A. Gebauer, A. Vivian, J. L. Sessler, *J. Chem. Soc., Perkin Trans. 2* **1999**, 2189. (f) H. Furuta, T. Ishizuka, A. Osuka, H. Dejima, H. Nakagawa, Y. Ishikawa, *J. Am. Chem. Soc.* **2001**, *123*, 6207. (g) M. Gil, J. Dobkowski, G. Wiosna-Sałyga, N. Urbanska, P. Fita, C. Radzewicz, M. Pietraszkiewicz, P. Borowicz, D. Marks, M. Glasbeek, J. Waluk, *J. Am. Chem. Soc.* **2010**, *132*, 13472. (h) P. Ciąćka, P. Fita, A. Listkowski, M. Kijak, S. Nonell, D.Kuzuhara, H. Yamada, C. Radzewicz, J. Waluk, *J. Phys. Chem. B* **2015**, *119*, 2292.

20 (a) T. Kumagai, F. Hanke, S. Gawinkowski, J. Sharp, K. Kotsis, J. Waluk, M. Persson, L. Grill, *Phys. Rev. Lett.* **2013**, *111*, 246101. (b) T. Kumagai, F. Hanke, S. Gawinkowski, J. Sharp, K. Kotsis, J. Waluk, M. Persson, L. Grill, *Nat. Chem.* **2014**, *6*, 41. (c) J. N. Ladenthin, T. Frederiksen, M. Persson, J. C. Sharp, S. Gawinkowski, J. Waluk, T. Kumagai, *Nat. Chem.* **2016**, *8*, 935.

21 (a) Z. Smedarchina, F. Zerbetto, *Chem. Phys.* **1989**, *136*, 285. (b) Z. Smedarchina, M. Z. Zgierski, W. Siebrand, P. M. Kozlowski, *J. Chem. Phys.* **1998**, *109*, 1014. (c) M. Boronat, E. Ortí, P. M. Viruela, F. Tomás, *J. Mol. Struct.* **1997**, *390*, 149.

22 (a) A. Sarai, *Chem. Phys. Lett.* **1981**, *83*, 50. (b) A. Sarai, *J. Chem. Phys.* **1982**, *76*, 5554. (c) A. Ghosh, J. Almlöf, *Chem. Phys. Lett.* **1993**, *213*, 519.

23 (a) H. Cybulski, M. Pecul, T. Helgaker, M. Jaszuński, *J. Phys. Chem. A* **2005**, *109*, 4162. (b) X. Lu, Y. He, J. Chen, J. Wang, H. Shi, *J. Phys. Chem. A* **2010**, *114*, 12731.

24 Reviews on this topic: (a) S. Fox, R. W. Boyle, *Tetrahedron* **2006**, *62*, 10039. (b) J. P. Lewtak, D. T. Gryko, *Chem. Commun.* **2012**, *48*, 10069. (c) H. Mori, T. Tanaka, A. Osuka, *J. Mater. Chem. C* **2013**, *1*, 2500. (d) M. Stępień, E. Gońka, M. Żyła, N. Sprutta, *Chem. Rev.* **2016**, ASAP (DOI: 10.1021/acs.chemrev.6b00076).

25 (a) L. Edwards, M. Gouterman, C. B. Rose, *J. Am. Chem. Soc.* **1976**, *98*, 7638. (b) T. D. Lash, B. H. Novak, *Angew. Chem., Int. Ed. Engl.* **1995**, *34*, 683. (c) S. Ito, T. Murashima, H. Uno, N. Ono, *Chem. Commun.* **1998**, 1661.

26 (a) R. Deshpande, L. Jiang, G. Schmidt, J. Rakovan, X. Wang, K. Wheeler, H. Wang, *Org. Lett.* **2009**, *11*, 4251. (b) L. Jiang, J. T. Engle, L. Sirk, C. S. Hartley, C. J. Ziegler, H. Wang, *Org. Lett.* **2011**, *13*, 3020. (c) S. Banala, T. Rühl, K. Wurst, B. Kräutler, *Angew. Chem. Int. Ed.* **2009**, *48*, 599.

27 (a) H. Aihara, L. Jaquinod, D. J. Nurco, K. M. Smith, *Angew. Chem. Int. Ed.* **2001**, *40*, 3439. (b) M. Nath, J. C. Huffman, J. M. Zaleski, *J. Am. Chem. Soc.* **2003**, *125*, 11484. (c) M. Nath, M. Pink, J. M. Zaleski, *J. Am. Chem. Soc.* **2005**, *127*, 478.

28 (a) A. N. Cammidge, P. J. Scaife, G. Berber, D. L. Hughes, *Org. Lett.* **2005**, *7*, 3413. (b) M. Tanaka, S. Hayashi, S. Eu, T. Umeyama, Y. Matano, H. Imahori, *Chem. Commun.* **2007**, 2069. (c) C. Jiao, K.-W. Huang, Z. Guan, Q.-H. Xu, J. Wu, *Org. Lett.* **2010**, *12*, 4046.

29 (a) H. S. Gill, M. Harmjanz, J. Santamaría, I. Finger, M. J. Scott, *Angew. Chem. Int. Ed.* **2004**, *43*, 485. (b) K. Kurotobi, K. S. Kim, S. B. Noh, D. Kim, A. Osuka, *Angew. Chem. Int. Ed.* **2006**, *45*, 3944.

30 C. Jiao, L. Zhu, J. Wu, *Chem. Eur. J.* **2011**, *17*, 6610.

31 (a) N. K. S. Davis, M. Pawlicki, H. L. Anderson, *Org. Lett.* **2008**, *10*, 3945. (b) N. K. S. Davis, A. L. Thompson, H. L. Anderson, *Org. Lett.* **2010**, *12*, 2124. (c) N. K. S. Davis, A. L. Thompson, H. L. Anderson, *J. Am. Chem. Soc.* **2011**, *133*, 30.

32 (a) K. Sendt, L. A. Johnston, W. A. Hough, M. J. Crossley, N. S. Hush, J. R. Reimers, *J. Am. Chem. Soc.* **2002**, *124*, 9299. (b) R. Paolesse, L. Jaquinod, F. S. Della, D. J. Nurco, L. Prodi, M. Montalti, C. D. Natale, A. D'Amico, A. D. Carlo, P. Lugli, K. M. Smith, *J. Am. Chem. Soc.* **2000**, *122*, 11295. (c) H. Uno, A. Masumoto, N. Ono, *J. Am. Chem. Soc.* **2003**, *125*, 12082. (d) M. Akita, S. Hiroto, H. Shinokubo, *Angew. Chem. Int. Ed.* **2012**, *51*, 2894.

33 (a) A. Tsuda, A. Nakano, H. Furuta, H. Yamochi, A. Osuka, *Angew. Chem. Int. Ed.* **2000**, *39*, 558. (b) A. Tsuda, H. Furuta, A. Osuka, *Angew. Chem. Int. Ed.* **2000**, *39*, 2549. (c) A. Tsuda, H. Furuta, A. Osuka, *J. Am. Chem. Soc.* **2001**, *123*, 10304. (d) A. Tsuda, A. Osuka, *Science* **2001**, *293*, 79. (d) Y. Nakamura, N. Aratani, H. Shinokubo, A. Takagi, T. Kawai, T. Matsumoto, Z. S. Yoon, D. Y. Kim, T. K. Ahn, D. Kim, A. Muranaka, N. Kobayashi, A. Osuka, *J. Am. Chem. Soc.* **2006**, *128*, 4119.

34 (a) R. B. Woodward, W. A. Ayer, J. M. Beaton, F. Bickelhaupt, R. Bonnet, P. Buchschacher, G. L. Closs, H. Dutler, J. Hannah, F. P. Hauck, S. Ito, A. Langemann, E. Le Goff, W. Leimgruber, W. Lwowski, J. Sauer, Z. Valenta, H. Volz, *J. Am. Chem. Soc.* **1960**, *82*, 3800. (b) R. B. Woodward, W. A. Ayer, J. M. Beaton, F. Bickelhaupt, R. Bonnet, P. Buchschacher, G. L. Closs, H. Dutler, J. Hannah, F. P. Hauck, S. Ito, A. Langemann, E. Le Goff, W. Leimgruber, W. Lwowski, J. Sauer, Z. Valenta, H. Volz, *Tetrahedron* **1990**, *46*, 7599.

35 (a) S. Fox, R. W. Boyle, *Chem. Commun.* **2004**, 1322. (b) D.-M. Shen, C. Liu, Q.-Y. Chen, *Chem. Commun.* **2005**, 4982. (c) D.-M. Shen, C. Liu, Q.-Y. Chen, *J. Org. Chem.* **2006**, *71*, 6508.

36 (a) S. Hayashi, Y. Matsubara, S. Eu, H. Hayashi, T. Umeyama, Y. Matano, H. Imahori, *Chem. Lett.* **2008**, *37*, 846. (b) T. D. Lash, B. E. Smith, M. J. Melquist, B. A. Godfrey, *J. Org. Chem.* **2011**, *76*, 5335. (c) A. M. V. M. Pereira, M. G. P. M. S. Neves, J. A. S. Cavaleiro, C. Jeandon, J.-P. Gisselbrecht, S. Choua, R. Ruppert, *Org. Lett.* **2011**, *13*, 4742.

37 (a) Y. Mitsushige, S. Yamaguchi, B. S. Lee, Y. M. Sung, S. Kuhri, C. A. Schierl, D. M. Guldi, D. Kim, Y. Matsuo, *J. Am. Chem. Soc.* **2012**, *134*, 16540. (b) H. Fliegl, N. Özcan, R. Mera-Adasme, F. Pichierri, J. Jusélius, D. Sundholm, *Mol. Phys.* **2013**, *111*, 1364.

38 (a) A. Nakano, N. Aratani, H. Furuta, A. Osuka, *Chem. Commun.* **2001**, 1920. (b) A. K. Sahoo, S. Mori, H. Shinokubo, A. Osuka, *Angew. Chem. Int. Ed.* **2006**, *45*, 7972. (c) N. Fukui, H. Yorimitsu, J. M. Lim, D. Kim, A. Osuka, *Angew. Chem. Int. Ed.* **2014**, *53*, 4395.

39 (a) N. Fukui, W.-Y. Cha, S. Lee, S. Tokuji, D. Kim, H. Yorimitsu, A. Osuka, *Angew. Chem. Int. Ed.* **2013**, *52*, 9728. (b) K. Ota, T. Tanaka, A. Osuka, *Org. Lett.* **2014**, *16*, 2974.

40 (a) T. Ishizuka, Y. Saegusa, Y. Shiota, K. Ohtake, K. Yoshizawa, T. Kojima, *Chem. Commun.* **2013**, *49*, 5939. (b) Y. Saegusa, T. Ishizuka, K. Komamura, S. Shimizu, H. Kotani, N. Kobayashi, T. Kojima, *Phys. Chem. Chem. Phys.* **2015**, *17*, 15001. (c) Y. Saegusa, T. Ishizuka, T. Kojima, S. Mori, M. Kawano, T. Kojima, *Chem. Eur. J.* **2015**, *21*, 5302. (d) Y. Saegusa, T. Ishizuka, Y. Shiota, K. Yoshizawa, T. Kojima, *J. Org. Chem.* **2017**, in press

41 (a) A. Suzuki, *Chem. Commun.* **2005**, 4759. (b) L. Yin, J. Liebscher, *Chem. Rev.* **2007**, *107*, 133. (c) S. Chamoin, S. Houldsworth, C. G. Kruse, W. Iwema Bakker, V. Snieckus, *Tetrahedron Lett.* **1998**, *39*, 4179. (d) M. O. Senge, Y. M. Shaker, M. Pintea, C. Ryppa, S. S. Hatscher, A. Ryan, Y. Sergeeva, *Eur. J. Org. Chem.* **2010**, 237.

42 Upon increasing the concentration, the ^{1}H NMR signal of the inner NH protons of **16c** was coalesced first from split, and then split again (Figure 6-3). The concentration effect on the NH tautomerism is currently under investigation.

43 H. S. Gutowsky, C. H. Holm, *J. Chem. Phys.* **1956**, *25*, 1228.

44 (a) I. Plowas, J. Swiergiel, J. Jadzyn, *J. Chem. Eng. Data* **2013**, *58*, 1741. (b) T. Teutenberg**,** S. Wiese, P. Wagner, J. Gmehling, *J. Chromatogr. A* **2009**, *1216*, 8480.

45 (a) H. Rumpel, H.-H. Limbach, *J. Am. Chem. Soc.* **1989**, *111*, 5429. (b) G. Scherer, H.-H. Limbach, *J. Am. Chem. Soc.* **1989**, *111*, 5946. (c) G. Scherer, H.-H. Limbach, *J. Am. Chem. Soc.* **1994**, *116*, 1230.

46 T. Leermann, F. R. Leroux, F. Colobert, *Org. Lett.* **2011**, *13*, 4479.

47 G. M. Sheldrick, SIR97 and SHELX97, Programs for Crystal Structure Refinement, University of Göttingen, Göttingen (Germany), 1997.

48 P. V. D. Sluis, A. L. Spek, *Acta Crystallogr.* **1990**, *A46*, 194.

49 A. D. Becke, *Phys. Rev. A* **1988**, 38, 3098.

50 C. Lee, W. Yang, R. G. Parr, *Phys. Rev. B* **1988**, 37, 785.

51 R. Ditchfield, W. J. Hehre, J.A. Pople *J. Chem. Phys.* **1971**, 54, 724.

52 W. J. Hehre, R. Ditchfield, J. A. Pople, *J. Chem. Phys.* **1972**, 56, 2257.

53 Gaussian 09, Revision D.01, M. J. Frisch, G. W. Trucks, H. B. Schlegel, G. E. Scuseria, M. A. Robb, J. R. Cheeseman, G. Scalmani, V. Barone, B. Mennucci, G. A. Petersson, H. Nakatsuji, M. Caricato, X. Li, H. P. Hratchian, A. F. Izmaylov, J. Bloino, G. Zheng, J. L. Sonnenberg, M. Hada, M. Ehara, K. Toyota, R. Fukuda, J. Hasegawa, M. Ishida, T. Nakajima, Y. Honda, O. Kitao, H. Nakai, T. Vreven, J. A. Montgomery, Jr., J. E. Peralta,

F. Ogliaro, M. Bearpark, J. J. Heyd, E. Brothers, K. N. Kudin, V. N. Staroverov, R. Kobayashi, J. Normand, K. Raghavachari, A. Rendell, J. C. Burant, S. S. Iyengar, J. Tomasi, M. Cossi, N. Rega, J. M. Millam, M. Klene, J. E. Knox, J. B. Cross, V. Bakken, C. Adamo, J. Jaramillo, R. Gomperts, R. E. Stratmann, O. Yazyev, A. J. Austin, R. Cammi, C. Pomelli, J. W. Ochterski, R. L. Martin, K. Morokuma, V. G. Zakrzewski, G. A. Voth, P. Salvador, J. J. Dannenberg, S. Dapprich, A. D. Daniels, Ö. Farkas, J. B. Foresman, J. V. Ortiz, J. Cioslowski, and D. J. Fox, Gaussian, Inc., Wallingford CT, 2009.

Chapter 7

QFP derivatives toward NLO properties

7-1. Introduction

Nonlinear optical (NLO) materials have been used for biological imaging and also for applications in telecommunication and date-storage devices.[1-3] In comparison to inorganic NLO materials, NLO materials based on organic chromophores can be easily modified by introduction of substituents to control the optoelectronic properties,[4] and intermolecular interaction of the molecules can be also employed to obtain high efficiency of NLO responses.[5] A variety of chromophores showing greatly enhanced molecular first hyperpolarizability values (β) have been designed and synthesized to date.[3,4] To qualitatively interpret the NLO responses of organic NLO chromophores, a two-state approximation model have been widely used.[6] In the model, the molecular first hyperpolalizability, β, can be estimated

$$\beta \propto \Delta\mu_{ge} \frac{\chi_{ge}}{(E_{ge})^2} \qquad (1)$$

with eq 1.[7] As expressed by eq 1, the intensity of β is qualitatively proportional to three factors, $\Delta\mu_{ge}$, χ_{ge} and $(E_{ge})^{-2}$. $\Delta\mu_{ge}$ is the difference of dipole moments between the ground and excited states of a chromophore, χ_{ge} is a transition-dipole moment, and E_{ge} is a HOMO-LUMO gap. Therefore, to obtain large β values, increasing dipole moments of the NLO molecules and narrowing the HOMO-LUMO gaps are considered to be effective.[6,7] Based on the strategies, NLO molecules, which are so-called "push-pull" system, have been synthesized; electron-donating and -withdrawing groups are introduced to diagonal positions of the π-conjugated molecules.[1] For instance, a stilbene derivative having an dimethylamino group as an electron-donor and a nitro group as an electron-acceptor have been reported to show large β values, 55×10^{-30} esu (Figure 7-1).[4a] In addition, extension of the alkene chains between the electron-donating and -withdrawing groups has been reported to increase the β values.[4b]

Due to its intense optical absorption, porphyrin and its derivatives have been widely used as building chromophores for optoelectronic applications including NLO materials.[7,8] To obtain large β

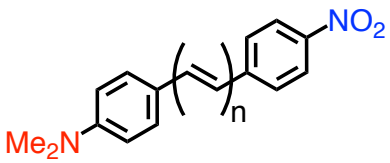

Figure 7-1. Structure of stilbene derivatives showing NLO properties.[4]

values, porphyrin derivatives are useful due to the narrow HOMO-LUMO gaps on the basis of the expanded π-conjugation with 18π aromatic circuit.[8] NLO chromophores made of porphyrin derivatives have been prepared on the basis of the "push-pull" design;[9-11] for instance, a "push-pull"-type (aryl-ethynyl)porphyrin, which has nitro- and

dimethylamino-phenylethynyl groups at the diagonal *meso*-positions, exhibited one of the largest β values (800×10^{-30} esu), together with high thermal stability.[9a] On the other hand, it is difficult to introduce both of electron-donating and electron-withdrawing groups directly at the aromatic circuit of the porphyrin core without π-conjugated bridge such as phenylethynyl moieties.[8] Therefore, the effects of direct introduction of the "push-pull" functional groups to the aromatic circuit of porphyrins on the NLO properties have yet to be well established.[10b]

To develop characteristic optoelectronic properties, modification of porphyrins by introduction of fused rings at the periphery of the porphyrin aromatic circuit has been intensively studied in recent years,[12-27] in light of the merits of the unique physical properties derived from the narrowed HOMO-LUMO gaps and facileness for formation of π-π stacked arrays using the planar highly expanded π-conjugated surfaces. The ring-fusion strategy has been successfully applied to obtain a chromophore showing an absorption band over 1400 nm based on one porphyrin unit.[19c] However, the ring-fusion reactions reported so far are highly limited and the synthetic procedures for the precursors are time-consuming.[12,19] Recently, an efficient procedure has been reported for preparation of quadruply fused porphyrins (QFPs), in which the four *meso*-aryl groups are covalently bonded to the β-carbons of the pyrrole rings at the *ortho*-positions.[28] Additionally, the π-conjugation circuit of QFP expands to the fused *meso*-aryl groups and the properties of QFP such as redox potentials are highly sensitive to the substituents at the fused aryl groups.[28b] The enhanced substituent effects of QFP on the electronic structures, exemplified by UV-vis spectrum and electrochemical studies,[28b] are also useful to obtain efficient NLO materials based on QFP.

In this chapter, the author describes preparation of NLO chromophores based on QFP to utilize its small HOMO-LUMO gap and sensitive substituent effects. In particular, to elucidate the impact of the "push-pull" effects on QFP toward the NLO properties, ZnQFP derivatives (**17** – **19**), having an electron-withdrawing group such as nitro group and a methoxy group as an electron-donating group at the diagonal positions of the molecule, have been prepared through stepwise processes. Furthermore, the emergence of the charge-transfer (CT) band and NLO responses of the "push-pull" ZnQFP derivatives have been explored.

7-2. Synthesis

Herein, to investigate the impact of the "push-pull" effects of substituents on the NLO properties of ZnQFP, various electron-withdrawing and -donating groups (EWG and EDG, respectively) has been introduced to $ZnTPPBr_4$ precursors (**20** – **22**) of ZnQFP (Scheme 7-1). Synthesis of the "push-pull" QFP derivatives have been done as follows: EDG and EWG were introduced at the *meso* positions through a stepwise manner to a TPP precursor (**23**), then the "push-pull" TPPs (**24** – **26**) were brominated at the four β-carbons to give the tetrabromo-derivatives, **27** – **29**, followed by Zn^{II} insertion to obtain precursors **20** – **22**, and the ring-fusing reaction for the precursors was performed with Pd clusters as a catalyst[29] in 1,4-dioxane. Because of the high thermal and air stability, a methoxy group was chosen as the EDG of the "push-pull" QFP. On the other hand, nitro, cyano and trifluoromethyl groups were introduced as EWG to "push-pull" QFP. Yields of the "push-pull" QFP derivatives at the final ring-fusion step were 84% for **17** having NO_2 group as EWG, 61% for **18** having CN group, and 17% for **19** having CF_3 group. Characterization of the "push-pull"

TPPs and QFPs was done by ^{1}H NMR spectroscopy, MALDI-TOF- MS spectrometry and single crystal X-ray diffraction analysis for **24**.

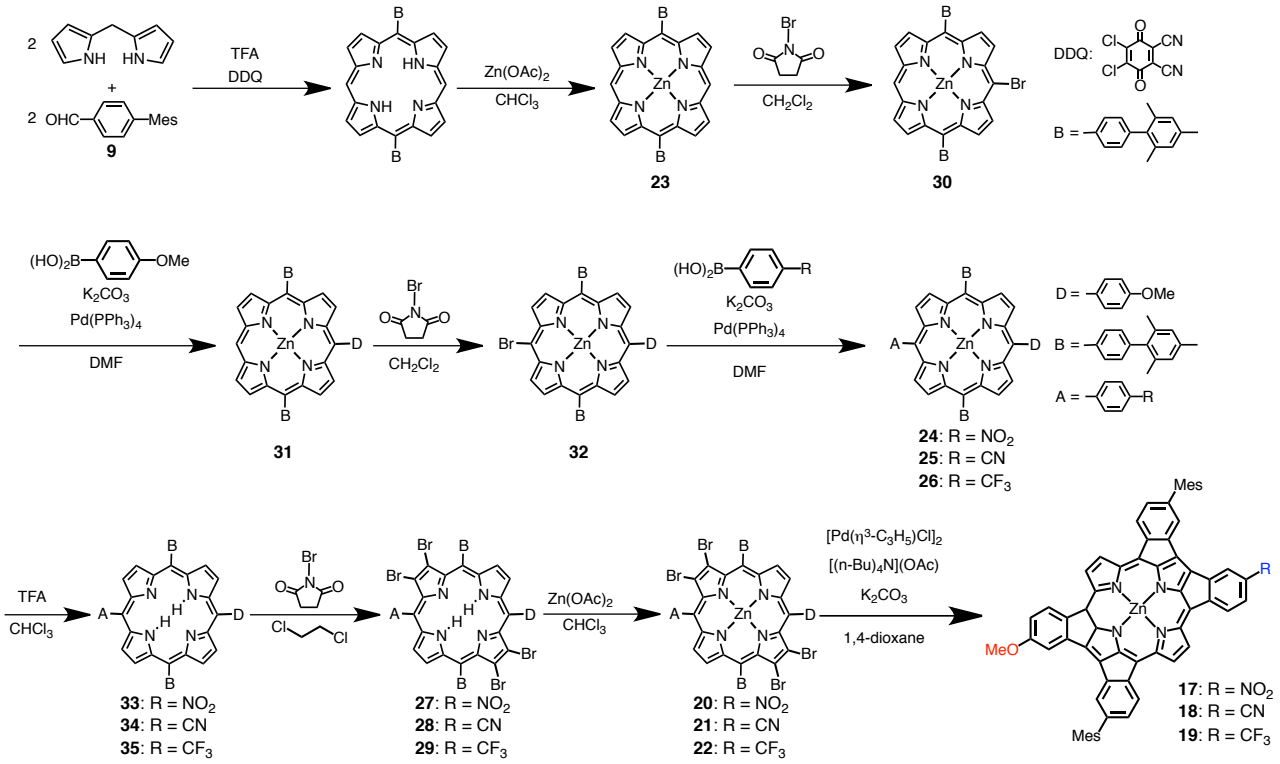

Scheme 7-1. The synthetic route of "push-pull" ZnQFPs.

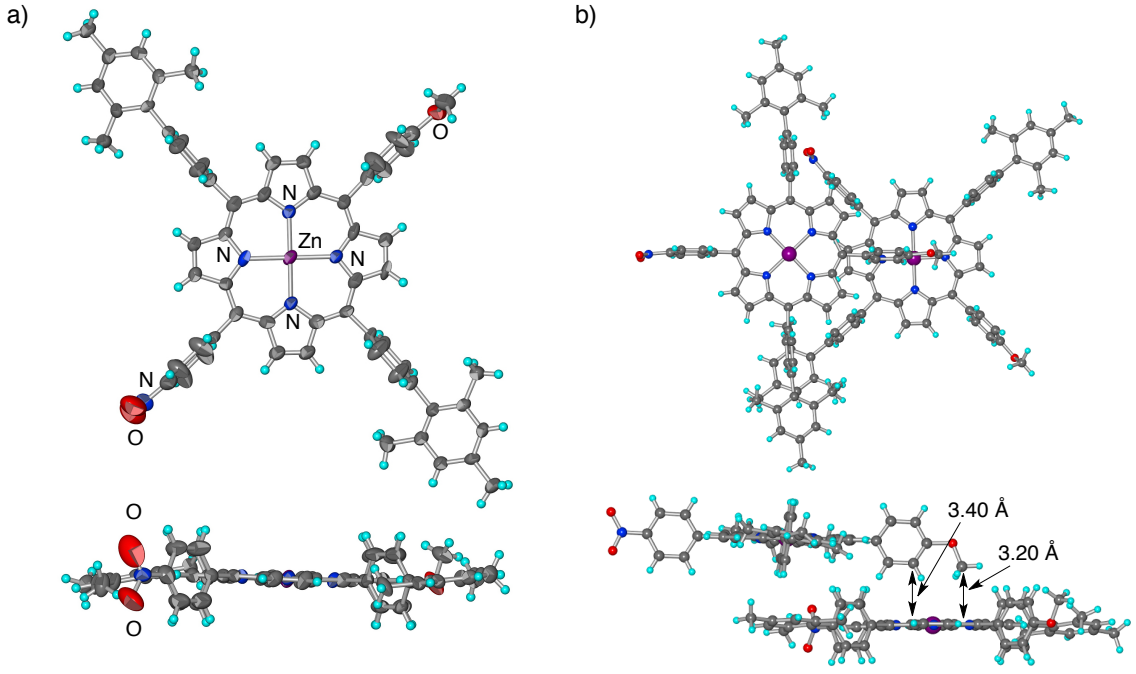

Figure 7-2. Top and side views of crystal structures of a "push-pull" TPP derivative, **24**, having OMe and NO_2 groups (a). The thermal ellipsoids are drawn at the 50% probability. Top and side views of the dimer structure of **24** (b).

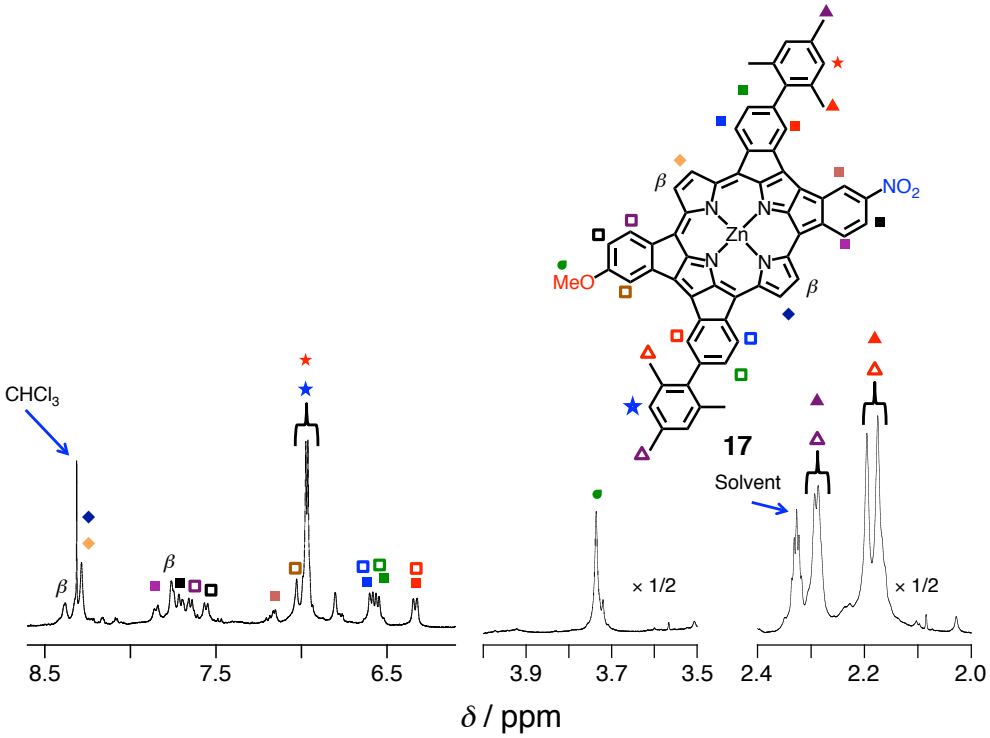

Figure 7-3. ^{1}H NMR spectrum of **17** in DMSO-d_6 at 298 K.

The single crystal of **24** was obtained from the solution in $CHCl_3$ in the presence of methanol vapor (Figure 7-2). The crystal structure revealed that the aryl moiety with a methoxy group is properly substituted at the diagonal position of the aryl moiety with a nitro group. Compound **24** showed edge-to-face and CH-π interaction in the crystal packing, in which the distance from the nearest phenyl carbon of the methoxy-phenyl group to the porphyrin plane was 3.40 Å and that from the carbon atom of the methoxy group to the porphyrin plane was 3.20 Å (Figure 7-2b).

The ^{1}H NMR spectra of "push-pull" ZnQFPs, **17** – **19**, in DMSO-d_6 showed relatively complicated pattern due to the low symmetric structures (Figure 7-3); for instance, the ^{1}H NMR signals of the methyl groups at the *ortho*- and *para*-positions of the two mesityl groups for **17** were observed as four singlet signals at 2.29, 2.28, 2.20, and 2.18 ppm with 1:1:2:2 integral ratio. The signal of the methoxy group was observed at 3.74 ppm in the ^{1}H NMR spectrum of **17**, and thus, the methoxy group was maintained after the ring-fusion reaction.

7-3. Optical properties of "push-pull" ZnQFPs

To confirm electronic effects of the introduction of "push-pull" substituents to QFP, the electronic absorption spectra of **17** – **19** were measured (Figure 7-4). As a result, the introduction of "push-pull" substituents caused bathochromic shifts of the absorption bands of **17** – **19**; for example, the absorption maxima of the longest Q-like band of **17** exhibited a bathochromic shift by 29 nm relative to that of **4b** (Figure 7-4a). On the other hand, the Soret and Q bands of "push-pull" ZnTPP derivatives, **24** – **26**, show the absorption maxima at similar wavelengths to those of ZnT(*p*-Mes)PP, having four mesityl-phenyl groups at the *meso* positions (Figure 7-4c).

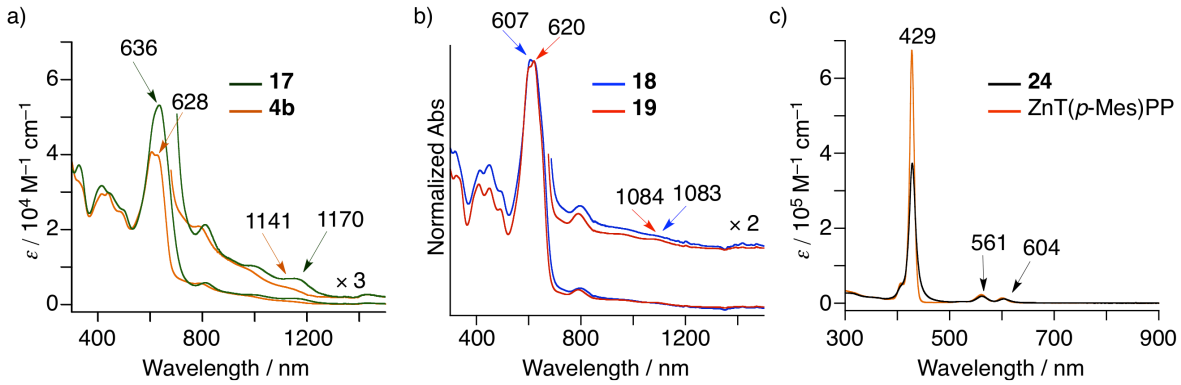

Figure 7-4. UV-vis spectra of and ZnQFP derivatives (a), "push-pull" ZnQFP, **18** (blue) and **19** (red) (b) and ZnTPP derivatives (c) in DMF.

Table 7-1. Absorption maxima of QFP and ZnTPP derivatives in DMF.

	λ_{max}(B)[a]	λ_{max}(Q)[a]	λ_{max}[a,b]
17 (R = NO_2)	636	1170	813
18 (R = CN)	607	1083	797
19 (R = CF_3)	620	1084	791
4b	628	1141	—
24 (R = NO_2)	429	604	—
ZnT(*p*-Mes)PP	429	604	—

[a] in nm, [b] Absorption maxima of a absorption band around 800 nm.

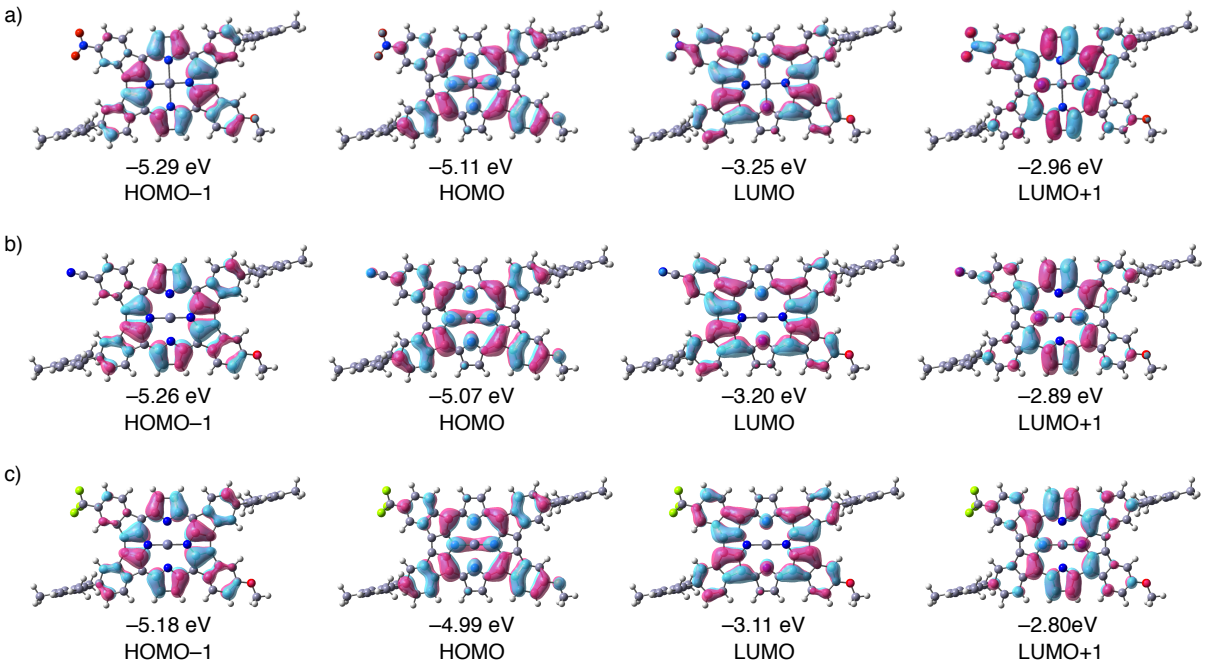

Figure 7-5. Frontier orbitals of DFT optimized structures of "push-pull" ZnQFP, **17** (a), **18** (b) and **19**(c).

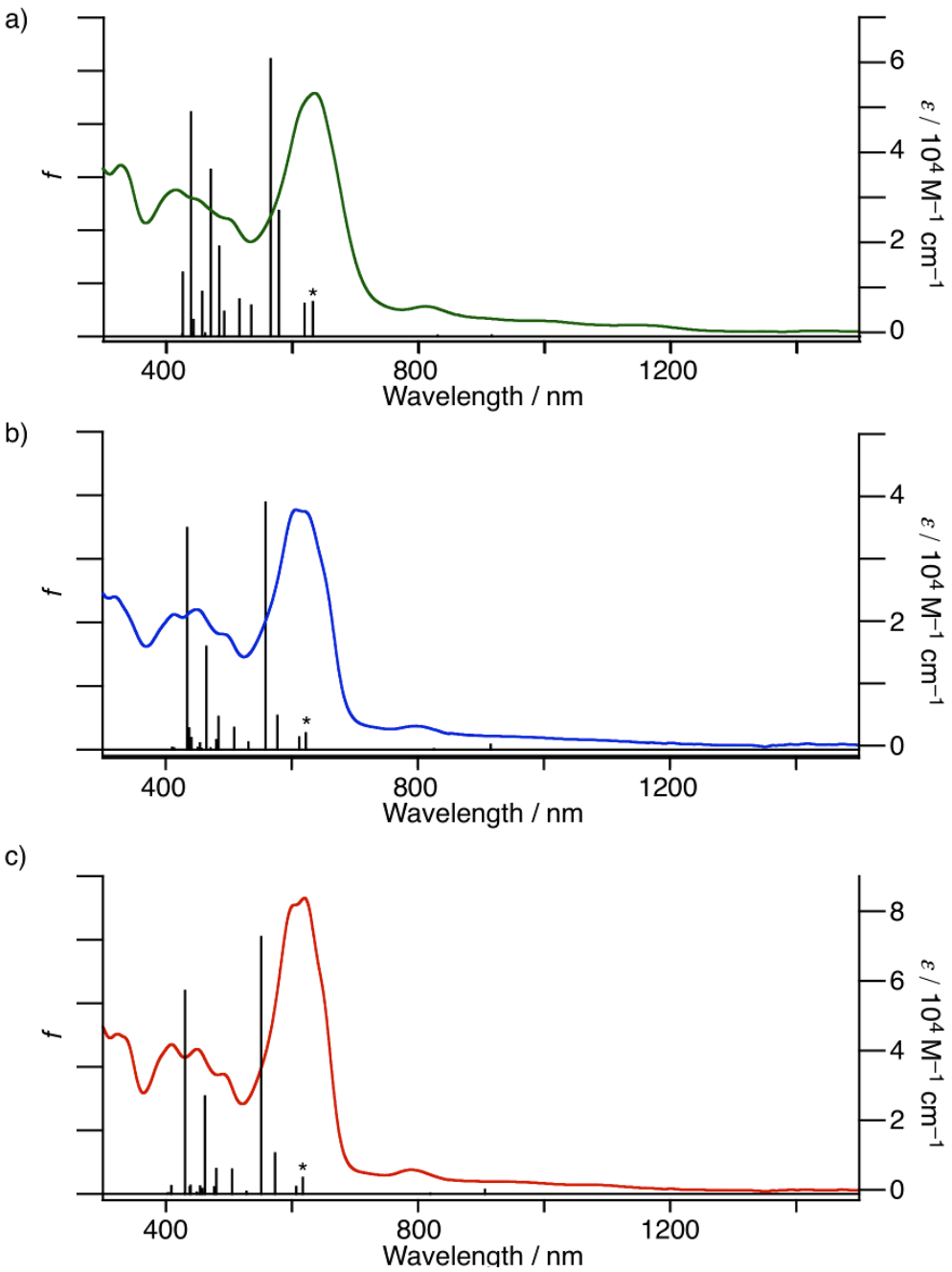

Figure 7-6. Experimental absorption spectra (colored solid lines), recorded in DMF at room temperature, and calculated transition energies and oscillator strengths (*f*) obtained by TD-DFT calculations at the B3LYP/6-31G** level of theory (black sticks) of **17** (a), **18** (b), **19** (c).

To assign the origins of the transitions to afford the absorption bands of "push-pull" ZnQFPs, TD-DFT calculations on **17** – **19** were performed at the B3LYP/6-31G** level of theory using their DFT-optimized structures (Figure 7-5). The calculated wavelengths and oscillator strengths for the electronic transitions are summarized in Table 7-2 and schematically depicted in Figure 7-6. The calculated stick spectra shown in Figure 7-6 well reproduce the excitation wavelengths and absorbance of the experimental spectra. The absorption bands around 600 nm of the "push-pull" ZnQFP, which can be assigned to the absorption bands around 800 nm in the experimental spectra, commonly derive from the (HOMO–1)-to-(LUMO+1) transitions, the former of which shows distribution on the fused

methoxy-phenyl moiety and the latter does it on the fused EWG-substituted aryl moiety (Figure 7-5); thus the transition bears a CT character. To gain in-depth insight into the CT bands of "push-pull" ZnQFPs, the UV-vis spectra of **17** were

Table 7-2. TD-DFT results for low-energy π-π* states of the "push-pull" ZnQFP derivatives. [a]

compound	wavelength, nm	oscillator strength	contribution (weight %)[b]
17	915.49	0.0184	H→L (93)
	829.77	0.0016	H–1→L (67), H→L+1 (31)
	632.06	0.0648	H–1→L+1 (67), H–2→L (9)
	618.61	0.0618	H–2→L (53), H→L+2 (18), H–1→L+1 (14)
	577.97	0.2360	H–3→L (53), H→L+1 (18), H–1→L (9), H–2→L (9)
	565.12	0.5220	H–9→L (30), H→L+1 (29), H–3→L (25), H–1→L (12), H–1→L+2 (10)
18	916.03	0.0151	H→L (94)
	825.54	0.0012	H–1→L (67), H→L+1 (31)
	622.52	0.0512	H–1→L+1 (63), H–2→L (18)
	612.10	0.0386	H–2→L (53), H–1→L+1 (19), H→L+2 (16)
	577.33	0.1060	H–3→L (73), H→L+1 (10)
	558.57	0.7771	H→L+1 (44), H–1→L (20), H–3→L (9)
19	906.36	0.0126	H→L (94)
	819.46	0.0011	H–1→L (67), H→L+1 (31)
	617.39	0.0501	H–1→L+1 (66), H–4→L (9)
	606.71	0.0219	H–2→L (58), H→L+2 (17), H–1→L+1 (15)
	573.17	0.1277	H–3→L (71), H→L (13)
	551.51	0.8084	H→L+1 (44), H–1→L (20), H–3→L (11)

[a] At the B3LYP/6-31G** level of theory. [b] H = HOMO, L = LUMO.

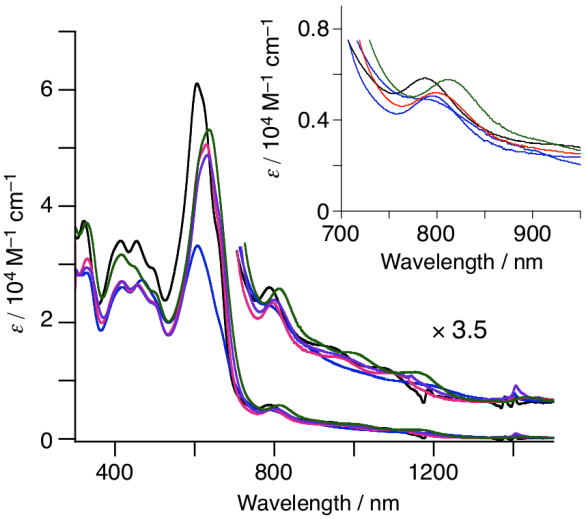

Figure 7-7. Solvent effects on UV-vis Absorbance of **17** in THF (black), *o*-dichlorobenzene (blue), pyridine (red), benzonitrile (purple), DMF (green).

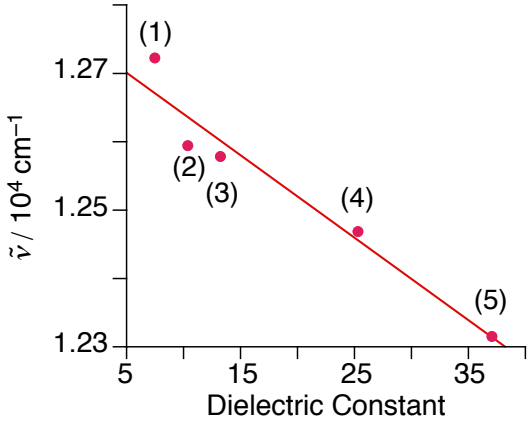

Figure 7-8. A plot of the absorption maxima of **17** around 800 nm relative to dielectric constants of solvents; (1) THF, (2) 1,2-dichlorobenzene, (3) pyridine, (4) benzonitrile and (5) DMF.

Table 7-3. Summary of absorption maxima of **17** in various solvents

	Dielectric constant	λ_{max} [a,b]	ν [a,c]
THF	7.5	786	12723
1,2-dichlorobenzene	10.4	794	12594
pyridine	13.2	795	12579
benzonitrile	25.3	802	12469
DMF	37.1	812	12315

[a] Absorption maxima of the absorption band around 800 nm, [b] in nm, [c] in cm^{-1}.

measured in five solvents, having different polarity (Figure 7-7 and Table 7-3); THF, 1,2-dichlorobenzene, pyridine, benzonitrile, and DMF were used in this study, and their dielectric constants are 7.5, 10.4, 13.2, 25.3, and 37.1, respectively.[30] The absorption band observed around 800 nm of **17** were well shifted upon changing the solvent. The wavenumber of the absorption maxima of the absorption band around 800 nm were plotted against the dielectric constant of the solvent (Figure 7-8), and the energies of the absorption maxima exhibited good linearity against the dielectric constants of the solvents, indicating that the absorption band around 800 nm derives from the CT transition, as suggested by the TD-DFT calculations.

7-4. NLO responses of "push-pull" ZnQFPs

To investigate the NLO properties of "push-pull" ZnQFPs, dynamic hyperpolarizability (β_{1300}) values for incident laser at 1300 nm were determined by hyper-Rayleigh light-scattering measurements.[31] The β_{1300} values are summarized in Table 7-4. The "push-pull" ZnQFP derivatives showed larger β_{1300} values than the corresponding ZnTPP derivatives, owing to direct introduction of EDG and EWG moieties to the aromatic circuit; for instance, the ZnQFP derivative, having a cyano group as an EWG, showed the largest β_{1300} value of 730×10^{-30} esu among the "push-pull"

ZnQFP derivatives studied here, and the β_{1300} value of the cyano-derivative was *ca.* 240 times larger than that of the corresponding ZnTPP derivative (**25**) having the same "push-pull" substituents. This large hyperpolarizability can be explained by the fact that the ring fusion enables the molecule to form a quinoid-like resonance structure (Figure 7-9), which supports increase of the $\Delta\mu_{ge}$ value.[4,8] It should be noted that only the cyano derivative, **18**, exhibited the large hyperpolarizability in comparison to those of **17** and **19**; however, the mechanism that compound **18** affords such large hyperpolarizability has yet to be clarified.[32]

Table 7-4. Dynamic hyperpolarizabilities in $CHCl_3$.

	β_{1300} / 10^{-30} esu
17 (R = NO_2)	58
18 (R = CN)	730
19 (R = CF_3)	64
24 (R = NO_2)	18
25 (R = CN)	3
26 (R = CF_3)	17

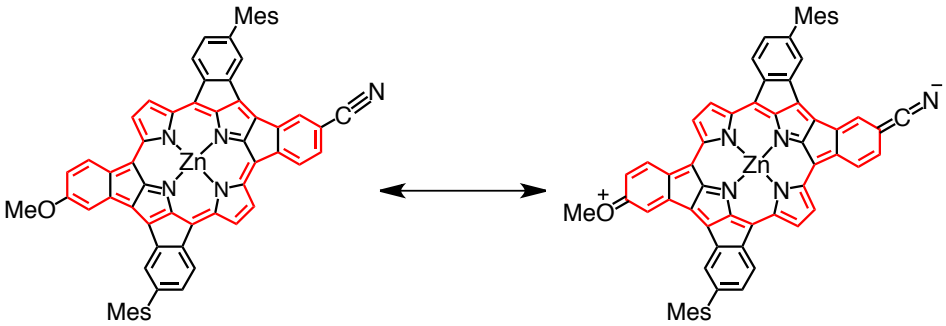

Figure 7-9. Resonance structures of **18**: a normal aromatic form (left) and a quinoid-like form (right).

In comparison to the β-values of other porphyrin derivatives having substituents directly introduced to the porphyrin core, the hyperpolarizability value of **18** is larger than those reported so far; for example, a porphyrin

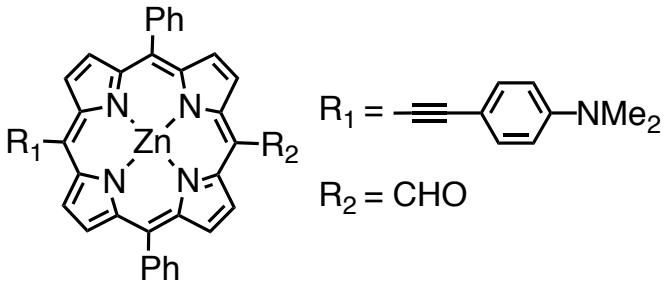

36

Figure 7-10. Structure of a "push-pull" porphyrin having EWG directly introduced at the porphyrin aromatic circuit.[10b]

derivative (**36**), having a formyl acceptor (Figure 7-10),[10b] which is directly introduced to the aromatic circuit without π-conjugated bridge such as phenylethyny group at the *meso*-position, exhibited the β_0 value as 82×10^{-30} esu. In the optimized structure of **36**, steric repulsion between the formyl group and the adjacent *β*-hydrogen causes twisting of the acceptor substituent against the porphyrin plane; the dihedral angle between the formyl and porphyrin planes is 26°. This loss of coplanarity results in less conjugation between the donor and acceptor substituents and the small NLO response. In contrast, the "push-pull" substituents of **18** exhibit coplanarity against the porphyrin plane; the substituents, CN and OMe group, are almost on the same plane including the porphyrin core (Figure 7-11).

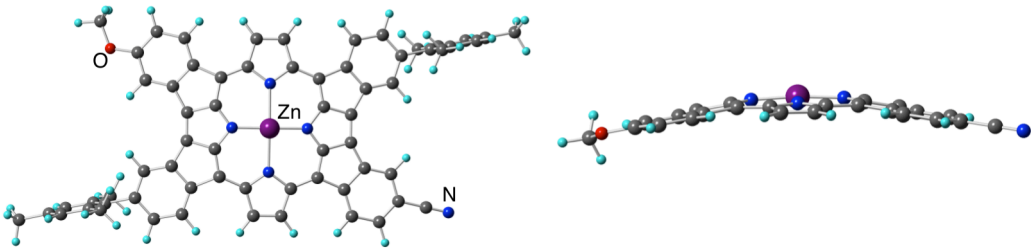

Figure 7-11. Top and side views of DFT-optimized structure of **18** at the B3LYP/6-31G** level of theory. The peripheral mesityl groups are omitted for clarity in side view.

7-4. Summary

The "push-pull" derivatives of ZnQFP, **17** – **19**, have been synthesized and characterized. Investigation on the electronic absorption spectra revealed that the "push-pull" ZnQFP exhibited characteristic CT bands around 800 nm, which derives from the electronic transition from the electron-donating moiety to the electron-accepting moiety. The absorption bands bear CT characters as reflected on the linear dependence on the solvent polarity, and as indicated by TD-DFT calculations. The dynamic hyperporalizability values (*β*) of **17** – **19** were determined by the hyper-Rayleigh light-scattering measurements. The expansion of the aromatic circuits to substituted ring-fused moieties significantly improved the *β* values of "push-pull" ZnQFP derivatives; especially the ZnQFP with a cyano group, **18**, showed the *ca.* 240 times larger *β* value than that of corresponding TPP derivatives, **25**.

Experimental section

General.

Chemicals and solvents were used as received from commercial sources unless otherwise mentioned. *o*-dichlorobenzene used for the UV-vis spectral measurements was distilled over CaH_2 before use. THF, pyridine, benzonitrile and DMF were distilled before use.

^{1}H NMR measurements were performed on Bruker AVANCE-400, -500 and -600 spectrometers. UV-vis absorption spectra were measured on a Shimadzu UV-3600 spectrophotometer. MALDI-TOF-MS spectrometry was performed on an AB SCIEX TOF/TOF 5800 spectrometer.

Synthesis.

General procedure of Pd-catalyzed ring-fusing reactions using Pd-nanoclusters derived from $[Pd(\eta^2\text{-}C_3H_5)Cl]_2$.[29] A solution of TBA·OAc (TBA = tetra(*n*-butyl)ammonium, 300 mg, 1.0 mmol), allyl-palladium(II) chloride dimer (2.8 mg, 7.7 μmol), and potassium carbonate (160 mg, 1.1 mmol) in 1,4-dioxane (1.0 mL) was heated at 110 ºC for 3 min. After the color of the solution changed to black, a tetrabromo-derivative of porphyrin (5.0 μmol) was quickly added to the solution. After stirring for 11 h at 110 °C, the reaction mixture was cooled to ambient temperature. After filtration, the filtrate was collected and the solvent was removed under vacuum. The residual solid was recrystallized from THF/ethanol (1:3, v/v) and dried under vacuum to obtain QFP derivatives.

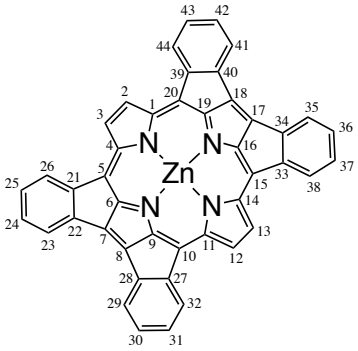

Zinc(II) 24,36-bismesityl-30-methoxy-42-nitro-quadruply-fused porphyrinato (17). A ring-fusion reaction was performed with **20** (5.3 mg, 4.1 μmol) as a starting material to obtain **17** (3.4 mg, 3.4 μmol, 84%), using the aforementioned general procedure. ^{1}H NMR (DMSO-d_6): δ 8.40 – 8.30 (m, 3H, β-H), 7.87 (d, J = 8.0 Hz, 1H, 44-Ph-H), 7.77 – 7.56 (m, 5H, 32,31,32,43,β-Ph-H), 7.03 (s, 1H, 41-Ph-H), 6.97 – 6.96 (m, 2H, mesityl-*m*-CH_3), 6.81 (s, 1H, 29- Ph-H), 6.61 (d, J = 8.0 Hz, 2H, 26,38-Ph-H), 6.56 (d, J = 8.0 Hz, 2H, 25,37-Ph-H), 6.35 – 6.34 (m, 2H, 23,35-Ph-H), 3.74 (s, 3H, OCH_3), 2.30 – 2.29 (m, 6H, mesityl-*p*-CH_3), 2.22 – 2.19 (m, 12H, mesityl- *o*-CH_3). UV-vis (DMF): λ_{max} [nm] (log (ε, M^{-1} cm^{-1})) = 328 (4.57), 413 (4.50), 450 (4.47), 500 (4.40), 637 (4.73), 813 (3.76), 1003 (3.41), 1173 (3.20). MS (MALDI-TOF, *9-aminoacridine matrix*): *m/z* = 979.4 (calcd. for $[M]^-$: 979.3).

Zinc(II) 24,36-bismesityl-30-cyano-42-methoxy-quadruply-fused porphyrinato (18). A ring-fusion reaction was performed with **21** (4.9 mg, 3.8 μmol) as a starting material to obtain **18** (2.2 mg, 2.3 μmol, 61%), using the aforementioned general procedure. ^{1}H NMR (DMSO-d_6): δ 8.36 – 8.28 (m, 3H, β-H), 7.79 – 7.55 (m, 5H, 31,32,43,44,β-Ph-H), 7.29 (s, 1H, 32-Ph-H), 7.01 (s, 1H, 41-Ph-H), 6.97 – 6.96 (m, 2H, mesityl-*m*-CH_3), 6.58 – 6.53 (m, 6H, 25,26,37,38-Ph-H), 6.34 – 6.33 (m, 2H, 23,35-Ph-H), 3.73 (s, 3H, OCH_3), 2.28 (s, 6H, mesityl-*p*-CH_3), 2.19 – 2.17 (m, 12H, mesityl-*o*-CH_3). UV-vis (DMF): λ_{max} [nm] (log (ε, M^{-1} cm^{-1})) = 320 (4.38), 415 (4.32), 448 (4.34), 498 (4.25), 623 (4.58), 794 (3.50), 967 (3.15), 1086 (3.00). MS (MALDI-TOF, *9-aminoacridine matrix*): *m/z* = 959.4 (calcd. for $[M]^-$: 959.3).

Zinc(II) 24,36-bismesityl-30-methoxy-42-trifluoromethy-quadruply-fused porphyrinato (19). A ring-fusion reaction was performed with **22** (11.5 mg, 8.7 μmol) as a starting material to obtain **19** (1.5 mg, 1.5 μmol, 17%), using the aforementioned general procedure. ^{1}H NMR (DMSO-d_6): δ 8.36 – 8.27 (m, 3H, β-H), 7.82 (d, J = 8.0 Hz, 1H, 44-Ph-H), 7.73 – 7.43 (m, 5H, 32,31,32,43,β-Ph-H), 7.15 (s, 1H, 41-Ph-H), 6.97 – 6.96 (m, 2H, mesityl-*m*-CH_3), 6.79 (s, 1H, 29-Ph-H), 6.61 (d, J = 8.0 Hz, 2H, 26,38-Ph-H), 6.58 – 6.53 (m, 2H, 25,37-Ph-H), 6.34 – 6.33 (m, 2H, 23,35-Ph-H), 3.73 (s, 3H, OCH_3), 2.28 (s, 6H, mesityl-*p*-CH_3), 2.20 – 2.17 (m, 12H, mesityl-*o*-CH_3). UV-vis (DMF): λ_{max} [nm] (log (ε, M^{-1} cm^{-1})) = 324 (4.38), 408 (4.62), 448 (4.61), 497 (4.51), 620 (4.92), 789 (3.76), 953 (3.36), 1081 (3.17). MS (MALDI-TOF, *dithranol matrix*): *m/z* = 1002.5 (calcd. for $[M]^+$: 1002.3).

Zinc(II) 2,3,12,13-tetrabromo-5,15-bis(4-mesitylphenyl)-10-(4-methoxyphenyl)-20-(4-nitrophenyl)- porphyrinato

(**20**). To a solution of **27** (14 mg, 12 μmol) in $CHCl_3$ (5 mL) was added a suspension of $Zn(OAc)_2 \cdot 2H_2O$ (24 mg, 56 μmol) in CH_3OH (3 mL) and the reaction mixture was refluxed for 1 h. The reaction mixture was poured into water and the organic phase was separated and then dried over Na_2SO_4. After removing the solvent, the residual solid was recrystallized from CH_2Cl_2/hexane (1:3, v/v) and the crystalline solid obtained was dried under vacuum to yield **20** (13 mg, 9.6 μmol, 83%). ^{1}H NMR ($CDCl_3$): δ 8.82 (d, J = 4.8 Hz, 1H, β-H), 8.78 (s, 2H, β-H), 8.59 – 8.57 (m, 3H, β-H, *o*-nitrophenyl-H), 8.27 (d, J = 8.6 Hz, 2H, *m*-nitrophenyl-H), 8.09 (d, J = 7.2 Hz, 4H, *o*-mesitylphenyl-H), 7.95 (d, J = 8.5 Hz, 2H, *o*-methoxyphenyl-H), 7.49 (d, J = 7.2 Hz, 4H, *m*-mesitylphenyl-H), 7.26 – 7.24 (m, 2H, *m*-methoxyphenyl-H), 7.09 (s, 4H, *m*-mesityl-H), 4.09 (s, 3H, OCH_3), 2.41 (s, 6H, mesityl-*p*-CH_3), 2.34 (s, 6H, mesityl-*o*-CH_3), 2.32 (s, 6H, mesityl-*o*-CH_3). UV-vis ($CHCl_3$): λ_{max} [nm] = 609, 568, 438. MS (MALDI- TOF, dithranol matrix): *m/z* = 1305.5 (calcd. for $[M]^+$: 1305.0).

Zinc(II) 2,3,12,13-tetrabromo-5,15-bis(4-mesitylphenyl)-10-(4-cyanophenyl)-20-(4-methoxyphenyl)-porphyrinato (21) To a solution of **28** (5.0 mg, 4.1 μmol) in $CHCl_3$ (1 mL) was added a suspension of $Zn(OAc)_2 \cdot 2H_2O$ (11 mg, 50 μmol) in CH_3OH (0.3 mL) and the reaction mixture was refluxed for 1 h. The reaction mixture was poured into water and the organic phase was separated and then dried over Na_2SO_4. After removing the solvent, the residual solid was recrystallized from CH_2Cl_2/hexane (1:3, v/v) and the crystalline solid obtained was dried under vacuum to yield **21** (4.9 mg, 3.8 μmol, 94%). ^{1}H NMR ($CDCl_3$): δ 8.81 (d, J = 4.8 Hz, 1H, β-H), 8.78 (s, 2H, β-H), 8.56 (d, J = 4.8 Hz, 1H, β-H), 8.20 (d, J = 8.0 Hz, 2H, *o*-cyanophenyl-H), 8.08 (dd, J = 7.9, 1.6 Hz, 4H, *o*-mesitylphenyl-H), 8.00 (d, J = 8.5 Hz, 2H, *o*-methoxyphenyl-H), 7.94 (d, J = 8.0 Hz, 2H, *m*-cyanophenyl-H), 7.48 (d, J = 7.9 Hz, 4H, *m*-mesityl- phenyl-H), 7.26-7.24 (m, 2H, *m*-methoxyphenyl-H), 7.09 (s, 4H, *m*-mesityl-H), 4.08 (s, 3H, OCH_3), 2.41 (s, 6H, mesityl-*p*-CH_3), 2.33 (s, 6H, mesityl-*o*-CH_3), 2.32 (s, 6H, mesityl-*o*-CH_3). UV-vis ($CHCl_3$): λ_{max} [nm] = 609, 568, 437. MS (MALDI-TOF, dithranol matrix): *m/z* = 1286.0 (calcd. for $[M + H]^+$: 1286.0).

Zinc(II) 2,3,12,13-tetrabromo-5,15-bis(4-mesitylphenyl)-10-(4-methoxyphenyl)-20-(4-trifluoromethylphenyl)-porphyrinato (22). To a solution of **29** (19 mg, 14 μmol) in $CHCl_3$ (6.5 mL) was added a suspension of $Zn(OAc)_2 \cdot 2H_2O$ (39 mg, 18 μmol) in CH_3OH (4 mL) and the reaction mixture was refluxed for 1 h. The reaction mixture was poured into water and the organic phase was separated and then dried over Na_2SO_4. After removing the solvent, the residual solid was recrystallized from CH_2Cl_2/hexane (1:3, v/v) and the crystalline solid obtained was dried under vacuum to yield **22** (17 mg, 13 μmol, 90%). ^{1}H NMR ($CDCl_3$): δ 8.80 (d, J = 4.8 Hz, 1H, β-H), 8.78 (s, 2H, β-H), 8.60 (d, J = 4.8 Hz, 1H, β-H), 8.20 (d, J = 8.0 Hz, 2H, *o*-trifluoromethylphenyl-H), 8.09 (d, J = 7.9 Hz, 4H, *o*-mesitylphenyl-H), 7.98 – 7.94 (m, 4H, *o*-methoxyphenyl-H, *m*-trifluoromethylphenyl-H), 7.48 (d, J = 7.9 Hz, 4H, *m*-mesitylphenyl-H), 7.26 – 7.24 (m, 2H, *m*-methoxyphenyl-H), 7.09 (s, 4H, *m*-mesityl-H), 4.09 (s, 3H, OCH_3), 2.41 (s, 6H, mesityl-*p*-CH_3), 2.34 (s, 6H, mesityl-*o*-CH_3), 2.33 (s, 6H, mesityl-*o*-CH_3). UV-vis ($CHCl_3$): λ_{max} [nm] = 609, 568, 437. MS (MALDI-TOF, dithranol matrix): *m/z* = 1327.8 (calcd. for $[M]^+$: 1328.0).

Zinc(II) 5,15-bis(4-mesitylphenyl)-porphyrinato (23). To a solution of dipyrromethane[33] (840 mg, 5.8 mmol) in CH_2Cl_2 (1150 mL), were added 4-mesityl-benzaldehyde (**9**; 1.3 g, 5.8 mmol). Then, TFA (430 μL, 2.6 mmol) was added and the reaction mixture was stirred at room temperature for 3 h. DDQ (2.0 g, 8.7 mmol) was added, followed by

addition of Et_3N (806 μL, 2.6 mmol). The reaction mixture was stirred at room temperature for further 1 h.[34] The mixture was filtered through an alumina pad eluted with CH_2Cl_2. Removal of the solvent gave a purple solid. The solid was dissolved in $CHCl_3$ (500 mL) and the solution was added to a suspension of $Zn(OAc)_2 \cdot 2H_2O$ (1.6 g, 7.3 mmol) in MeOH (20 mL), and the reaction mixture was refluxed for 2 h. The reaction mixture was poured into water and the organic phase was separated and then dried over Na_2SO_4. After removing the solvent, the purple solid was chromatographed on a silica gel column using CH_2Cl_2/pyridine (100:3, v/v) as an eluent. The red purple fraction was collected and the solvent was removed under vacuum. The residual solid was recrystallized from CH_2Cl_2/CH_3OH (1:3, v/v) and dried under vacuum to obtain **23** (1.4 g, 1.8 mmol, 63%). ^{1}H NMR ($CDCl_3$): δ 10.38 (s, 2H, *meso*-H), 9.43 (d, J = 4.5 Hz, 8H, β-H), 9.19 (d, J = 4.5 Hz, 8H, β-H), 8.32 (d, J = 8.0 Hz, 4H, *o*-Ph), 7.59 (d, J = 8.0 Hz, 4H, *m*-Ph), 7.15 (s, 4H, *m*-mesityl-H), 2.46 (s, 6H, mesityl-*p*-CH_3), 2.42 (s, 12H, mesityl-*o*-CH_3). UV-vis ($CHCl_3$): λ_{max} [nm] = 409, 532, 572. MS (MALDI-TOF, dithranol matrix): m/z = 761.0 (calcd. for $[M + H]^+$: 761.3).

Zinc(II) 5,15-bis(4-mesitylphenyl)-10-(4-methoxyphenyl)-20-(4-nitrophenyl)porphyrinato (**24**). To a solution of tris(dibenzylideneacetone)dipalladium ($Pd_2(dba)_3$; 3.7 mg, 3.6 μmol) and triphenylphosphine (14 mg, 46 μmol) in DMF was stirred at room temperature for 1 min. After the color of the solution changed to light green, **32** (81 mg, 86 μmol), 4-nitrophenylboronic acid (88 mg, 510 μmol) and potassium carbonate (220 mg 1.6 mmol) were quickly added to the solution and stirred at 90 °C for 2 h.[35] After stirring, the reaction mixture was cooled to ambient temperature. The solution was added to H_2O, and the precipitate was filtered. The residual solid was chromatographed on a silica gel column by using CH_2Cl_2/hexane/Et_3N (100 : 100 : 0.5, v/v/v) as an eluent. The second fraction was collected and the solvent was removed under vacuum. The residual solid was recrystallized from CH_2Cl_2/MeOH (1:3, v/v) and dried under vacuum to obtain **24** (67 mg, 68 μmol, 79%). ^{1}H NMR ($CDCl_3$): δ 8.99 – 8.81 (m, 8H, β-H), 8.60 (d, J = 8.8 Hz, 2H, *o*-nitrophenyl-H), 8.41 (d, J = 8.8 Hz, 2H, *m*-nitrophenyl-H), 8.23 (d, J = 8.0 Hz, 4H, *o*-mesitylphenyl-H), 8.13 (d, J = 8.5 Hz, 2H, *o*-methoxyphenyl-H), 7.50 (d, J = 8.0 Hz, 4H, *o*-mesitylphenyl-H), 7.28 – 7.26 (m, 2H, *m*-methoxyphenyl-H), 7.09 (s, 4H, *m*-mesityl-H), 4.09 (s, 3H, methoxy-H), 2.41 (s, 6H, mesityl-*p*-CH_3), 2.34 (s, 12H, mesityl-*o*-CH_3). UV-vis ($CHCl_3$): λ_{max} [nm] = 422, 549, 590. MS (MALDI-TOF, dithranol matrix): m/z = 987.9 (calcd. for $[M + H]^+$: 988.3).

Zinc(II) 5,15-bis(4-mesitylphenyl)-10-(4-cyanophenyl)-20-(4-methoxyphenyl)porphyrinato (25). To a solution of $Pd_2(dba)_3$ (3.4 mg, 3.7 μmol) and triphenylphosphine (13 mg, 50 μmol) in DMF was stirred at room temperature for 1 min. After the color of the solution changed to light green, **32** (107 mg, 106 μmol), 4-cyanophenylboronic acid (99 mg, 630 μmol) and potassium carbonate (463 mg 3.3 mmol) were quickly added to the solution and stirred at 90 °C for 16 h. Then, the reaction mixture was cooled to ambient temperature. The solution was added to H_2O, and the precipitate was filtered. The residual solid was chromatographed on a silica gel column by using CH_2Cl_2/hexane/Et_3N (100 : 50 : 0.5, v/v/v) as an eluent. The second fraction was collected and the solvent was removed under vacuum. The residual solid was recrystallized from CH_2Cl_2/MeOH (1:3, v/v) and dried under vacuum to yield **25** (85 mg, 88 μmol, 83%). ^{1}H NMR ($CDCl_3$): δ 9.01 – 8.81 (m, 8H, β-H), 8.36 (d, J = 8.3 Hz, 2H, *o*-cyanophenyl-H), 8.25 (d, J = 7.8 Hz, 4H, *o*-mesitylphenyl-H), 8.14 (d, J = 8.3 Hz, 4H, *m*-cyanophenyl-H), 8.05 (d, J = 8.5 Hz, 2H, *o*-methoxyphenyl-H), 7.52 (d,

J = 8.0 Hz, 4H, *o*-mesitylphenyl-H), 7.29 (d, *J* = 8.5 Hz, 2H, *m*-methoxyphenyl-H), 7.10 (s, 4H, *m*-mesityl-H), 4.10 (s, 3H, methoxy-H), 2.43 (s, 6H, mesityl-*p*-CH_3), 2.36 (s, 12H, mesityl-*o*-CH_3). UV-vis ($CHCl_3$): λ_{max} [nm] = 422, 550, 587. MS (MALDI-TOF, dithranol matrix): *m*/*z* = 967.7 (calcd. for $[M + H]^+$: 967.3).

Zinc(II) 5,15-bis(4-mesitylphenyl)-10-(4-methoxyphenyl)-20-(4-trifluoromethylphenyl)- porphyrinato (26). To a solution of $Pd_2(dba)_3$ (3.7 mg, 3.6 μmol) and triphenylphosphine (17 mg, 64 μmol) in DMF was stirred at room temperature for 1 min. After the color of the solution changed to light green, **32** (101 mg, 106 μmol), 4-trifluorophenylboronic acid (125 mg, 660 μmol) and potassium carbonate (240 mg 1.7 mmol) were quickly added to the solution and stirred at 90 °C for 9 h. Then, the reaction mixture was cooled to ambient temperature. The solution was added to H_2O, and the precipitate was filtered. The residual solid was chromatographed on a silica gel column using CH_2Cl_2/hexane/Et_3N (100 : 100 : 0.5, v/v/v) as an eluent. The second fraction was collected and the solvent was removed under vacuum. The residual solid was recrystallization from CH_2Cl_2/MeOH (1:3, v/v) and dried under vacuum to obtain **26** (84 mg, 83 μmol, 78%). ^{1}H NMR ($CDCl_3$): δ 9.00 – 8.86 (m, 8H, β-H), 8.36 (d, *J* = 7.8 Hz, 2H, *o*-trifluoromethylphenyl-H), 8.26 (d, *J* = 8.1 Hz, 4H, *o*-mesitylphenyl-H), 8.15 (d, *J* = 8.6 Hz, 2H, *o*-methoxyphenyl-H), 8.01 (d, *J* = 7.8 Hz, 2H, *m*-trifluoromethylphenyl-H), 7.51 (d, *J* = 8.1 Hz, 4H, *o*-mesitylphenyl-H), 7.29 (d, *J* = 8.6 Hz, 2H, *m*-methoxyphenyl-H), 7.09 (s, 4H, *m*-mesityl-H), 4.09 (s, 3H, methoxy-H), 2.43 (s, 6H, mesityl-*p*-CH_3), 2.36 (s, 12H, mesityl-*o*-CH_3). UV-vis ($CHCl_3$): λ_{max} [nm] = 421, 549, 586. MS (MALDI-TOF, dithranol matrix): *m*/*z* = 1010.1 (calcd. for $[M]^+$: 1010.3).

2,3,12,13-tetrabromo-5,15-bis(4-mesitylphenyl)-10-(4-methoxyphenyl)-20-(4-nitrophenyl)porphyrin (**27**). To a solution of **33** (19 mg, 22 μmol) in 1,2-dichloroethane (4 mL) was added recrystallized *N*-bromosuccinimide (NBS; 23 mg, 130 μmol) and the reaction mixture was refluxed for 3 h. After cooling to room temperature, the reaction mixture was washed with water to remove any soluble succinimide impurities. The brown-colored solid was chromatographed on a silica gel column using CH_2Cl_2/hexane (1:1, v/v) as an eluent. The second fraction was collected and the solvent was removed under vacuum. The residual solid was recrystallized from CH_2Cl_2/CH_3OH (1:3, v/v) and dried under vacuum to yield **27** (16 mg, 13 μmol, 58%). ^{1}H NMR ($CDCl_3$): δ 8.86 (d, *J* = 5.0 Hz, 1H, β-H), 8.79 (s, 2H, β-H), 8.65 (d, *J* = 8.7 Hz, 2H, *o*-nitrophenyl-H), 8.61 (d, *J* = 5.0 Hz, 1H, β-H), 8.40 (d, *J* = 8.7 Hz, 2H, *m*-nitrophenyl-H), 8.23 (dd, *J* = 8.2 Hz, *J* = 2.5 Hz, 4H, *o*-mesitylphenyl-H), 8.12 (d, *J* = 8.6 Hz, 2H, *o*-methoxyphenyl-H), 7.57 (d, *J* = 8.2 Hz, 4H, *m*-mesitylphenyl-H), 7.34 (d, *J* = 8.6 Hz, 2H, *m*-methoxyphenyl-H), 7.11 (s, 4H, *m*-mesityl-H), 4.10 (s, 3H, OCH_3), 2.43 (s, 6H, mesityl-*p*-CH_3), 2.33 (s, 12H, mesityl-*o*-CH_3), –2.68 (br s, 1H, inner N*H*), –2.71 (br s, 1H, inner N*H*). UV-vis ($CHCl_3$): λ_{max} [nm] = 692, 541, 445. MS (MALDI-TOF, dithranol matrix): *m*/*z* = 1241.8 (calcd. for $[M + H]^+$: 1242.1).

2,3,12,13-Tetrabromo-5,15-bis(4-mesitylphenyl)-10-(4-cyanophenyl)-20-(4-methoxyphenyl)- porphyrin (28). To a solution of **34** (30 mg, 33 μmol) in 1,2-dichloroethane (7 mL) was added recrystallized NBS (36 mg, 199 μmol) and the reaction mixture was refluxed for 2 h. After cooling to room temperature, the reaction mixture was washed with water to remove any soluble succinimide impurities. The brown-colored solid was chromatographed on a silica gel column using CH_2Cl_2/hexane (1:1, v/v) as an eluent. The second fraction was collected and the solvent was removed under

vacuum. The residual solid was recrystallized from CH_2Cl_2/CH_3OH (1:3, v/v) and dried under vacuum to yield **28** (22 mg, 18 μmol, 55%). ^{1}H NMR ($CDCl_3$): δ 8.86 (d, J = 5.7 Hz, 1H, β-H), 8.79 (s, 2H, β-H), 8.60 (d, J = 5.7 Hz, 1H, β-H), 8.34 (d, J = 8.3 Hz, 2H, *o*-cyanophenyl-H), 8.24-8.21 (m, 4H, *o*-mesitylphenyl-H), 8.11 (d, J = 8.6 Hz, 2H, *o*-methoxyphenyl-H), 8.08 (d, J = 8.3 Hz, 2H, *m*-cyanophenyl-H), 7.57 (d, J = 7.9 Hz, 4H, *m*-mesitylphenyl-H), 7.34 (d, J = 8.6 Hz, 2H, *m*-methoxyphenyl-H), 7.11 (s, 4H, *m*-mesityl-H), 4.10 (s, 3H, OCH_3), 2.43 (s, 6H, mesityl-*p*-CH_3), 2.33 (s, 12H, mesityl-*o*-CH_3), –2.70 (br s, 1H, inner N*H*), –2.73 (br s, 1H, inner N*H*). UV-vis ($CHCl_3$): λ_{max} [nm] = 692, 542, 444. MS (MALDI-TOF, dithranol matrix): m/z = 1222.1 (calcd. for $[M + H]^+$: 1222.1).

2,3,12,13-Tetrabromo-5,15-bis(4-mesitylphenyl)-10-(4-methoxyphenyl)-20-(4-trifluoromethyl- phenyl)-porphyrin (29). To a solution of **35** (29 mg, 32 μmol) in 1,2-dichloroethane (7 mL) was added recrystallized NBS (32 mg, 190 μmol) and the reaction mixture was refluxed for 2.5 h. After cooling to room temperature, the reaction mixture was washed with water to remove any soluble succinimide impurities. The brown-colored solid was chromatographed on a silica gel column using CH_2Cl_2/hexane (1:1, v/v) as an eluent. The second fraction was collected and the solvent was removed under vacuum. The residual solid was recrystallized from CH_2Cl_2/CH_3OH (1:3, v/v) and dried under vacuum to yield **29** (20 mg, 16 μmol, 49%). ^{1}H NMR ($CDCl_3$): δ 8.85 (d, J = 5.0 Hz, 1H, β-H), 8.79 (s, 2H, β-H), 8.65 (d, J = 5.0 Hz, 1H, β-H), 8.33 (d, J = 8.3 Hz, 2H, *o*-trifluoromethylphenyl-H), 8.23 (dd, J = 8.1, 1.7 Hz 4H, *o*-mesitylphenyl-H), 8.11 (d, J = 8.6 Hz, 2H, *o*-methoxyphenyl-H), 8.04 (d, J = 8.3 Hz, 2H, *m*-trifluoromethylphenyl-H), 7.57 (d, J = 8.1 Hz, 4H, *m*-mesitylphenyl-H), 7.34 (d, J = 8.6 Hz, 2H, *m*-methoxyphenyl-H), 7.10 (s, 4H, *m*-mesityl-H), 4.10 (s, 3H, OCH_3), 2.43 (s, 6H, mesityl-*p*-CH_3), 2.33 (s, 12H, mesityl-*o*-CH_3), –2.73 (br s, 2H, inner N*H*). MS (MALDI-TOF, dithranol matrix): m/z = 1264.1 (calcd. for $[M]^+$: 1264.1).

Zinc(II) 5-bromo-10,20-bis(4-mesitylphenyl)-porphyrinato (30). To a solution of **23** (250 mg, 0.33 mmol) in CH_2Cl_2 (320 mL) and CH_3OH (30 mL) were added NBS (62 mg, 0.36 mmol). Then, the reaction mixture was stirred at room temperature for 20 min. Acetone (30 mL) was added and the reaction mixture was poured into water.[34] The organic phase was separated and then dried over Na_2SO_4. After removing the solvent, the residual solid was recrystallized from CH_2Cl_2/CH_3OH (1:3, v/v) and dried under vacuum to obtain **30** (180 mg, 0.23 mmol, 69%). ^{1}H NMR ($CDCl_3$): δ 10.21 (s, 1H, *meso*-H), 9.80 (d, J = 4.5 Hz, 8H, β-H), 9.35 (d, J = 4.5 Hz, 8H, β-H), 9.09 – 9.07 (m, 4H, β-H), 8.26 (d, J = 8.0 Hz, 4H, *o*-Ph), 7.56 (d, J = 8.0 Hz, 4H, *m*-Ph), 7.14 (s, 4H, *m*-mesityl-H), 2.46 (s, 6H, mesityl-*p*-CH_3), 2.42 – 2.39 (m, 12H, mesityl-*o*-CH_3). UV-vis ($CHCl_3$): λ_{max} [nm] = 419, 547, 591. MS (MALDI-TOF, dithranol matrix): m/z = 840.9 (calcd. for $[M + H]^+$: 841.2).

Zinc(II) 5,15-bis(4-mesitylphenyl)-10-(4-methoxyphenyl)-20-porphyrinato (31). To a solution of $Pd_2(dba)_3$ (7.7 mg, 8.6 μmol) and triphenylphosphine (24 mg, 87 μmol) in DMF was stirred at room temperature for 1 min. After the color of the solution changed to light green, **30** (176 mg, 0.21 mmol), 4-methoxyphenylboronic acid (252 mg, 1.6 mmol) and potassium carbonate (123 mg, 0.89 mmol) were quickly added to the solution and stirred at 90 °C for 1 h. Then, the reaction mixture was cooled to ambient temperature. The solution was added to H_2O, and the precipitate was filtered. The residual solid was chromatographed on a silica gel column using CH_2Cl_2/hexane (1:2, v/v) as an eluent and the second fraction was collected and the solvent was removed under vacuum. The residual solid was recrystallized from

CH_2Cl_2/hexane (1:3, v/v) and dried under vacuum to obtain **31** (117 mg, 0.14 μmol, 64%). ^{1}H NMR ($CDCl_3$): δ 10.21 (s, 1H, *meso*-H), 9.40 (d, J = 4.5 Hz, 2H, β-H), 9.13 (d, J = 4.5 Hz, 2H, β-H), 9.02 – 8.99 (m, 4H, β-H), 8.27 (d, J = 8.1 Hz, 4H, *o*-mesitylphenyl-H), 8.14 (d, J = 7.8 Hz, 2H, *o*-methoxy- phenyl-H), 7.51 (d, J = 8.1 Hz, 4H, *o*-mesitylphenyl-H), 7.27 (d, J = 7.8 Hz, 2H, *m*-methoxyphenyl-H), 7.11 (s, 4H, *m*-mesityl-H), 4.10 (s, 3H, methoxy-H), 2.43 (s, 6H, mesityl-*p*-CH_3), 2.40 (s, 6H, mesityl- *o*-CH_3) 2.37 (s, 6H, mesityl-*o*-CH_3). UV-vis ($CHCl_3$): λ_{max} [nm] = 419, 547, 590. MS (MALDI-TOF, dithranol matrix): m/z = 866.6 (calcd. for $[M]^+$: 866.3).

Zinc(II) 5-bromo-10,20-bis(4-mesitylphenyl)-15-(4-methoxyphenyl)-porphyrinato (32). To a solution of **31** (250 mg, 0.33 mmol) in CH_2Cl_2 (320 mL) and CH_3OH (30 mL) were added NBS (62 mg, 0.36 mmol). Then, the reaction mixture was stirred at room temperature for 20 min and acetone (30 mL) was added. The reaction mixture was poured into water and the organic phase was separated and then dried over Na_2SO_4.[36] After removing the solvent, the residual solid was recrystallized from CH_2Cl_2/CH_3OH (1:3, v/v) and dried under vacuum to obtain **32** (180 mg, 0.23 mmol, 69%). ^{1}H NMR ($CDCl_3$): δ 9.75 (d, J = 4.5 Hz, 2H, β-H), 9.01 (d, J = 4.5 Hz, 2H, β-H), 8.91 – 8.90 (m, 4H, β-H), 8.23 (d, J = 8.1 Hz, 4H, *o*-mesitylphenyl-H), 8.10 (d, J = 7.8 Hz, 2H, *o*-methoxyphenyl-H), 7.51 (d, J = 8.1 Hz, 4H, *o*-mesitylphenyl-H), 7.27 (d, J = 7.8 Hz, 2H, *m*-methoxyphenyl-H), 7.11 – 7.10 (m, 4H, *m*-mesityl-H), 4.10 (s, 3H, methoxy-H), 2.43 (s, 6H, mesityl-*p*-CH_3), 2.39 (s, 6H, mesityl-*o*-CH_3) 2.35 (s, 6H, mesityl-*o*-CH_3). UV-vis ($CHCl_3$): λ_{max} [nm] = 428, 560, 602. MS (MALDI-TOF, dithranol matrix): m/z = 946.5 (calcd. for $[M]^+$: 946.2).

5,15-bis(4-mesitylphenyl)-10-(4-methoxyphenyl)-20-(4-nitrophenyl)porphyrin (**33**). To a solution of **24** (52 mg, 52 μmol) in $CHCl_3$ (30 mL), was added TFA (4.5 mL, 60 mmol) and the reaction mixture was stirred for 10 min at room temperature. The reaction mixture was washed with Na_2HCO_3 aq and water, and dried over Na_2SO_4. The solvent was removed under vacuum and the residual solid was recrystallized from CH_2Cl_2/EtOH (1:3, v/v) to obtain purple crystals of **33** (46 mg, 50 μmol, 96%). ^{1}H NMR ($CDCl_3$): δ 8.97 (d, J = 4.8 Hz, 2H, β-H), 8.94 (s, 4H, β-H), 8.78 (d, J = 4.8 Hz, 2H, β-H), 8.65 (d, J = 8.6 Hz, 2H, *o*-nitrophenyl-H), 8.43 (d, J = 8.6 Hz, 2H, *m*-nitrophenyl-H), 8.27 (d, J = 8.0 Hz, 4H, *o*-mesitylphenyl-H), 8.16 (d, J = 8.5 Hz, 2H, *o*-methoxyphenyl-H), 7.54 (d, J = 8.0 Hz, 4H, *m*-mesitylphenyl-H), 7.32 (d, J = 8.6 Hz, 2H, *m*-methoxyphenyl-H), 7.12 (s, 4H, *m*-mesityl-H), 4.12 (s, 3H, OCH_3), 2.44 (s, 6H, mesityl-*p*-CH_3), 2.36 (s, 12H, mesityl-*o*-CH_3), –2.70 (br s, 2H, inner N*H*). UV-vis (CH_2Cl_2): λ_{max} [nm] = 648, 592, 556, 519, 423. MS (MALDI-TOF, dithranol matrix): m/z = 926.6 (calcd. for $[M + H]^+$: 926.4).

5,15-bis(4-mesitylphenyl)-10-(4-cyanophenyl)-20-(4-methoxyphenyl)porphyrin (34). To a solution of **25** (75 mg, 78 μmol) in $CHCl_3$ (30 mL), was added TFA (4.5 mL, 60 mmol) and the reaction mixture was stirred for 10 min at room temperature. The reaction mixture was washed with Na_2HCO_3 aq and water, and dried over Na_2SO_4. The solvent was removed under vacuum and the residual solid was recrystallized from CH_2Cl_2/EtOH (1:3, v/v) to obtain dark blue crystals of **34** (68 mg, 75 μmol, 96%). ^{1}H NMR ($CDCl_3$): δ 8.96 (d, J = 4.8 Hz, 2H, β-H), 8.94 (s, 4H, β-H), 8.76 (d, J = 4.8 Hz, 2H, β-H), 8.38 (d, J = 8.0 Hz, 2H, *o*-cyanophenyl-H), 8.26 (d, J = 8.0 Hz, 4H, *o*-mesitylphenyl-H), 8.15 (d, J = 8.5 Hz, 2H, *o*-methoxy- phenyl-H), 8.08 (d, J = 8.0 Hz, 2H, *m*-cyanophenyl-H), 7.54 (d, J = 8.0 Hz, 4H, *m*-mesitylphenyl-H), 7.31 (d, J = 8.6 Hz, 2H, *m*-methoxyphenyl-H), 7.11 (s, 4H, *m*-mesityl-H), 4.11 (s, 3H, OCH_3), 2.44 (s, 6H, mesityl-*p*-CH_3), 2.36 (s, 12H, mesityl-*o*-CH_3), –2.72 (br s, 2H, inner N*H*). UV-vis ($CHCl_3$): λ_{max} [nm] =

648, 594, 554, 518, 422. MS (MALDI-TOF, dithranol matrix): *m/z* = 906.6 (calcd. for $[M + H]^+$: 906.4).

5,15-bis(4-mesitylphenyl)-10-(4-methoxyphenyl)-20-(4-trifluoromethylphenyl)-porphyrin (35). To a solution of **25** (73 mg, 72 μmol) in $CHCl_3$ (30 mL), was added TFA (4.5 mL, 60 mmol) and the reaction mixture was stirred for 10 min at room temperature. The reaction mixture was washed with Na_2HCO_3 aq and water, and dried over Na_2SO_4. The solvent was removed under vacuum and the residual solid was recrystallized from CH_2Cl_2/MeOH (1:3, v/v) to yield purple crystals of **35** (67 mg, 71 μmol, 98%). ^{1}H NMR ($CDCl_3$): δ 8.95-8.94 (m, 6H, β-H), 8.80 (d, J = 5.2 Hz, 2H, β-H), 8.37 (d, J = 7.9 Hz, 2H, *o*-trifluoromethylphenyl-H), 8.27 (d, J = 7.8 Hz, 4H, *o*-mesitylphenyl-H), 8.16 (d, J = 8.6 Hz, 2H, *o*-methoxyphenyl-H), 8.04 (d, J = 7.9 Hz, 2H, *m*-trifluoromethylphenyl-H), 7.54 (d, J = 7.8 Hz, 4H, *m*-mesitylphenyl-H), 7.31 (d, J = 8.6 Hz, 2H, *m*-methoxyphenyl-H), 7.11 (s, 4H, *m*-mesityl-H), 4.11 (s, 3H, OCH_3), 2.44 (s, 6H, mesityl-*p*-CH_3), 2.36 (s, 12H, mesityl-*o*-CH_3), –2.71 (br s, 2H, inner N*H*). UV-vis (CH_2Cl_2): λ_{max} [nm] = 648, 592, 554, 518, 421. MS (MALDI-TOF, dithranol matrix): *m/z* = 831.9 (calcd. for $[M]^+$: 831.4).

X-ray diffraction analysis.

A single crystal of **24** was obtained by recrystallization from the chloroform solution with a vapor deposition method using acetonitrile as a poor solvent. The single crystal was mounted on a mounting loop. All diffraction data were collected at 120 K by using a Bruker APEXII diffractometer equipped with graphite-monochromated Mo $K\alpha$ (λ = 0.71073 Å) by the ω-2θ scan. The structures were solved by direct methods using SIR97 and SHELX97.[37] Crystallographic data for these compounds are summarized in Table 7-5.

Table 7-5. Crystallographic data for **24**.

crystal system	monoclinic
space group	$P2_1$
T / K	120
formula	$C_{63}H_{51}N_5O_3$
FW	926.11
a / Å	10.643(5)
b /Å	15.283(5)
c /Å	15.182(5)
α / °	90
β / °	92.141(5)
γ / °	90
V / Å^3	2465.6(16)
Z	2
λ / Å	0.71073 (Mo $K\alpha$)
D_c / g cm^{-3}	1.380
reflns measured	13917
reflns unique	9860
$R1$ ($I > 2\sigma(I)$)	0.0683
$wR2$ (all)	0.1817
GOF	1.029

Computational method.

To obtain the optimized structure of compound **1**, DFT calculations were performed with optimized local minima on the potential energy surfaces using the B3LYP method[38,39] combined with the 6-31G(d,p) basis set.[40,41] The Gaussian 09 program package[42] was used for all DFT calculations.

Hyper-Rayleigh scattering (HRS) measurements.

HRS experiments were performed using the incident laser light at 1300 nm. The chromophores were dissolved in $CHCl_3$ with the concentration range of 2.5 – 10 μM. Disperse red 1 ($\beta_{1300} = 54 \times 10^{-30}$ esu in $CHCl_3$)[43] was utilized as a reference chromophore. Note that these experiments were performed at low chromophore concentrations where the linearity of the HRS signal as a function of chromophore concentration confirmed that no significant self-absorption of the SHG signal occurred in these experiments.

Reference and notes

1 J. Zyss, I. Ledoux, *Chem. Rev.* **1994***, 94,* 77.

2 P. A. Sullivan, L. R. Dalton, *Acc. Chem. Res.* **2010**, *43*, 10.

3 S. R. Marder, *Chem. Commun.* **2006**, 131.

4 (a) S. R. Marder, D. N. Beratan, L.-T. Cheng, *Science*, **1991**, *252*, 103. (b) S. R. Marder, L. Cheng, B. G. Tiemann, A. C. Friedli, M. Blanchard-Desce, J. W. Perry, J. Skindhøj, *Science* **1994**, *263*, 511. (c) S. R. Marder, B Kippelen, A. K.-Y. Jen, N. Peyghambarian, *Nature* **1997**, *388*, 845. (d) T. Verbiest, S. Hourechts, M. Kauranen, K. Clays, André Persoons, *J. Mater. Chem.* **1997**, *7*, 2175.

5 (a) T. Verbiest, S. V. Elshocht, M. Kauranen, L. Hellemans, J. Snauwaert, C. Nuckolls, T. J. Katz, A. Persoons, *Science*, **1998**, *282*, 913. (b) C. Nuckolls, T. J. Katz, T. Verbiest, S. V. Elshocht, H, Kuball, S. Kiesewalter, A. J. Lovinger, A. Persoons, *J. Am. Chem. Soc.* **1998**, *120*, 8656.

6 (a) S. J. Lalama, A. F. Garito, *Phys. Rev. A* **1979**, *20*, 1179. (b) J. L. Oudar, D. S. Chemia, *J. Chem. Phys.* **1977**, *66*, 2664.

7 X. Hu, D. Xiao, S. Keiman, I. Asselberghs, M. J. Therien, K. Clays, W. Yang, D. N. Beratan, *J. Phys. Chem. C* **2010**, *114*, 2349.

8 M. O. Senge, M. Fazekas, E. G. A. Notaras, W. J. Blau, M. Zawadzka, O. B. Locos, E. M. Ni Mhuircheartaigh, *Adv. Mater.* **2007**, *19*, 2737.

9 (a) S. M. LeCours, H.-W. Guan, S. G. DiMagno, C. H. Wang, M. J. Therien, *J. Am. Chem. Soc.* **1996**, *118*, 1497. (b) T.-G. Zhang, Y. Zhao, I. Asselberghs, A. Persoons, K. Clays, M. J. Therien, *J. Am. Chem. Soc.* **2005**, *127*, 9710. (c) T.-G. Zhang, Y. Zhao, K. Song, I. Asselberghs, A. Persoons, K. Clays, M. J. Therien, *Inorg. Chem.* **2006**, *45*, 9703. (d) T. Ishizuka, L. E. Sinks, K. Song, S.-T. Hung, A. Nayak, K. Clays, M. J. Therien, *J. Am. Chem. Soc.*

2011, *133*, 2884. (e) N. Jiang, G. Zuber, S. Keinan, A. Nayak, W. Yang, M. J. Therien, D. N. Beratan, *J. Phys. Chem. C* **2012**, *116*, 9724.

10 (a) K. S. Suslick, C. T. Chen, G. R. Meredith and L.-T. Cheng, *J. Am. Chem. Soc.* **1992**, *114*, 6928, (b) M. Yeung, A. C. H. Ng, M. G. B. Drew, E. Vorpagel, E. M. Breitung, R. J. McMahon, D. K. P. Ng, *J. Org. Chem.* **1998**, *63*, 7143. (c) I. D. L. Albert, T. J. Marks, M. A. Ratner, *Chem. Mater.* **1998**, *10*, 753.

11 (a) K. De Mey, J. Pérez-Moreno, J. E. Reeve, I. López-Duarte, I. Boczarow, H. L. Anderson and K. Clays, *J. Phys. Chem. C* **2012**, *116*, 13781. (b) X. Hu, D. Xiao, S. Keinan, I. Asselberghs, M. J. Therien, K. Clays, W. Yang, D. N. Beratan, *J. Phys. Chem. C* **2010**, *114*, 2349.

12 (a) S. Fox, R. W. Boyle, *Tetrahedron* **2006**, *62*, 10039. (b) J. P. Lewtak, D. T. Gryko, *Chem. Commun.* **2012**, *48*, 10069. (c) H. Mori, T. Tanaka, A. Osuka, *J. Mater. Chem. C* **2013**, *1*, 2500. (d) M. Stępień, E. Gońka, M. Żyła, N. Sprutta, *Chem. Rev.* **2017**, ASAP (DOI: 10.1021/acs.chemrev.6b00076).

13 (a) L. Edwards, M. Gouterman, C. B. Rose, *J. Am. Chem. Soc.* **1976**, *98*, 7638. (b) T. D. Lash, B. H. Novak, *Angew. Chem. Int. Ed. Engl.* **1995**, *34*, 683. (c) S. Ito, T. Murashima, H. Uno, N. Ono, *Chem. Commun.* **1998**, 1661.

14 (a) R. Deshpande, L. Jiang, G. Schmidt, J. Rakovan, X. Wang, K. Wheeler, H. Wang, *Org. Lett.* **2009**, *11*, 4251. (b) L. Jiang, J. T. Engle, L. Sirk, C. S. Hartley, C. J. Ziegler, H. Wang, *Org. Lett.* **2011**, *13*, 3020. (c) S. Banala, T. Rühl, K. Wurst, B. Kräutler, *Angew. Chem. Int. Ed.* **2009**, *48*, 599.

15 (a) H. Aihara, L. Jaquinod, D. J. Nurco, K. M. Smith, *Angew. Chem. Int. Ed.* **2001**, *40*, 3439. (b) M. Nath, J. C. Huffman, J. M. Zaleski, *J. Am. Chem. Soc.* **2003**, *125*, 11484. (c) M. Nath, M. Pink, J. M. Zaleski, *J. Am. Chem. Soc.* **2005**, *127*, 478.

16 (a) N. Cammidge, P. J. Scaife, G. Berber, D. L. Hughes, *Org. Lett.* **2005**, *7*, 3413. (b) M. Tanaka, S. Hayashi, S. Eu, T. Umeyama, Y. Matano, H. Imahori, *Chem. Commun.* **2007**, 2069. (c) C. Jiao, K.-W. Huang, Z. Guan, Q.-H. Xu, J. Wu, *Org. Lett.* **2010**, *12*, 4046.

17 (a) H. S. Gill, M. Harmjanz, J. Santamaría, I. Finger, M. J. Scott, *Angew. Chem. Int. Ed.* **2004**, *43*, 485. (b) K. Kurotobi, K. S. Kim, S. B. Noh, D. Kim, A. Osuka, *Angew. Chem. Int. Ed.* **2006**, *45*, 3944.

18 Jiao, L. Zhu, J. Wu, *Chem. Eur. J.* **2011**, *17*, 6610.

19 (a) N. K. S. Davis, M. Pawlicki, H. L. Anderson, *Org. Lett.* **2008**, *10*, 3945. (b) N. K. S. Davis, A. L. Thompson, H. L. Anderson, *Org. Lett.* **2010**, *12*, 2124. (c) N. K. S. Davis, A. L. Thompson, H. L. Anderson, *J. Am. Chem. Soc.* **2011**, *133*, 30.

20 (a) K. Sendt, L. A. Johnston, W. A. Hough, M. J. Crossley, N. S. Hush, J. R. Reimers, *J. Am. Chem. Soc.* **2002**, *124*, 9299. (b) R. Paolesse, L. Jaquinod, F. Della Sala, D. J. Nurco, L. Prodi, M. Montalti, C. Di Natale, A. D'Amico, A. Di Carlo, P. Lugli, K. M. Smith, *J. Am. Chem. Soc.* **2000**, *122*, 11295. (c) H. Uno, A. Masumoto, N. Ono, *J. Am. Chem. Soc.* **2003**, *125*, 12082. (d) M. Akita, S. Hiroto, H. Shinokubo, *Angew. Chem. Int. Ed.* **2012**, *51*, 2894.

21 (a) Tsuda, A. Nakano, H. Furuta, H. Yamochi, A. Osuka, *Angew. Chem. Int. Ed.* **2000**, *39*, 558. (b) A. Tsuda, H.

Furuta, A. Osuka, *Angew. Chem. Int. Ed.* **2000**, *39*, 2549. (c) A. Tsuda, H. Furuta, A. Osuka, *J. Am. Chem. Soc.* **2001**, *123*, 10304. (d) A. Tsuda, A. Osuka, *Science* **2001**, *293*, 79. (e) Y. Nakamura, N. Aratani, H. Shinokubo, A. Takagi, T. Kawai, T. Matsumoto, Z. S. Yoon, D. Y. Kim, T. K. Ahn, D. Kim, A. Muranaka, N. Kobayashi, A. Osuka, *J. Am. Chem. Soc.* **2006**, *128*, 4119.

22 (a) R. B. Woodward, W. A. Ayer, J. M. Beaton, F. Bickelhaupt, R. Bonnet, P. Buchschacher, G. L. Closs, H. Dutler, J. Hannah, F. P. Hauck, S. Ito, A. Langemann, E. Le Goff, W. Leimgruber, W. Lwowski, J. Sauer, Z. Valenta, H. Volz, *J. Am. Chem. Soc.* **1960**, *82*, 3800. (b) R. B. Woodward, W. A. Ayer, J. M. Beaton, F. Bickelhaupt, R. Bonnet, P. Buchschacher, G. L. Closs, H. Dutler, J. Hannah, F. P. Hauck, S. Ito, A. Langemann, E. Le Goff, W. Leimgruber, W. Lwowski, J. Sauer, Z. Valenta, H. Volz, *Tetrahedron* **1990**, *46*, 7599.

23 (a) S. Fox, R. W. Boyle, *Chem. Commun.* **2004**, 1322. (b) D.-M. Shen, C. Liu, Q.-Y. Chen, *Chem. Commun.* **2005**, 4982. (c) D.-M. Shen, C. Liu, Q.-Y. Chen, *J. Org. Chem.* **2006**, *71*, 6508.

24 (a) S. Hayashi, Y. Matsubara, S. Eu, H. Hayashi, T. Umeyama, Y. Matano, H. Imahori, *Chem. Lett.* **2008**, *37*, 846. (b) T. D. Lash, B. E. Smith, M. J. Melquist, B. A. Godfrey, *J. Org. Chem.* **2011**, *76*, 5335. (c) A. M. V. M. Pereira, M. G. P. M. S. Neves, J. A. S. Cavaleiro, C. Jeandon, J.-P. Gisselbrecht, S. Choua, R. Ruppert, *Org. Lett.* **2011**, *13*, 4742.

25 (a) Y. Mitsushige, S. Yamaguchi, B. S. Lee, Y. M. Sung, S. Kuhri, C. A. Schierl, D. M. Guldi, D. Kim, Y. Matsuo, *J. Am. Chem. Soc.* **2012**, *134*, 16540. (b) H. Fliegl, N. Özcan, R. Mera-Adasme, F. Pichierri, J. Jusélius, D. Sundholm, *Mol. Phys.* **2013**, *111*, 1364.

26 (a) Nakano, N. Aratani, H. Furuta, A. Osuka, *Chem. Commun.* **2001**, 1920. (b) A. K. Sahoo, S. Mori, H. Shinokubo, A. Osuka, *Angew. Chem. Int. Ed.* **2006**, *45*, 7972. (c) N. Fukui, H. Yorimitsu, J. M. Lim, D. Kim, A. Osuka, *Angew. Chem. Int. Ed.* **2014**, *53*, 4395.

27 (a) N. Fukui, W.-Y. Cha, S. Lee, S. Tokuji, D. Kim, H. Yorimitsu, A. Osuka, *Angew. Chem. Int. Ed.* **2013**, *52*, 9728. (b) K. Ota, T. Tanaka, A. Osuka, *Org. Lett.* **2014**, *16*, 2974.

28 Please see other chapters of this thesis. See also: (a) T. Ishizuka, Y. Saegusa, Y. Shiota, K. Ohtake, K. Yoshizawa, T. Kojima, *Chem. Commun.* **2013**, *49*, 5939. (b) Y. Saegusa, T. Ishizuka, K. Komamura, S. Shimizu, H. Kotani, N. Kobayashi, T. Kojima, *Phys. Chem. Chem. Phys.* **2015**, *17*, 15001. (c) Y. Saegusa, T. Ishizuka, T. Kojima, S. Mori, M. Kawano, T. Kojima, *Chem. Eur. J.* **2015**, *21*, 5302.

29 S. Higashibayashi, H. Sakurai, *Chem. Lett.* **2007**, *36*, 18.

30 V. Gutmann, *Coord. Chem. Rev.* **1976**, *18*, 225.

31 (a) K. Clays, A. Persoons, *Phys. Rev. Lett.* **1991**, *66*, 2980. (b) K. Clays, A. Persoons, *Rev. Sci. Instrum.* **1992**, *63*, 3285.

32 DFT calculations on **17** – **19** have bee performed to theoretically estimate the hyperpolarizability and the estimated β (β_{theor}) of **18** is larger than those of **17** and **19**: β_{theor} is estimated to be 10×10^{-30} esu for **17**, 11×10^{-30} esu for **18**, 5×10^{-30} esu for **19**. However, the difference in the theoretical values is not so large as that in the experimental values.

33 J. K. Laha, S. Dhanalekshmi, M. Taniguchi, A. Ambroise, J. S. Lindsey, *Org. Proc. Res. Dev.* **2003**, *7*, 799.

34 G. R. Geier, III, B. J. Littler, J. S. Lindsey, *Perkin Trans. 2* **2001**, 701.

35 Ryan, A. Gehrold, R. Perusitti, M. Pintea, M. Fazekas, O. B. Locos, F. Blaikie, M. O. Senge, *Eur. J. Org. Chem.* **2011**, 5817.

36 M. Alba, N. Pazos-Perez, B. Formentin, M. Tebbe, M. A. Correa-Duarte, P. Granero, J. Ferré-Borrull, R. Alvarez, J. Pallares, A. Fery, A. R. de Lera, L. F. Marsal, R. A. Alvarez-Puebla, *Angew. Chem. Int. Ed.* **2013**, *52*, 6459.

37 G. M. Sheldrick, SIR97 and SHELX97, Programs for Crystal Structure Refinement, University of Göttingen, Göttingen (Germany), 1997.

38 A. D. Becke, *Phys. Rev. A* **1988**, 38, 3098.

39 C. Lee, W. Yang, R. G. Parr, *Phys. Rev. B* **1988**, 37, 785.

40 R. Ditchfield, W. J. Hehre, J. A. Pople *J. Chem. Phys.* **1971**, 54, 724.

41 W. J. Hehre, R. Ditchfield, J. A. Pople, *J. Chem. Phys.* **1972**, 56, 2257.

42 Gaussian 09, Revision D.01, M. J. Frisch, G. W. Trucks, H. B. Schlegel, G. E. Scuseria, M. A. Robb, J. R. Cheeseman, G. Scalmani, V. Barone, B. Mennucci, G. A. Petersson, H. Nakatsuji, M. Caricato, X. Li, H. P. Hratchian, A. F. Izmaylov, J. Bloino, G. Zheng, J. L. Sonnenberg, M. Hada, M. Ehara, K. Toyota, R. Fukuda, J. Hasegawa, M. Ishida, T. Nakajima, Y. Honda, O. Kitao, H. Nakai, T. Vreven, J. A. Montgomery, Jr., J. E. Peralta, F. Ogliaro, M. Bearpark, J. J. Heyd, E. Brothers, K. N. Kudin, V. N. Staroverov, R. Kobayashi, J. Normand, K. Raghavachari, A. Rendell, J. C. Burant, S. S. Iyengar, J. Tomasi, M. Cossi, N. Rega, J. M. Millam, M. Klene, J. E. Knox, J. B. Cross, V. Bakken, C. Adamo, J. Jaramillo, R. Gomperts, R. E. Stratmann, O. Yazyev, A. J. Austin, R. Cammi, C. Pomelli, J. W. Ochterski, R. L. Martin, K. Morokuma, V. G. Zakrzewski, G. A. Voth, P. Salvador, J. J. Dannenberg, S. Dapprich, A. D. Daniels, Ö. Farkas, J. B. Foresman, J. V. Ortiz, J. Cioslowski, D. J. Fox, Gaussian, Inc., Wallingford CT, 2009.

43 G. Olbrechts, K. Wostyn, K. Clays, A. Persoons, *Opt. Lett.* **1999**, *24*, 403.

Chapter 8

Supramolecular interaction of fullerenes with monomeric ZnQFP

8-1. Introduction

Fullerene and its derivatives exhibit reversible multistep redox processes and high first reduction potentials, and thus, they can act as efficient electron acceptors in photovoltaic cells[1] and can exhibit n-type semi-conducting properties.[2] Based on the high electron affinity, fullerenes have been also employed to form supramolecular assemblies with electron-donating molecules, and the supramolecules obtained have been reported to exhibit unique optoelectronic functionality.[3] In particular, supramolecular assemblies consisting of fullerenes and porphyrins have especially attracted great interest from a wide range of chemists,[3-6] since the assemblies can conduct efficient photoinduced electron-transfer reactions.[7, 8] However, porphyrin derivatives generally show planar structures, whereas fullerenes have curved surfaces,[9] and thus, planar porphyrins are not well matched with the curved surfaces of fullerenes to form strong π–π interactions. Therefore, the interaction between fullerenes and monomeric porphyrins is too weak to be observed in solution.[10] Consequently, for efficient complexation of fullerenes with porphyrins in solution, porphyrin hosts need to be dimers or higher oligomers.[4,5,11] For example, a porphyrin dimer connecting at each *meta*-position of *meso*-aryl moieties of the porphyrin unit with a flexible spacer have been well studied as a host molecules of fullerenes, and the dimer indicated the large association constant with fullerenes ($K_{assoc} \sim 7 \times 10^5$ M^{-1} in benzene) and performed selective extraction of higher fullerenes.[4] On the other hand, a concave-structured molecule with a curved surface is expected to form more stable molecular complexes with convex-shaped fullerenes on the basis of a suitable fit to gain stronger intermolecular π-π interactions.[12] For instance, calix-[5]arene receptors, which show curved π-surfaces, have been reported to bind C_{60} in organic solvents such as toluene, benzene, carbon disulfide and 1,2-dichlorobenzene (DCB).[13]

As described in Chapter 2, the author has reported the synthesis of a Zn^{II} complex of a quadruply fused porphyrin (ZnQFP, **4a**) and found that the planar structure of **4a**, which is most stable as suggested by DFT calculations, changes to a concave structure by axial coordination of pyridine at the zinc center (see Chapter 2 and 3 of this thesis).[14] In this chapter, the author describes utilization of the extensively π-conjugated concave surface of a pyridine-coordinated ZnQFP derivative to recognize the convex surfaces of fullerenes.

8-2. Determination of the association constant between ZnQFP and pyridine

A ZnQFP derivative (**4b**) having mesityl groups at the fused benzene rings (Figure 8-1)[15] was used to improve the solubility to facilitate binding of fullerenes, C_{60} and C_{70}. At first, the association constant between **4b** and pyridine (K_{py}) was determined. UV/Vis titration experiments of **4b** with pyridine in *o*-dichlorobenzene (DCB) at 298 K indicated the binding constant for the 1:1 complex to be $K_{py} = (2.0 \pm 0.6) \times 10^6$ M^{-1} (Figure 8-2). The structure of the pyridine

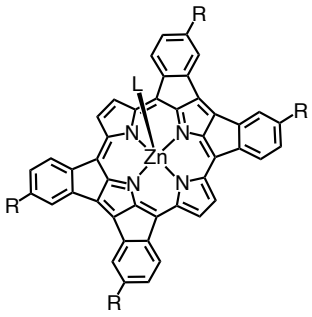

4a (R = H, L = none), **4a**-py (R = H, L = pyridine)
4b (R = mesityl, L = none), **4b**-py (R = mesityl, L = pyridine)

Figure 8-1. Molecular structures of ZnQFP derivatives, **4a** and **4b**.

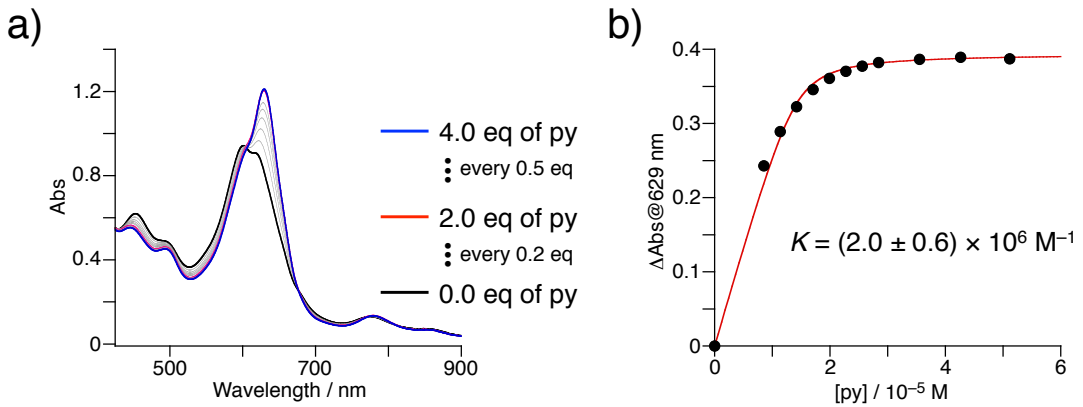

Figure 8-2. (a) UV-Vis spectral changes of **4b**-py in DCB upon addition of pyridine at 298 K and (b) the titration curve of the absorbance at 629 nm.

complex of **4b** (**4b**-py) was revealed by single-crystal X-ray diffraction analysis (Figure 8-3). The asymmetric unit included a half molecule of **4b**-py. In the crystal, the porphyrin core, consisting of four pyrrole rings, four *meso*-carbons and four fused *meso*-benzene rings is bowl-shaped and the mean deviation of the core 48 atoms is 0.389 Å, which is larger than that of **4a**-py (0.212 Å).[14a] The Zn^{II} center is positioned at 1.278 Å above from the mean plane to the direction of the coordinated pyridine.

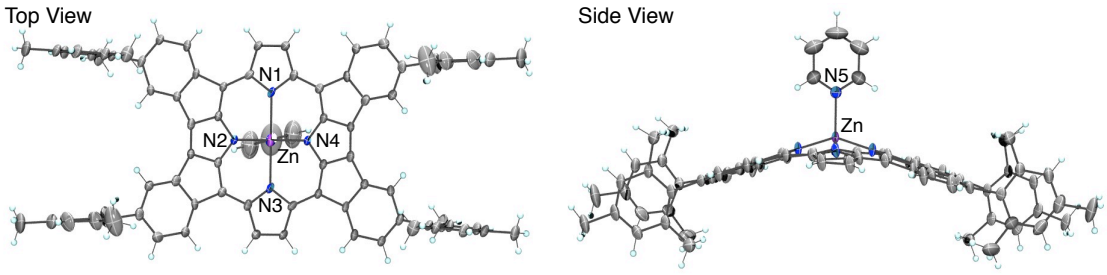

Figure 8-3. ORTEP drawings of the crystal structure of **4b**-py. The thermal ellipsoids are drawn with 40% probability.

8-3. Interaction between ZnQFP and fullerenes in solution

To confirm the interaction between **4b**-py and fullerenes in solution, the solution of **4b**-py in DCB (7.5×10^5 M^{-1})[16] was titrated with a solution of fullerenes in DCB (1.9×10^3 M^{-1}) at 298 K (Figure 8-4). In all cases using C_{60} and C_{70}, the Q bands of **4b**-py showed hypsochromic shifts. The binding constants were obtained from the titration curves based on the absorbance at 778 nm for C_{60} and that at 688 nm for C_{70}, using a nonlinear least-squares regression program.[17] Based on equations (1) and (2), where Ful is fullerene, the stepwise constants, K_1 and K_2, were estimated to

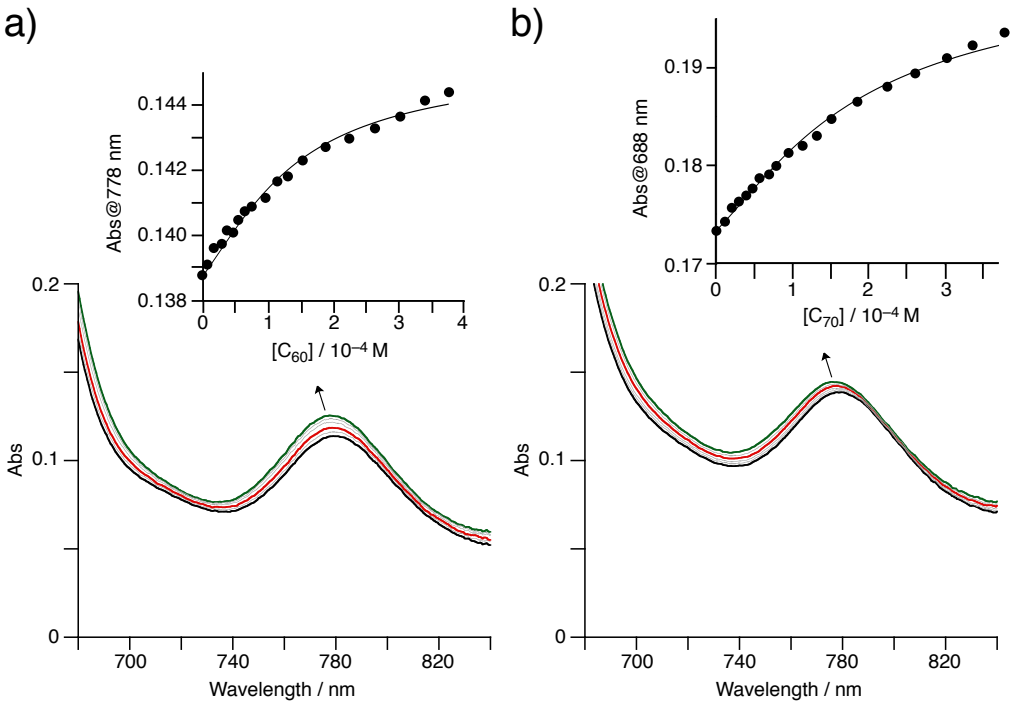

Figure 8-4. UV-Vis spectral change of **4b**-py in DCB with C_{60} (a) and C_{70} (b) in the presence of pyridine (7.9×10^{-5} M) at 298 K. Inset: the fitting curves of the absorbance at 778 nm for (a) and 688 nm for (b).

$$\textbf{4b}\text{-py} + \text{Ful} \rightleftharpoons (\textbf{4b}\text{-py})(\text{Ful});\ K_1 = \frac{[(\textbf{4b}\text{-py})(\text{Ful})]}{[\textbf{4b}\text{-py}][\text{Ful}]} \qquad (1)$$

$$\textbf{4b}\text{-py} + (\textbf{4b}\text{-py})(\text{Ful}) \rightleftharpoons (\textbf{4b}\text{-py})_2(\text{Ful});\ K_2 = \frac{[(\textbf{4b}\text{-py})_2(\text{Ful})]}{[\textbf{4b}\text{-py}][\text{Ful}][\textbf{4b}\text{-py}]} \qquad (2)$$

$$2\,\textbf{4b}\text{-py} + \text{Ful} \rightleftharpoons (\textbf{4b}\text{-py})_2(\text{Ful});\ \beta_2 = K_1 \times K_2 = \frac{[(\textbf{4b}\text{-py})_2(\text{Ful})]}{[\textbf{4b}\text{-py}]^2[\text{Ful}]} \qquad (3)$$

be $(1.1 \pm 0.1) \times 10^4$ and $(1.2 \pm 0.2) \times 10^3$ M^{-1} for C_{60} and $(1.3 \pm 0.1) \times 10^4$ and $(2.2 \pm 0.3) \times 10^3$ for C_{70}, respectively (Table 8-1). Therefore, the total binding constants (β_2) for the complexes of QFP: fullerene = 2:1 were calculated to be $(1.3 \pm 0.3) \times 10^7$ for C_{60} and $(2.9 \pm 0.2) \times 10^7$ M^{-2} for C_{70} (Table 8-1). As far as the author knows, this is the first example that the molecular binding between monomeric porphyrins and fullerenes has been demonstrated in

solution.[10,12c] Additionally, the constants are not significantly different between C_{60} and C_{70}. Although the K_1 values are larger than the K_2 values for both C_{60} and C_{70}, the differences are not large enough to clearly observe the stepwise binding from the 2:1 to 1:1 fashions. In fact, the Job's plots for the association between **4b**-py and fullerenes, obtained under relatively concentrated conditions at 298 K (total concentration of **4b**-py and fullerenes:

Table 8-1. Binding constants of **4b**-py with fullerene, C_{60} and C_{70}.[a]

Fullerene	Method	K_1 / 10^3 M^{-1}	K_2 / 10^3 M^{-1}	β_2 / 10^7 M^{-2}
C_{60}	UV/Vis	11 ± 1	1.2 ± 0.2	1.3 ± 0.3
	^{1}H NMR	10 ± 1	1.2 ± 0.1	1.2 ± 0.1
C_{70}	UV/Vis	13 ± 1	2.2 ± 0.3	2.9 ± 0.2
	^{1}H NMR	12 ± 1	2.3 ± 0.5	2.8 ± 0.6

[a] In DCB at 298 K, obtained from a nonlinear least-squares regression analysis of the absorbance changes at 778 nm for C_{60} and 688 nm for C_{70} and ^{1}H NMR chemical shift changes of the β-pyrrole proton of **4b**-py.

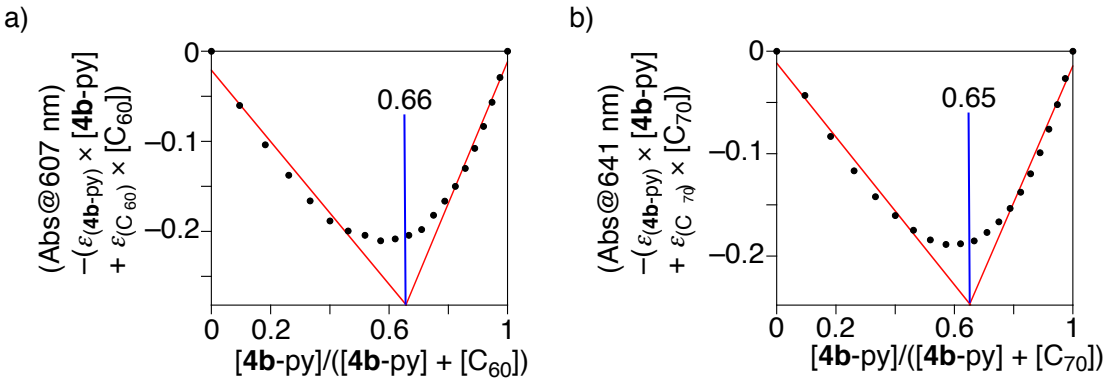

Figure 8-5. Job's plots for **4b**-py and C_{60} (a) and for **4b**-py and C_{70} (b) in DCB at 298 K. The total concentration of **4b**-py and the fullerene was set to be 1.7×10^{-4} M.

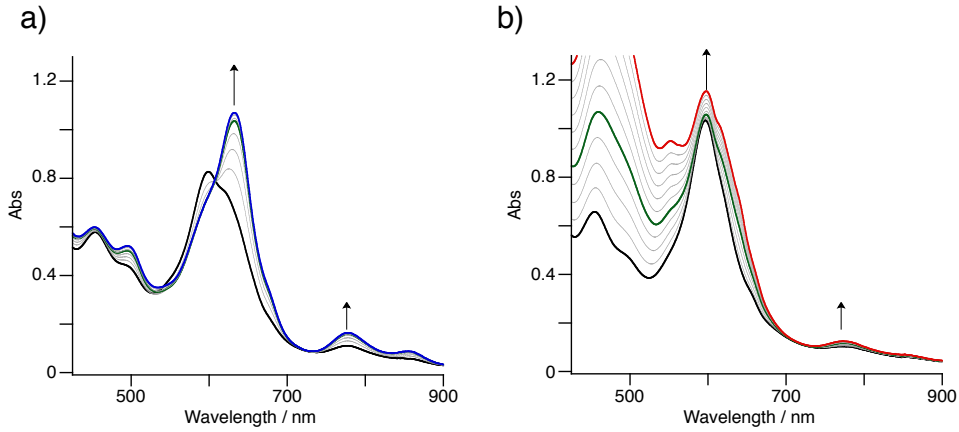

Figure 8-6. UV-Vis spectral changes of **4b** (7.5×10^{-5} M) in DCB with C_{60} (a) and C_{70} (b) in the absence of pyridine at 298 K.

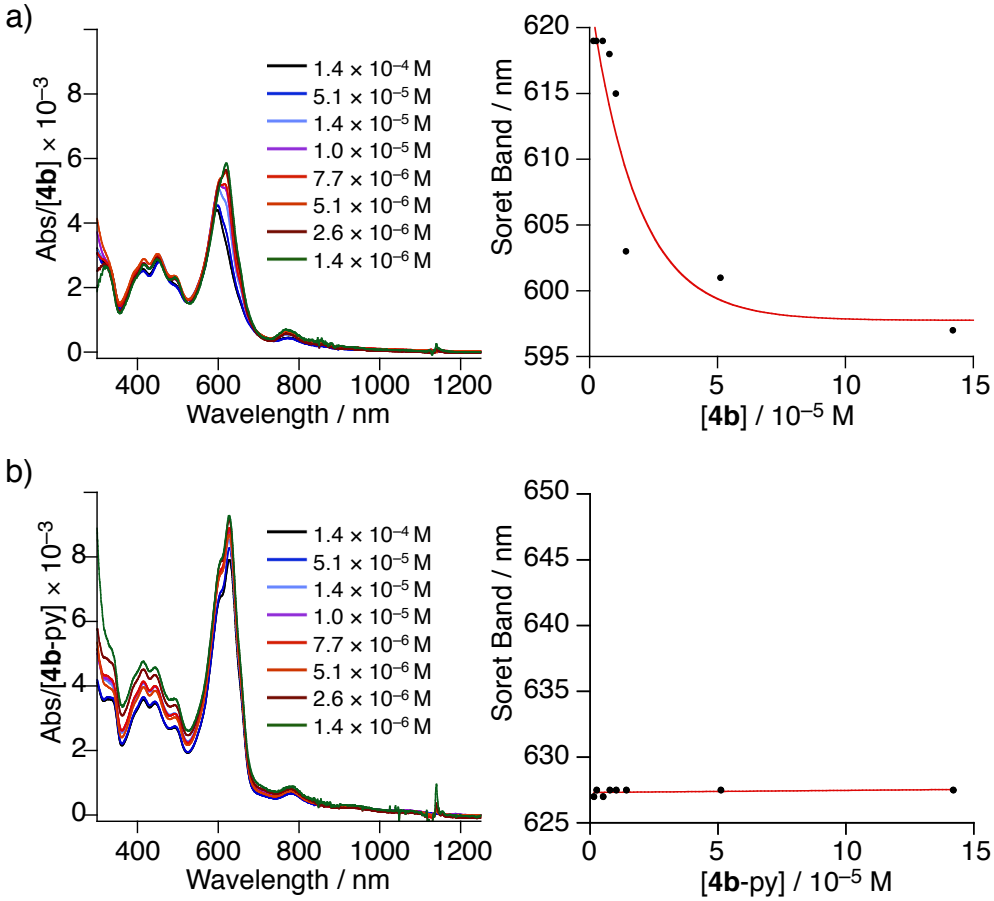

Figure 8-7. UV-Vis spectral changes of **4b** (a) and **4b**-py (b) depending on the concentration in DCB at 298 K.

1.7×10^{-4} M), indicated the formation of the 2:1 complex (Figure 8-5). The titration experiments of **4b** with fullerenes in the absence of pyridine in DCB (Figure 8-6) were also conducted. As results, the addition of fullerenes brought drastic absorption changes, in comparison to the cases in the presence of pyridine. These changes probably derive from the association with fullerenes, causing structural changes of **4b** from the planar form to the bowl-shaped structure to strengthen the π-π interaction with fullerenes. Compound **4b**, however, exhibits self-aggregation in DCB at the concentration of the titration experiments (7.5×10^{-5} M). Increasing the concentration of **4b** in DCB caused a blue shift of the Soret band; for instance, 619 nm at 1.4×10^{-6} M and 597 nm for 1.4×10^{-4} M (Figure 8-7). In contrast, the Soret band of **4b**-py did not show any dependence on the concentration in DCB in the presence of pyridine. These results indicate that compound **4b** exhibits H-type π-π stacking under concentrated conditions and the pyridine coordination to give rise to deformation of the porphyrin core prevents the π-π stacking. Therefore, the self-aggregation of **4b** by the π-π stacking disturbs the analysis of the titration experiments with fullerenes in the absence of pyridine in the solution.

For further confirmation of the association between **4b**-py and fullerenes in solution, ^{1}H NMR titration experiments were also performed in DCB-d_4 at 298 K (Figures 8-8, 8-9 and 8-10). Addition of C_{60} caused upfield shifts of the *p*-CH_3 groups of the peripheral mesityl groups in **4b**-py (8.8×10^{-4} M) from $\delta = 2.159$ ppm in the absence of C_{60} to $\delta = 2.147$ ppm in the presence of 3 equiv of C_{60}. Slight downfield shifts of the *o*-CH_3 groups of the mesityl groups

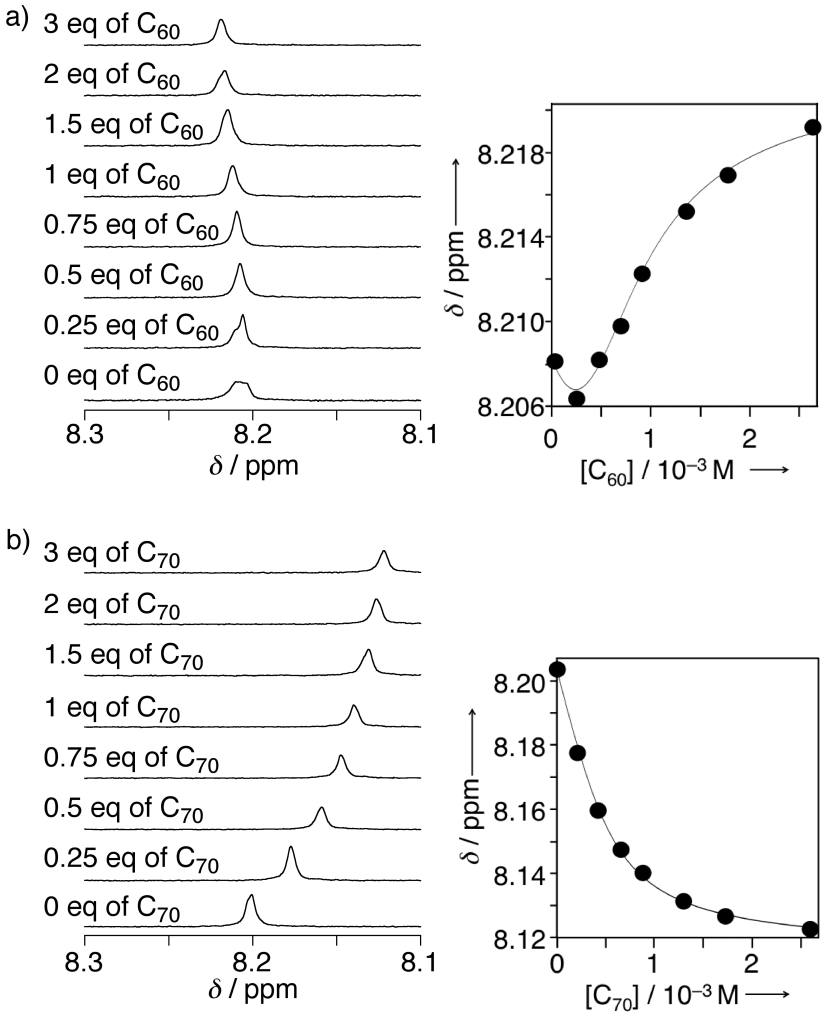

Figure 8-8. Left: 1H NMR spectral change of **4b**-py in DCB-d_4 with addition of: a) C_{60}, and b) C_{70} in the presence of pyridine (1.2×10^{-2} M) at 298 K. Right: the fitting curves of the signal of pyrrole-β-protons.

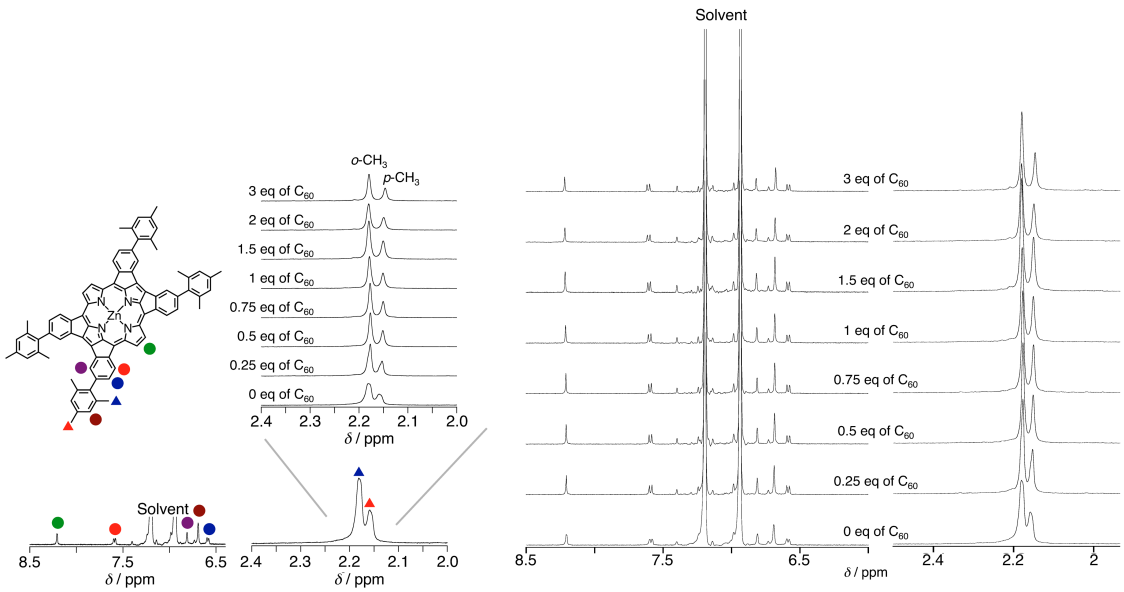

Figure 8-9. ^{1}H NMR spectral changes of **4b**-py (8.8×10^{-4} M) upon addition of C_{60} in DCB-d_4 at 298 K.

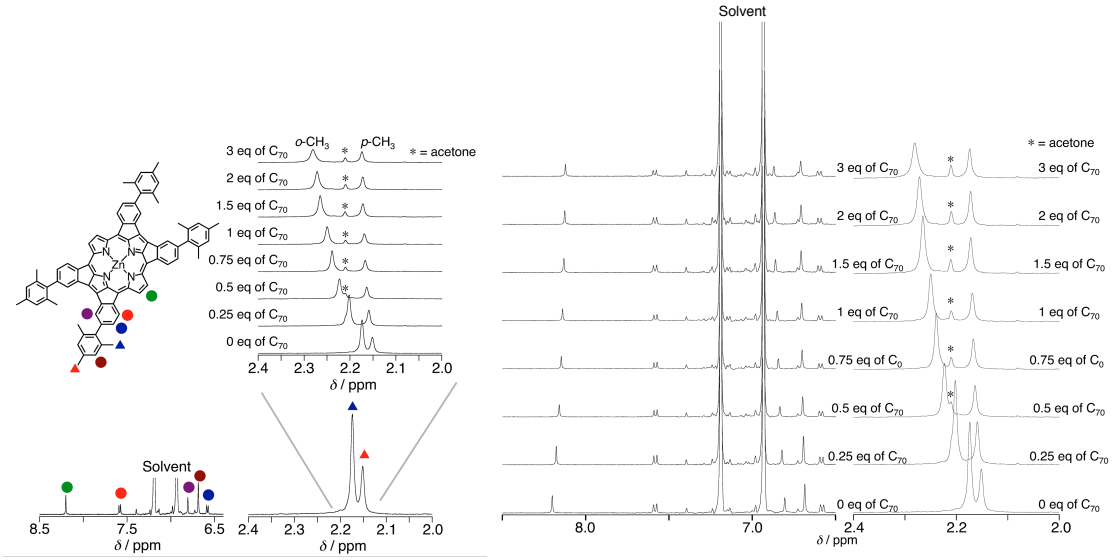

Figure 8-10. ^{1}H NMR spectral changes of **4b**-py (8.8×10^{-4} M) upon addition of C_{70} in DCB-d_4 at 298 K.

and the pyrrole-β-protons were also observed with increasing amount of C_{60} (Figure 8-8a). The shift widths of the NMR signals of **4b**-py were relatively small in the titration with C_{60}. In sharp contrast, addition of C_{70} to the solution of **4b**-py in DCB-d_4 induced clear shifts of the ^{1}H NMR signals (Figure 8-8b and 8-10). The chemical shift changes of the ^{1}H NMR signals for the *o*- and *p*-CH_3 groups of the mesityl groups and the β-pyrrole protons of **4b**-py were used to estimate the association constants, K_1, K_2, and β_2, using the nonlinear least-squares regression program (Table 8-1).[17] All of the association constants obtained from the analyses of the chemical shift changes are comparable to those obtained with UV/Vis titration experiments (Table 8-1). The downfield shift of the *o*-CH_3 groups can be explained by CH-π interaction with C_{70} and the upfield shift of the β-pyrrole protons can be ascribed to the ring-current effect of aromatic C_{70} surfaces in the associated complexes. This explanation is well matched with the crystal structure of the 2:1 complex between **4b**-py and C_{70} (see below). In addition, the downfield shifts of the *p*-CH_3 groups indicate the decrease of the electron densities of the mesityl groups upon formation of the associated complexes between **4b**-py and C_{70}, probably caused by charge-transfer (CT) interaction from **4b**-py to C_{70} (see the electrochemical studies described below). On the other hand, the shift widths of the ^{1}H NMR signals for the *o*-CH_3 groups and the β-pyrrole protons for the C_{60} complexes are modest, which can be elucidated by considering the small volume of C_{60} relative to the cavity composed of the *o*-CH_3 groups of **4b**-py. The small shift of the pyrrole-β-Hs can probably be ascribed to the fact that the C_{60} molecule is not located on top of the β-Hs in the solution due to its smaller size than C_{70}.

8-4. The association structure between ZnQFP and fullerenes in the crystal

The structures of supramolecular assemblies of **4b**-py with fullerenes were explicitly revealed by single-crystal X-ray diffraction analysis (Figure 8-11). The single crystal of the 2:1 complex between **4b**-py and C_{70} was obtained with slow evaporation of the solvent from the toluene solution (Figure 8-11a). The C_{70} molecule, which exhibited

crystallographic disorder, was covered with two molecules of **4b**-py and the longer axis of C_{70} was tilted to **4b**-py by 29.4°. The concave surface of **4b**-py and the convex surface of C_{70} are well matched with each other to form strong π-π interactions. On the other hand, the single crystal obtained from the solution of **4b**-py and C_{60} in DCB in the presence of methanol vapor, which is a poor solvent, gave a preliminary crystal structure of the 2:1 complex (Figure 8-11b). Interestingly, alteration of the poor solvent to acetonitrile vapor gave a single crystal of the 1:1 complex with C_{60} (Figure 8-11c), where the half sphere of C_{60} was covered with a molecule of **4b**-py. The uncovered surface of C_{60} was used to form a π-π stacked pair of the two C_{60} molecules, in which the C-C bonds between six- and five-membered

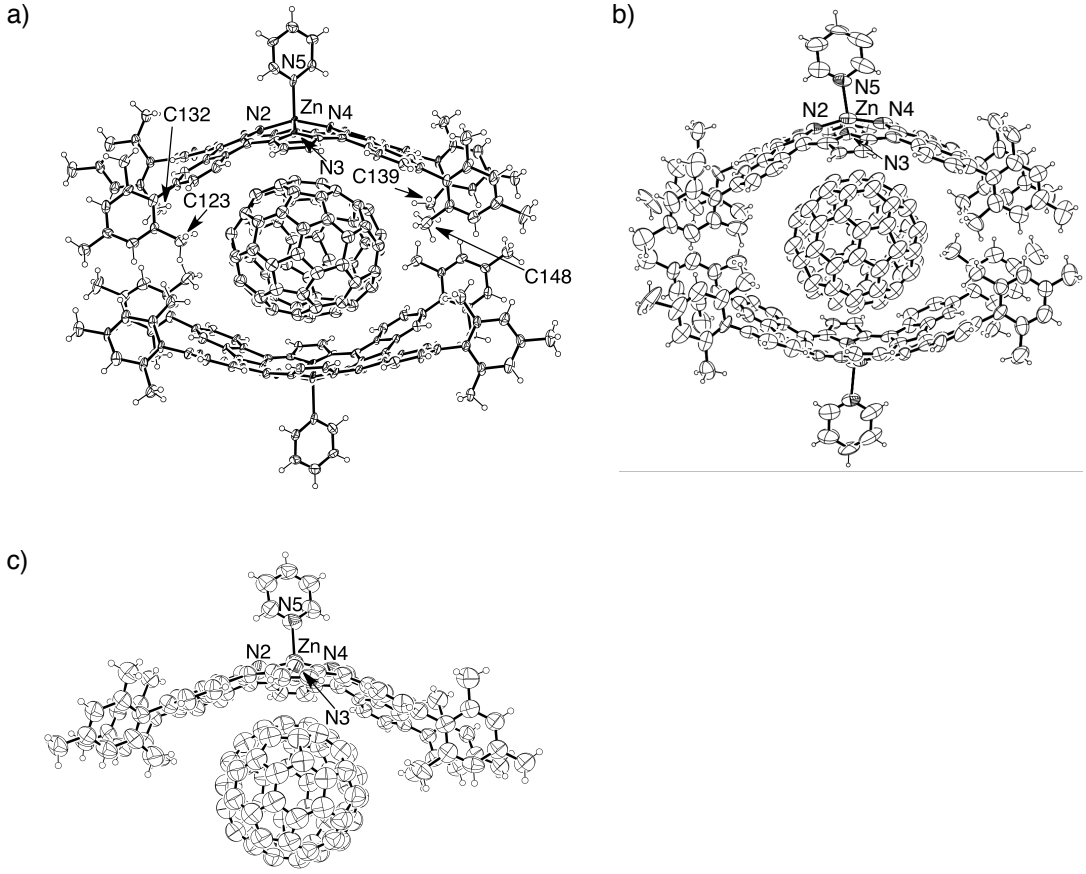

Figure 8-11. ORTEP drawings of crystal structures of (**4b**-py)$_2$·C_{70} (a) and **4b**-py·C_{60} (c). The thermal ellipsoids are drawn with 50% probability. One of the disordered pairs of the fullerenes is shown for clarity. The preliminary crystal structure of (**4b**-py)$_2$·C_{60} (b). The thermal ellipsoids are drawn with 50% for (a) and (c), 25% probability for (b).

rings came closer and the closest C···C distance in the paired C_{60} molecules was 2.89(4) Å. The porphyrin cores in all associated structures determined are more distorted relative to that of free **4b**-py. The mean deviations of the core 48 atoms of **4b**-py are 0.584, 0.571, and 0.502 Å for the 1:1 and 2:1 complexes with C_{60} and the 2:1 complex with C_{70}, respectively. This increase in the degree of the curved distortion for the porphyrin structures in the associated complexes should be induced to strengthen the π-π interaction with the fullerenes.[18] The distances for the π-π interactions between the planes of **4b**-py and fullerenes are estimated to be 3.30, 3.23, and 3.23 Å, for the 1:1 and 2:1 complexes with C_{60} and the 2:1 complex with C_{70}, respectively. Additionally, the molecular size of C_{70} is matched to

Table 8-2. Redox potentials of **4b**-py and fullerenes, C_{60} and C_{70}, in DCB in the presence of TBAP (0.2 M) and pyridine (0.012 M) at 298 K.

	$E_{1/2}$ / V vs Fc/Fc^+						
	$Por^{2-}/Por^{\bullet-}$	$Por^{\bullet-}/Por$	$Por/Por^{\bullet+}$	$Por^{\bullet+}/Por^{2+}$	$Ful^{\bullet 3-}/Ful^{2-}$	$Ful^{2-}/Ful^{\bullet-}$	$Ful^{\bullet-}/Ful$
4b-py	–1.58[a]	–1.28[a]	+0.11[a]	+0.52[a]	—	—	—
C_{60}	—	—	—	—	–1.97	–1.48	–1.07
4b-py + C_{60}	–1.60[a]	–1.20	+0.16	+0.53[a]	–2.01	–1.50	–1.06
ΔE, V	+0.02	+0.08	+0.05	+0.01	–0.04	–0.02	+0.01
C_{70}	—	—	—	—	–1.79	–1.37	–1.00
4b-py + C_{70}	–1.57	–1.26	+0.13	+0.52	–1.89	–1.44	–1.06
ΔE, V	+0.01	+0.02	+0.02	+0.00	–0.06	–0.07	–0.06

[a] obtained from DPV.

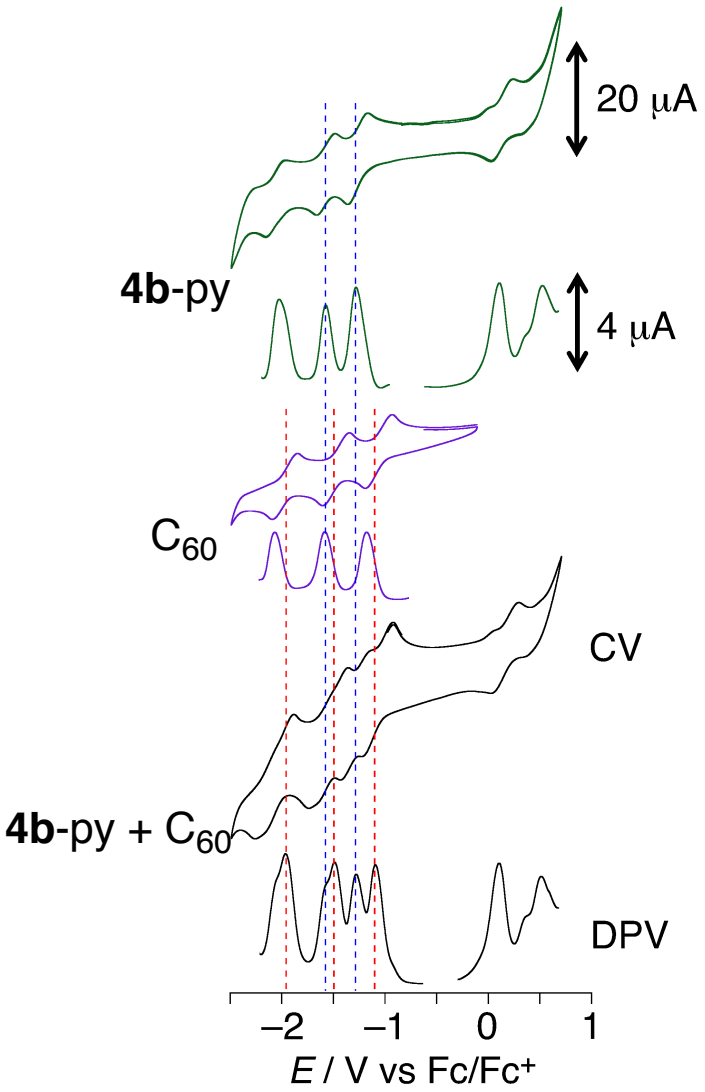

Figure 8-12. Cyclic voltamograms and differential pulse voltammograms for **4b**-py (green, top), C_{60} (purple, middle), **4b**-py + C_{60} (black, bottom), in DCB containing TBAP (0.2 M) as an electrolyte at 298 K.

the cavity provided by four *o*-CH_3 groups of **4b**-py and three among the four CH_3 groups are close enough in the distances to form CH-π interactions with the trapped C_{70}. The distances from C_{70} to the four *o*-CH_3 groups, which are represented by C123, C132, C139, and C148 in Figure 8-12a, are 3.33(3) 3.81(4), 4.95(3), and 3.64(4) Å, respectively.

On the other hand, the size of C_{60} is small for the cavity and thus the C_{60} molecule both in the 1:1 and 2:1 complexes is located on a side of the two fused rings of **4b**-py. As a consequence, the distances from C_{60} to two *o*-CH_3 groups are in the range of the C-H···π distances (*ca.* 3.8 Å), whereas the other two show longer distances from the C_{60} molecule (*ca.* 4.2 Å).

8-5. Electrochemical studies on the association between ZnQFP and fullerenes

The association between **4b**-py and fullerenes affects the redox potentials of both **4b**-py and fullerenes in DCB (Table 8-2, and Figures 8-12 and 8-13). The cyclic and differential-pulse voltammograms (CV and DPV) of **4b**-py in DCB (1.3×10^{-3} M) exhibited two oxidation waves at +0.11 and +0.52 V vs Fc/Fc^+ and two reduction

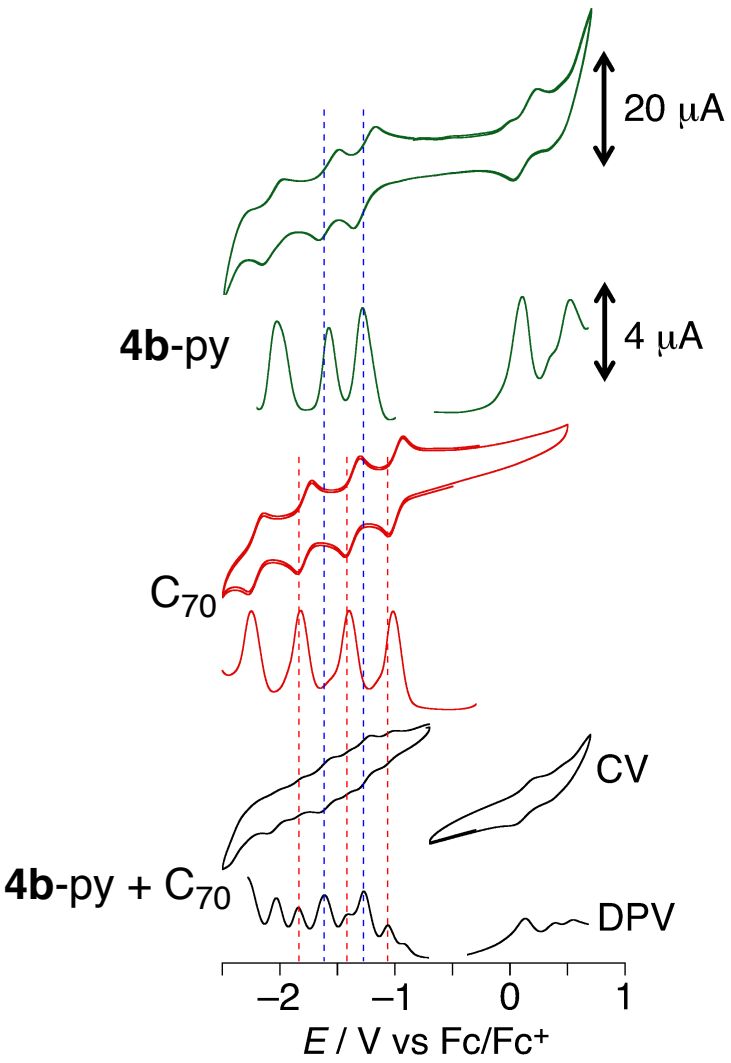

Figure 8-13. Cyclic voltamograms and differential-pulse voltammograms for **4b**-py (green, top), C_{70} (purple, middle), **4b**-py + C_{70} (black, bottom), in DCB containing TBAP (0.2 M) as an electrolyte at 298 K.

waves at –1.28 and –1.58 V vs Fc/Fc^+ in the presence of pyridine (1.2×10^{-2} M) and tetrabutylammonium perchlorate (TBAP, 0.2 M) as an electrolyte at 298 K. The CVs and DPVs of C_{60} and C_{70} measured under the same conditions displayed three reduction waves at –1.06, –1.50 and –2.01 V vs Fc/Fc^+ for C_{60}, and –1.00, –1.37 and –1.79 V vs Fc/Fc^+ for C_{70}. The 2:1 mixture of **4b**-py (1.3×10^{-3} M) and the C_{70} (6.4×10^{-4} M)[19] showed the redox waves with significant shifts (Table 8-2). The redox potentials of **4b**-py were positively shifted in the association with C_{70}, whereas those of C_{70} exhibited negative shifts. The tendencies of the potential shifts can be accounted for by the CT interaction from **4b**-py to the fullerenes.[20] As a result of the CT interaction, the electron density of **4b**-py decreased, whereas that of fullerenes increased; this makes reduction of fullerenes and oxidation of **4b**-py harder in the associated complexes. The degree of potential shifts of C_{70} was larger than that of **4b**-py, because of the difference between the degree of associated C_{70} and that of **4b**-py;[19] in total 72% of **4b**-py formed complexes with C_{70}, whereas 97% of C_{70} participated in complexation with **4b**-py under the experimental conditions. The 2:1 mixture of **4b**-py (1.3×10^{-3} M) and C_{60} (6.4×10^{-4} M) showed the redox waves with modest shifts. This can be explained on the basis of the fact that the first redox potential of C_{60} is lower than that of C_{70}; therefore the CT interaction between **4b**-py and C_{60} is weaker than that between **4b**-py and C_{70}.

8-6. Conclusion

The association equilibriums between the mononuclear Zn^{II} complex of a QFP derivative, **4b**-py, and fullerenes, C_{60} and C_{70}, have been fully investigated spectroscopically and electrochemically. This is the first example to demonstrate encapsulation of fullerenes using a monomeric porphyrinoid in solution. The concave surface of **4b**-py is well matched to the convex surface of fullerenes for strong π-π interactions, especially for C_{70}. In addition, the CH-π interaction of the *o*-CH_3 groups of the mesityl groups and the CT interaction assisted the association between **4b**-py and fullerenes. The molecular sizes of the fullerenes significantly affected the ^{1}H NMR spectral changes and redox potential shifts of **4b**-py. The structures of the associated complexes were explicitly elucidated by X-ray diffraction analysis. The fullerenes are fully covered by the concave surfaces of two **4b**-py molecules in the 2:1 complexes. In contrast, in the crystal structure of the 1:1 complex of C_{60}, the C_{60} molecules formed a π-π stacked pair using the partial surface, uncovered by one **4b**-py molecule.

8-7. Experimental section

General.

Chemicals and solvents were used as received from commercial sources unless otherwise mentioned. Especially, C_{60} was purchased from TCI and C_{70} was kindly gifted by Prof. Takeshi Akasaka (FAIS and Tokyo Gakugei Univ.). 1,4-dioxane for the synthesis was distilled over Na/benzophenone. DCB for the electrochemical measurements was distilled before use. ^{1}H NMR measurements were performed on a Bruker AVANCE400 spectrometer. UV-vis absorption spectra were measured in DCB on a Shimadzu UV-3600 spectrophotometer. MALDI-TOF-MS spectrometry was performed on an AB SCIEX TOF/TOF 5800 spectrometer by using dithranol as a matrix. Electrochemical

measurements were performed on an ALS/CH Instruments Electrochemical Analyzer Model 710D.

X-ray diffraction analysis.

The single crystals were mounted on mounting loops. All diffraction data were collected at 120 K by using a Bruker APEXII diffractometer equipped with graphite- monochromated Mo $K\alpha$ (λ = 0.71073 Å) by the ω-2θ scan for **4b**-py and (**4b**-py)$_2$·C$_{70}$, or a Rigaku Mercury CCD system at Photon Factory-Advanced Ring for Pulse X-rays (PF-AR NW2A) of High Energy Accelerator Research Organization (KEK) at 183 K for (**4b**-py)$_2$·C$_{60}$ and **4b**-py·C$_{60}$. The structures were solved by direct methods by using SIR97 and SHELX-97.[21] Crystallographic data for these compounds are summarized in Table 8-3. CCDC-1038721 (**4b**-py), -1038724 ((**4b**-py)$_2$·C$_{60}$), -1038723 (**4b**-py·C$_{60}$), and -1038722

Table 8-3. Crystallographic data for **4b**-py and the association complexes between **4b**-py and fullerenes.

compound	**4b**-py	(**4b**-py)$_2$·C$_{60}$	**4b**-py·C$_{60}$	(**4b**-py)$_2$·C$_{70}$
crystal system	monoclinic	monoclinic	triclinic	triclinic
space group	*C*2/*c*	*C*2/*c*	*P* $\bar{1}$	*P* $\bar{1}$
T / K	120	120	120	120
formula	C$_{80}$H$_{60}$N$_4$Zn·C$_5$H$_5$N	2(C$_{80}$H$_{60}$N$_4$Zn) ·2(C$_5$H$_5$N)·C$_{60}$	C$_{80}$H$_{60}$N$_4$Zn ·C$_5$H$_5$N·C$_{60}$	2(C$_{80}$H$_{60}$N$_4$Zn) ·2(C$_5$H$_5$N)·C$_{70}$
FW	1221.87	3164.41	1942.53	3219.13
a / Å	36.090(8)	21.243(4)	12.9302(13)	15.552(10)
b / Å	8.3851(18)	44.002(8)	13.9359(17)	18.05(2)
c / Å	28.580(6)	23.481(5)	29.001(4)	20.375(13)
α / º	36.090(8)	21.243(4)	12.9302(13)	15.552(10)
β / º	8.3851(18)	44.002(8)	13.9359(17)	18.05(2)
γ / º	28.580(6)	23.481(5)	29.001(4)	20.375(13)
V / Å^3	7818(3)	21725(7)	4575.0(10)	4872(7)
Z	4	8	2	2
λ / Å	0.71073 (Mo $K\alpha$)	0.6890 (synchrotron)	0.6890 (synchrotron)	0.71073 (Mo $K\alpha$)
D_c / g cm^{-3}	1.038	0.967	1.410	1.119
reflns measured	14327	62593	36269	14333
reflns unique	8381	15427	4821	5385
*R*1 ($I > 2\sigma(I)$)	0.0825	0.1586	0.1026	0.0856
*wR*2 (all)	0.1759	0.4500	0.2130	0.2227
GOF	1.069	1.171	1.125	1.021

((**4b**-py)$_2$·C$_{70}$) contain the supplementary crystallographic data. A molecule of **4b**-py and two co-crystallized tetrahydrofuran molecules are involved in the asymmetric unit. The two co-crystallized tetrahydrofuran molecules in the crystal of **4b**-py were highly disordered and deleted by using the "Squeeze" program.[22]

Estimation of association constants between 4b and pyridine. To the solution of **4b** in DCB was titrated with the solution of pyridine and the absorbance change was fitted with eq 8-4 (Figure 8-2).

$$\text{Abs} = (\varepsilon_{PyP} / (2 \times K)) \times (1 + K \times [py] + K \times [P]_0) - ((1 + K \times [py] + K \times [P]_0)^2 - 4 \times K^2 \times [py] \times [P]_0)^{1/2} \quad (4)$$

Here, ε_P, [P], [py], ε_{PyP}, and K, refer to the absorption coefficient of **4b**, the concentration of **4b**, the concentration of pyridine, the absorption coefficient of the associated complex between **4b** and pyridine, and the binding constant, respectively.

Reference and notes

1 (a) R. E. Haufler, J. Conceicao, L. P. F. Chibante, Y. Chai, N. E. Byrne, S. Flanagan, M. M. Haley, S. C. O'Brien, C. Pan, Z. Xiao, W. E. Billups, M. A. Ciufolini, R. H. Hauge, J .L. Margrave, L. J. Wilson, R. F. Curl, R. E. Smalley, *J. Phys. Chem.* **1990**, *94*, 8634. (b) P.-M. Allemand, A. Koch, F. Wudl, Y. Rubin, F. Diederich, M. M. Alvarez, S. J. Anz, R. L. Whetten, *J. Am. Chem. Soc.* **1991**, *113*. 1050.

2 (a) B. C. Thompson, J. M. J. Fréchet, *Angew. Chem. Int. Ed.* **2008**, *47*, 58. (b) J.-L. Brédas, J. R. Durrant, *Acc. Chem. Res.* **2009**, *42*, 1689. (c) D. Nocera, D. M. Guldi, *Chem. Soc. Rev.* **2009**, *38*, 1. (d) D. M. Guldi, B. M. Illescas, C. M. Atienza, M. Wielopolski, N. Martín, *Chem. Soc. Rev.* **2009**, *38*, 1587.

3 (a) D. Canevet, E. M. Pérez, N. Martín, *Angew. Chem. Int. Ed.* **2011**, *50*, 9248. (b) P. D. W. Boyd, C. A. Reed, *Acc. Chem. Res.* **2005**, *38*, 235. (c) K. Tashiro, T. Aida, *Chem. Soc. Rev.* **2007**, *36*, 189.

4 (a) K. Tashiro, T. Aida, J.-Y. Zheng, K. Kinbara, K. Saigo, S. Sakamoto, K. Yamaguchi, *J. Am. Chem. Soc.* **1999**, *121*, 9477. (b) J.-Y. Zheng, K. Tashiro, Y. Hirabayashi, K. Kinbara, K. Saigo, T. Aida, S. Sakamoto, K. Yamaguchi, *Angew. Chem. Int. Ed*. **2001**, *40*, 1857. (c) Y. Shoji, K. Tashiro, T. Aida, *J. Am. Chem. Soc.* **2004**, *126*, 6570. (d) M. Yanagisawa, K. Tashiro, M. Yamasaki, T. Aida, *J. Am. Chem. Soc.* **2007**, *129*, 11912. (e) F. Hajjaj, K. Tashiro, H. Nikawa, N. Mizorogi, T. Akasaka, S. Nagase, K. Furukawa, T. Kato, T. Aida, *J. Am. Chem. Soc.* **2011**, *133*, 9290.

5 (a) P. D. W. Boyd, M. C. Hodgson, C. E. F. Rickard, A. G. Oliver, L. Chaker, P. J. Brothers, R. D. Bolskar, F. S. Tham, C. A. Reed, *J. Am. Chem. Soc.* **1999**, *121*, 10487. (b) D. Sun, F. S. Tham, C. A. Reed, L. Chaker, P. D. W. Boyd, *J. Am. Chem. Soc.* **2002**, *124*, 6604. (c) A. Hosseini, S. Taylor, G. Accorsi, N. Armaroli, C. A. Reed, P. D. W. Boyd, *J. Am. Chem. Soc.* **2006**, *128*, 15903.

6 (a) H. Nobukuni, Y. Shimazaki, F. Tani, Y. Naruta, *Angew. Chem. Int. Ed.* **2007**, *46*, 8975. (b) J. Zhang, X. Zheng, R. Jiang, Y. Yu, Y. Li, H. Liu, Q. Li, Z. Shuaic, Y. Li, *RSC Adv.* **2014**, *4*, 27389.

7 (a) G. Bottari, O. Trukhina, M. Ince, T. Torres, *Coord. Chem. Rev.* **2012**, *256*, 2453. (b) G. Bottari, G. de La Torre, D. M. Guldi, T. Torres, *Chem. Rev.* **2010**, *110*, 6768. (c) S. Fukuzumi, T. Kojima, *J. Mater. Chem.* **2008**, *18*, 1427.

8 (a) H. Nobukuni, Y. Shimazaki, H. Uno, Y. Naruta, K. Ohkubo, T. Kojima, S. Fukuzumi, S. Seki, H. Sakai, T. Hasobe, F. Tani, *Chem. Eur. J.* **2010**, *16*, 11611. (b) B. Grimm, J. Schornbaum, C. M. Cardona, J. D. van Paauwe, P. D. W. Boyd, D. M. Guldi, *Chem. Sci.* **2011**, *2*, 1530. (c) T. Kamimura, K. Ohkubo, Y. Kawashima, H. Nobukuni, Y. Naruta, F. Tani, S. Fukuzumi, *Chem. Sci.* **2013**, *4*, 1451.

9 (a) R. D. Jonson, D. S. Bethune, C. S. Yannoni, *Acc. Chem. Res.* **1992**, *25*, 169. (b) A. V. Nicolaev, T. J. S. Dennis, K. Prassides, A. K. Soper, *Chem. Phys. Lett.* **1994**, *223*, 143.

10 X. Fang, Y.-Z. Zhu, J.-Y. Zheng, *J. Org. Chem.* **2014**, *79*, 1184.

11 (a) G. Gil-Ramirez, S. D. Karlen, A. Shundo, K. Porfyrakis, Y. Ito, G. A. D. Briggs, J. J. L. Morton, H. L. Anderson, *Org. Lett.* **2010**, *12*, 3544. (b) J. Song, N. Aratani, H. Shinokubo, A. Osuka, *J. Am. Chem. Soc.* **2010**, *132*, 16356. (c) A. R. Mulholland, C. P. Woodward, S. J. Langford, *Chem. Commun.* **2011**, *47*, 1494.

12 (a) E. M. Pérez, N. Martín, *Chem. Soc. Rev.* **2008**, *37*, 1512. (b) E. M. Pérez, L. Sánchez, G. Fernández, N. Martín, *J. Am. Chem. Soc.* **2006**, *128*, 7172. (c) I. Sánchez-Molina, C. G. Claessens, B. Grimm, D. M. Guldi, T. Torres, *Chem. Sci.* **2013**, *4*, 1338.

13 T. Haino, M. Yanase, Y. Fukazawa, *Angew. Chem. Int. Ed. Engl.* **1997**, *36*, 259.

14 (a) T. Ishizuka, Y. Saegusa, Y. Shiota, K. Ohtake, K. Yoshizawa, T. Kojima, *Chem. Commun.* **2013**, *49*, 5939. (b) Y. Saegusa, T. Ishizuka, K. Komamura, S. Shimizu, H. Kotani, N. Kobayashi, T. Kojima, *Phys. Chem. Chem. Phys.* **2015**, *17*, 15001. (c) Y. Saegusa, T. Ishizuka, T. Kojima, S. Mori, M. Kawano, T. Kojima, *Chem. Eur. J.* **2015**, *21*, 5302.

15 The synthetic details are reported in Chapter 2 of this thesis.

16 The solutions of **4b** for the titration experiments with fullerenes included pyridine (7.9×10^{-5} M), and thus, over 96% of **4b** in the solution were coordinated with pyridine, based on the association constant (K_{py}) between **4b** and pyridine at 298 K.

17 K. Hirose, *J. Inclusion Phenom. Macrocyclic Chem.* **2001**, *39*, 193.

18 A. L. Litvinov, D. V. Konarev, A. Yu. Kovalevsky, I. S. Neretin, P. Coppens, R. N. Lyubovskaya, *Cryst. Growth Des.* **2005**, *5*, 1807.

19 In the 2:1 mixed solution of **4b**-py (1.3×10^{-3} M) and C_{60} (6.4×10^{-4} M) for the electrochemical studies at 298 K, **4b**-py: C_{60} = 2:1 and 1:1 complexes co-existed and the percentages based on **4b**-py are 44% for the 2:1 complex and 22% for the 1:1 complex and the percentages based on C_{60} are 47% for the 2:1 complex and 47% for the 1:1 complex, respectively. In the solution of **4b**-py (1.3×10^{-3} M) and C_{70} (6.4×10^{-4} M), the percentages based on **4b**-py are 55% for the 2:1 complex and 17% for the 1:1 complex and the percentages based on C_{70} are 60% for the 2:1 complex and 37% for the 1:1 complex, respectively.

20 K. Tashiro, T. Aida, *J. Inclusion Phenom. Macrocyclic Chem.* **2001**, *41*, 215.

21 G. M. Sheldrick, SIR97 and SHELX97, Programs for Crystal Structure Refinement, University of Göttingen, Göttingen (Germany), 1997.

22 P. V. D. Sluis, A. L. Spek, *Acta Crystallogr.* **1990**, *A46*, 194.

Concluding remarks

In this thesis, to elucidate the significant effects of the ring fusion on the electronic structures of the porphyrin derivatives, a novel quadruply-fused porphyrin, QFP (**4**), in which the *meso*-aryl groups are covalently bonded to the *β*-carbons of the pyrrole rings at the *ortho*-positions, has been prepared with a facilely prepared precursor in a high yield. The crystal structure of **4** revealed the expansion of the π-conjugation circuits to the fused *meso*-aryl groups, as reflected on the long bond lengths between the *ipso*- and *ortho*-carbons bonded to the *β*-pyrrole carbon. Remarkable red shifts of the absorption bands were observed for **4**, reflecting the narrowed HOMO-LUMO gaps, and the remarkable contribution of antiaromatic resonance forms to the magnetic properties was recognized in the ^{1}H NMR spectra.

The author has investigated substituent effects, introduced at two different kinds of positions of QFP, on optical and electrochemical properties and structural features of QFP; one is the *para*-positions of the fused *meso*-aryl groups and the other is the *β*-positions of the non-fused pyrroles. The former derivatives were synthesized by introduction of the substituents to the precursor TPP derivatives at the *para* positions of the *meso*-phenyl groups, and the latters were prepared by direct functionalization of QFPs *via* bromination of the *β*-positions of the non-fused pyrroles. Introduction of substituents to the aromatic circuit of QFPs at the fused *meso*-aryl groups more largely affects the first oxidation potentials than that of *meso*-aryl substituted Zn^{II}TPPs; that is, the substituent effect is more significant on the HOMO level than the LUMO level. On the other hand, introduction of substituents at the *β*-positions of the non-fused pyrroles affects both of the HOMO and LUMO levels to the same extent. Furthermore, *β*-tetrabrominated QFP shows a characteristic dimeric structure involving a η^3-QFP ligand in the crystal and in non-coordinating solvents such as CH_2Cl_2 due to steric repulsion between the Br groups and the fused aromatic rings as well as the strong coordination of a solvent molecule and a pyrrole nitrogen atom of the other molecule. The enhanced substituent effects of ZnQFPs on the electronic structure contribute to the large NLO responses of "push-pull" ZnQFP derivatives having both EWG and EDG at the fused aryl moieties; especially, a ZnQFP derivative having a cyano group and a methoxy group as an EWG and an EDG, respectively, displayed a *ca*. 240-times larger dynamic hyperporalizability than that of the corresponding "push-pull" TPP derivative.

Freebase derivatives of QFP, **12c**, and its mesitylated derivative, **16c**, have been synthesized and characterized by various spectroscopies and X-ray diffraction analysis. Structural rigidity caused by the ring fusion induces the stepwise diprotonation of H_2QFP through the destabilization of the diprotonated form. The crystal structures of **12c** and **16c** revealed rhombic distortion of the porphyrin core, and the deformation of the porphyrin core leads to decrease in the reaction rates for the NH tautomerism of **16c**. The author also has revealed that the ZnQFP derivatives show dome-type distortion with a continuous concave surface involving the fused aryl moieties and porphyrin core, upon introduction of an axial ligand such as pyridine on the Zn^{II} center. The concave surface of the ZnQFP derivative was utilized to form stable associated complexes with fullerenes based on the convex-concave structural complementarity in solution due to enhanced intermolecular π-π interaction; in the associated complexes, the electrochemical properties of

fullerenes was controlled by the CT interaction with the Zn^{II}QFP complex.

Throughout this research, the author has succeeded in revealing the effects of ring fusion in QFPs, having five-membered rings at the periphery, on the aromatic and optical properties and has provided a novel molecular design to afford useful functional molecules through the ring fusion of porphyrin derivatives. The synthetic procedure of QFPs, developed in this work, is facile and efficient, and the synthetic precursors can be easily prepared. Additionally, introduction of substituents to QFPs is also facile, and through the modification, QFP derivatives can be synthesized to show desired physical properties including optical and redox functionality. QFP derivatives exhibit long wavelength absorption reaching to the near infrared region, and the properties are useful to produce photovoltaic cells and other optoelectronic devices, working with a wide wavelength range of irradiation light from the UV to NIR region. Therefore, the effectiveness of the ring-fusion approach has been demonstrated to develop functional dyes to be applied to future molecular devices. Developments of molecular devices based on organic dyes, which do not include precious metals as components but can utilize a wide range of solar energy, is very important to solve the energy and resource problems that the world is facing at present.

List of publications

1) Multiply-fused porphyrins—effects of extended π-conjugation on the optical and electrochemical properties
T. Ishizuka, Y. Saegusa, Y. Shiota, K. Ohtake, K. Yoshizawa, T. Kojima, *Chem. Commun.* **2013**, *49*, 5939-5941.

2) Ring-fused porphyrins: extension of π-conjugation significantly affects the aromaticity and optical properties of the porphyrin π-systems and the Lewis acidity of the central metal ions
Y. Saegusa, T. Ishizuka, K. Komamura, S. Shimizu, H. Kotani, N. Kobayashi, T. Kojima, *Phys. Chem. Chem. Phys.* **2015**, *17*, 15001-15011.

3) Supramolecular Interaction of Fullerenes with a Curved π-Surface of a Monomeric Quadruply Ring-Fused Porphyrin
Y. Saegusa, T. Ishizuka, T. Kojima, S. Mori, M. Kawano, T. Kojima, *Chem. Eur. J.* **2015**, *21*, 5302-5306.

4) Acid-Base Properties of a Freebase Form of a Quadruply Ring-Fused Porphyrin—Stepwise Protonation Induced by Rigid Ring-Fused Structure
Y. Saegusa, T. Ishizuka, Y. Shiota, K. Yoshizawa, T. Kojima, *J. Org. Chem.* **2017**, *82*, 322-330.

Acknowledgement

The author would like to give special thanks to Professor Takahiko Kojima for his excellent guidance, encouragement, patience and insightful comments on the author's research. The author would also appreciate very much prof. Kojima's valuable suggestions about chemistry and one's life. The author's sincere thanks also go to Dr. Tomoya Ishizuka for his guidance throughout this research by proving constructive and fruitful scientific advises with great patience and effort to edit this thesis. The author's thanks also go to Dr. Hiroaki Kotani for his helpful suggestion in chemistry.

The author would like to express his sincere gratitude to Prof. Kazunari Yoshizawa and Prof. Yoshihito Shiota in Kyusyu University for their kind collaboration in DFT calculations. The author would like to appreciate Prof. Masaki Kawano and Dr. Tatsuhiro Kojima in POSTECH, who now moved to Tokyo Institute of Technology and Osaka University, respectively, for his kind collaboration in X-ray diffraction measurements at High Energy Accelerator Research Organization (KEK). Dr. Shigeki Mori in Ehime University is gratefully appreciated for X-Ray diffraction Analysis. The author would like to thank Prof. Nagao Kobayashi in Shinshu University, Prof. Souji Shimizu in Kyusyu University and Prof. Taniyuki Furuyama in Kanazawa University for DFT calculations and MCD measurements. The author also thanks Dr. Shuhei Higashibayashi in Institute for Molecular Science for guidance to Pd-clusters preparations. The author would like to appreciate Prof. Shigehisa Akine in Kanazawa University for nonlinear least-squares regression program. Prof. Takeshi Akasaka in FAIS and Tokyo Gakugei University is gratefully appreciated for gift of C_{70}. The author is grateful to Prof. Masanori Sakamoto and Mr. Daichi Eguchi in Kyoto University for their kind collaboration. The author would like to appreciate Prof. Taka-aki Ishibashi and Dr. Masanari Okuno in University of Tsukuba for hyper-Rayleigh light-scattering measurements. The author would like to express one's gratitude to Prof. Miki Hasegawa and Dr. Ayumi Ishii in Aoyama Gakuin University for NIR emission spectrometry.

The author would like to thank all the labmates in the Kojima laboratory, Department of Chemistry, University of Tsukuba, who have experienced a lot of joys together as well as a few of difficulty. The author owes them so much for experiencing a cheerful laboratory life. The author would like to appreciate Mr. Kazuhisa Ohtake and Mr. Keiyu Komamura in University of Tsukuba for their research on QFP. In addition, Ms. Miyuki Nakahara should be appreciated her solicitudes and kind support in administrative processes.

Finally, the author sincerely appreciates his family for their support and pecuniary assistance throughout his life.

February 2019

Yuta Saegusa

Kojima Laboratory
Department of Chemistry
University of Tsukuba